R-07-56

Geology – Background complementary studies

Forsmark modelling stage 2.2

Editors:

Michael B Stephens, Geological Survey of Sweden

Kristina Skagius, Kemakta Konsult AB

September 2007

Svensk Kärnbränslehantering AB
Swedish Nuclear Fuel
and Waste Management Co
Box 5864
SE-102 40 Stockholm Sweden
Tel 08-459 84 00
+46 8 459 84 00
Fax 08-661 57 19
+46 8 661 57 19

ISSN 1402-3091
SKB Rapport R-07-56

Geology – Background complementary studies

Forsmark modelling stage 2.2

Editors:

Michael B Stephens, Geological Survey of Sweden

Kristina Skagius, Kemakta Konsult AB

September 2007

Preface

During Forsmark model stage 2.2, seven complementary geophysical and geological studies were initiated by the geological modelling team, in direct connection with and as a background support to the deterministic modelling of deformation zones. One of these studies involved a field control on the character of two low magnetic lineaments with NNE and NE trends inside the target volume. The interpretation of these lineaments formed one of the late deliveries to SKB that took place after the data freeze for model stage 2.2 and during the initial stage of the modelling work. Six studies involved a revised processing and analysis of reflection seismic, refraction seismic and selected oriented borehole radar data, all of which had been presented earlier in connection with the site investigation programme. A prime aim of all these studies was to provide a better understanding of the geological significance of indirect geophysical data to the geological modelling team. Such essential interpretative work was lacking in the material acquired in connection with the site investigation programme. The results of these background complementary studies are published together in this report.

The titles and authors of the seven background complementary studies are presented below. Necessary editing work has been carried out by Michael B. Stephens and Kristina Skagius. Summaries of the results of each study, with a focus on the implications for the geological modelling of deformation zones, are presented in the master geological report, stage 2.2 /Stephens et al. 2007/. The sections in the master report, where reference is made to each background complementary study and where the summaries are placed, are also provided below. The individual reports are listed in the order that they are referred to in the master geological report and as they appear in this report.

Reference to each report in the master geological report /Stephens et al. 2007/ is carried out in accordance with the following example:

Petersson J, Andersson U B, Berglund J, 2007. Scan line fracture mapping and magnetic susceptibility measurements across two low magnetic lineaments with NNE and NE trend, Forsmark. In Stephens M B and Skagius K (edits.), Geology − Background complementary studies. Forsmark modelling stage 2.2. SKB R-07-56, Svensk Kärnbränslehantering AB.

Reference

Stephens M B, Fox A, La Pointe P, Simeonov A, Isaksson H, Hermanson J, Öhman J, 2007. Geology. Forsmark modelling stage 2.2. SKB R-07-45, Svensk Kärnbränslehantering AB.

Scan line fracture mapping and magnetic susceptibility measurements across two low magnetic lineaments with NNE and NE trend, Forsmark

Jesper Petersson, Ulf B Andersson, Johan Berglund
Vattenfall Power Consultant AB

Contents

1 Introduction

A detailed ground magnetic survey in the Forsmark area /Isaksson et al. 2006/ has revealed several low magnetic lineaments with NNE to NE trend in the north-western part of the candidate area. In order to confirm their possible relation to geological structures, such as fracture zones, a relatively well exposed outcrop that clearly coincides with two of these lineaments was chosen for detailed investigations. The outcrop, referred to as PFM000704 in the bedrock mapping work /Stephens et al. 2003/, is located about 400 m north of drill site 6 (Figure 1-1). The more distinct low magnetic lineament (MFM2273G) is inferred to be 659 m in length and shows an average trend of 29°, whereas the other lineament (MFM2088G) is 68 m in length and trends approximately 54° /cf. Isaksson et al. 2006/.

Two more or less parallel traverses (LFM001027 and LFM001028), 7–10 m apart, were uncovered in a direction perpendicular to the low magnetic lineaments, with the purpose to investigate their geological character with the help of scan line fracture mapping and magnetic susceptibility measurements. The total lengths of these two traverses are 40.5 and 46.0 m, respectively, and their widths range generally from 1.5 to 2.5 m. A summary of the results from the scan line mapping work is presented in Figure 1-2.

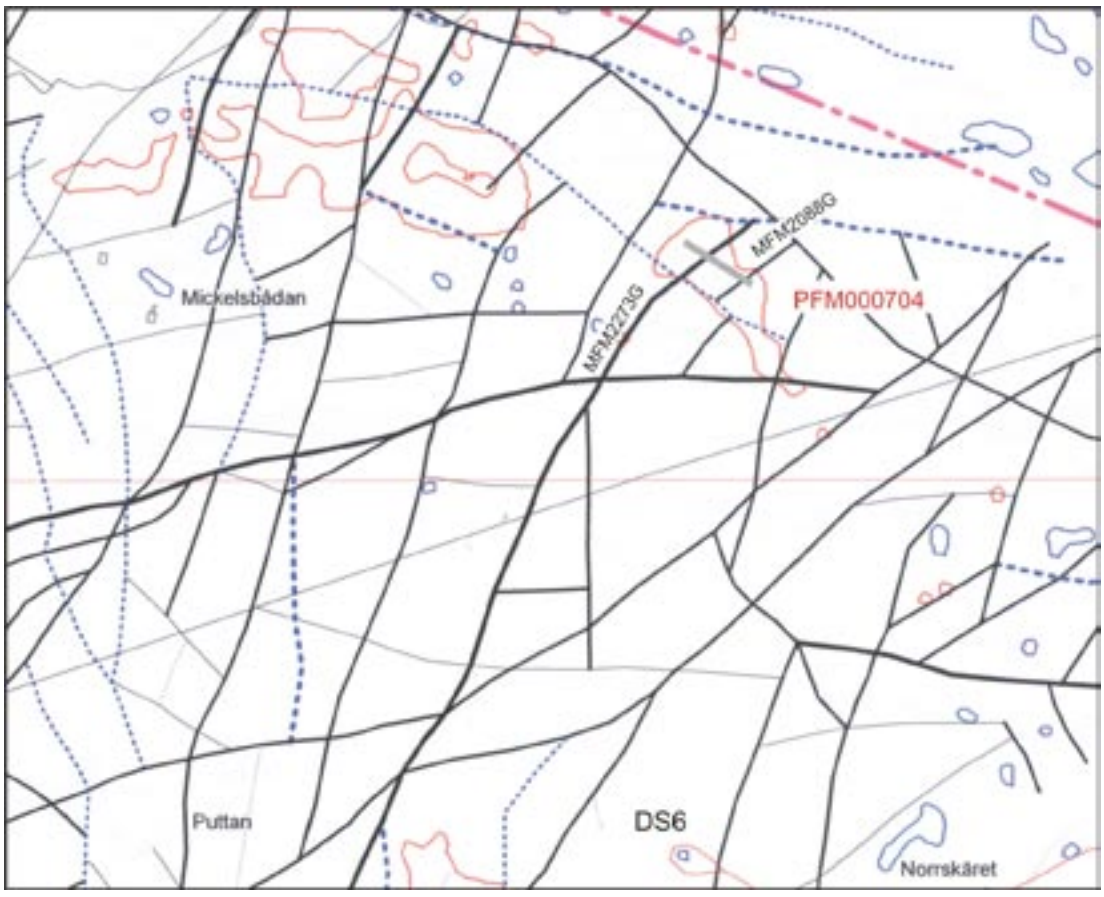

Figure 1-1. *Lineament map based on the detailed ground survey of the magnetic total field /Isaksson et al. 2006/. Outcrops intersected by lineaments are marked by red contours, whereas the other outcrops have blue contours. The location of the traverses is also shown.*

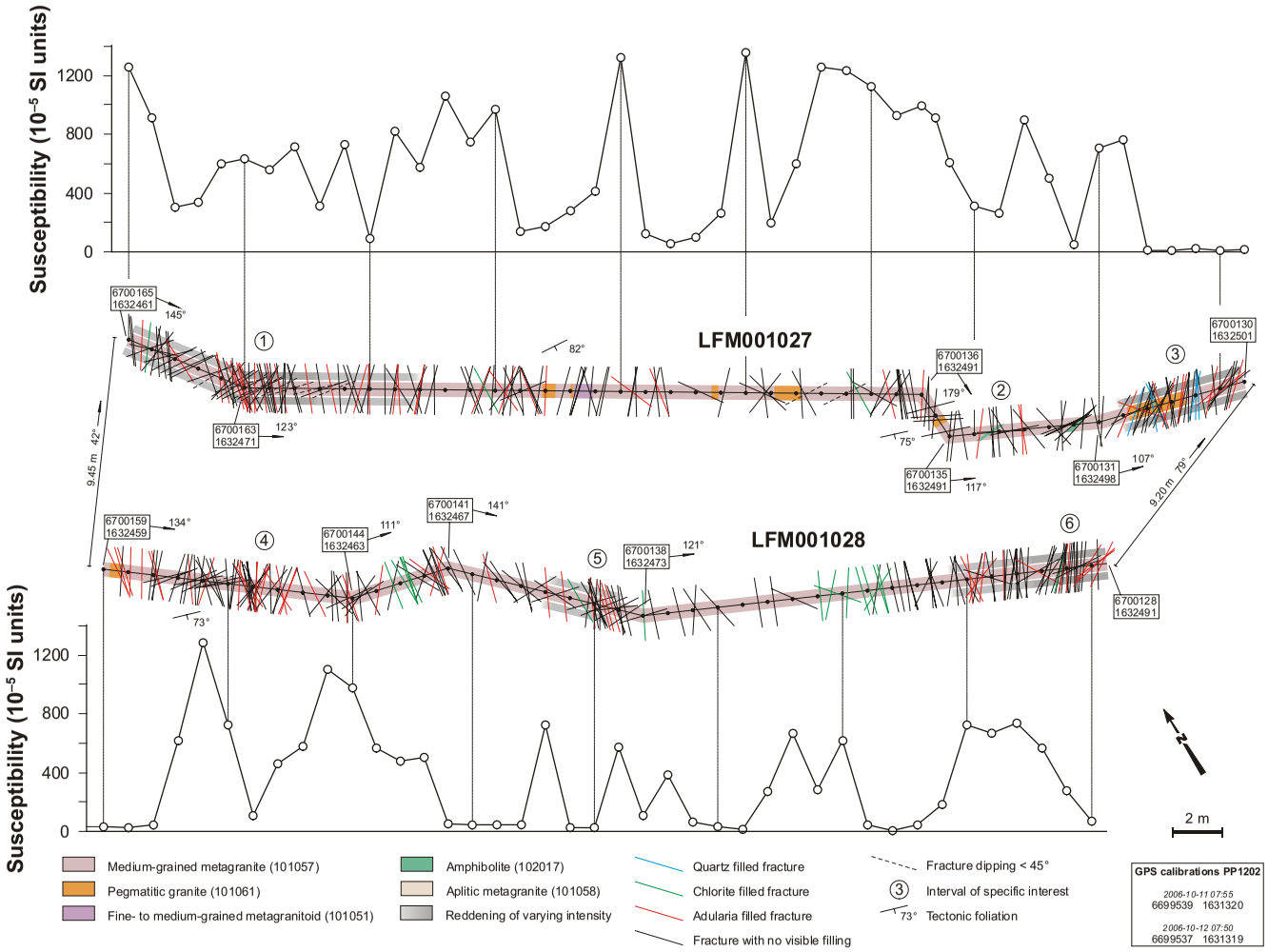

Figure 1-2. *Summary of the results from the scan line mapping along LFM001027 and LFM001028. Individual fractures are separated on the basis of their dip and predominant mineral filling. The length shown on the diagram is identical for all fractures regardless of their actual length. Reddening (oxidation) associated with intervals of increased fracture frequency is illustrated by a grey tone of varying intensity. Encircled numbers mark intervals referred to in the text. Exact locations of magnetic susceptibility measurement areas are indicated by black dots along the scan lines. The distance between individual dots is 1 m. GPS coordinates are given for the start and end points of the scan lines. The trend of individual scan line sections is indicated. Note that, for presentation purposes, the scan lines have been rotated 32° anticlockwise.*

2 Execution

Scan lines were marked by measuring-tapes, lined up along the centre of each traverse. Coordinates in RT90 for the start and end points of the scan lines were defined by GPS measurements. Fix point PP1202 was used for accuracy estimates. During the course of the work, the precision of the GPS measurements turned out to be inadequate. The GPS measurements were, therefore, complemented by compass orientations of individual scan line sections. The magnetic declination in the area is 4.4°.

All rock descriptions and identification of fracture minerals were based solely on ocular inspection. The orientation of ductile structures, rock contacts and fractures were measured by using a Silva compass with inclinometer. The scan line fracture mapping did not strictly follow the SKB method description for detailed fracture mapping (SKB MD 132.003, v. 1.0). The mapping involved documentation of orientation (i.e. strike and dip), width, aperture, mineralogy and possible movement indicators. Other fracture parameters given in the method description, such as terminations, lithological relations, waviness, etc, were not registered in the present study. The truncation level was set to 4 dm.

The instrument used to measure magnetic susceptibility was a SM-20 magnetic susceptibility meter (GF instruments, Czech Republic) with a sensitivity of 10^{-6} SI units (see *www.gfinstruments.cz* for more details). Measurements were registered at approximately 1 m intervals along both the scan lines. Each measurement represents the mean of eight instrument readings within an area with a radius less than about 0.5 m. Special care was taken to avoid composite measurements comprising readings from more than one rock type. Totally, scan lines LFM001027 and LFM001028 comprise 41 and 47 measurement areas, respectively. The storage capacity of the SM-20 magnetic susceptibility meter is 100 readings. The total number of readings along the profile is 704 (i.e. 8×88). Since no portable PC was available, all readings were written down manually, and later fed into Microsoft Excel. The digital data and the original protocol were checked twice for consistency, and after delivery exported to the SKB database Sicada. The data are also presented in Tables 2-1 and 2-2.

Table 2-1. Magnetic susceptibility measurements along LFM001027. The measurements start at the north-western end of the traverse and are given as 10^{-5} SI units.

Distance from NW	Readings 1	2	3	4	5	6	7	8	Mean
0	31.2	34.1	33.0	32.1	9.8	33.9	44.1	32.6	31.4
1	29.8	22.2	15.3	26.5	23.7	29.5	17.7	19.4	23.0
2	38.5	50.6	25.1	22.8	61.8	65.6	47.6	45.7	44.7
3	1,060	1,380	460	494	108	514	394	536	618
4	1,460	1,430	1,220	1,040	1,200	1,420	1,220	1,310	1,288
5	401	957	396	717	1,550	984	257	552	727
6	20.7	26.9	356	190	86.8	21.5	126	30.0	107
7	206	179	73.7	1,000	793	21.6	723	687	460
8	926	365	79.6	992	61.6	1,380	690	142	580
9	1,280	1,260	1,130	743	1,050	1,180	1,170	1,000	1,102
10	1,200	1,040	797	629	1,080	997	1,220	833	974
11	419	860	687	796	186	636	413	559	569
12	1,050	734	238	14.8	363	72.8	453	933	482
13	51.8	861	666	767	74.4	853	496	283	506
14	40.2	23.6	47.6	79.8	19.4	58.3	66.3	74.4	51.2
15	77.4	67.7	11.5	11.6	55.1	46.5	54.7	30.1	44.3
16	20.7	45.2	31.6	38.9	25.1	114	31.1	40.5	43

Distance from NW	Readings 1	2	3	4	5	6	7	8	Mean
17	16.7	31.9	40.6	81.8	67.0	63.0	20.0	39.9	45.1
18	1,020	569	447	754	842	701	788	665	723
19	35.8	16.6	20.2	54.9	37.6	9.3	7.0	9.2	23.8
20	55	27.7	7.0	18.9	6.5	87.3	10.8	8.8	27.8
21	619	1,210	368	511	371	41.6	921	537	572
22	780	19.2	5.0	17	15.3	4.0	26.9	7.4	109
23	805	10.6	58.1	404	736	554	159	357	386
24	70	14.6	5.6	6.7	124	155	25.5	109	64
25	17.4	12.6	179	10.9	30.1	8.0	6.6	8.0	34.1
26	11.6	9.8	8.7	6.4	7.6	12.5	10.9	10.2	9.7
27	267	208	194	281	269	410	276	285	274
28	311	540	739	847	579	830	870	629	668
29	25	5.2	219	835	617	274	24.6	279	285
30	367	461	348	843	661	695	789	801	621
31	11.3	223	9.0	8.4	13.4	49.4	9.6	14.4	42.3
32	8.7	12.9	11.7	7.3	9.1	8.5	6.8	9.1	9.3
33	13	8.4	22.4	5.2	169	102	6.7	29.7	45
34	195	357	560	62.4	21.1	161	85	33.1	184
35	197	481	828	831	751	879	1,010	813	724
36	138	839	254	905	1,070	589	593	962	669
37	434	737	908	442	1,070	1,090	756	449	736
38	802	226	854	314	551	1,000	175	625	568
39	224	284	344	408	193	418	220	134	278
40	25.5	65.6	113	48.7	73.1	6.0	140	105	72

Table 2-2. Magnetic susceptibility measurements along LFM001028. The measurements start at the north-western end of the traverse and are given as 10^{-5} SI units.

Distance from NW	Readings 1	2	3	4	5	6	7	8	Mean
0	1,210	1,400	1,280	1,470	1,170	1,270	1,040	1,180	1,252
1	387	1,550	787	1,180	816	780	1,070	649	902
2	43.0	30.0	823	564	20.7	36.5	834	51.0	300
3	207	418	177	149	161	729	132	736	339
4	778	514	609	380	510	961	572	429	594
5	1,020	367	793	840	168	775	426	617	626
6	913	787	47.8	138	99.2	793	783	897	557
7	838	757	649	712	808	436	692	818	714
8	183	173	376	501	71.1	210	832	158	313
9	879	160	921	1,260	883	25.3	850	806	723
10	29.5	34.8	26.6	154	210	91.6	60.5	110	90
11	1,160	51.6	677	874	674	1,040	1,240	816	817
12	1,070	923	471	538	465	120	407	560	569
13	1,110	1,320	466	517	1,210	1,250	1,280	1,250	1,050
14	8	314	17.4	1,040	1,280	1,010	1,260	1,030	745
15	1,000	890	70.2	1,310	1,110	1,030	1,370	907	961
16	831	37.5	20.7	17.9	9.8	23.6	71.8	74.5	136

Distance from NW	Readings 1	2	3	4	5	6	7	8	Mean
17	883	27.7	14.8	241	110	32.9	33.8	3.5	168
18	138	187	1,260	123	45.7	51.5	194	194	274
19	36.8	125	757	989	690	25.0	567	46.2	404
20	1,250	1,160	1,520	1,220	1,220	1,420	1,430	1,320	1,318
21	119	77.3	101	175	133	71.1	176	132	123
22	47.7	36.8	80.8	25.2	37.6	35.7	99.1	72.2	54.4
23	22.1	27.6	35.3	39.7	3.2	465	124	61.5	97
24	110	1,220	16.2	553	38.4	22.1	93.2	40.1	262
25	983	924	1,560	1,470	1,480	1,530	1,260	1,550	1,345
26	11.8	12.9	51.9	1,380	15.7	34.1	16.2	15.3	192
27	1,600	783	1,300	13.9	56	963	44.5	9.7	596
28	1,230	1,800	1,090	1,440	1,290	966	1,090	1,110	1,252
29	984	1,210	1,510	1,200	954	1,350	1,360	1,260	1,228
30	827	815	1,280	1,120	1,250	1,490	1,190	946	1,115
31	829	1,050	785	696	1,280	835	926	975	922
32	1,140	676	1,040	813	960	1,160	1,020	1,080	986
33	849	1,060	1,180	895	235	923	988	1,110	905
34	904	472	1,080	15.0	12.5	1,220	1,090	23.6	602
35	321	151	32.5	59.5	121	872	661	242	308
36	175	606	611	10	387	116	89.8	117	264
37	931	1,100	1,010	1,100	240	950	637	1,120	886
38	76.7	76.3	1,230	490	55.0	337	904	807	497
39	37.5	41.5	54.2	53	49.7	54.6	42.6	51.3	48.1
40	625	995	1,060	218	1,000	797	272	627	699
41	441	495	900	637	1,180	754	477	1,200	760
42	6.1	6.2	4.4	7.6	3.5	3.8	15.0	6.2	6.6
43	5.1	9.0	4.4	3.1	4.8	15.3	4.6	11.3	7.2
44	83.0	27.1	44.7	6.4	15.4	11.5	13.1	5.6	25.9
45	8.4	6.8	16.2	6.7	8.2	7.6	5.8	8.4	8.5
46	23.8	8.1	8.0	22.3	8.1	12.9	18.1	11.5	14.1

3 Rock type and ductile structures

More than 90% of the exposed bedrock along the two scan lines consists of a medium-grained metagranite (rock code 101057), which exhibits a weak to distinct tectonic foliation with a general orientation of 100–126°/73–82°. Other rock units include a few occurrences of pegmatitic granite (rock code 101061), two decimetre-wide dykes of amphibolite, an occurrence of fine- to finely medium-grained metagranitoid (rock code 101051) and two vein-like occurrences of aplitic metagranite (rock code 101058).

All rock trends and contacts are more or less parallel with the tectonic fabric. Individual occurrences are typically a few decimetres in scan line length. The most extensive occurrence of pegmatitic granite forms a continuous occurrence at 41.20–43.53 m length along LFM001027. In addition, there is a ca 1 m wide amphibolite dyke with mingling structures that is parallel to

the scan line and runs a few metres south-west of LFM001028. Two orientation measurements of the north-eastern dyke contact yielded 121°/75° and 126°/79° (right-hand-rule method). All rocks along the scan lines have experienced metamorphism under amphibolite-facies conditions.

4 Fractures

The total number of fractures registered along scan lines LFM001027 and LFM001028 is 208 and 229, respectively, i.e. approximately 5 fractures/metre. Confident fracture dips were only possible to measure for 270 of the fractures (i.e. 62%). The majority of fractures dip steeply, generally greater than 70°. However, there are 13 fractures with dips less than 40°. The strike of the fractures varies considerably along the scan lines. The most conspicuous fracture set, to which the majority of the fractures belong, strikes NE–SW. The gently dipping fractures strike WNW–ESE and mainly occur in the north-western ends of the two scan lines. Naturally, a certain bias can be expected due to the scan line orientations. However, the focus here is on the presentation of raw data without any line bias correction.

Fracture filling minerals are detectable in 122 of the fractures. In order of decreasing abundance, these minerals include adularia, chlorite and quartz. Individual fractures may contain more than one mineral. 153 fractures exhibit oxidized or reddened walls. Two thirds of these fractures occur along scan line LFM001028. More extensive reddening, which cannot be bound to individual fractures, occurs in some of the sections with increased fracture frequency.

There are five intervals of highly increased fracture frequency. Two intervals occur along scan line LFM001027 and three along scan line LFM001028 (Figure 1-2). The fracture frequency typically exceeds 10 fractures/metre in these intervals. The majority of the fractures within all five intervals belong to the steep NE–SW fracture set. Furthermore, the more gently dipping, WNW–ESE fractures are frequent in some of these intervals. Individual intervals of highly increased fracture frequency, as well as the fractures associated with two amphibolite dykes, are described briefly below. Each interval is given a number (1–6), which corresponds to the numbers in Figures 1-2, 4-1 and 4-2.

LFM001027

1. 3.93–7.01 m. Predominantly steeply dipping fractures with NNE-SSW strike (Figure 4-2). Subordinate, yet distinct, fractures with WNW-ESE strike, which typically dip gently (< 40°) towards NNE, are also present. Adularia is the only distinguishable fracture filling. Some fractures exhibit oxidized or reddened walls. Additionally, the entire interval has been affected by a weak oxidation (Figure 4-1).
2. Amphibolite dykes intersecting the scan line at 35.52–35.74 and 39.01–39.28 m. The dykes are about 1 dm in width and strike approximately 80–95°. Both dykes are intensely fractured along their southern contacts (Figure 4-1). However, this does not emerge in the scan line mapping, since virtually all the fractures are shorter than the truncation level.
3. 41.42–45.66 m. Predominantly steep, NE-SW fracture set (Figure 4-2). Fractures that belong to this set, but are shorter than the truncation level are frequent. The high fracture frequency appears to persist under the vegetation cover in the southeastward continuation of the scan line. Adularia and quartz, typically in close association, are the only distinguishable infilling minerals. Oxidation of the fracture wall rock occurs frequently. Some of the fractures exceed 1 mm in width. The entire interval has been affected by oxidation of weak to medium intensity (Figure 4-1).

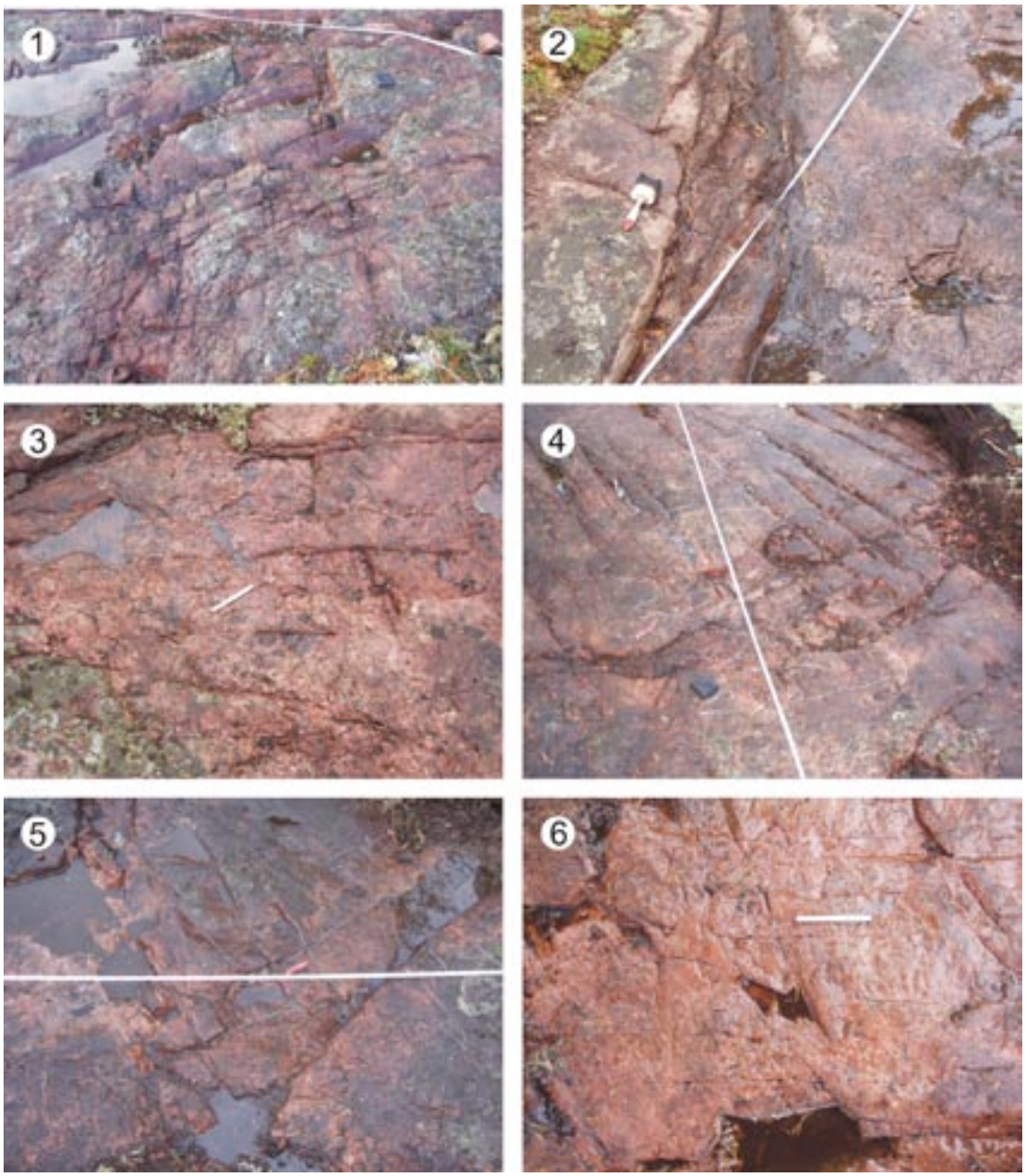

Figure 4-1. *Photographs that show intervals of highly increased fracture frequency and altered (oxidised) bedrock along LFM001027 and LFM001028. (1) A steep, NE-SW fracture set intersected by gently dipping fractures that strike WNW-ESE. View towards the south. (2) Decimetre-wide amphibolite dyke with intensely fractured southern contact. The general strike of the dyke is approximately 90°. View towards the west. (3) Steep, NE-SW fractures. The majority are shorter than the truncation level (i.e. 4 dm). View towards the east. (4) Steep, approximately NE–SW fractures intersected by a gently dipping, WNW-ESE fracture set. View towards the NE. (5) Steep, approximately NE-SW fractures intersected by a gently dipping, WNW-ESE fracture set. View towards the NE. (6) Steep, NE-SW fractures. The majority are shorter than the truncation level (i.e. 4 dm). View towards the east. Scales: compass 10×6.5 cm, pen length 14 cm, brush length 23 cm and length of pocket knife 9 cm.*

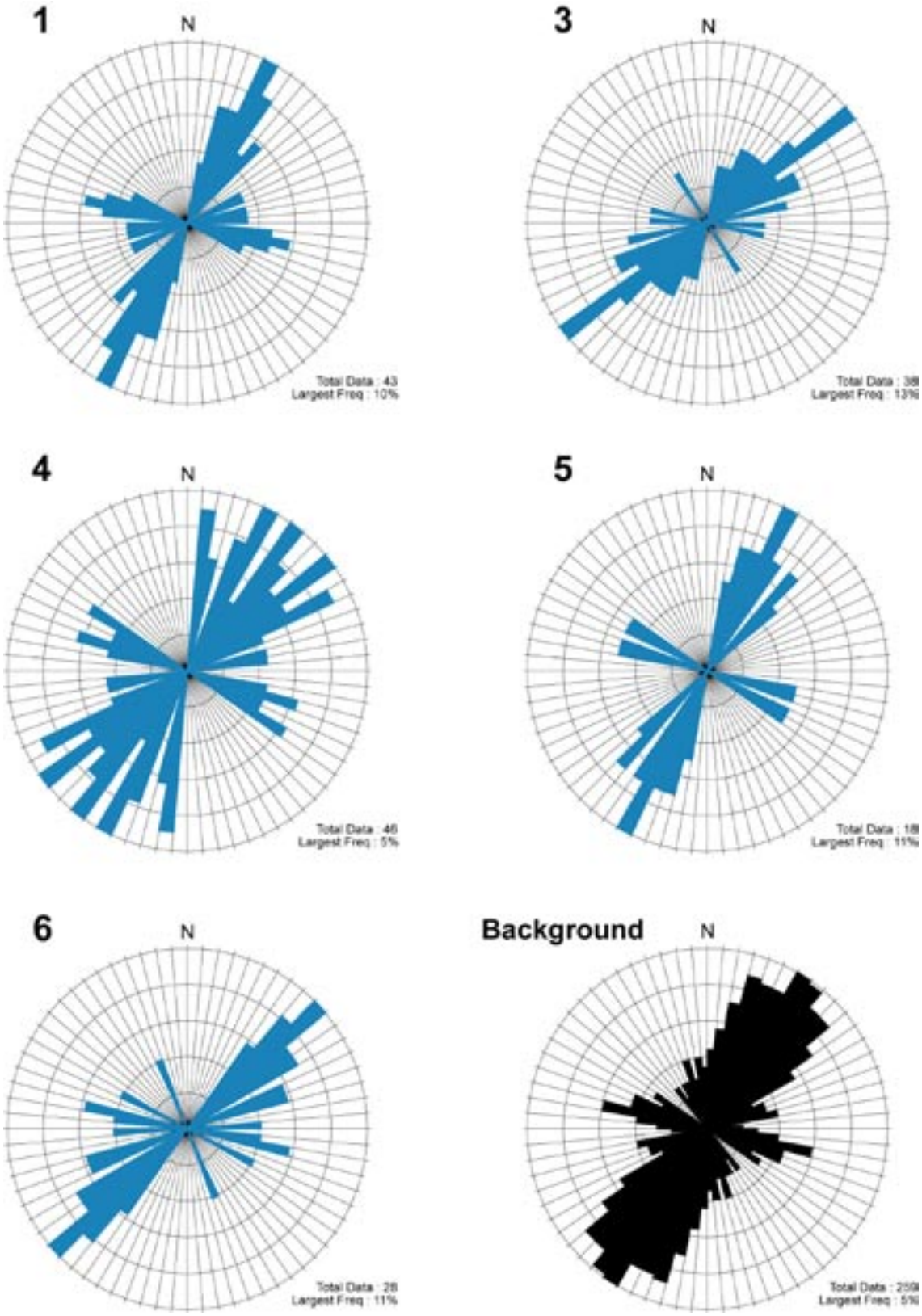

Figure 4-2. *Rose diagrams that show the strike of all fractures in the five intervals of highly increased fracture frequency along LFM001027 and LFM001028. All gently dipping fractures belong to the WNW set. The strikes of fractures outside these intervals are presented in a separate diagram for comparison (background). Note that the frequency contours vary between the diagrams.*

4. 2.84–7.43 m. Predominantly steeply dipping fractures that strike from NNE-SSW to NE-SW (Figures 4-1 and 4-2). Subordinate, yet distinct, fractures with WNW-ESE strike, which typically dip gently (< 40°) towards the NNE, are also present. Adularia is the only distinguishable fracture filling. A few fractures exhibit oxidized walls.
5. 19.74–21.08 m. Predominantly steep fractures with NNE-SSW strike, and subordinately, fractures with WNW-ESE strike (Figure 4-2). Adularia is the only distinguishable fracture filling. Some fractures exhibit oxidized walls. Most of the interval has been affected by faint oxidation (Figure 4-1).
6. 37.81–40.40 m. Predominantly steep NE-SW fracture set. Fractures that belong to this set, but are shorter than the truncation level are frequent. The high fracture frequency appears to persist under the vegetation cover in the southeastward continuation of the scan line. Except for one chlorite-bearing fracture, adularia is the only distinguishable fracture filling. The entire interval has been affected by oxidation of weak intensity (Figure 4-1).

5 Magnetic susceptibility

Magnetic susceptibility was primarily measured in the predominant medium-grained metagranite (101057), since most of the other rock units are too thin to yield reliable data. However, four of the 88 measurement areas were located in occurrences of pegmatitic granite (101061).

Typically, the metagranite exhibits a rather low magnetic susceptibility, averaging at c. $480 \cdot 10^{-5}$ SI units. However, the susceptibility does, even in decimetre scale, vary considerably and ranges from $3.2 \cdot 10^{-5}$ to $1{,}490 \cdot 10^{-5}$ SI. The average susceptibility of the pegmatitic granite is c. $190 \cdot 10^{-5}$, with a range from $3.5 \cdot 10^{-5}$ to $1{,}600 \cdot 10^{-5}$ SI. Generally, the susceptibility tends to decrease with an increasing intensity of oxidation (see Figure 1-2). However, the overall pattern is not always clear. The distinct susceptibility decrease at interval 3 may be related, in part, to the pegmatitic granite. Furthermore, it must be emphasized that the exposed surface of this highly fractured area largely corresponds to gently dipping fracture planes, which are variably affected by oxidation. For this reason, it is not clear to what extent the decrease in magnetic susceptibility is related to these gently dipping fracture planes.

6 Discussion and conclusions

The spatial relationship between the more intensely fractured intervals along the two scan lines is not obvious. However, the general characteristics of the intervals, such as predominant fracture orientations and infilling mineralogy, suggest that there is a correlation between the highly fractured intervals 1 and 4, and 3 and 6, and that each of these pairs belongs to the same fracture zone. However, a possible continuation of interval 5 in LFM001027 is more doubtful, suggesting that the extent of some fracture zones in the area is limited.

The principal purpose of the investigation concerned a possible relationship between the more intensely fractured and altered intervals in the bedrock and the two low magnetic lineaments with NNE and NE trend, revealed by the detailed ground magnetic survey. A direct correlation using the magnetic susceptibility values is obviously not possible because of the equivocal susceptibility pattern along the scan lines. The uncertainty in the position of the lineaments as well as in the GPS measurements in this field study also limits confidence in such correlation work. However, reduced magnetic susceptibility values are present in the vicinity of the highly

fractured intervals 1 and 4, and 3 and 6 (see also above). Furthermore, the highly fractured intervals also show rock alteration (oxidation). Thus, although there are some limitations, it is suggested that intervals 1 and 4 correspond to the westernmost lineament, i.e. MFM2273G, whereas intervals 3 and 6 correspond to lineament MFM2088G.

In conclusion, the scan line fracture mapping has revealed that at least two low magnetic lineaments with NNE and NE trend correspond to intervals of high fracture frequency and rock alteration (oxidation). The corollary follows that these lineaments represent minor fracture zones in the bedrock.

7 References

Isaksson I, Thunehed T, Pitkänen T, Keisu M, 2006. Forsmark site investigation. Detailed ground and marine magnetic survey and lineament interpretation in the Forsmark area – 2006. SKB P-06-261, Svensk Kärnbränslehantering AB.

Stephens M B, Bergman T, Andersson J, Hermansson T, Wahlgren C-H, Albrecht L, Mikko H, 2003. Forsmark. Bedrock mapping. Stage 1 (2002) – Outcrop data including fracture data. SKB P-03-09, Svensk Kärnbränslehantering AB.

Integrated interpretation of surface and borehole (VSP) seismic data along profiles 2 and 5, Forsmark, Sweden

Christopher Juhlin
Dept. of Earth Sciences, Uppsala University

Contents

Summary

Borehole KFM02A intersects several hydraulically conductive fracture zones, in particular a major zone at 415–520 m. This zone and two of the others can be correlated to reflections observed on the surface seismic data acquired during the Stage 1 surveys. However, the 3D geometry of the fracture zones and the fact that the borehole does not lie on the profiles makes a definite correlation uncertain. Moreover, the presence of higher density mafic rock in the borehole implies that the reflections could conceivably result from lithological contrasts rather than from the fracture zones. Therefore, surface seismic and vertical seismic profile (VSP) data have been quantitatively integrated and compared to geological and geophysical data from KFM02A.

The main result is that the F1 reflection, the strongest reflection on the surface seismic data near the borehole, can definitely be identified as intersecting the borehole at about 500 m. This is close to the base of the heavily fractured interval at 415–520 m and far from any high density mafic rocks, indicating that the F1 reflection is generated from the base of this fractured interval. The A2 reflection is not as clearly observed on the VSP data, but appears to intersect the borehole somewhat below 400 m, suggesting that it originates from the top of the fractured interval. The deeper B4 reflector was not covered by the VSP survey and its exact intersection depth with the borehole cannot be determined, but it probably intersects the borehole at around 920 m. A thick section of high density tonalitic rock at this depth with a 10 m thick fracture zone on top suggests that the nature of the B4 reflector differs from that of the A2 and F1 reflectors.

Surface seismic profiles 2 and 5 from the Stage 1 survey, acquired in 2002, cross one another near borehole KFM02A. Profile 2 was extended to the south-west in the Stage 2 survey in 2004 and a prominent south-west moderately dipping reflection, J1, was observed on this extension. It projects to the surface along the southernmost part of profile 2 from the Stage 1 survey, but was not observed on the profile. Therefore, profile 2 from Stage 1 and profile 2b from Stage 2 were merged and reprocessed in order to increase the potential of tracing J1 to the surface. In spite of detailed processing, it has not been possible to trace the reflector to shallower than 200 m from the surface. In the reprocessed section of profiles 2 and 2b, several reflections are clearer than on the original processing, due to using slightly different processing parameters. Thus, the central part of profile 5 was also reprocessed along a new CDP line with a more advantageous geometry for migrating profile 5 and correlating with the KFM02A borehole. Migration of the reprocessed section shows that the A2, A3 and F1 reflections contain small offsets that may be related to sub-vertical faulting.

Finally, the northern part of profile 5 was reprocessed to see if F1 could be further traced to the north. The reflection has been split into 3 sections with the northernmost section extending to about 6699400 N, where it is either cut by a sub-vertical fracture zone or by weaker south-east dipping reflectors. A new reflection was identified in the reprocessing, A8, that strikes WSW-ENE and dips about 35° to the SSE. Its orientation is somewhat uncertain since no crossing line data are available. However, it is observed on raw shot gathers and has an orientation similar to other reflections in the set A group.

1 Introduction

Reflection seismic data were acquired in the Forsmark area in north-eastern Uppland, Sweden in 2002 (Stage 1) and 2004 (Stage 2) by Uppsala University, under contract from SKB. Approximately 40 km of high-resolution (10 m shot and receiver spacing) reflection seismic data have been shot along 15 different profiles during the two campaigns (Figure 1-1). Results have been

reported in /Juhlin et al. 2002, Juhlin and Bergman 2004, Juhlin and Palm 2005/. Borehole seismic data (VSP) were acquired in 2004 by Vibrometric Oy and the results were reported in /Cosma et al. 2005/.

The purpose of the present study was two-fold. A clear south-west dipping reflection (J1) was observed in the stage 2 data on profile 2. The structure generating this reflection appears to cut across the Eckarfjärden deformation zone (ZFMNW0003) and extends onto profile 2 of the stage 1 data, but could not be traced to the surface. Profiles 2 of Stage 1 and Stage 2 were processed independently of one another even though they overlap (Figure 1-1). By reprocessing the two profiles together, it was hoped that an improved section of where the profiles overlap could be obtained and that it would easier to determine if the J1 reflection can or cannot be traced to the surface.

The second goal of this study was make an integrated interpretation of the surface seismic data from profiles 2 and 5 together with the borehole seismic data and geophysical logs from borehole KFM02A. The integrated interpretation focuses on studying the source of the reflectivity observed on the surface seismic sections in the vicinity of the borehole. Vertical seismic profile (VSP) data allows, in principle, the exact intersection points of reflectors with the borehole to be determined. If reflections in the VSP can be correlated to reflections in the surface seismics, then the source of the surface seismic reflections can be determined. In order to implement this exercise, part of profile 5 was also reprocessed to facilitate this integration and interpretation.

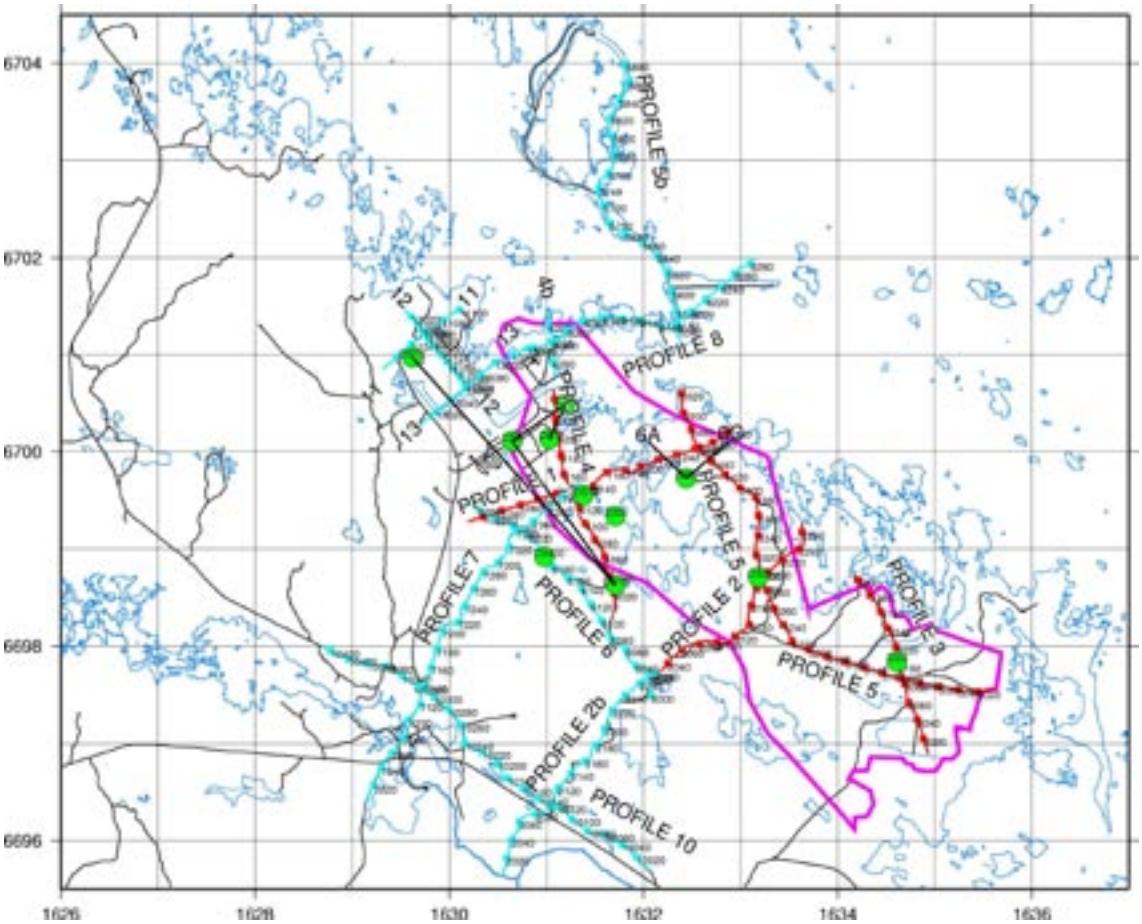

Figure 1-1. *Stage 2 profiles acquired in 2004 are shown as light blue lines. Station locations for profiles acquired in 2002 (Stage 1) are shown with red lines. Green circles are deep, cored boreholes available at model stage 2.2. Candidate area is marked by purple line.*

2 Reprocessing of profiles 2 and 2b, the central part of profile 5 and the northern part of profile 5

2.1 Profiles 2 and 2b

Data from profiles 2 and 2b were projected onto a single straight line (Figure 2-1) prior to stacking. Processing parameters from the Stage 2 data /Juhlin and Palm 2005/ were used for the entire merged profile. A large window (1001100 ms) was used for residual statics in order to omit any bias in the final image. The merged final stacked time section is shown in Figure 2-2. For comparison, the independently processed stacked sections from profile 2 (Stage 1) and 2b (Stage 2) are shown in Figure 2-3.

The sections differ primarily in the central portions where the merged processing appears to have performed better. In the upper 0.3 s north-east of the Eckarfjärden deformation zone (ZFMNW0003), a number of short south-west dipping reflections have appeared that were not observed earlier. Inspection of shot gathers indicates that these are not artifacts, but real.

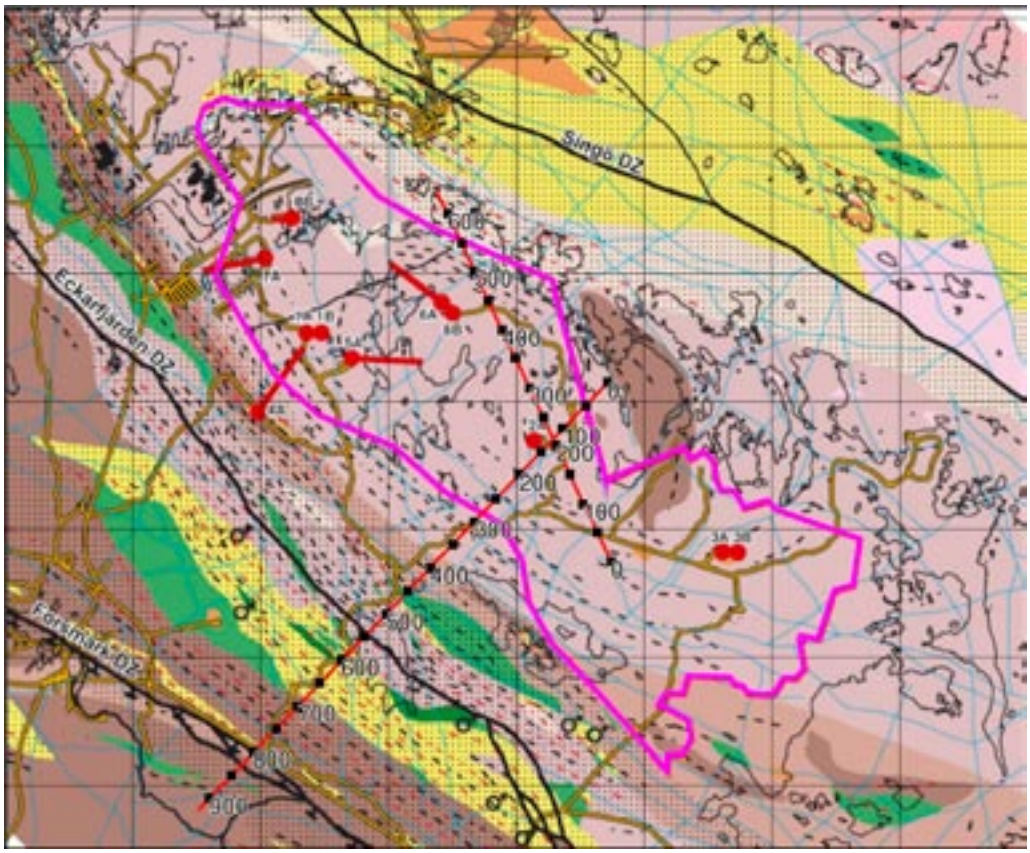

Figure 2-1. *CDP stacking lines (red) used for the reprocessing of profiles 2 and 2b and the central and northern parts of profile 5 in this report plotted on top of the geological map of the Forsmark area. Candidate area is marked by purple line. The longer NE-SW running line represents merged profiles 2 and 2b while the shorter NW-SE running line represents the reprocessed central and northern parts of profile 5.*

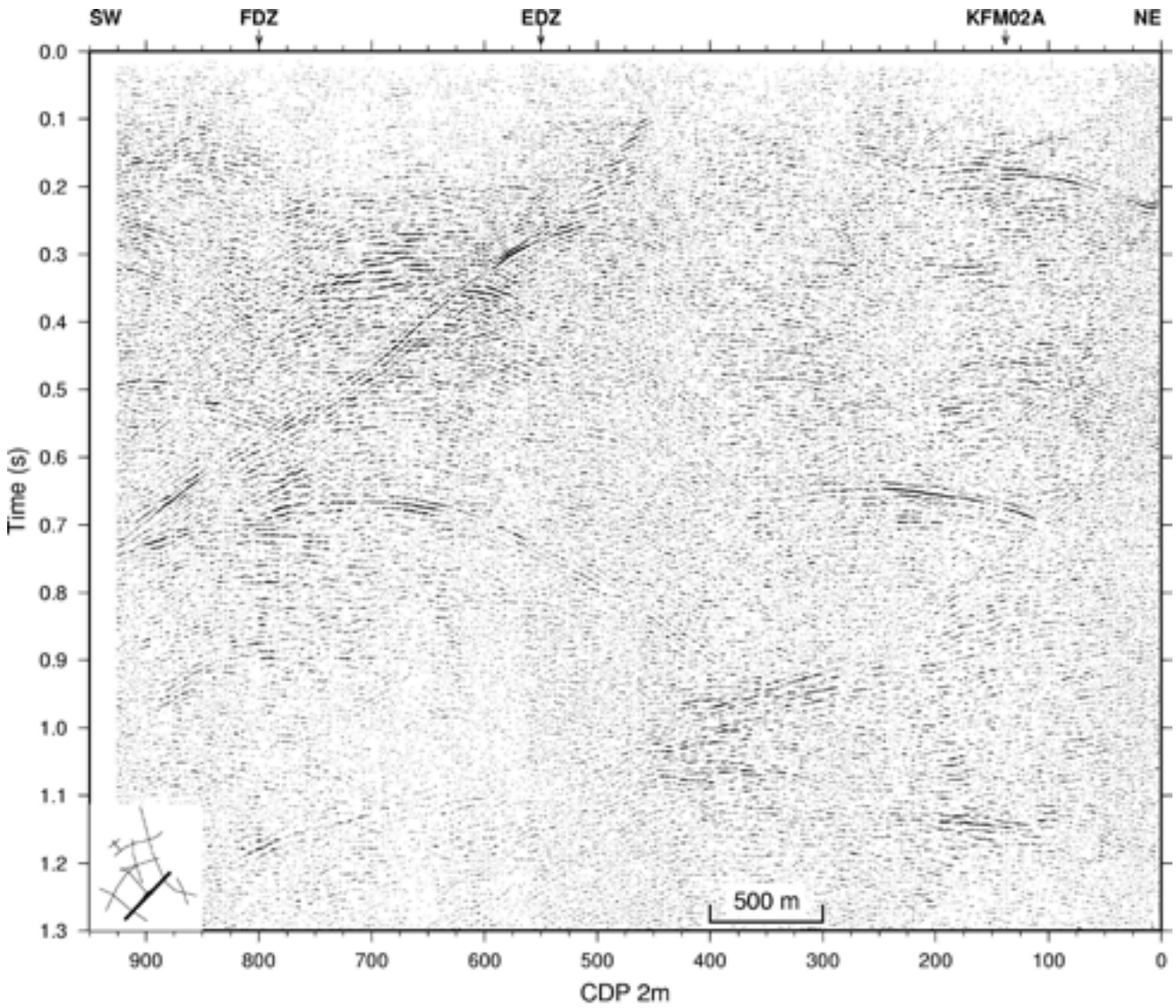

Figure 2-2. *Stacked section of merged profile 2 down to 1.3 seconds. Location of section indicated in lower left corner.*

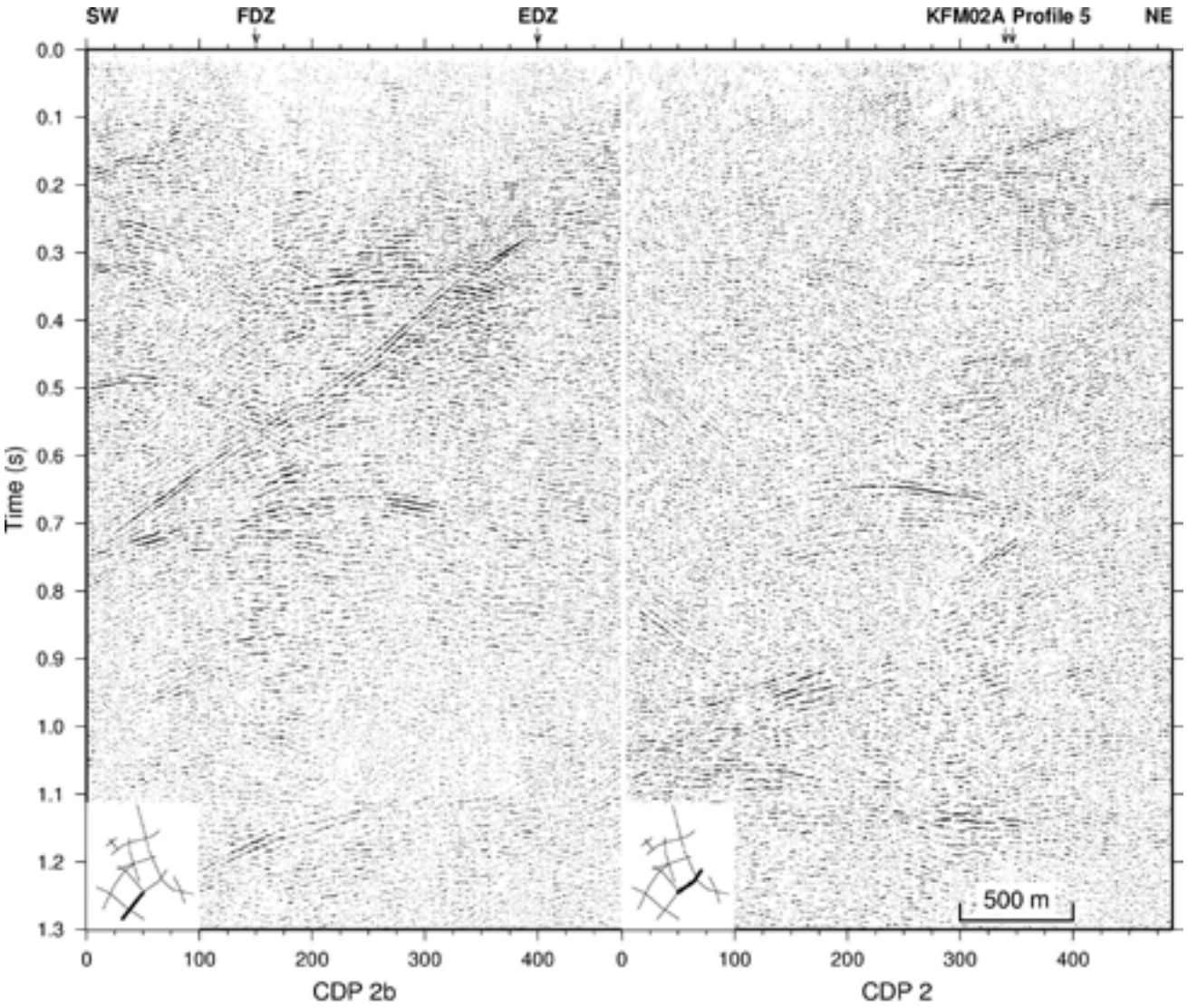

Figure 2-3. *Stacked sections of profiles 2 and 2b from /Juhlin and Palm 2005/ down to 1.3 seconds. Location of sections indicated in lower left corners.*

In addition to these reflections, the image along profile 2 (Stage 1) appears sharper than in the earlier processing. This may be due to that somewhat lower frequencies were used in the filtering and the longer residual statics window. Figures 2-4 and 2-5 show more detailed sections of the merged and previous processing, respectively, near the Eckarfjärden deformation zone. It should be noted that the apparent break in the prominent south-west dipping reflection directly below the Eckarfjärden deformation zone in Figure 2-4 moves to the north-east after migration (Figure 4-2) and is not a direct indication of the vertical orientation of the Eckarfjärden deformation zone. Figures 2-6 and 2-7 show more detailed sections of the merged and previous processing, respectively, near the KFM02A borehole.

2.2 Central part of profile 5 around KFM02A

In the original processing of profile 5 /Juhlin et al. 2002/, a CDP line was chosen that contains a bend south of the KFM02A borehole. The location of this bend was somewhat arbitrary, but was required to follow the general trend of the source-receiver midpoints. For migrating data along the central portion of profile 5, the selected location of this bend is not an optimum, since reflections have to "migrate around the bend". Therefore, the central part of profile 5 was reprocessed along a new CDP line that continues further to the south-east, allowing data from further south to be included in the migration. Processing parameters were chosen as in the reprocessing of profiles 2 and 2b. The somewhat lower frequencies used and the wider residual statics window also result in a section where the reflections are somewhat more distinct (Figure 2-8) compared to the earlier processing (Figure 2-9).

A migrated section of the reprocessed stack is shown in Figure 2-10. Note that the image is blurred and biased in the south-east, since the reflections dip in this direction. Aside from this geometrical effect, the image gives a good representation of the true subsurface geometry of the main reflectors along the CDP line. This is confirmed by the observation that the location of the main reflectors, as determined from the cross dip analysis of profiles 2 and 5 /Juhlin and Bergman 2004/, fall nearly on top of the main reflectors in the migrated image (Figure 2-11). Only B5 does not fall on top of its corresponding reflection in the migrated image. This is due to that the orientation of B5 was based on where profiles 3 and 5 cross, not where profiles 2 and 5 cross, and has, therefore, been projected a long distance. The true location of B5 corresponds closely to the strong reflection below B4 in the migrated image (Figure 2-11). Based on the migrated image, the main reflectors expected to be encountered in the KFM02A borehole are A3, A2, F1 and B4.

2.3 Northern part of profile 5

The CDP line chosen for reprocessing is shown in Figure 2-1. Note that the CDP numbering system is again different from that in the original processing and from the processing from the central part of profile 5 near KFM02A. The same processing parameters were used as for the central part of profile 5 and profiles 2 and 2b in this report. The reprocessed stacked section shows there is a group of set F reflections, consisting of 3 sections (Figure 2-12), F1, F2 and F3. A migrated version is shown in Figure 2-13. After reprocessing, a new reflection has been identified, A8 (Figures 2-12 and 2-13). Although not as clear as the other set A reflections, it is seen on shot gathers and can be traced nearly to the surface on these gathers.

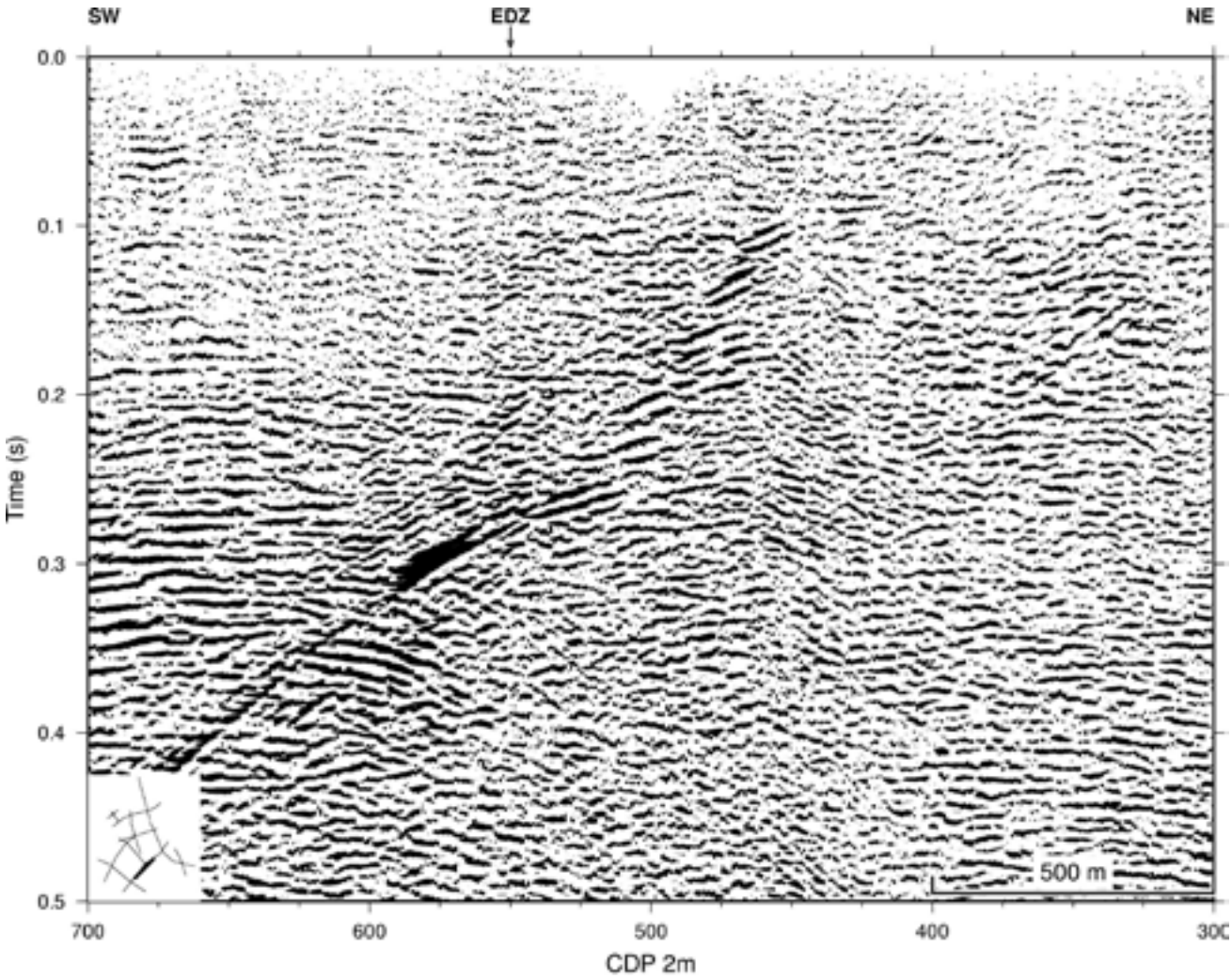

Figure 2-4. *Stacked section of merged profile 2 near the Eckarfjärden deformation zone and down to 0.5 seconds. Location of section indicated in lower left corner.*

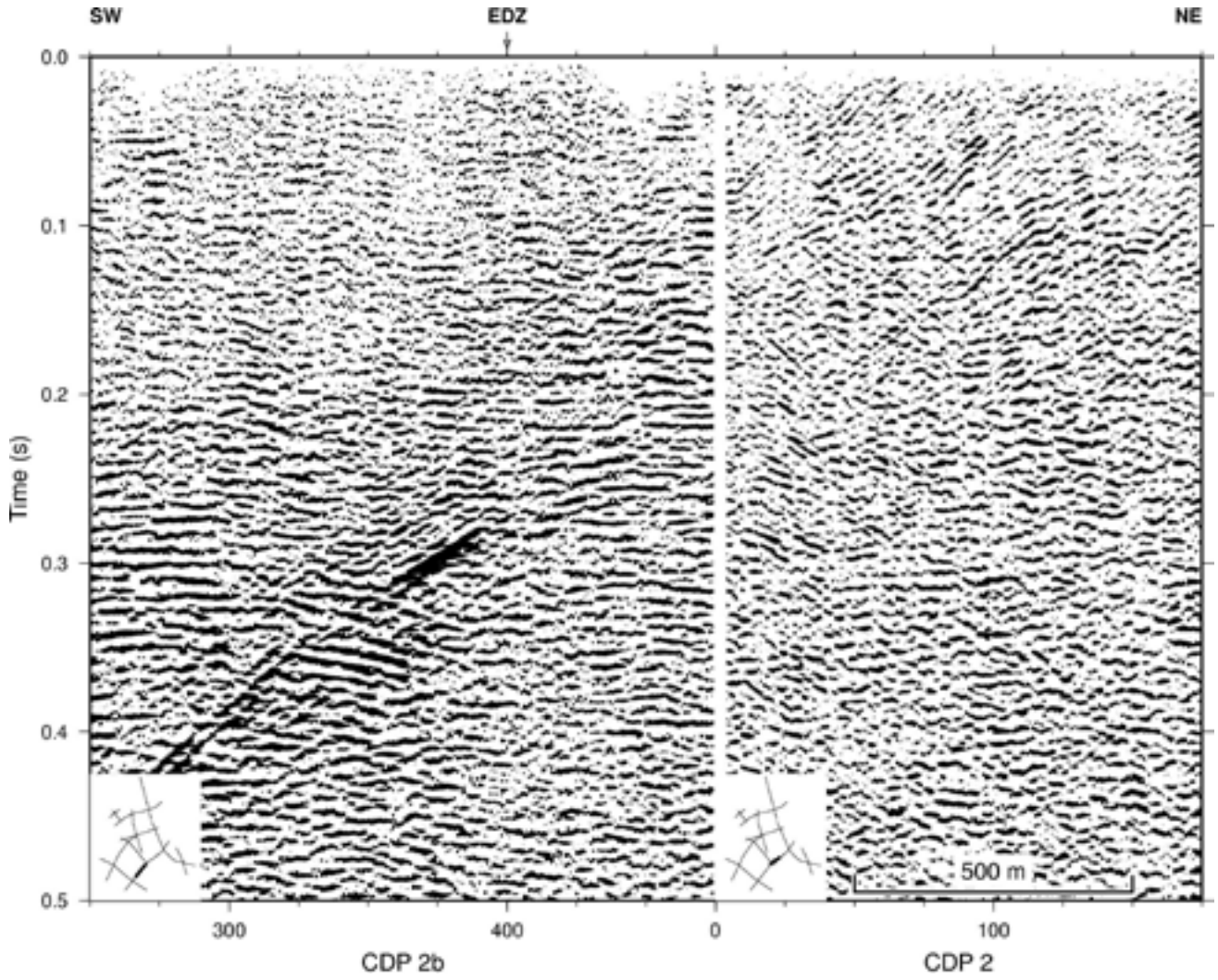

Figure 2-5. *Stacked sections of profiles 2 and 2b from /Juhlin and Palm 2005/ near the Eckarfjärden deformation zone and down to 0.5 seconds. Location of sections indicated in lower left corners.*

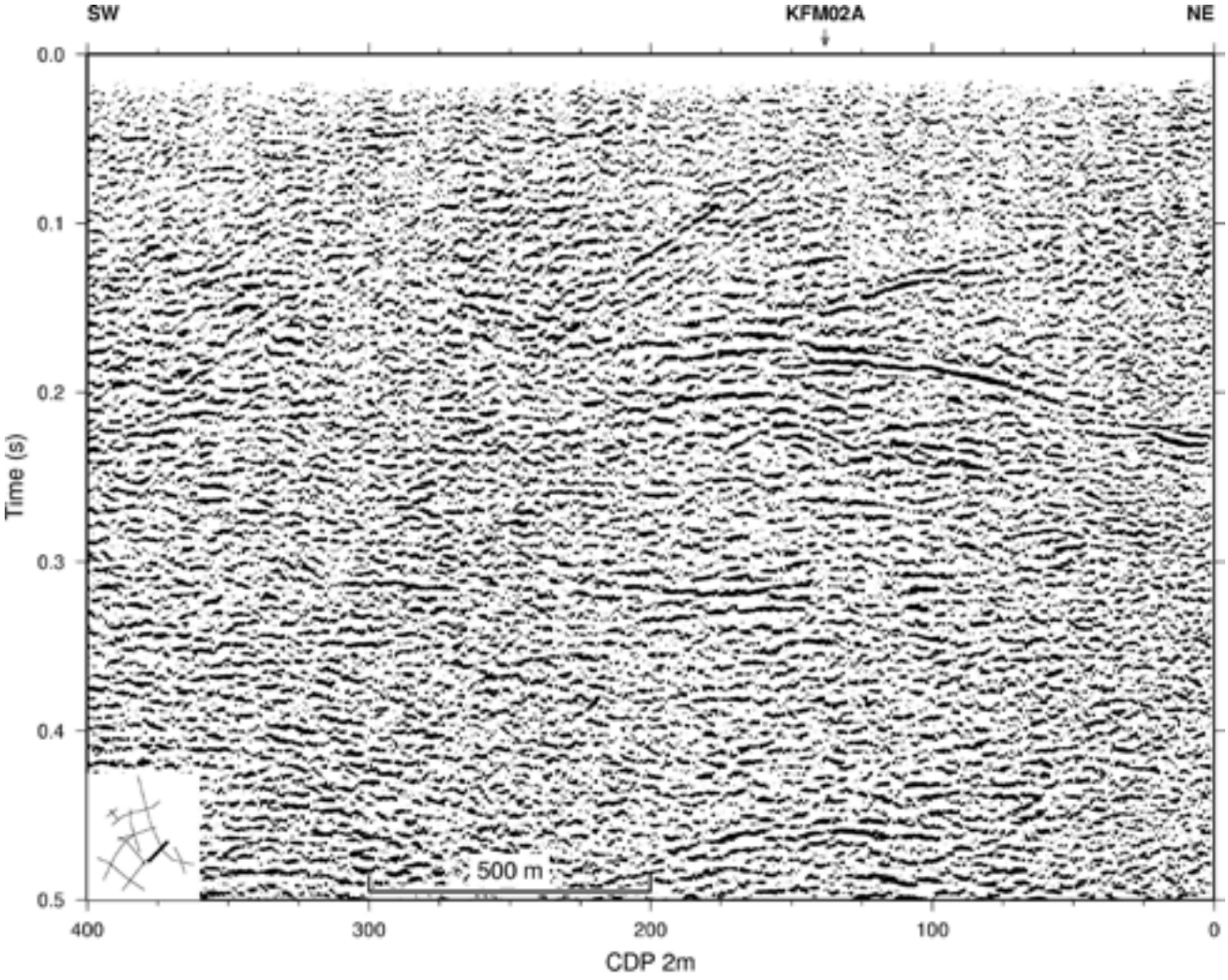

Figure 2-6. *Stacked section of merged profile 2 near to borehole KFM02A and down to 0.5 seconds. Location of section indicated in lower left corner.*

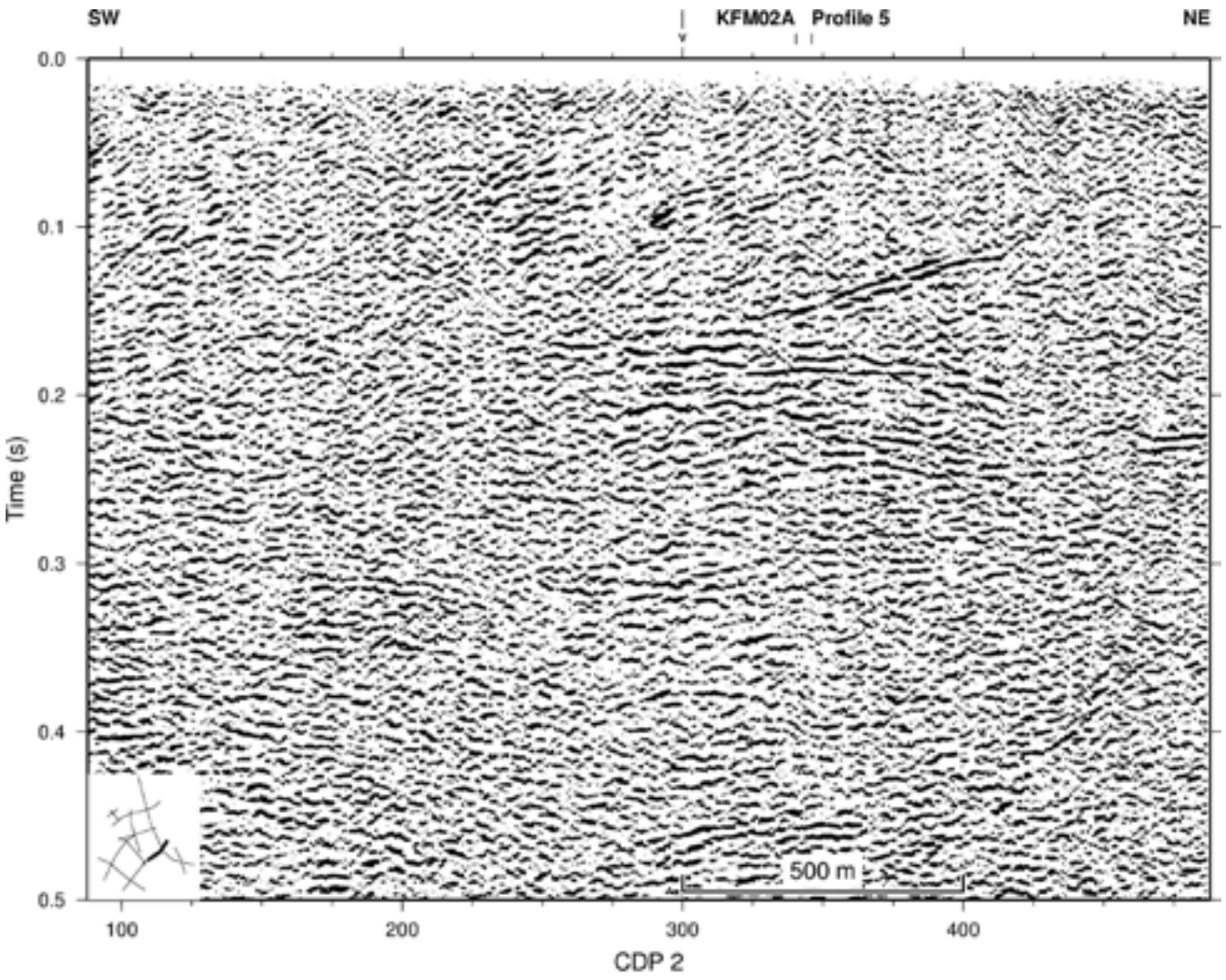

Figure 2-7. *Stacked section of profile 2 as presented in Stage 1 /Juhlin et al. 2002/ near to borehole KFM02A and down to 0.5 seconds. Location of section indicated in lower left corner.*

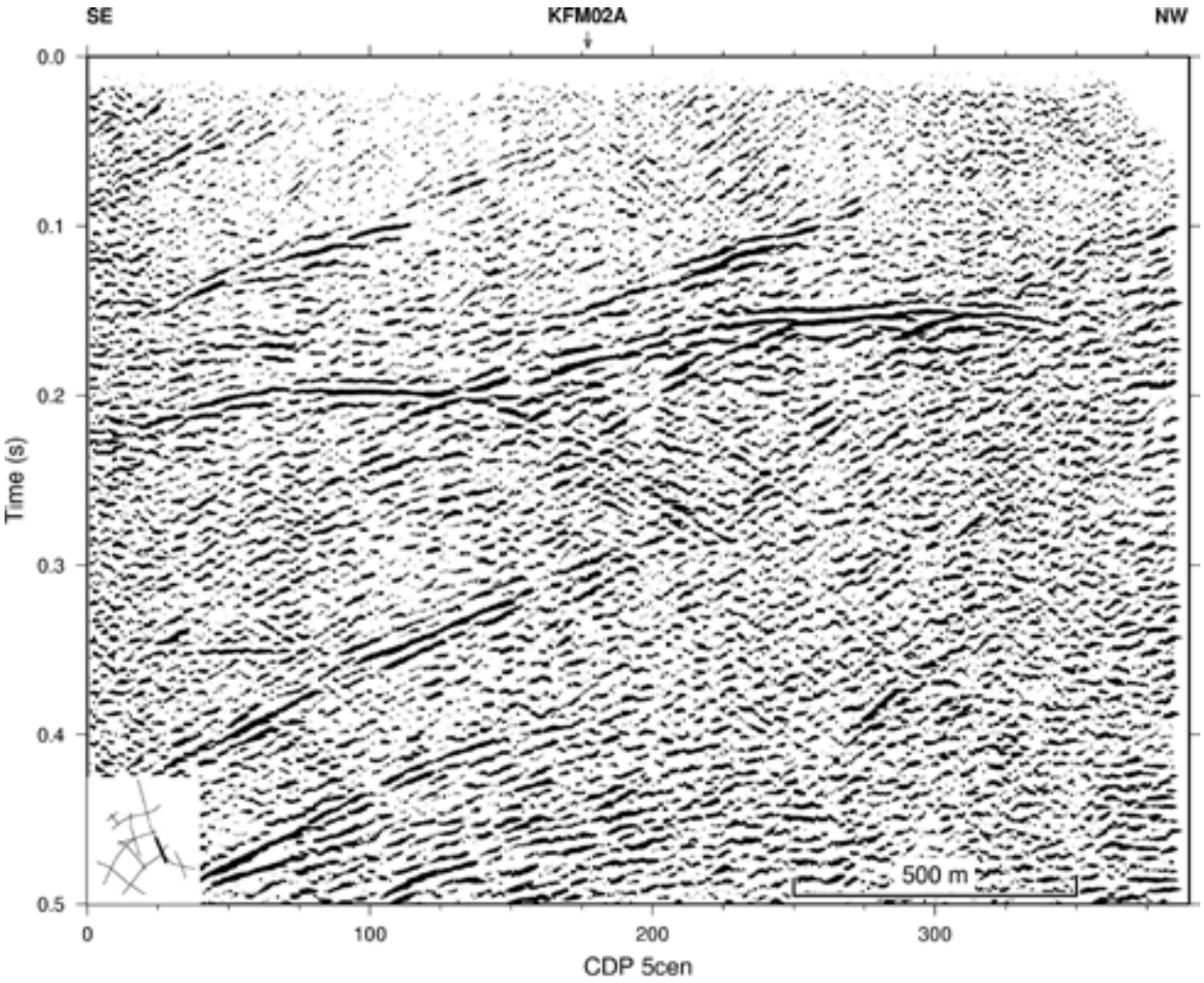

Figure 2-8. *Reprocessed stacked section of profile 5 near to borehole KFM02A and down to 0.5 seconds. Location of section indicated in lower left corner.*

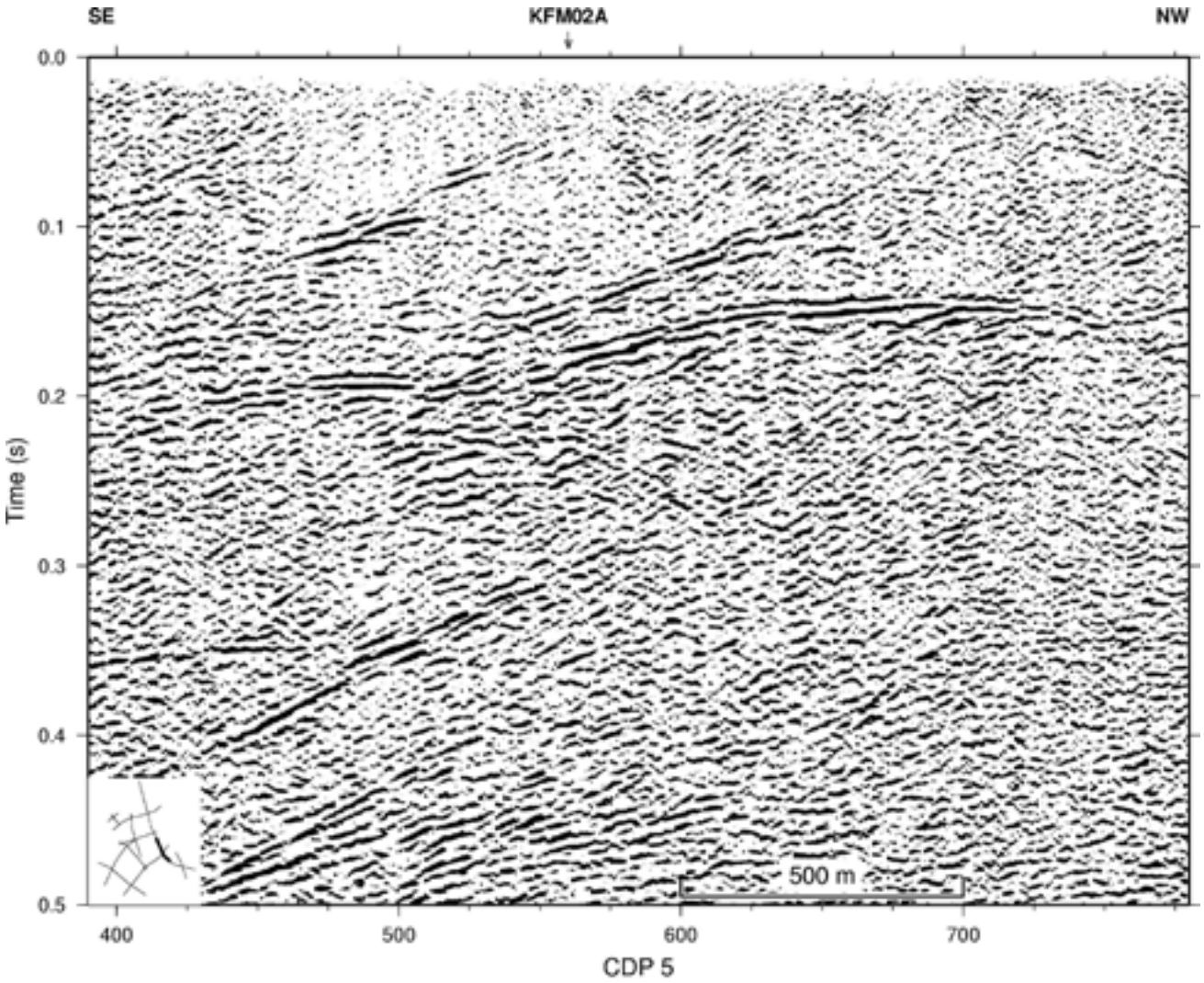

Figure 2-9. *Stacked section of the central part of profile 5 as presented in Stage 1 /Juhlin et al. 2002/ near to borehole KFM02A and down to 0.5 seconds. Location of section indicated in lower left corner.*

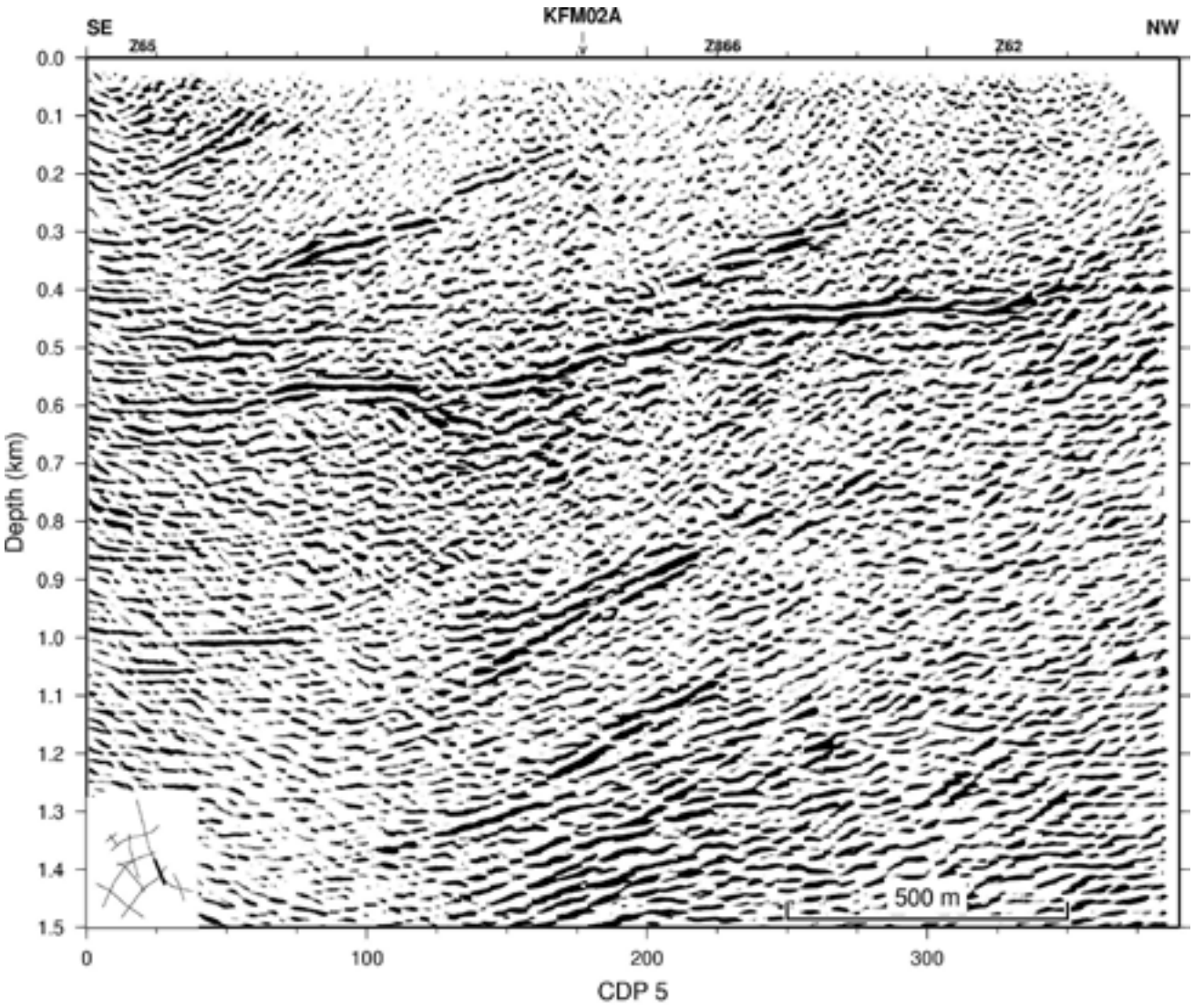

Figure 2-10. *Migrated section of reprocessed profile 5 near to borehole KFM02A and down to 0.5 seconds. Location of section indicated in lower left corner.*

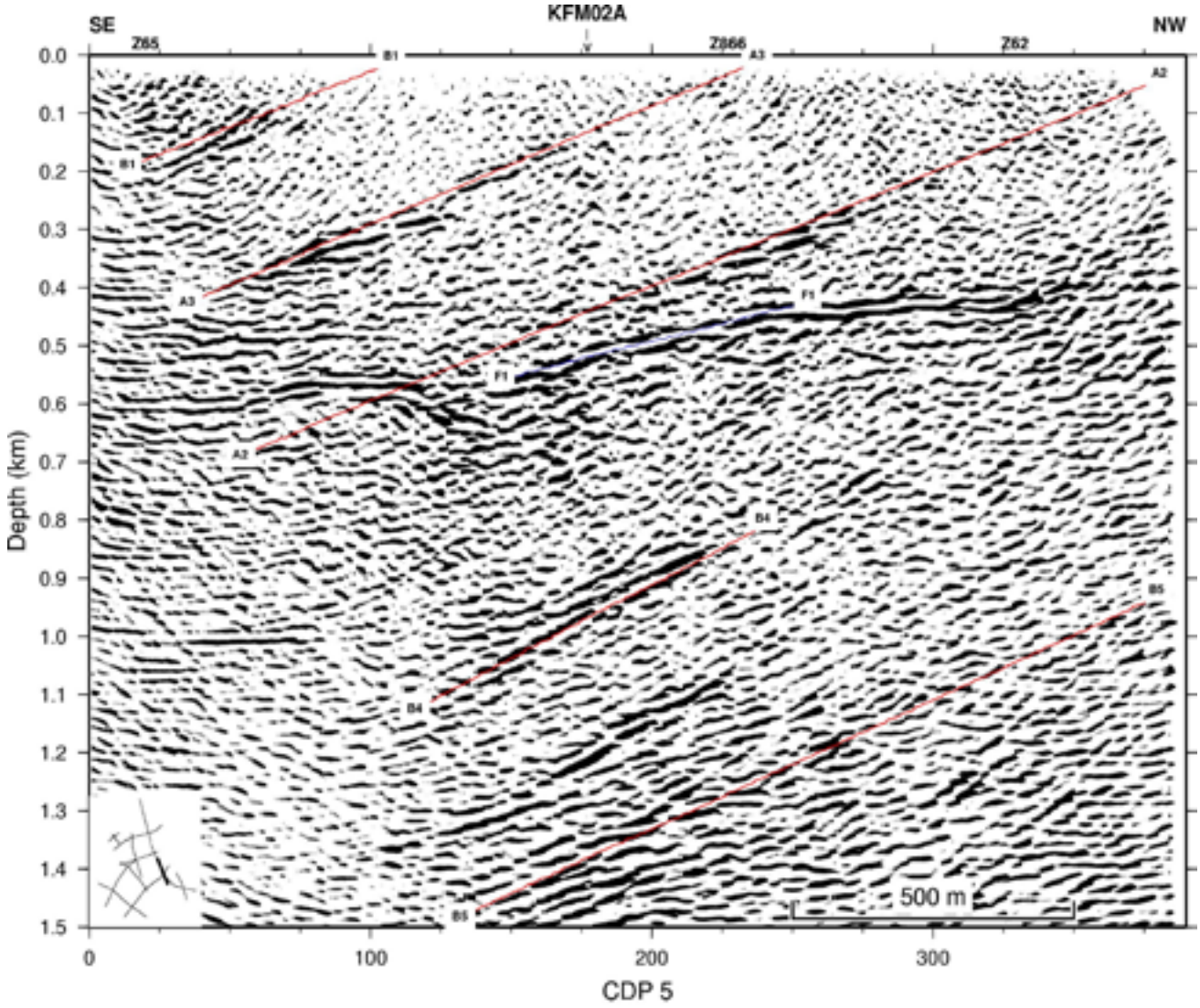

Figure 2-11. *Migrated section of reprocessed profile 5 near to borehole KFM02A and down to 0.5 seconds. Location of section indicated in lower left corner. Depths of the selected reflectors have been projected onto the section. The depths of these reflectors correspond to the depths where the reflectors would be intersected if a borehole were to be drilled along the profile. They should be viewed as nearly true depths.*

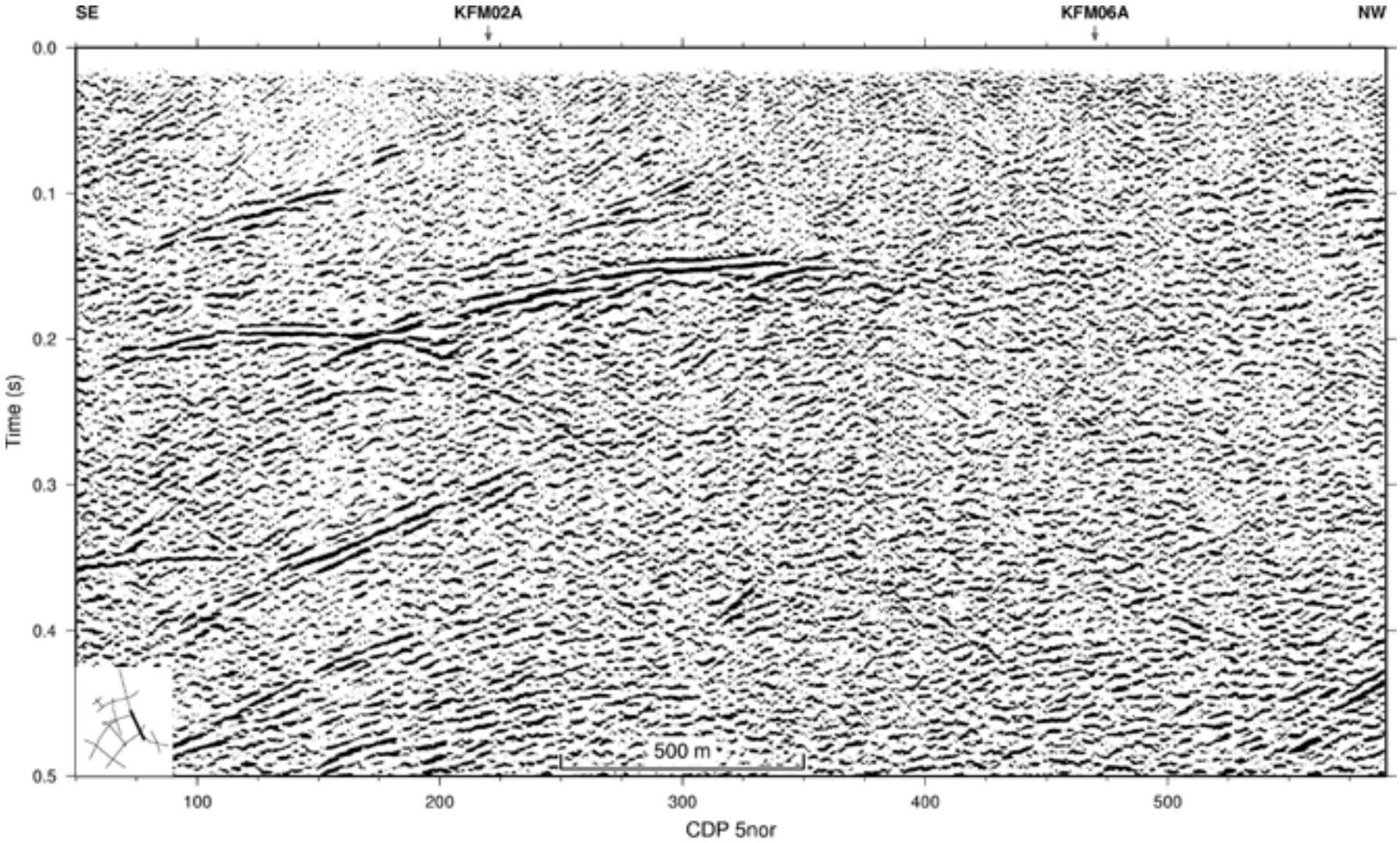

Figure 2-12. *Reprocessed stacked section of the northern part of profile 5 down to 0.5 seconds. Location of section indicated in lower left corner.*

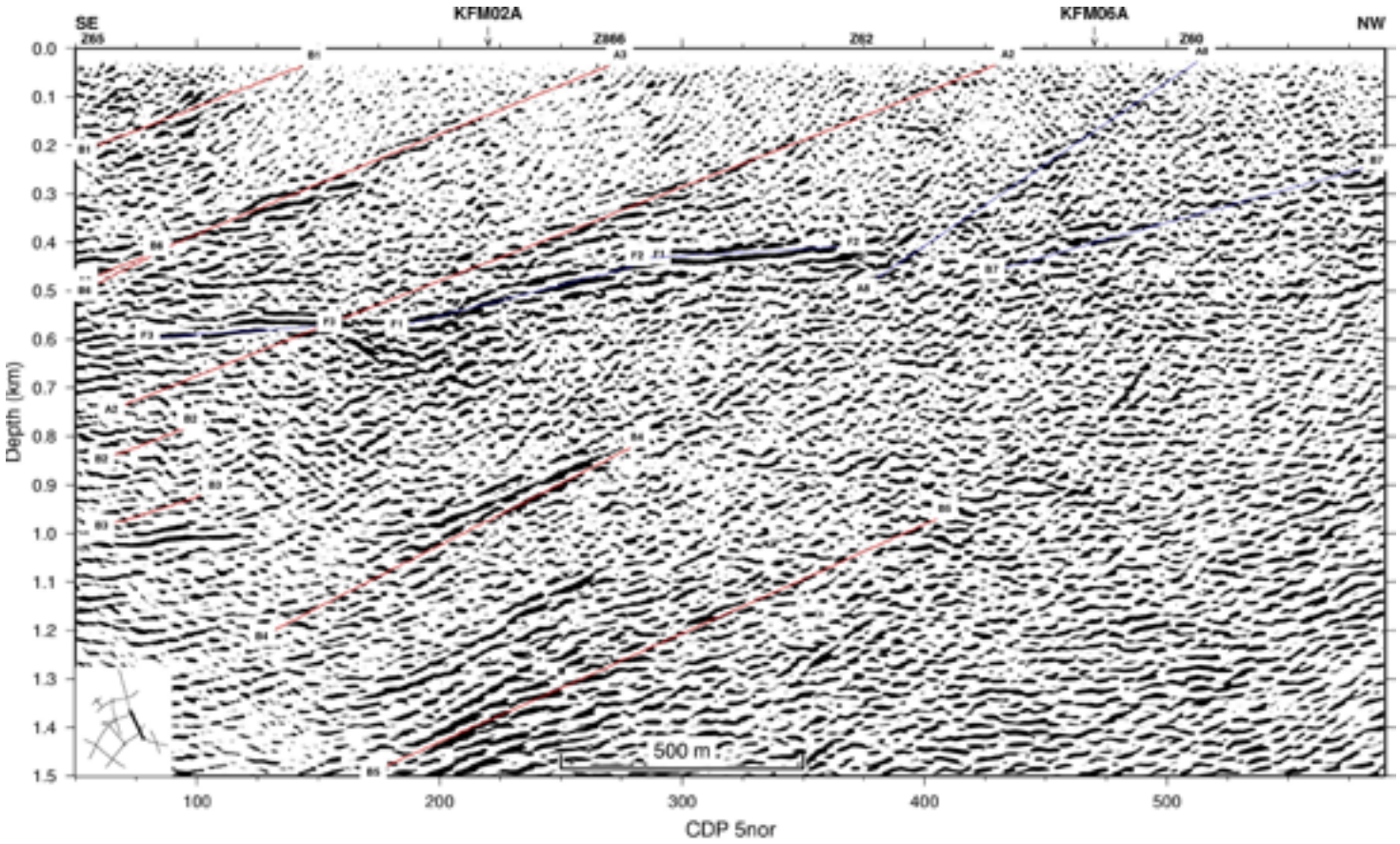

Figure 2-13. *Migrated section of reprocessed northern part of profile 5 down to 0.5 seconds. Location of section indicated in lower left corner. Depths of the selected reflectors have been projected onto the section. The depths of these reflectors correspond to the depths where the reflectors would be intersected if a borehole were to be drilled along the profile. They should be viewed as nearly true depths.*

3 VSP data from KFM02A

3.1 Background

Vertical seismic profile (VSP) data were acquired in the KFM02A borehole in 2004 using 10 different source points (Figure 3-1). The depth interval of the survey was 100 m to 775 m with a receiver interval spacing of 5 m. These VSP data were processed and interpreted by /Cosma et al. 2005/ using methods developed specifically for multi-source VSP surveys. The orientation of both gently and steeply dipping reflectors was obtained.

The main aim of the present study is to investigate the origin of the gently dipping reflections observed on the surface seismic profiles near the KFM02A borehole, in particular reflectors A2, F1 and B4. Reflections from these zones should also be present in the VSP data. By tracing these reflections to where they intersect the borehole, it should be possible to determine the exact depth the reflector is penetrated by the borehole. Changes in rock properties in the borehole at this depth provide clues to the source of the reflection. This procedure is, in principle, straightforward. However, complicating factors generally arise in a crystalline rock environment. These include:

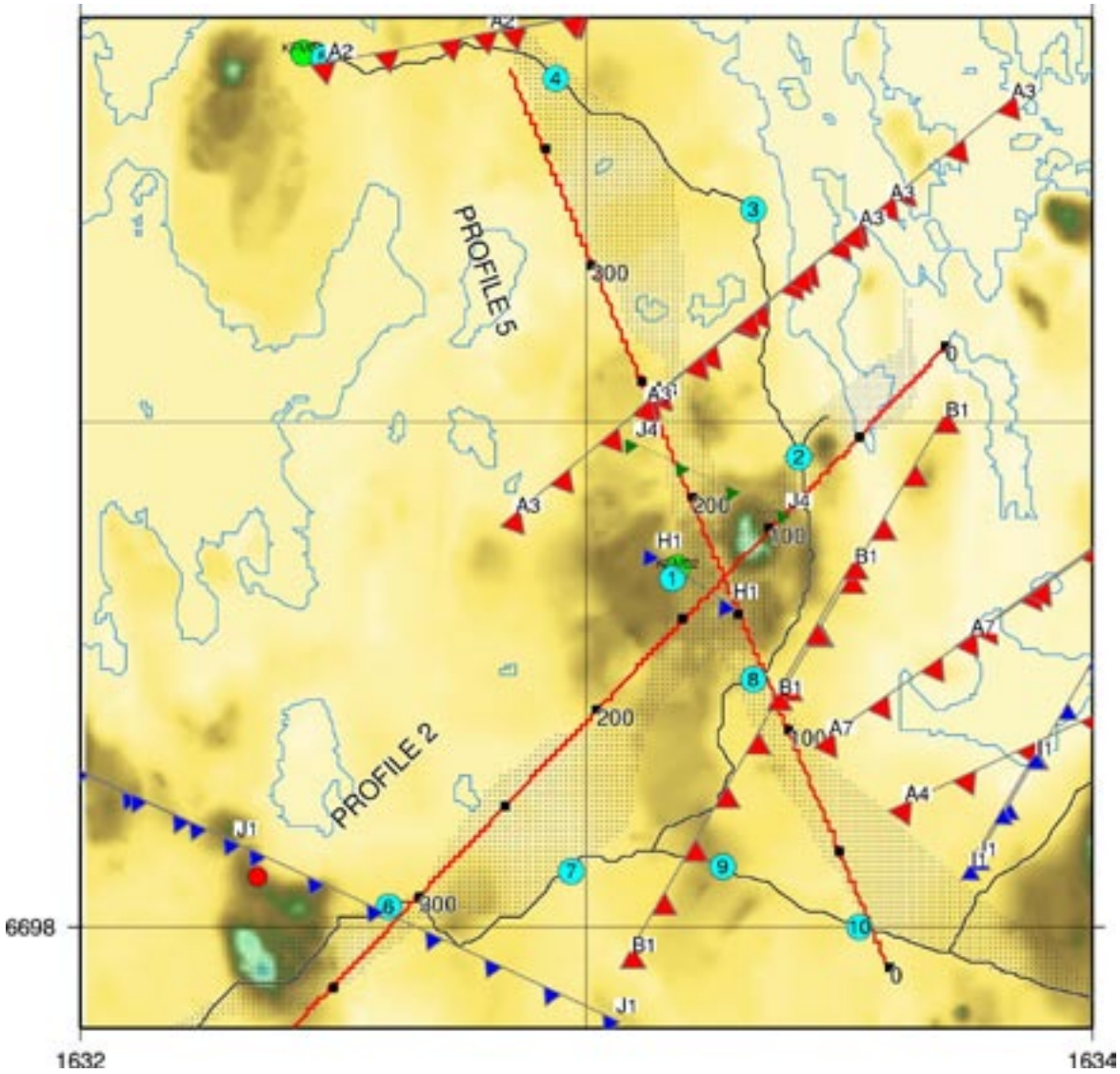

Figure 3-1. *Location of KFM02A VSP source points (cyan circles) and reprocessed profiles 2 and 5 (red lines) in relation to the KFM02A borehole (DS2 green circle). Black dots show midpoint spread along the seismic profiles.*

1. The surface seismic profile does not cross exactly over the borehole, implying that the reflections observed are not generated where the reflector intersects the borehole.
2. Even if the profile crosses exactly over the borehole, the reflections may come from out-of-the-plane of the profile, implying again that the borehole does not intersect the reflector where the reflections are generated.
3. VSP data are single fold whereas surface seismic profiles are multi-fold, resulting in that reflections will be significantly weaker in the VSP data. This may make it difficult to correlate reflections on the surface seismics with reflections on the VSP.
4. Angles of incidence are generally higher in VSP data, resulting in that P-waves that have been converted to S-waves, both transmitted and reflected, are more often present in the data. These converted waves may mask P-wave reflections, or be mistaken for P-wave reflections.

3.2 VSP Processing

VSP processing in this study followed standard methods developed for imaging gently dipping reflectors (Table 3-1). Figure 3-2 shows essentially the raw data after some preliminary processing. The wave-field is dominated by downgoing P- and S-waves, the arrival time of which increases with increasing depth. Reflections from sub-horizontal zones, which will generally have arrival times that decrease with increasing depth, are difficult to identify (Figure 3-3). After spectral whitening and filtering (Figure 3-4), there are more indications of reflections from sub-horizontal zones in the VSP data (Figure 3-5). After removal of down-going P- and S-waves, reflected waves dominate the wave-field (Figures 3-6 to 3-9). However, it is still difficult to pick out distinct reflections as is possible on the surface seismic data. Reflections from more steeply dipping zones, and even interference between reflections from sub-horizontal zones, mask the potentially distinct reflections. The clearest reflection observed in the VSP data is found on SP 2 and intersects the borehole at about 500 m (Figure 3-8). Its travel-time corresponds closely to that expected of a reflection from the F1 zone (Figure 3-9). Reflections with travel-times corresponding to the F1 zone are also relatively clearly seen on SP 1 and SP 8 (Figure 3-9), also there intersecting the borehole at about 500 m.

Table 3-1. Processing parameters applied to VSP data from KFM02A.

Step	Process
1	Read decoded vertical component SEGY data
2	Apply –50 ms shift to zero time
3	Gain by $t^{0.5}$
4	Bandpass filter: 40-60-300-450 Hz
5	Kill noisy traces
6	Infill killed traces: aperture size 7
7	Spectral whitening: 40-60-200-250 Hz
8	Bandpass filter: 60-90-240-360 Hz
9	Align first breaks at 5,750 m/s
10	Mute at first break
11	Remove downgoing Pwaves: 15/1/5,750 (traces/samples/velocity)
12	Bandpass filter: 40-60-300-450 Hz
13	Remove downgoing Swaves: 15/1/3,300 (traces/samples/velocity)
14	Bandpass filter: 40-60-300-450 Hz
15	Trace equalization: 0–500 ms
16	Convert to two-way travel-time: velocity 5,750 m/s
17	2D median filter: enhance sub-horizontal events

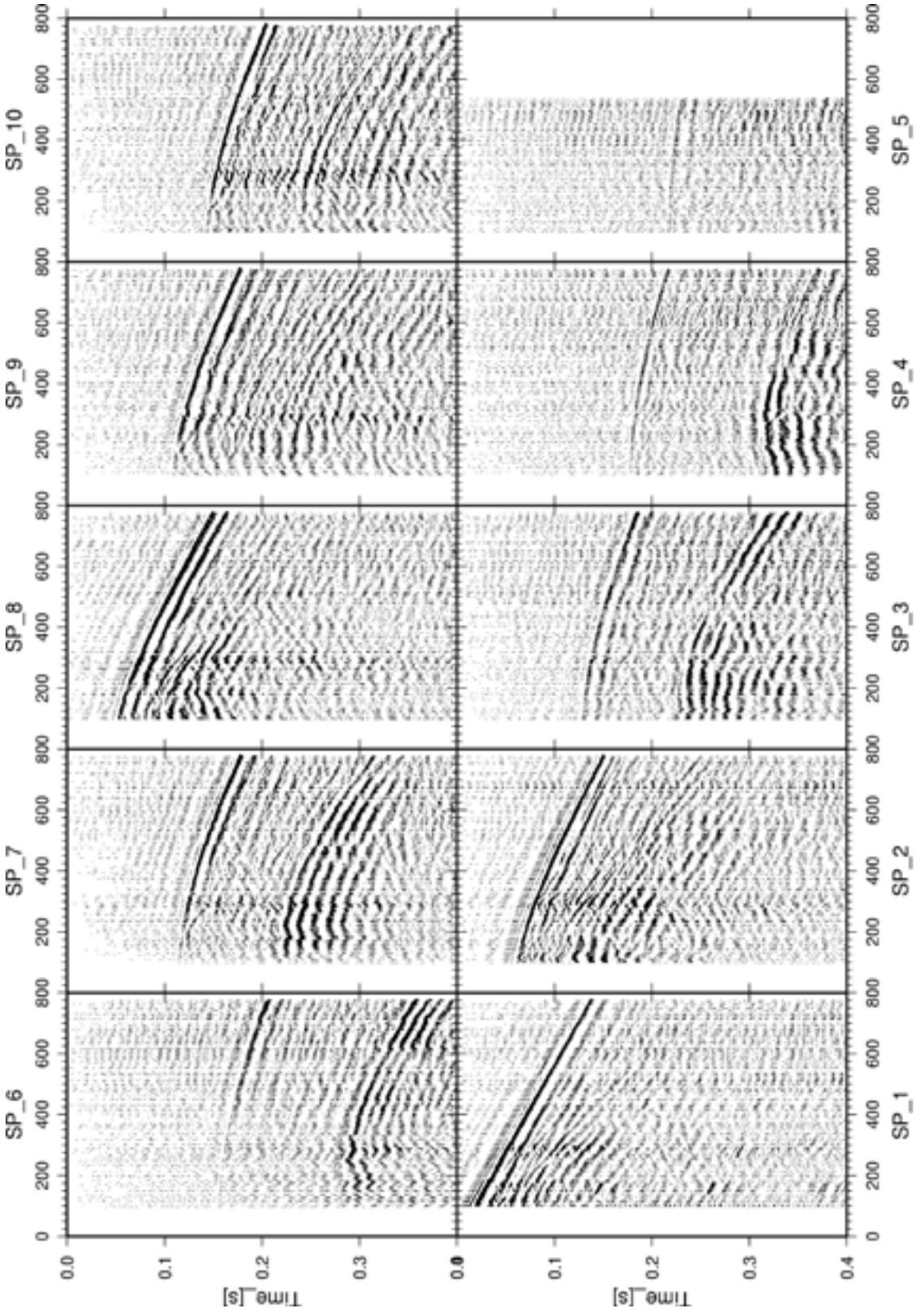

Figure 3-2. *VSP data from all 10 source points processed up to step 6 in Table 3-1. Horizontal axis is depth in metres in borehole.*

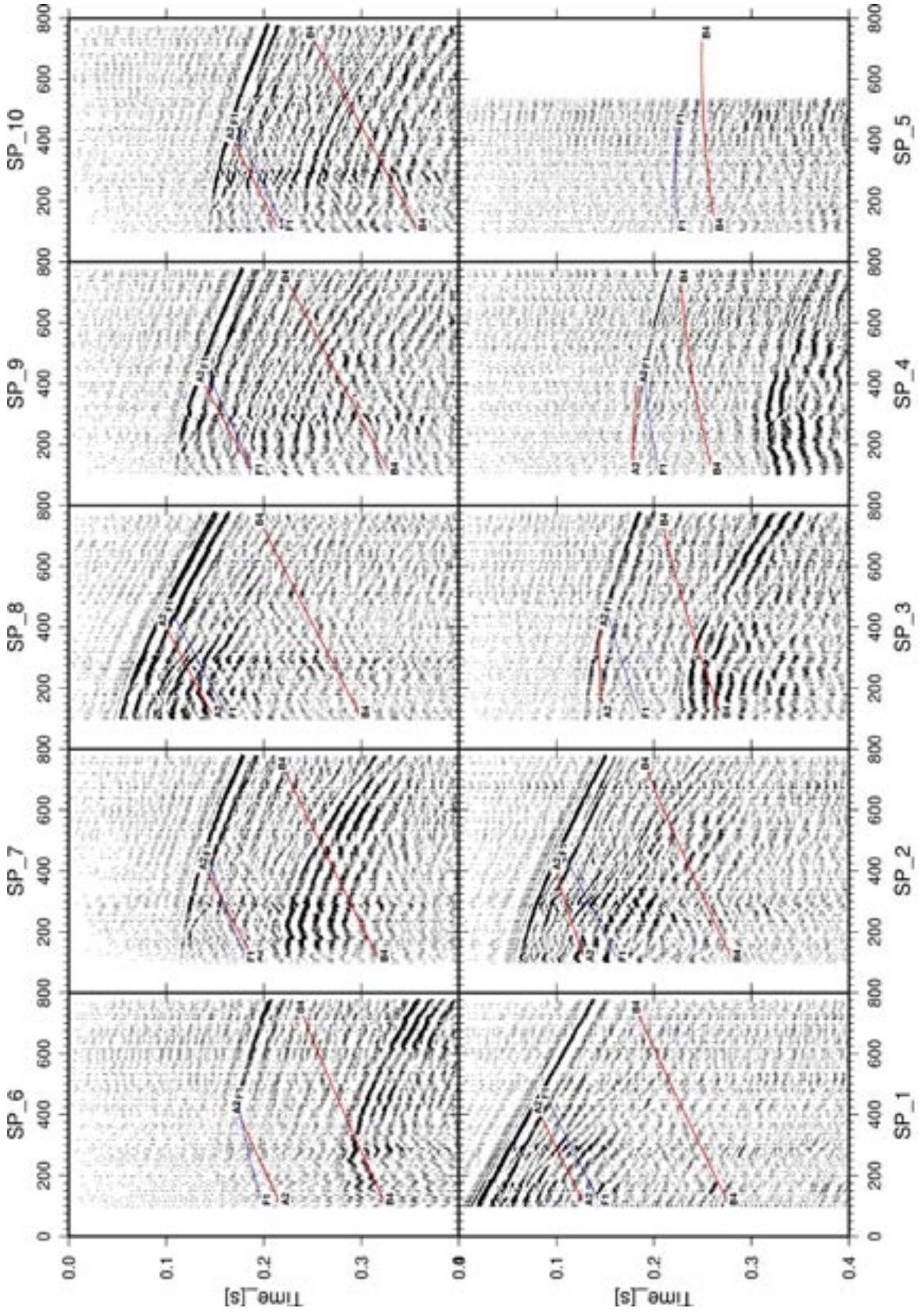

Figure 3-3. *VSP data from all 10 source points processed up to step 6 in Table 3-1 with predicted travel-times for reflectors A2, B4 and F1 superimposed. X-axis is depth in metres.*

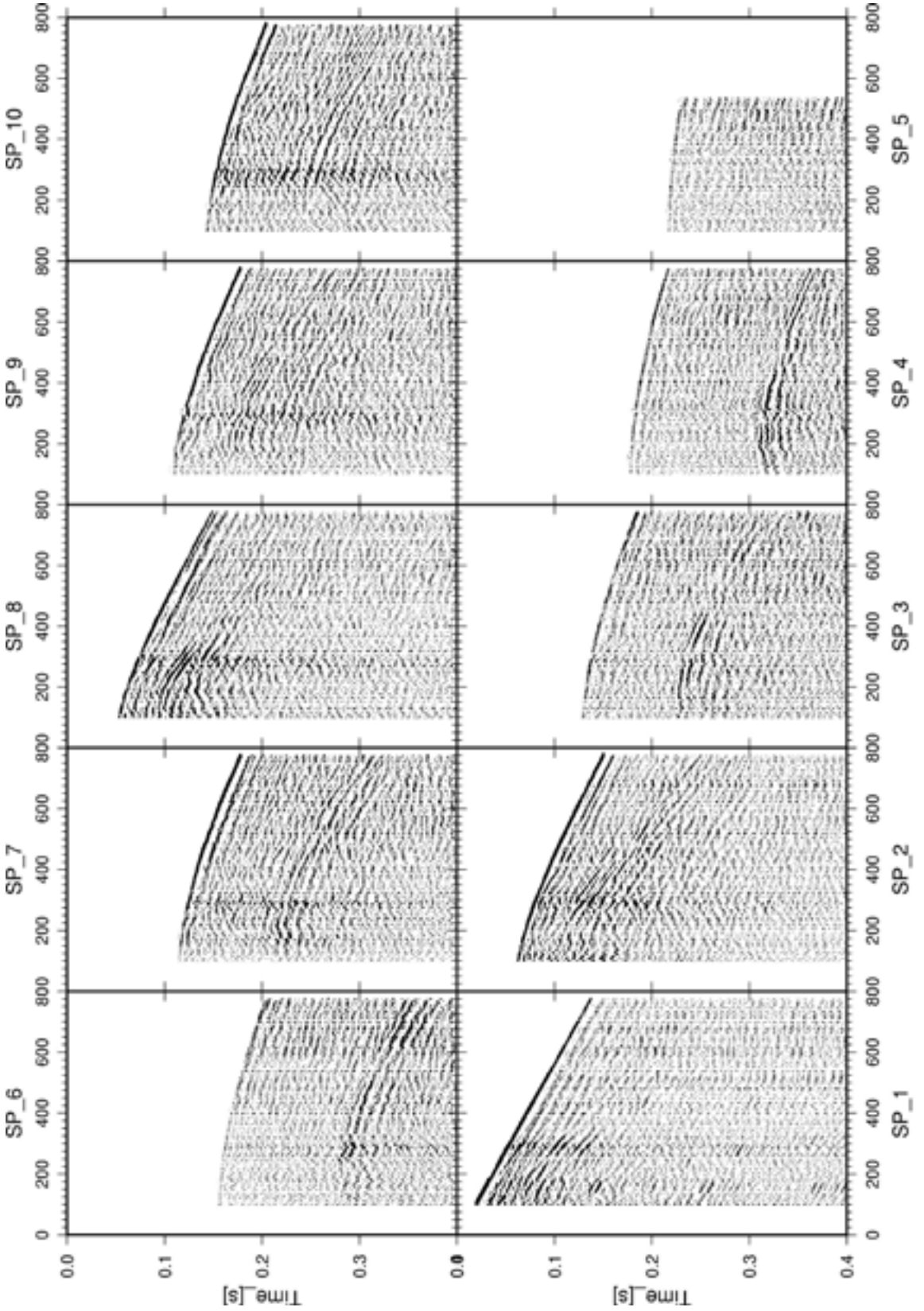

Figure 3-4. *VSP data from all 10 source points processed up to step 10 in Table 3-1. X-axis is depth in metres.*

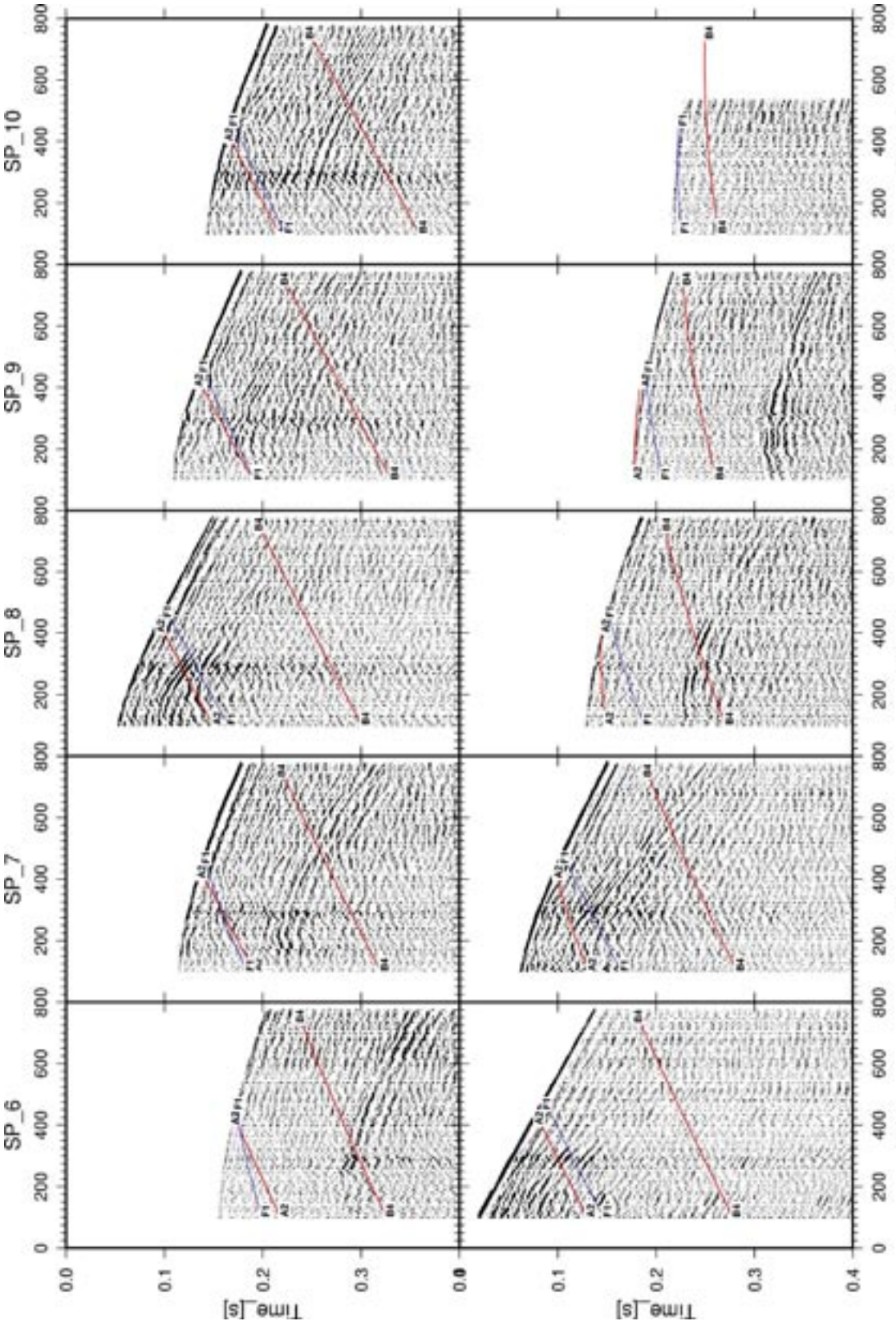

Figure 3-5. *VSP data from all 10 source points processed up to step 10 in Table 3-1 with predicted travel-times for reflectors A2, B4 and F1 superimposed. X-axis is depth in metres.*

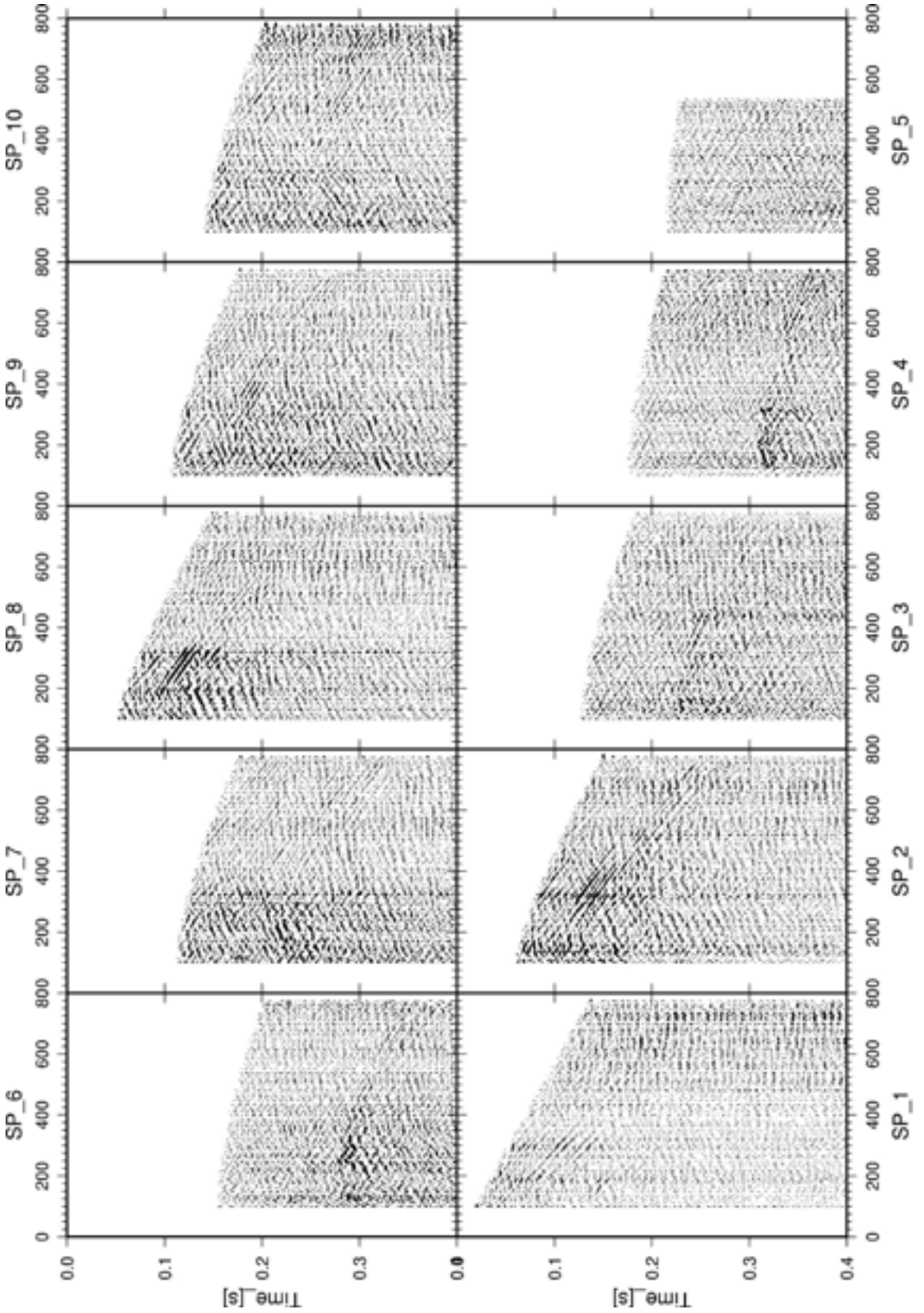

Figure 3-6. *VSP data from all 10 source points processed up to step 12 in Table 3-1. X-axis is depth in metres.*

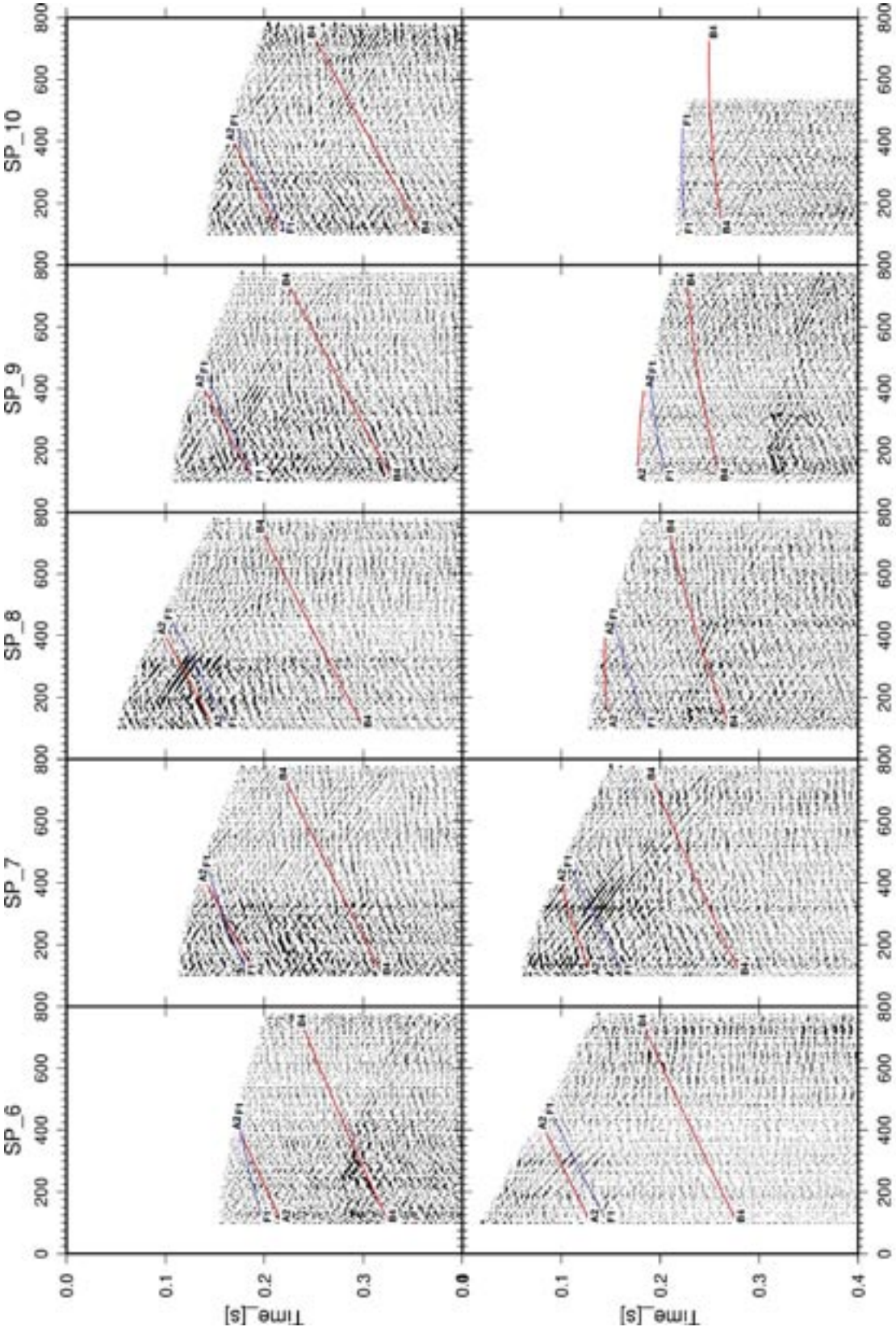

Figure 3-7. *VSP data from all 10 source points processed up to step 12 in Table 3-1 with predicted travel-times for reflectors A2, B4 and F1 superimposed. X-axis is depth in metres.*

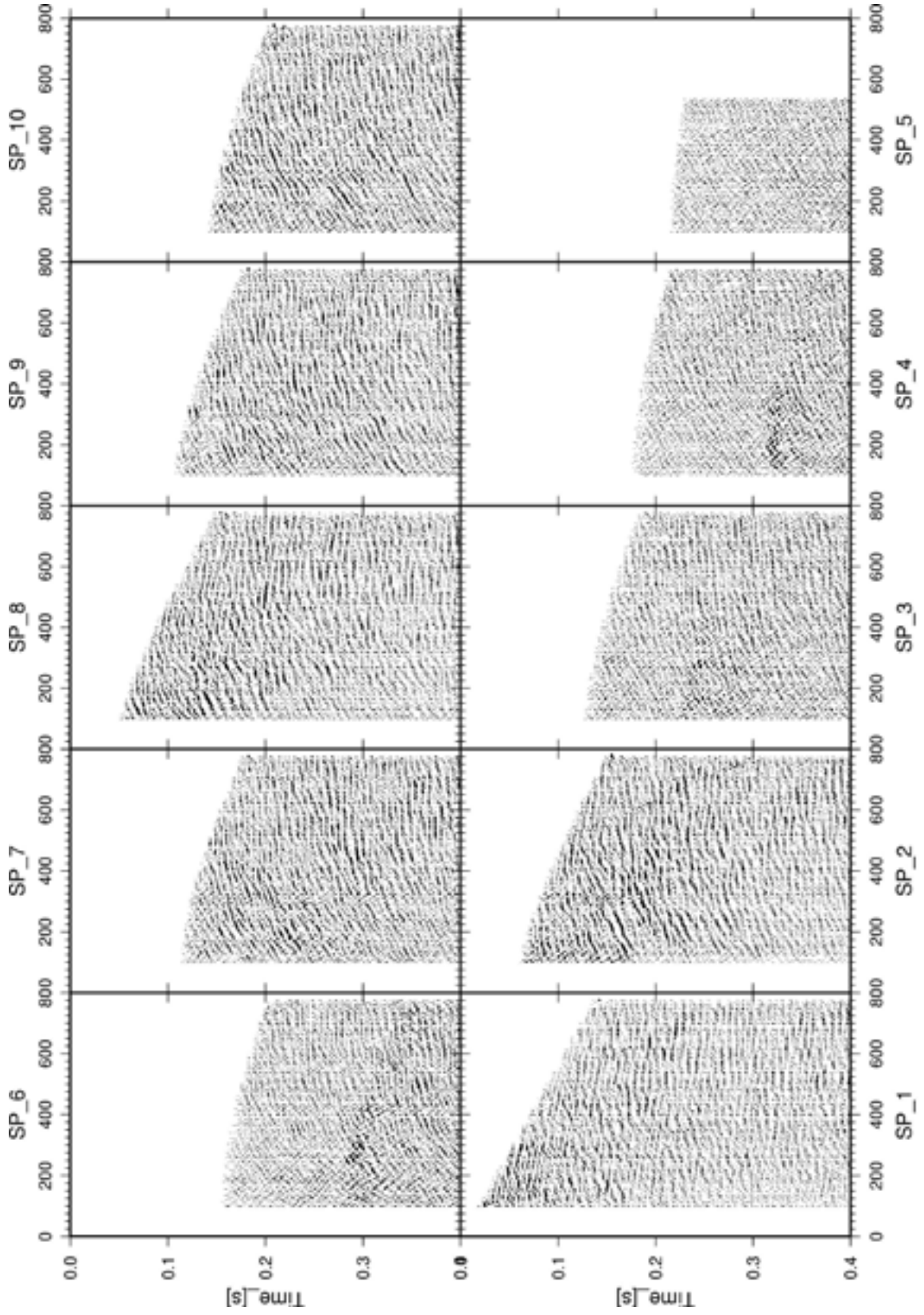

Figure 3-8. *VSP data from all 10 source points processed up to step 14 in Table 3-1. X-axis is depth in metres.*

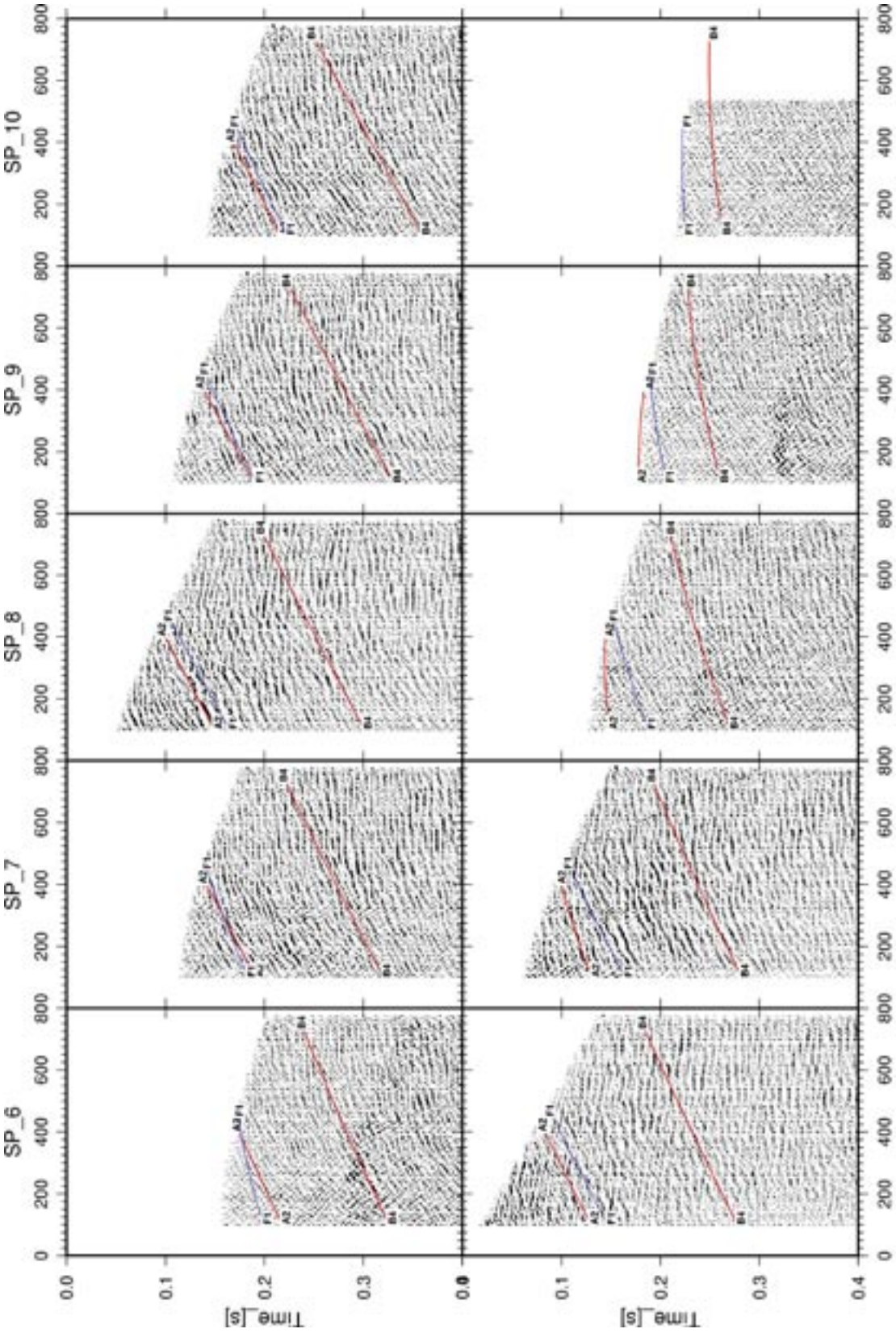

Figure 3-9. *VSP data from all 10 source points processed up to step 14 in Table 3-1 with predicted travel-times for reflectors A2, B4 and F1 superimposed. X-axis is depth in metres.*

In order to compare the VSP data more directly with the surface seismic data, the sections were converted to two-way-travel-time (TWT). If the source-receiver offset is not too large, reflections from sub-horizontal interfaces will now have an approximate sub-horizontal orientation (Figures 3-10 and 3-11), and will arrive at approximately the same TWT as the corresponding reflections on the surface seismic profiles.

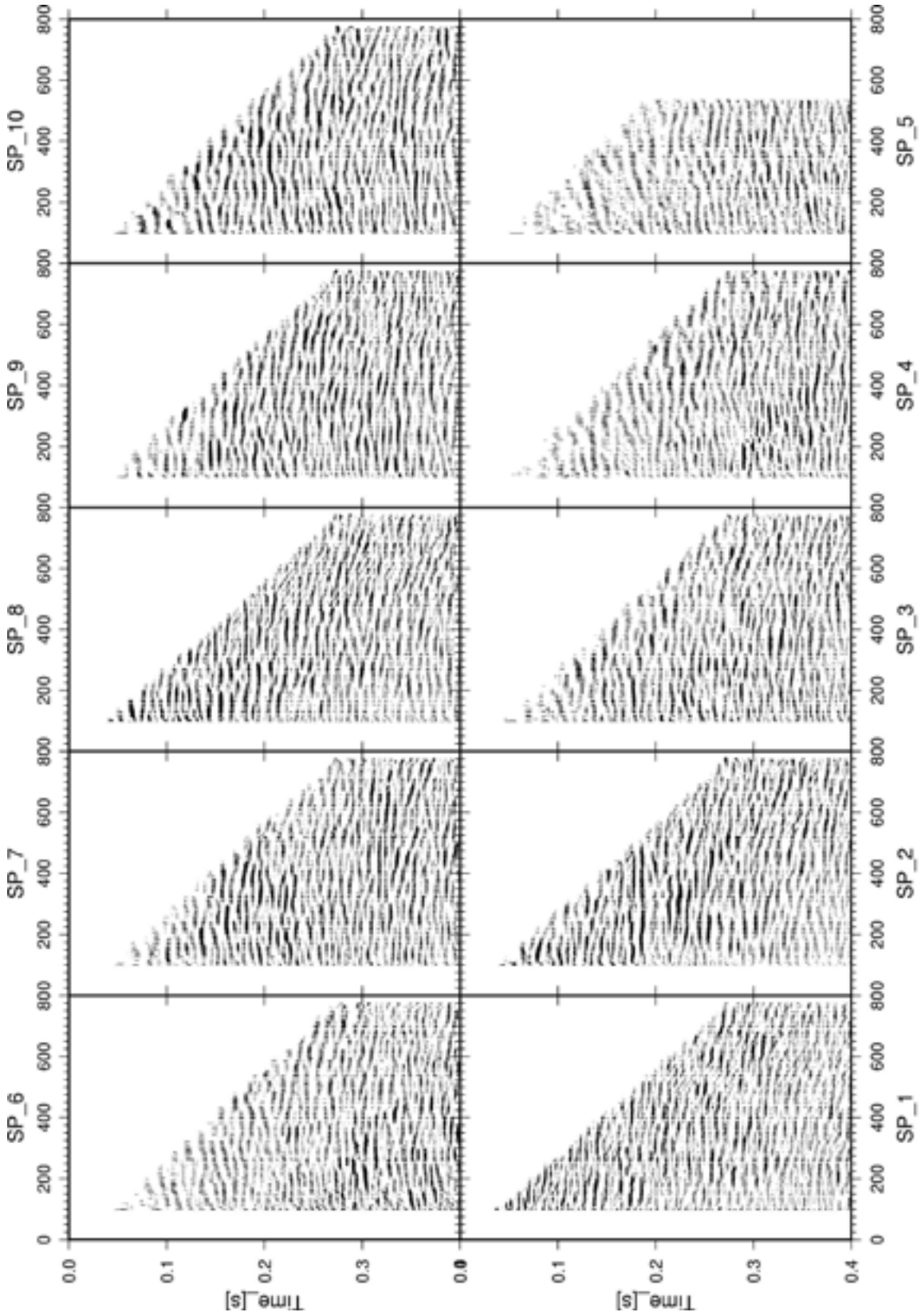

Figure 3-10. *VSP data from all 10 source points processed up to step 17 in Table 3-1. X-axis is depth in metres.*

When viewing the VSP data, the onset of a reflection corresponds to the top of a reflector. Thus, the maximum amplitude of a reflection will not correspond to the top of a reflector. To determine where a reflector intersects the borehole, the location of the onset of the reflection needs to be identified.

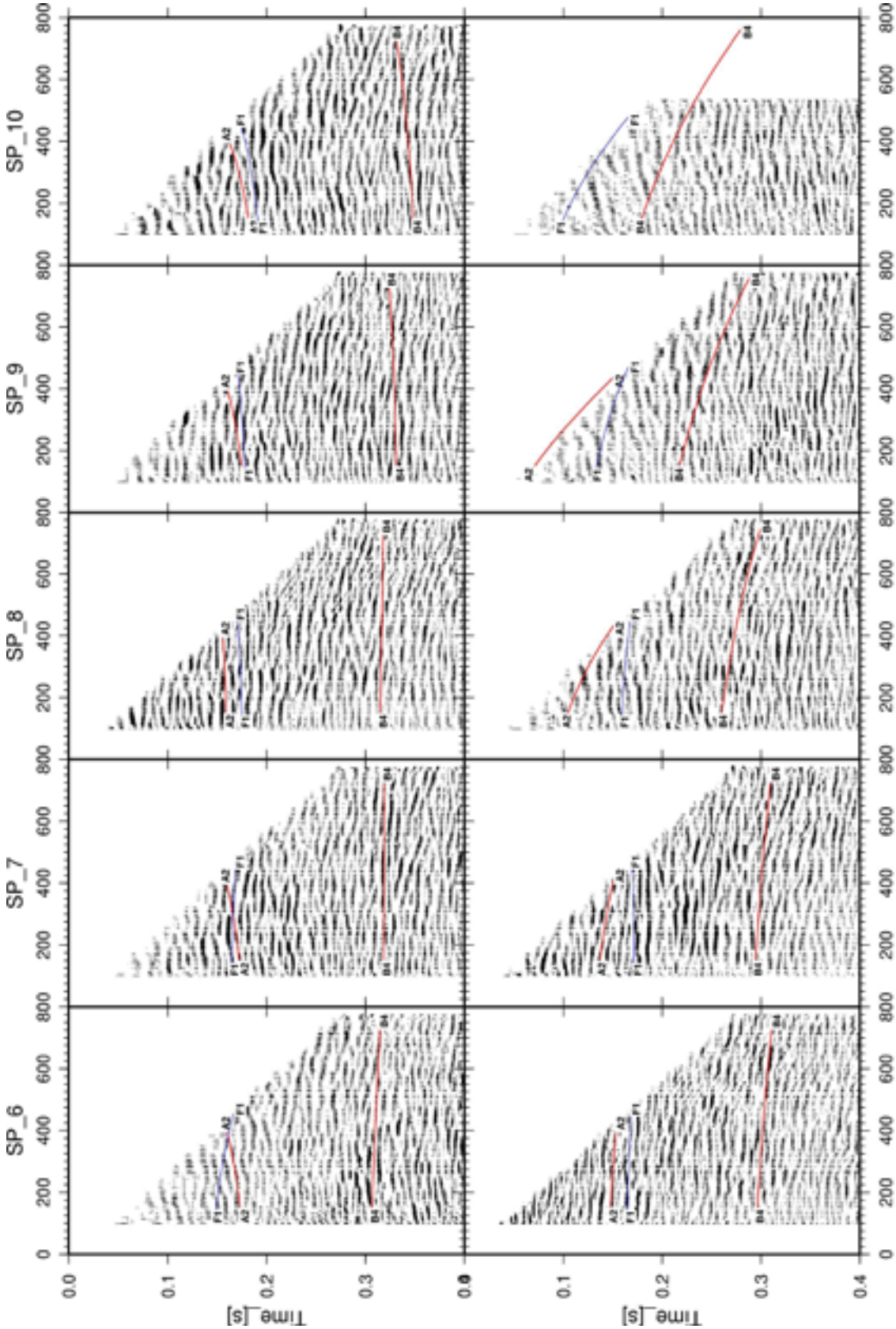

Figure 3-11. *VSP data from all 10 source points processed up to step 17 in Table 3-1 with predicted travel-times for reflectors A2, B4 and F1 superimposed. X-axis is depth in metres.*

4 Discussion of results

4.1 Profile 2 and 2b

Selected reflections from Stage 1 and Stage 2 have been plotted on top of the new merged section (Figure 4-1). Inspection of this figure shows that no new pronounced reflections have appeared in the reprocessing. Reflections from J1 fall close to predicted locations starting on the south-western end of the profile at 0.75 s and continuing to about CDP 500 at 0.2 s. Above 0.2 s, it is still difficult to trace J1 to the surface. The strong reflectivity along J1 at about 0.3 s at CDP 575 should also be noted. The high amplitude of the reflections may be due to larger quantities of mafic rock.

In order to study the geometry of J1 and the short SW dipping reflections above it, the merged section has been migrated (Figure 4-2). The migration is 2D and assumes that all reflections are from within-the-plane of the profile. This assumption is nearly correct for the J1 reflection, but the orientation of the short SW dipping reflections above J1 is not known and it is possible that they emanate from out-of-the-plane of the profile. If they are from within the plane, then the migrated image indicates that they form a cap on the J1 reflector and are part of the J1 structure or zone. A borehole at CDP 450 down to 300 m would then penetrate the J1 structure. By simple projection on the time section (Figure 4-1), J1 is predicted to intersect the surface at about CDP 300. The migrated image indicates that J1 steepens as it approaches the surface and projects to about CDP 400, although it cannot be traced closer than 200 m from the surface. This is within a zone of strongly foliated or banded rock on the geological map (Figure 2-1), suggesting that there may be some connection between the reflector and this banded rock.

Although not very reliable, it should be noted that there are two, steeply SW dipping, weak reflections on the migrated section (Figure 4-2) that project to the surface close to the Eckarfjärden deformation zone. These may be an indication of its orientation and would explain why it does not offset the J1 reflector directly below it.

4.2 Interpretation of reflectivity in KFM02A

Seismic reflections arise when the down-going wave encounters changes in the velocity and/or density of the rock, provided that these changes occur over a large enough area and are reasonably continuous. If the boundary between geological units is limited or not sufficiently continuous, then the down-going wave will be scattered and little energy will be reflected back, even if the velocity and density contrasts are large. Signs of scattered waves may be found in diffraction patterns in the seismic data.

In order to identify where sub-horizontal reflections originate in the borehole, the VSP data from selected source points that were transformed to two-way-time (Figure 3-10) have been depth-converted using a velocity of 5,750 m/s. These depth-converted VSP sections have been plotted alongside the migrated surface seismic and the sonic and density logs from KFM02A (Figures 4-3 to 4-6). It needs to be kept in mind that there are two intervals where the sonic velocity has not been properly calculated, these are at 350–380 m and below 900 m. The full waveform sonic display shows no indication of such low velocities over these intervals. In the interval 250–300 m (corresponding to the porous granite described by /Möller at al. 2003/), the sonic velocity is also extremely low (as low as 3.5 km/s), but here the full waveform sonic shows clear delays, indicating that these velocities have been correctly determined. The full waveform sonic is highly irregular in the interval 415–520 m, indicating this interval to be significantly fractured and altered. It should also be noted that the depths of the reflectors indicated in the surface seismics in Figures 4-3 to 4-6 refer to depth below the wellhead of the KFM02A borehole (location: 1633182 E, 6698712 N). They differ from the intersection depths reported in /Juhlin and Bergman 2004/, where the planned location of the KFM02A borehole was used (location: 1633200 E, 6698670 N), not the actual location.

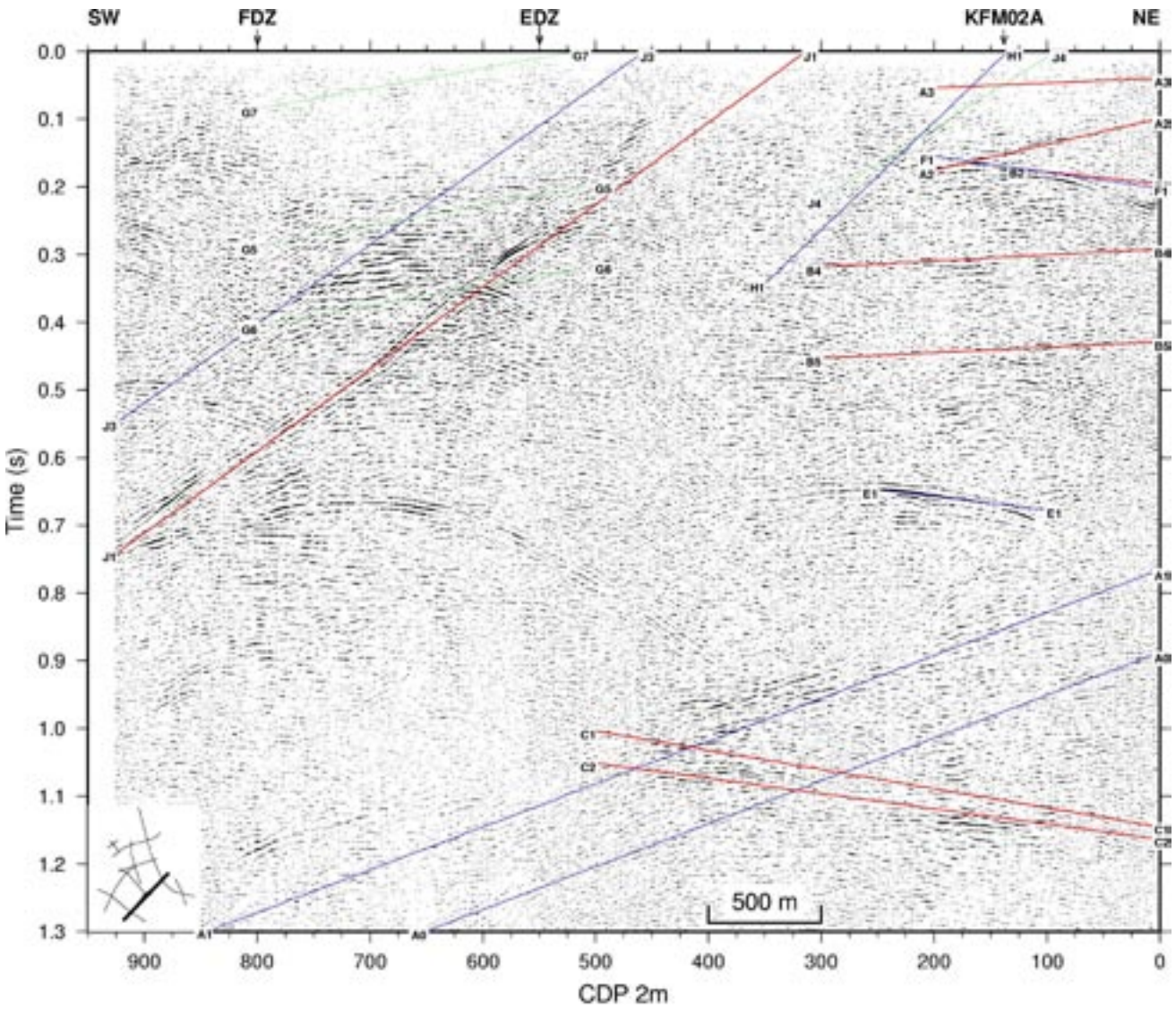

Figure 4-1. *Stacked section of merged profile 2 down to 1.3 seconds with selected reflections marked. Location of section indicated in lower left corner.*

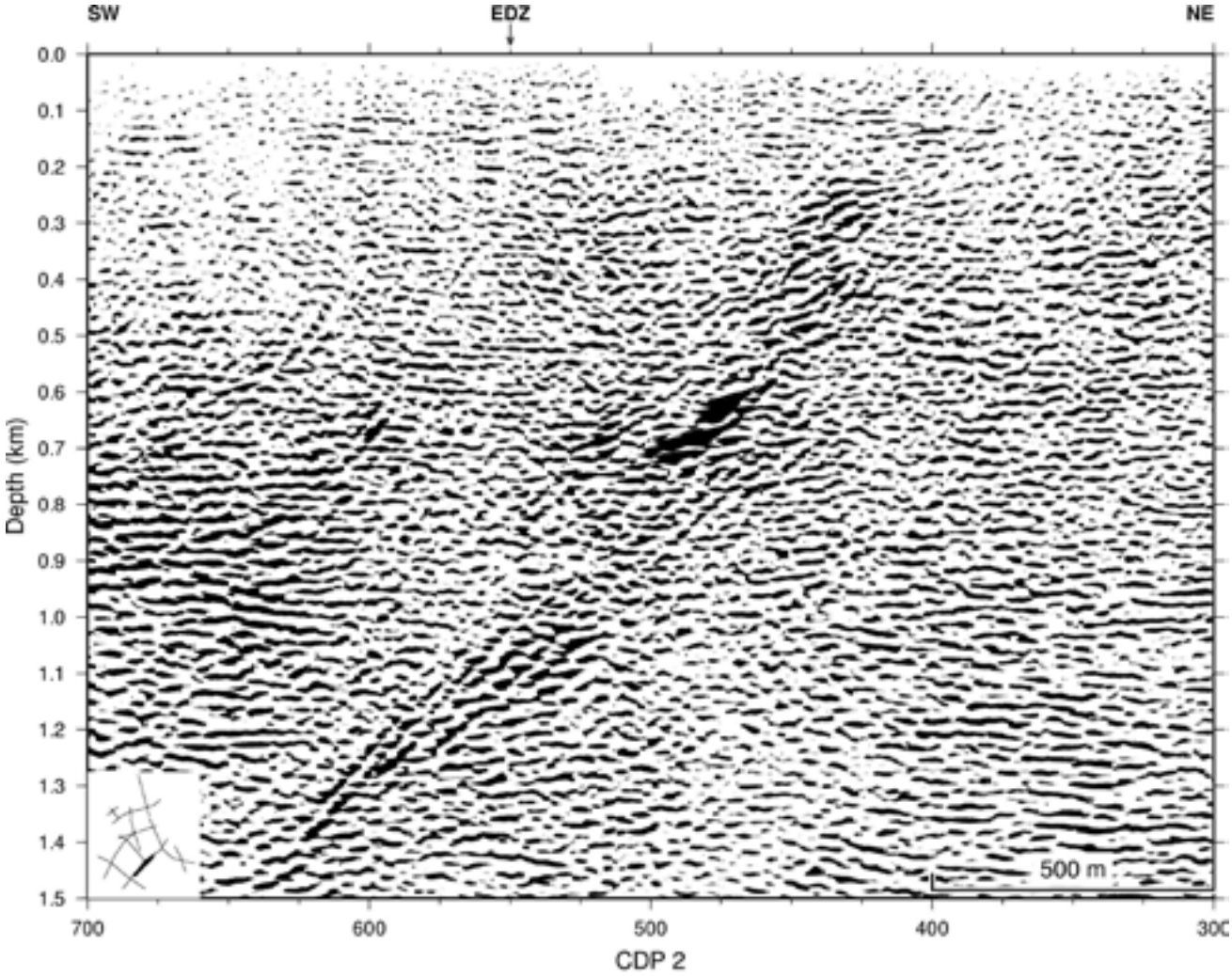

Figure 4-2. *Migrated section of merged profile 2 down to 1.5 km. Location of section indicated in lower left corner. Migration assumes all reflections originate from within-the-plane of the profile.*

The clearest reflection observed on the VSP data is found on SP 2 and intersects the borehole at about 500 m (Figure 4-3). Its onset time agrees well with that predicted for the F1 reflector and this reflector is also clearly imaged on profile 5 near the KFM02A borehole at this depth. A depth of 500 m is close to the bottom of the highly fractured interval 415–520 m /Carlsten et al. 2004/, suggesting that the F1 reflection originates from the base of this interval. Thus, it is the contrast between the fractured rock above and the more intact rock below that generates the strong F1 reflection observed on the surface seismics. Reflections that can be correlated to the F1 reflector, although not as clearly as on SP 2, are also observed on VSP data from SP 1 and SP 8 (Figures 4-4 and 4-5), also intersecting the borehole at about 500 m. Signs of the F1 reflection are seen on the VSP data from the other source points (Figure 3-11), but either the predicted onset time is not sub-horizontal, or the arrivals from the A2 reflector are predicted to interfere with the F1 reflection, and thereby mask one another. SP 1, SP 2 and SP 8 are those source points closest to the borehole, and have the best geometry for mapping the F1 reflector close to the borehole. It should also be noted that the F1 reflection is clearest north of the borehole (Figure 4-7), which suggests that SP 2 should contain the best image of the reflection, in agreement with observations.

Reflections that can be correlated to the A2 reflector are also observed on SP 1, SP 2 and SP 8 (Figures 4-3 and 4-5). The onsets of these reflections do not match the predicted onsets based

on the surface seismic data as well as the F1 onsets do. This can be explained by the orientation of the A2 reflector being somewhat different near the borehole than predicted from the surface seismic data. The correlated reflections are also not as clear as the ones correlated to the F1 reflector. This is to be expected from the surface seismic data, where the F1 reflection is stronger and more clearly imaged below the KFM02A borehole on profiles 2 and 5 (Figures 2-6 and 2-11). The onset of these apparent A2 reflections on the VSP data intersects the borehole at about 410 m. This is about 30 m shallower than predicted from the surface seismic data, but coincides closely with the top of the heavily fractured interval at 415–520 m /Carlsten et al. 2004/. Inspection of the selection of the A2 reflection on the surface seismic data (Figure 4-7) shows that it could indeed intersect the borehole somewhat shallower than what is predicted based on the selection procedure.

The depth to reflector B4 is about 950 m directly below the KFM02A wellhead. Since the borehole dips at 85° to the north, the predicted depth of penetration is at about 930 m, some 50 m offset from the wellhead and corresponding to about CDP 185 on profile 5. It is expected to be most clearly imaged on source points lying south of the borehole (Figure 4-7). Clear reflections from VSP data on SP 7 can be correlated with the B4 reflector (Figure 4-6), although signs of it are observed on all source points south of the borehole. Since the VSP survey did not extend down deeper than 775 m, the exact depth at which it penetrates the borehole cannot be determined. However, the reflection projects into the borehole at about 920 m, close to the depth expected based on the surface seismic data. This is in the middle of a high density, tonalitic metagranitoid /Carlsten et al. 2004/, suggesting that it is the density contrast between this unit and the surrounding lower density granitic rock that is generating the B4 reflection.

This interpretation requires that this high density rock is continuous, with approximately the same thickness laterally away from the borehole for several hundreds of metres, if not more. Note that the density log shows a rather gradual transition between the surrounding rock and the tonalitic rock, indicating the boundary may not be sharp. There are also a number of fracture zones close to the B4 reflector, the uppermost one is at about 900 m and is characterized by a clear 10 m thick low velocity anomaly signature. This low velocity zone could also contribute to the reflectivity. Given that the reflectivity appears to start shallower than 900 m at the borehole location, it is possible that it is a combination of this fracture zone and the high density rock that is generating the reflectivity associated with the B4 reflection that is observed on the surface seismic data.

The A3 reflector is projected to intersect the borehole at about 115 m, too shallow to be imaged by the VSP data. However, the fracture zone and underlying amphibolite at 120–130 m are candidates for this reflector. The amphibolite is quite thin and its contribution to the reflection coefficient from the density contrast is less than that from the velocity contrast of the fracture zone. In addition, other amphibolites, in particular those at about 800 m and 850 m do not generate any clear reflections. Thus, it is possible that the A3 reflection is generated by the low velocity zone at 120–130 m.

Apart from the porous granite at 250–300 m, the only other prominent low velocity zone that does not have a corresponding reflection identified on the surface seismic data is the one 160–180 m. This zone also corresponds to the A3 reflector. Since the borehole is offset from the profiles by about 100 m, it is not possible to draw any definite conclusions about this zone. However, another more speculative possibility exists. The zone at 160–180 m could correspond to the more steeply dipping reflection seen on profile 2 and tentatively referred to as J4 (Figure 4-8). This reflection would have the same strike as the prominent J1 reflection to the south and dip at about 40° to the south-west. The earlier interpreted H1 reflection may actually have been mistaken for this event. If the J4 reflection has the assumed orientation, it overlaps the A3 reflection on profile 5 (Figure 4-7), making it difficult to ensure a reliable orientation. A migrated image of profile 2 shows that the potential J4 zone could limit the F1 and A2 reflectors towards the south-west (Figure 4-9). It should also be noted that only the J4 reflection is migrated reasonably properly on the section. The other reflections have a significant out-of-the-plane of the profile component.

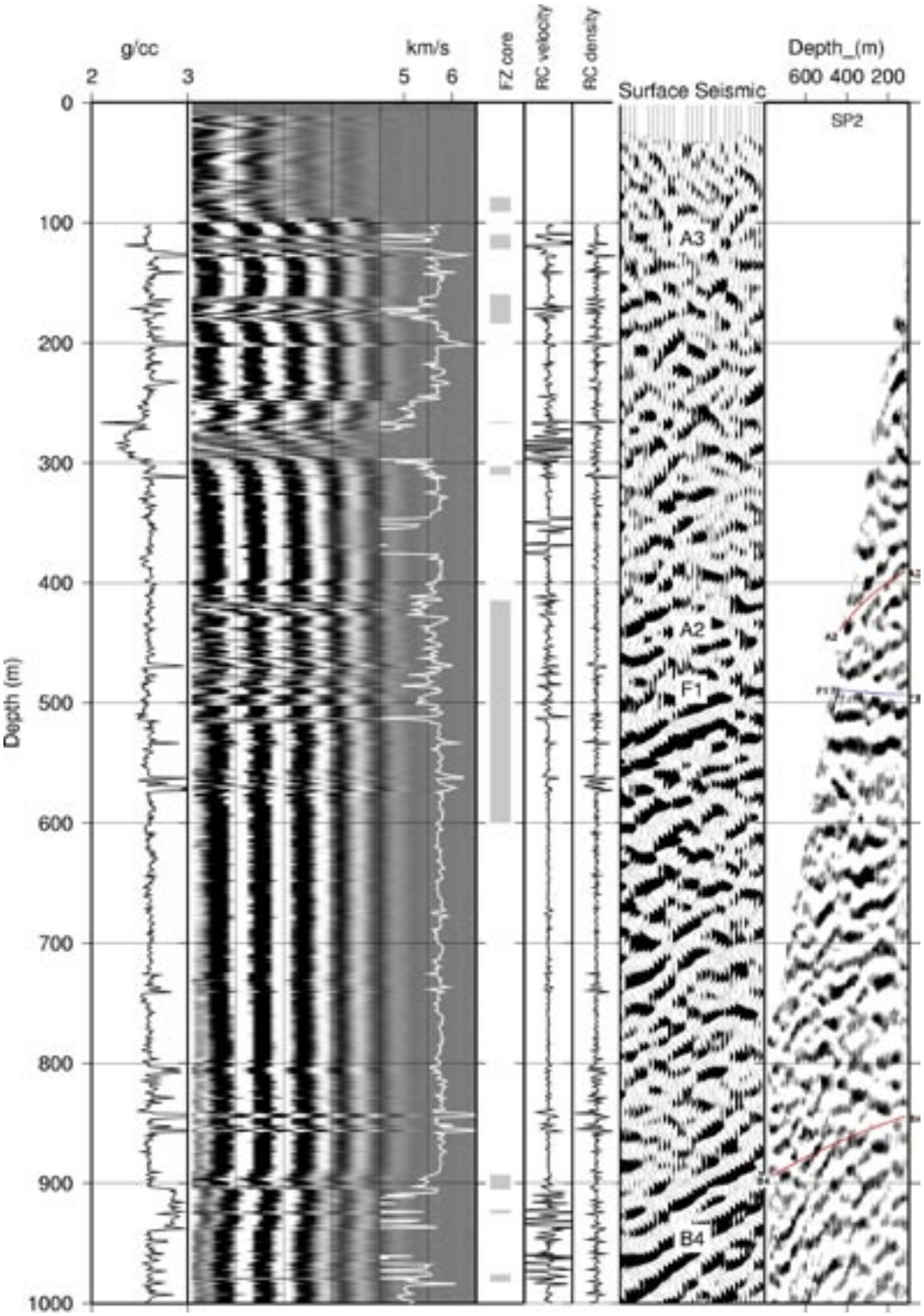

Figure 4-3. *Density and sonic logs from the KFM02A borehole compared to the migrated seismic section along profile 5 and SP 2 from the VSP. P-wave sonic velocity is plotted on top of the full waveform sonic seismograms from the near receiver. Shaded portions in the FZ core panel indicate where the major deformation zones in the core have been identified /Carlsten et al. 2004/. Reflection coefficients (RC) have been calculated using only the sonic and only the density log, to allow a comparison of the importance of the contrasts in these two parameters. They are plotted on a scale ranging from –0.1 to 0.1. Borehole was cased to 100 m.*

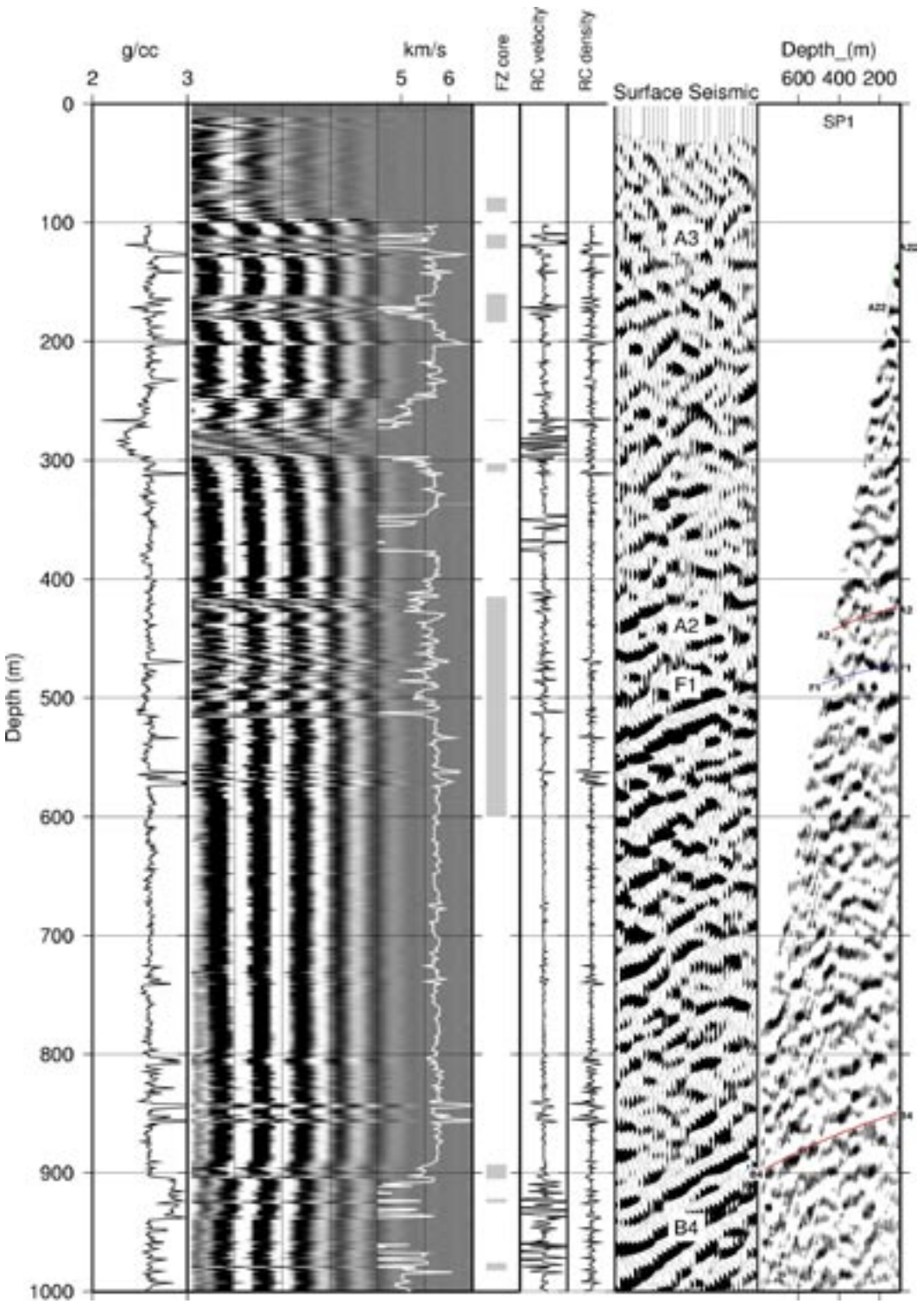

Figure 4-4. *Density and sonic logs from the KFM02A borehole compared to the migrated seismic section along profile 5 and SP 1 from the VSP. P-wave sonic velocity is plotted on top of the full waveform sonic seismograms from the near receiver. Shaded portions in the FZ core panel indicate where the major deformation zones in the core have been identified /Carlsten et al. 2004/. Reflection coefficients (RC) have been calculated using only the sonic and only the density log, to allow a comparison of the importance of the contrasts in these two parameters. They are plotted on a scale ranging from –0.1 to 0.1. Borehole was cased to 100 m.*

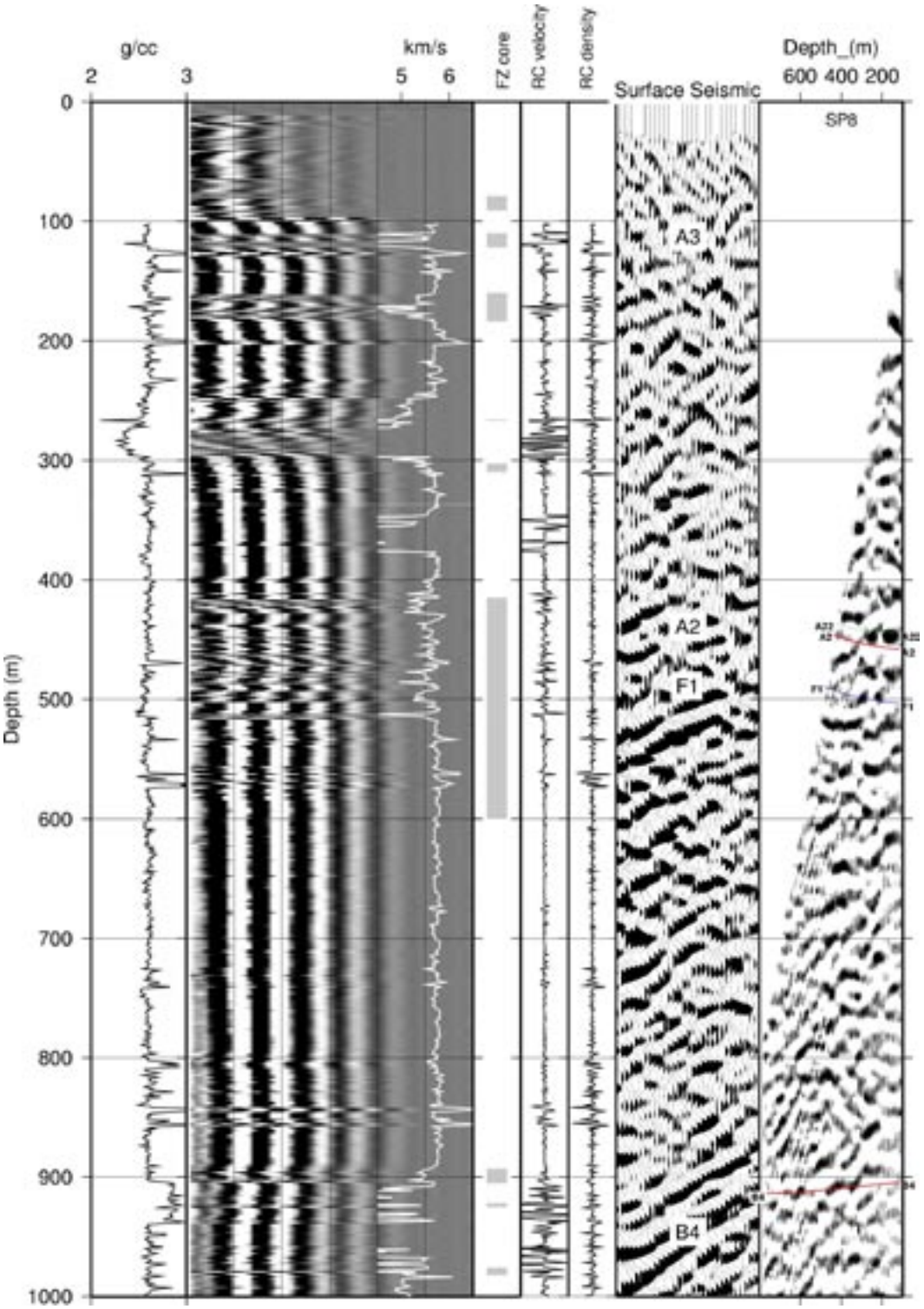

Figure 4-5. *Density and sonic logs from the KFM02A borehole compared to the migrated seismic section along profile 5 and SP 8 from the VSP. P-wave sonic velocity is plotted on top of the full waveform sonic seismograms from the near receiver. Shaded portions in the FZ core panel indicate where the major deformation zones in the core have been identified /Carlsten et al. 2004/. Reflection coefficients (RC) have been calculated using only the sonic and only the density log, to allow a comparison of the importance of the contrasts in these two parameters. They are plotted on a scale ranging from –0.1 to 0.1. Borehole was cased to 100 m.*

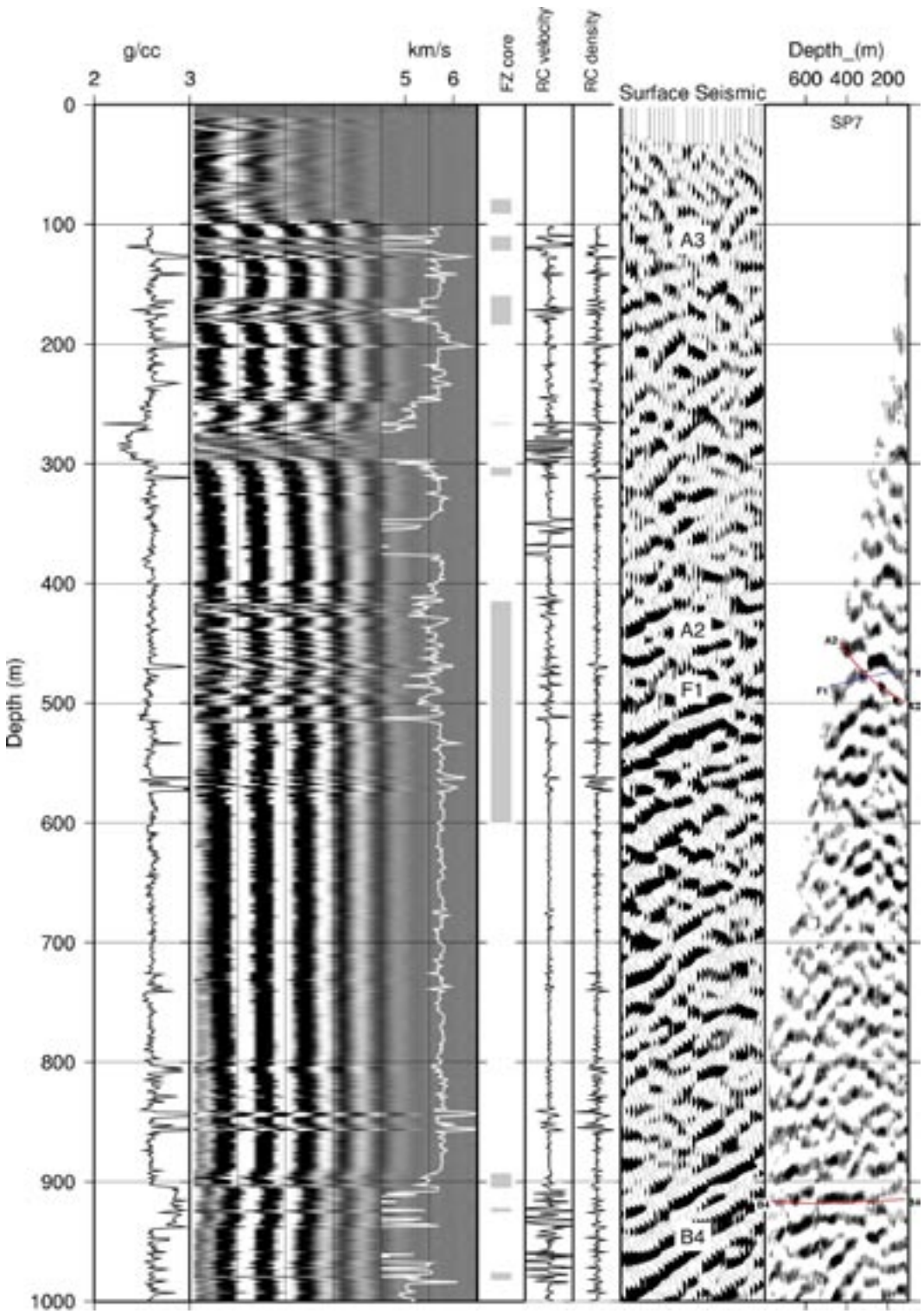

Figure 4-6. *Density and sonic logs from the KFM02A borehole compared to the migrated seismic section along profile 5 and SP 7 from the VSP. P-wave sonic velocity is plotted on top of the full waveform sonic seismograms from the near receiver. Shaded portions in the FZ core panel indicate where the major deformation zones in the core have been identified /Carlsten et al. 2004/. Reflection coefficients (RC) have been calculated using only the sonic and only the density log, to allow a comparison of the importance of the contrasts in these two parameters. They are plotted on a scale ranging from –0.1 to 0.1. Borehole was cased to 100 m.*

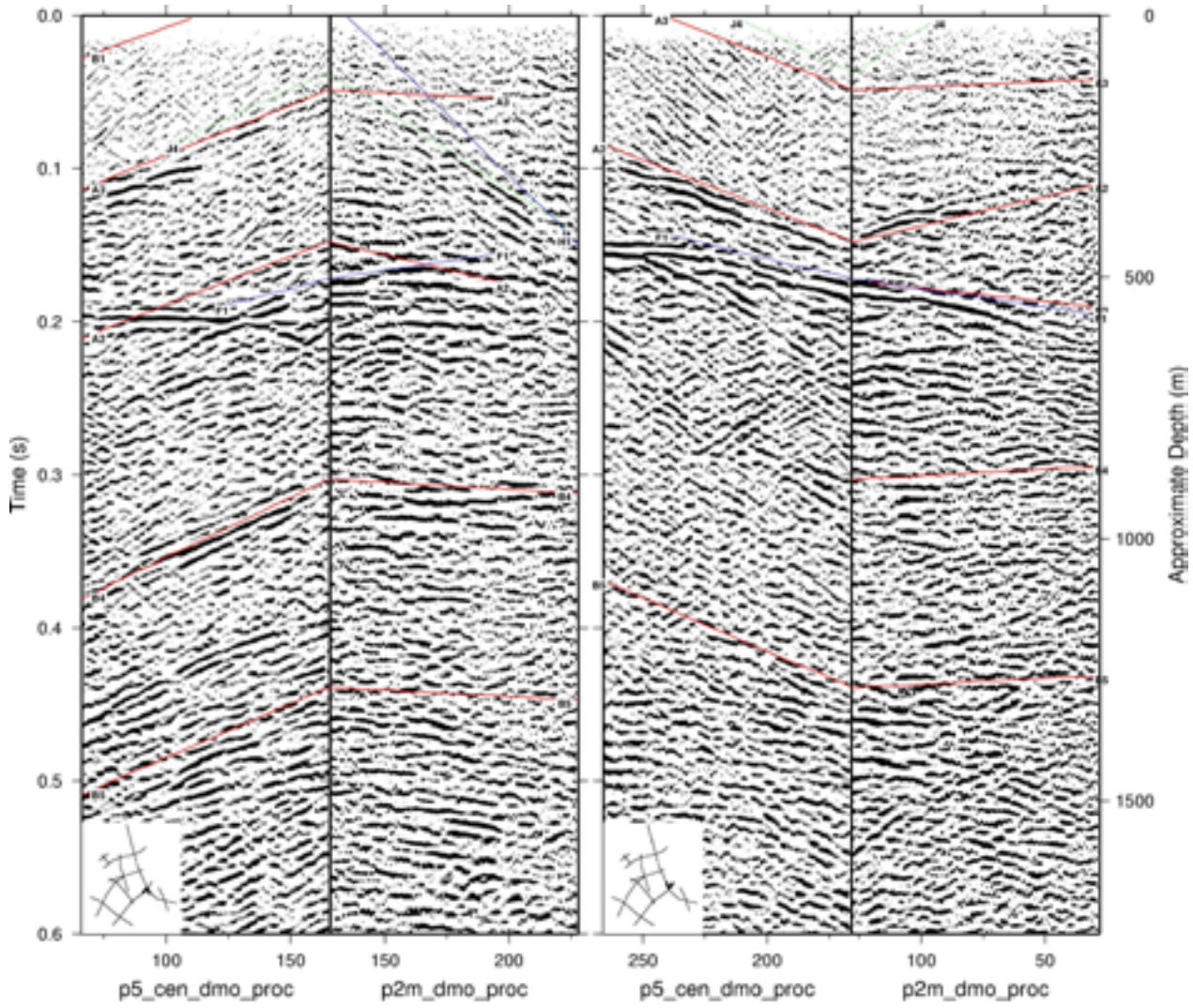

Figure 4-7. *Parts of profiles 2 and 5 viewed from the south (left) and the north (right). Predicted reflection onset times based on /Juhlin and Bergman 2004/ are marked with lines.*

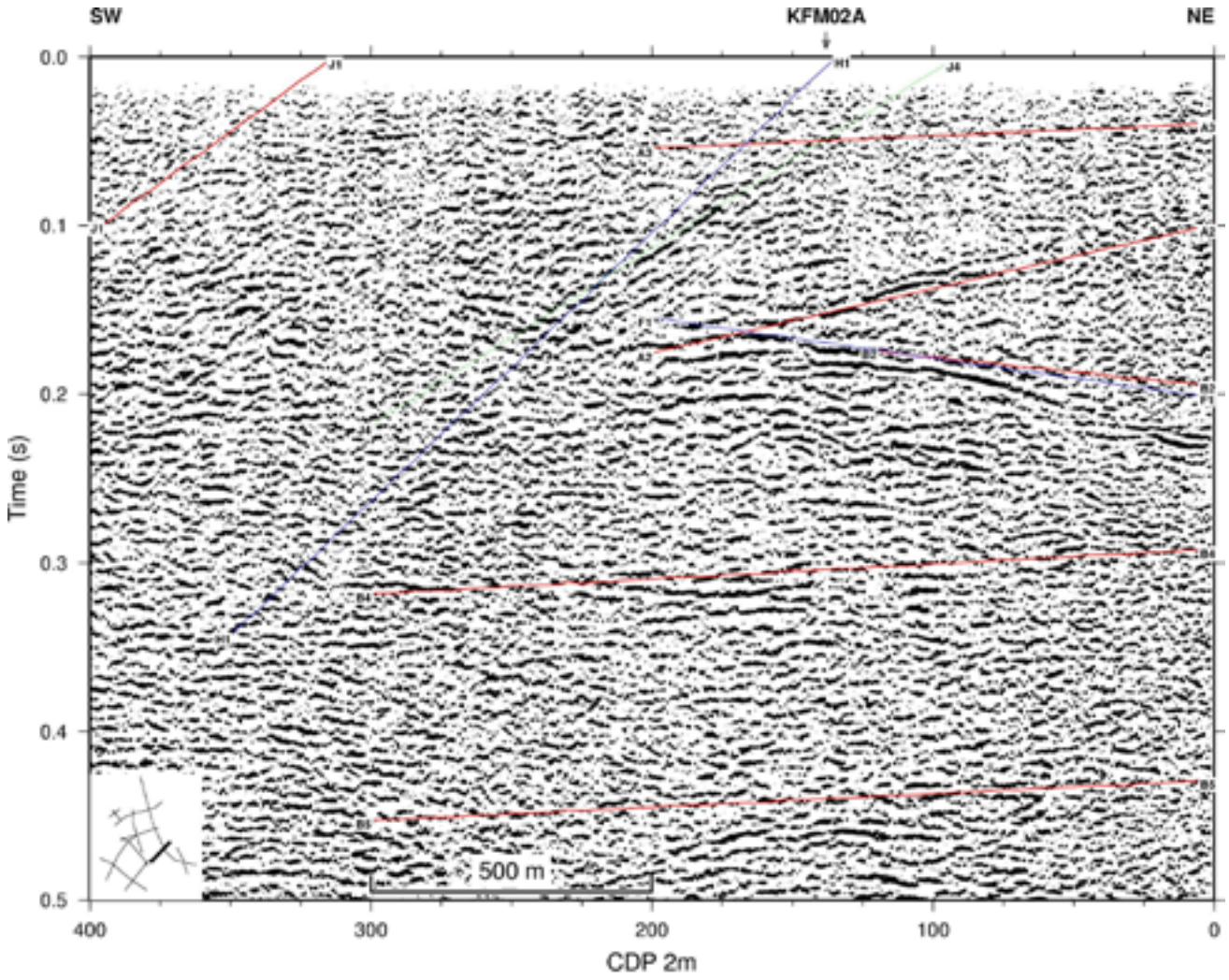

Figure 4-8. *Stacked section of merged profile 2 down to 0.5 seconds with selected reflections marked. Location of section indicated in lower left corner.*

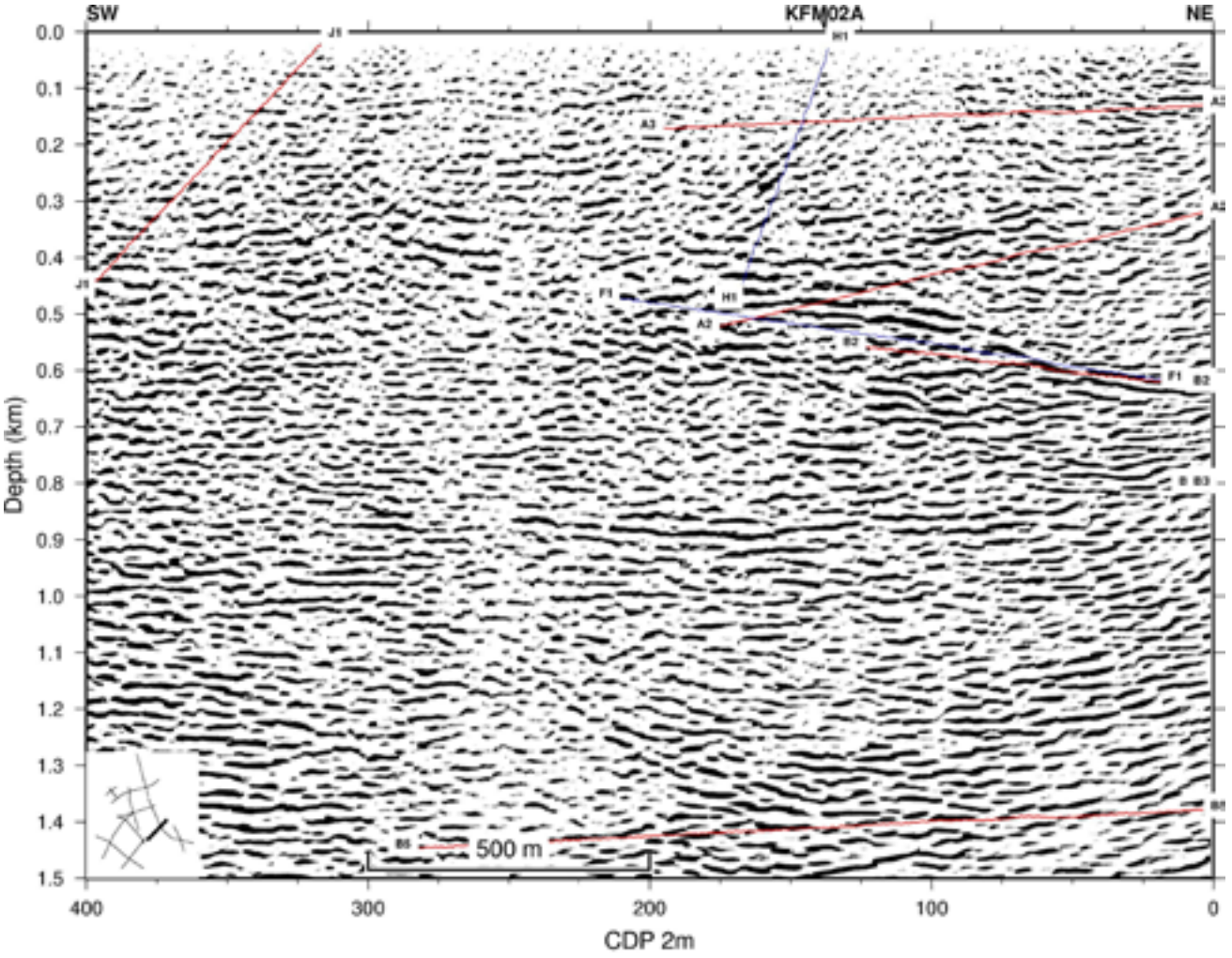

Figure 4-9. *Migrated section of merged profile 2 near the KFM02A borehole down to 1.5 km. Location of section indicated in lower left corner. Migration assumes all reflections originate from within-the-plane of the profile.*

4.3 Porous granite

An interesting discovery in the KFM02A borehole was the long interval between 250 m and 300 m containing porous (vuggy) granite or episyenite /Möller et al. 2003/. This interval has anomalously low velocities and densities. If it were laterally continuous it would generate very strong reflections. However, no clear response in the surface seismic data is seen from this body, suggesting that it is limited in its lateral dimensions. Is it observed on the VSP data?

The clearest indication of this body on the VSP is found in the variations in arrival time of the direct S-wave at a depth of about 250 m on the unprocessed VSP data (Figure 3-2). No clear reflections appear to be generated by it, suggesting that it is limited laterally and that it has an irregular geometry. SP 6 shows the greatest variations in the direct S-wave arrival in the interval 150 m to 300 m at about 0.3 s. Since the body intersects the borehole between 250 m and 300 m, this suggests that the body extends towards the surface on the south side of the borehole towards SP 6 and does not extend much deeper towards the north. Diffraction patterns with an apex at about 300 m depth are also seen in data from some of the unprocessed VSP source points, in particular SP 2 (Figure 3-2). These diffractions have an S-wave velocity, suggesting they originate from forward scattering at the base of the body on the north side of the borehole.

4.4 Northern part of profile 5 – reflectors F1, F2, F3 and A8

The orientation of F1 is well constrained from crossing profile 2, while the orientations of F2 and F3 are more uncertain. In orienting F2 and F3, a strike similar to F1 has been assumed and the dip adjusted to match the reflection travel-times. Inspection of the migrated section (Figure 2-13) shows that the set F reflections appear to form an undulating surface that may contain offsets at some locations. This surface appears to end at about CDP 375 (6699400 N), where it either terminates or becomes more diffuse, perhaps merging into the B7 reflection zone. Towards the south, the set F reflections extend to about 6698500 N, consistent with observations on profile 2.

Given the constraints from shot gathers and the stacked section, it has been possible to give an estimate of the orientation of the A8 reflector (Table 4-1) and locate where it projects to the surface (Figure 4-10). It possibly cuts the F1 reflector (Figure 2-13), and perhaps even extends further down than modelled. It should be noted that the A8 reflection is not observed on crossing profile 1. It projects into profile 1 at very early times where profile 1 crosses profile 5 and it

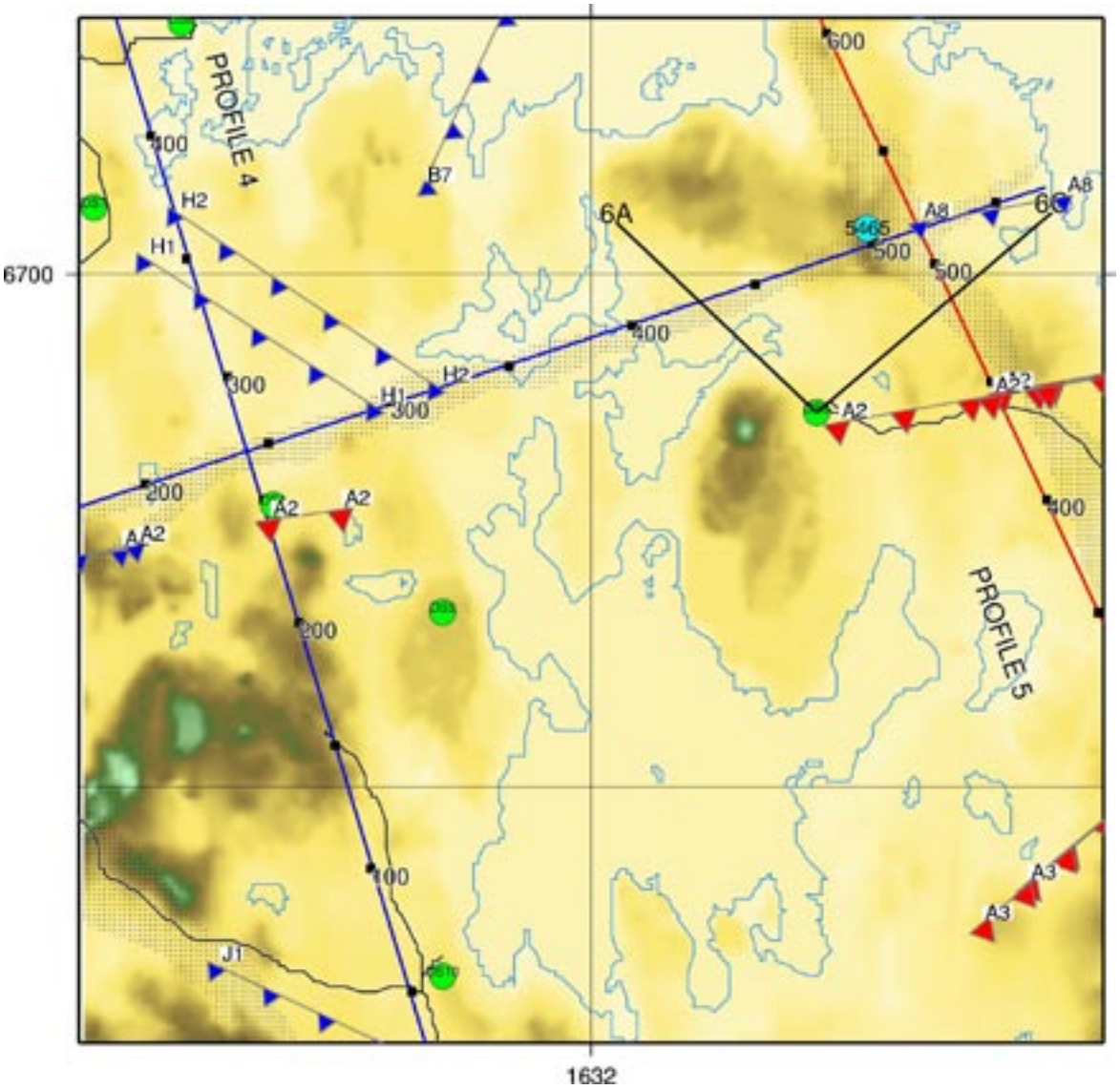

Figure 4-10. *Location of boreholes at drill site 6, the A8 reflector and profile1 (running WE). A8 is seen to intersect the surface close to receiver 5,465 (cyan circle) and to project up to the surface close to CDP 520 on the reprocessed northern part of profile 5. A8 cuts profile 1 at too shallow a depth to be imaged near the crossing point of the profiles. Black dots show midpoint spread along the seismic profiles.*

Table 4-1. Orientation of the new reflectors discussed in this report. F1 is also included from earlier reports. Distance refers to distance from the arbitrary origin (6699 km N, 1633 km W) to the closest point on the reflector at the surface. Depth refers to depth below the surface at this origin. Strike is measured clockwise from north. Rank indicates how sure the observation of each reflection is on profiles that the reflection is observed on; 1 – definite, 2- probable, 3-possible.

Reflector	Strike	Dip	Distance (m)	Depth (m)	Rank	Profiles observed on
F1	20	20		400	1	2.5
F2	20	5		420	2	5
F3	20	5		500	2	5
A8	80	35	1,150		2	5

would not be expected to be seen there. However, it is also not seen further west along profile 1, where it would be expected to be observed at 100–200 ms. Therefore, its lateral extent towards the west appears to be very limited.

As noted in /Juhlin et al. 2002/, many of the reflections appear to die out towards the north on profile 5, particularly the set A and set B reflections. The set F reflections also follow this pattern. Both the B7 and A8 reflections, which lie in the northernmost part of the profile, are quite diffuse here. This may be due to the reflectors that generate them being "broken up" and not as laterally homogeneous as further towards the south-east.

4.5 Concluding remarks

4.5.1 VSP

Integration of the VSP data with the surface seismic data has proven useful for:

1. Obtaining a realistic velocity profile that can be used for depth conversion of the seismic data.
2. Identification of where the F1 and A2 reflectors intersect the borehole. The F1 reflection originates from near the base of the heavily fractured interval at 415–520 m and the A2 reflection from near the top of this fractured interval.
3. Confirmation that the porous granite is probably limited in its lateral extent.
4. Even though the B4 reflector was not intersected by the VSP survey, it is likely that it intersects the borehole at about 920 m, in good agreement with the surface seismics. A thick section of high density tonalitic rock is present at this depth, but also a 10 m thick fracture zone. Both probably contribute to the reflectivity of the B4 reflector.

It is surprising that first arrivals from all source points to all receiver points in the KFM02A borehole, and also in the KFM01A borehole /Cosma et al. 2005/, indicate a nearly constant velocity media of 5,750 m/s, irrespective of azimuth or depth. Given the variations in fracturing and the metamorphic grade of the rock, one would expect some azimuthal or depth dependence. Perhaps the lack of velocity variations is due to the high stresses in the bedrock. Alternatively, it could be due to some preprocessing that has been applied to the VSP data that has not been mentioned in the reports.

One problem in using the VSP data is the lower signal to noise ratio compared to the surface seismic data. This is due to the VSP data being single fold. It could be useful in the future to carry out moving source profiling (MSP). This allows stacking of VSP data to increase the signal to noise ratio. Such profiles would focus on certain depths so as to more clearly map the lateral extent of certain reflectors.

4.5.2 Profiles 2 and 2b

Reprocessing of profiles 2 and 2b as one profile produced a seismic section that was superior to simply merging of the two previously processed profiles. This was partly due to taking advantage of the overlapping data, but also to using slightly different processing parameters. A major goal for the processing was to determine if the J1 reflector can be traced to the surface. In spite of detailed velocity analysis and inspection of shot gathers, it was not possible to trace the reflector shallower than about 200 m from the surface. In the reprocessed a section, a reflection (J4) with a similar apparent dip as the J1 reflection and possibly a similar strike was observed. If correctly oriented, it would intersect borehole KFM02A at about 150 m, in a fracture zone. However, this depth also corresponds approximately to the position of the A3 reflector. The J4 orientation is highly speculative and has not been confirmed. However, if correct, the J4 reflector could limit the F1 and A2 reflectors to the south-west.

4.5.3 Profile 5

An interesting point to note on the migrated section of profile 5 (Figures 2-10 and 2-11) is that the A3, A2 and F1 reflectors appear to be faulted with offsets on the order of 10 m to 20 m. F1 also appears to be faulted on the migrated section of profile 2 (Figure 4-9). If real, it may be possible to use 3D reflection seismics to map sub-vertical faults in this area. On the reprocessed northern part of profile 5, a previously unidentified reflection, A8, is indicated. It appears to have a strike and dip similar to the previously identified set A reflections.

4.5.4 Sonic velocity log

Sonic velocities were not calculated properly along two sections of borehole KFM02A. Plotting the sonic waveform data together with the sonic velocity provides a method of control for determining where the sonic log is reliable. The waveform data should be reprocessed and a dependable sonic log be archived in the SKB database, rather than the one that is presently archived.

4.6 Possible future studies

Apart from carrying out a 3D surface seismic survey over the KFM02A borehole, which is probably necessary to fully understand the geometrical relationships between the reflectors and the observations in the borehole and on the surface, there are several smaller studies that could be made:

1. Due to the crooked line acquisition geometry, there is considerable spread in the mid-points from profiles 2 and 5 near the KFM02A borehole (Figure 3-1). This implies that there already is some 3D sub-surface coverage in the area. It may be possible to map the A3, A2 and F1 reflections to limited extent in 3D in this area and tie borehole observations to observations on the CDP stacking lines.
2. A 2D very high resolution (1 m or 2 m station spacing) survey over borehole KFM02A and running in the SW-NE direction may detect the porous granite and allow its lateral dimensions to be estimated. Such a survey would also better tie the borehole observation to the profile 5.
3. Moving source profiling to better image the F1 and A2 reflectors. This could be carried out in conjunction with point 2 above, with simultaneously recording on the surface and in the borehole simultaneously.

5 References

Carlsten S, Petersson J, Stephens M, Mattsson H, Gustafsson J, 2004. Geological single-hole interpretation of KFM02A and HFM04–05 (DS2). Forsmark site investigation. SKB P-04-117, Svensk Kärnbränslehantering AB.

Cosma C, Enescu N, Balu L, 2005. Vertical seismic profiling from the boreholes KFM01A and KFM02A. Forsmark site investigation. SKB P-05-168, Svensk Kärnbränslehantering AB.

Juhlin C, Bergman B, 2004. Reflection seismics in the Forsmark area. Updated interpretation of Stage 1 (previous report R-02-43). Updated estimate of bedrock topography (previous report P-04-99). SKB P-04-158, Svensk Kärnbränslehantering AB.

Juhlin C, Bergman B, Palm H, 2002. Reflection seismic studies in the Forsmark area Stage 1. SKB R-02-43, Svensk Kärnbränslehantering AB.

Juhlin C, Palm H, 2005. Reflection seismic studies in the Forsmark area, 2004 Stage 2. SKB R-05-42, Svensk Kärnbränslehantering AB.

Möller C, Snäll S, Stephens M B, 2003. Dissolution of quartz, vug formation and new grain growth associated with post-metamorphic hydrothermal alteration in KFM02A. Forsmark site investigation. SKB P-03-77, Svensk Kärnbränslehantering AB.

Correlation of 2D surface seismic, vertical seismic profile (VSP), and geological and sonic data in boreholes KFM01A and KFM02A, Forsmark: Background analysis

Nicoleta Enescu, Calin Cosma
Vibrometric AB

Contents

1 Aims of the study

The purpose of this work was to:

- Refine the vertical seismic profile (VSP) results from boreholes KFM01A and KFM02A at Forsmark /Cosma et al. 2005/.
- Attempt to correlate these results with the 2D surface seismic as well as the geological and sonic wave data in each borehole, as inferred from the respective single-hole interpretations /Carlsten et al. 2004ab/.

The work involved an analysis and an integration of the VSP data with the 2D surface seismic and geological and sonic wave data from the two boreholes. The results of the correlation work are presented in tabular format in this report. They form a basis for a broader evaluation that is presented in section 3.10.3 in the main stage 2.2 geological report /Stephens et al. 2007/.

2 Background data

In this study, VSP measurements and interpreted results from boreholes KFM01A and KFM02A at Forsmark /Cosma et al. 2005/ were used together with depth migrated sections of 2D reflection seismic profiles along lines 1, 2, 4 and 5 (Figure 2-1; see /Juhlin et al. 2002, Juhlin and Bergman 2004/) and the single-hole interpretations of geological and geophysical data in these two boreholes in the form of Well-Cad plots /Carlsten et al. 2004ab/. Full wave sonic data from the two boreholes were also evaluated, but were not used to aid the refined interpretation produced by this study.

Profile 5 was projected along the line of profile 5b, to produce one profile along a straight line. Furthermore, profiles 2 and 2b were merged into one longer profile. The resulting geometry is shown in Figure 2-2.

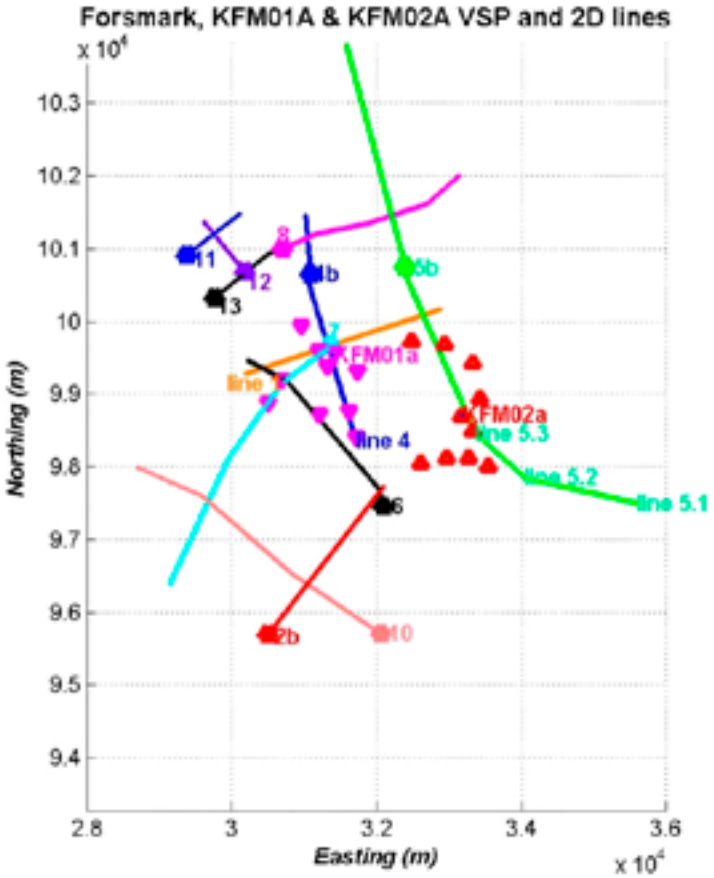

Figure 2-1. *Location of the measured 2D seismic reflection profiles, boreholes KFM01A and KFM02A, and the VSP shot points. View from top.*

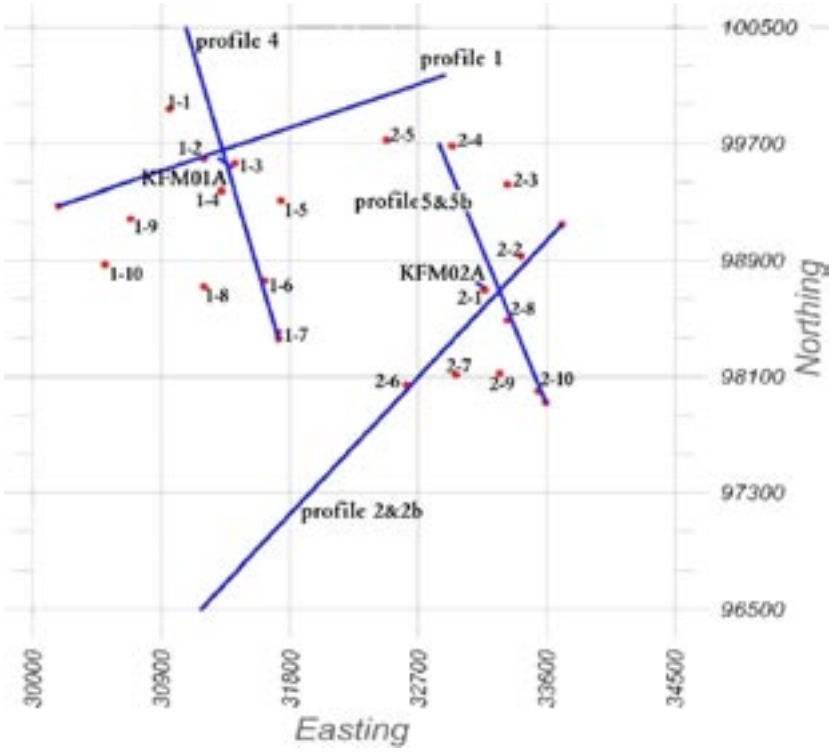

Figure 2-2. *Location of profiles 1, 2, 4 and 5 for which the 2D depth migrated profiles have been used in this interpretation, boreholes KFM01A and KFM02A, and the VSP shot points. View from top.*

3 Refined interpretation of the VSP data, in relation to 2D seismic profiles 1, 2, 4 and 5 and the single-hole interpretations for KFM01A and KFM02A

The figures below show the interpreted reflectors along the VSP profiles from KFM01A (Figures 3-1 to 3-4) and KFM02A (Figures 3-5 to 3-8), and along the 2D depth migrated profiles along lines 1, 2, 4 and 5 (Figures 3-9 to 3-12). Average values for the parameters that determine each interpreted reflector (49) are presented in Table 3-1 and the results are visualized in Figures 3-13 to 3-19. An average set of parameters were computed for the VSP profiles measured in the same borehole, generating in this way only one set of reflector parameter values for each borehole. The detailed list of parameters is provided in Appendix 1.

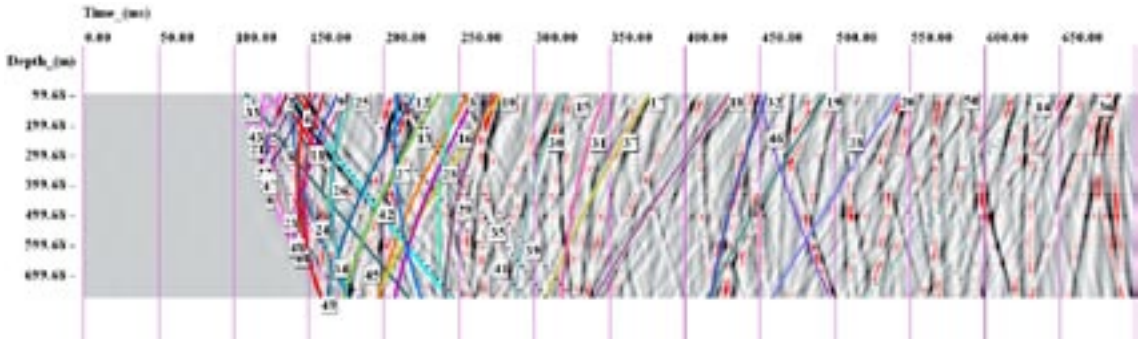

Figure 3-1. *VSP profile from SP01 close to KFM01A, with interpreted reflector events.*

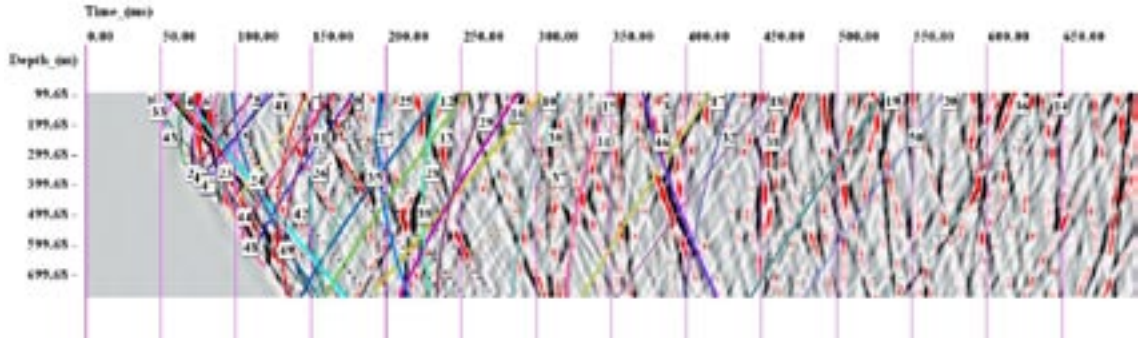

Figure 3-2. *VSP profile from SP02 close to KFM01A, with interpreted reflector events.*

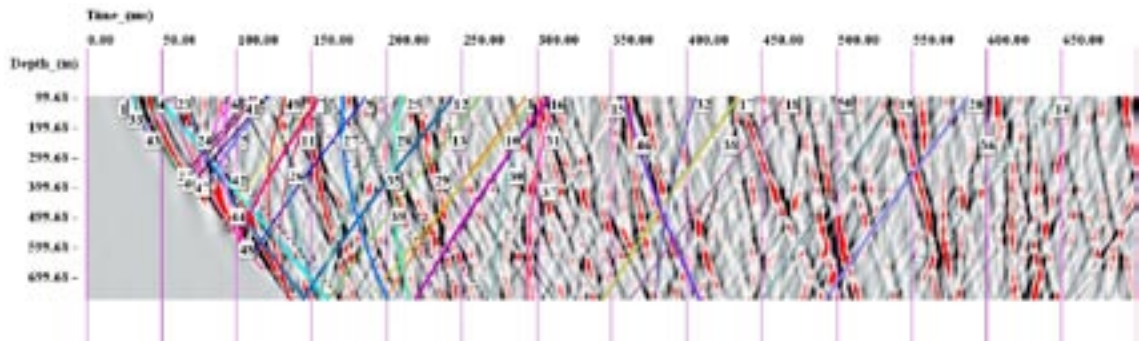

Figure 3-3. *VSP profile from SP03 close to KFM01A, with interpreted reflector events.*

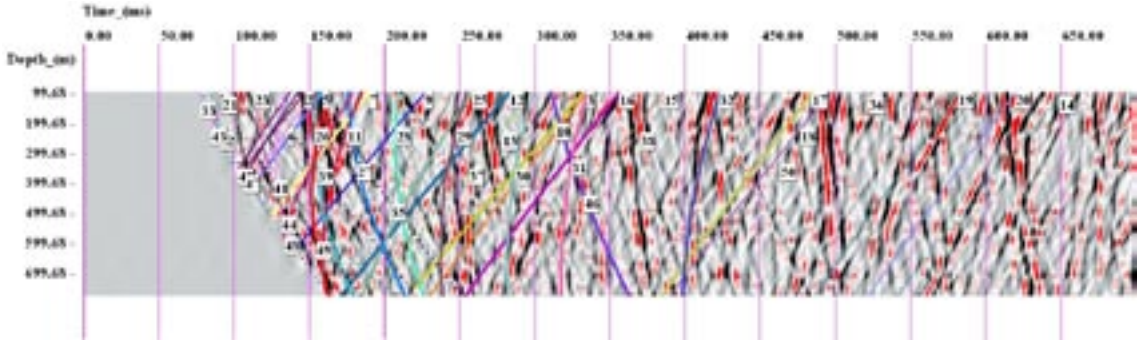

Figure 3-4. *VSP profile from SP05 close to KFM01A, with interpreted reflector events.*

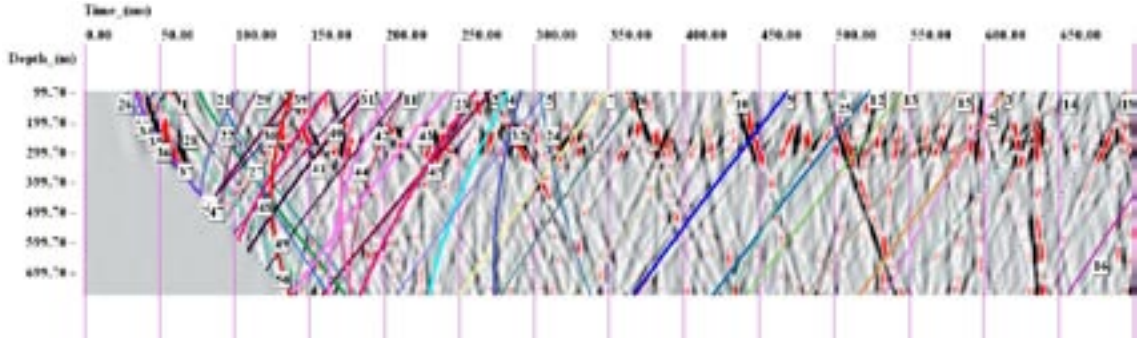

Figure 3-5. *VSP profile from SP01 close to KFM02A, with interpreted reflector events.*

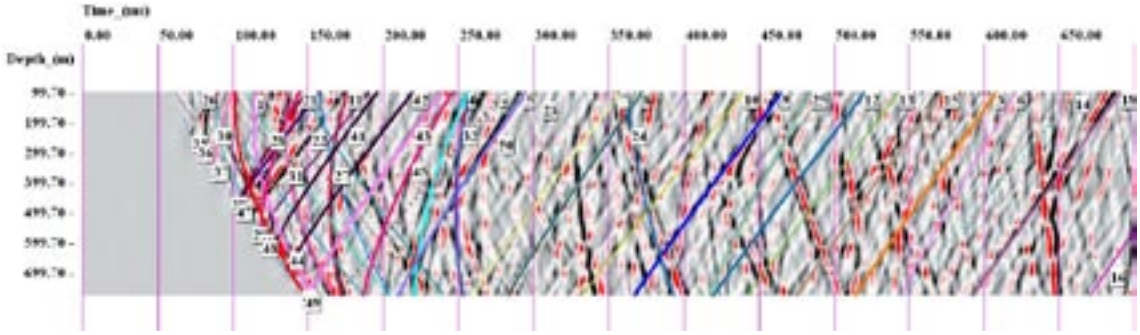

Figure 3-6. *VSP profile from SP02 close to KFM02A, with interpreted reflector events.*

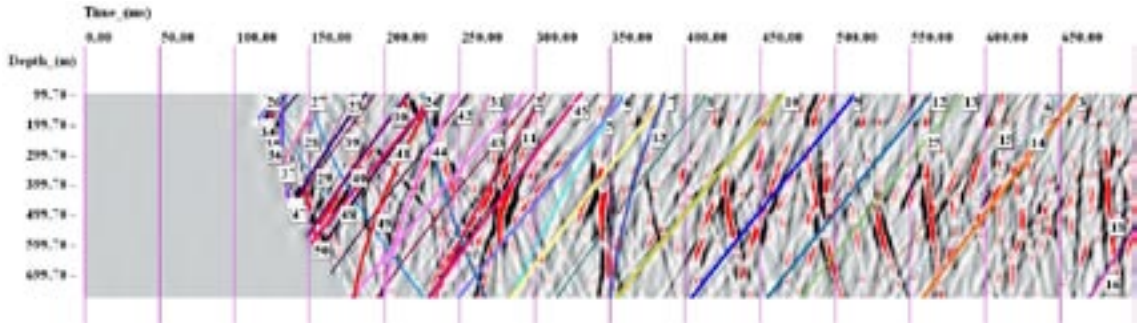

Figure 3-7. *VSP profile from SP07 close to KFM02A, with interpreted reflector events.*

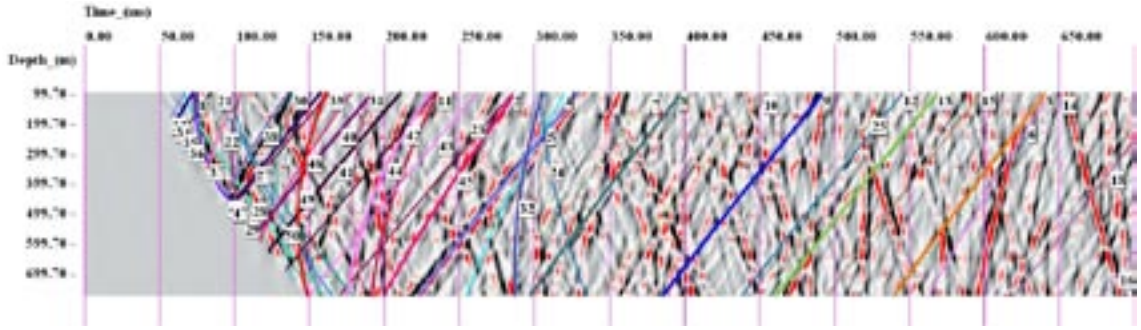

Figure 3-8. *VSP profile from SP08 close to KFM02A, with interpreted reflector events.*

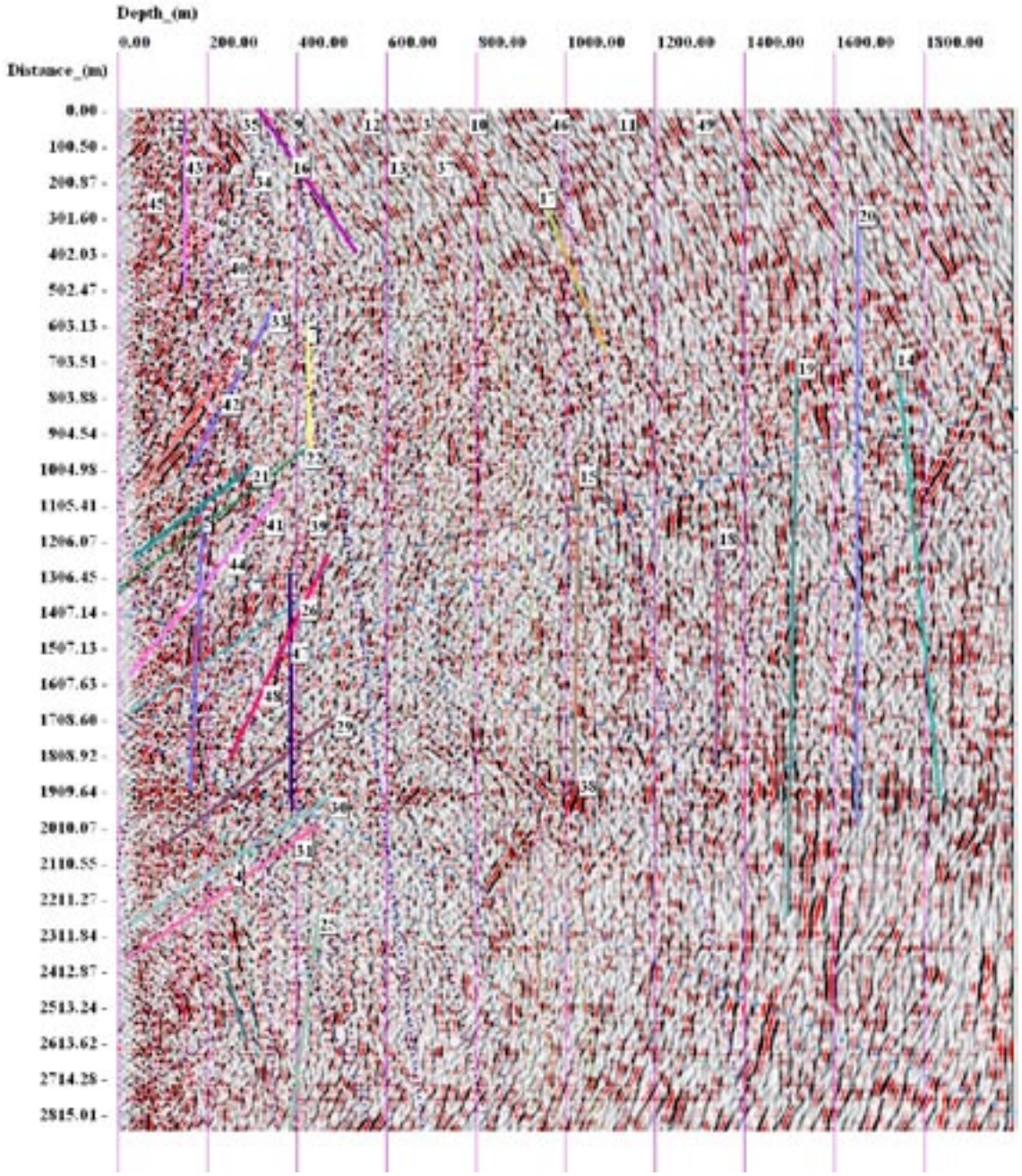

Figure 3-9. *2D depth migrated seismic profile along line 1, with interpreted reflector events.*

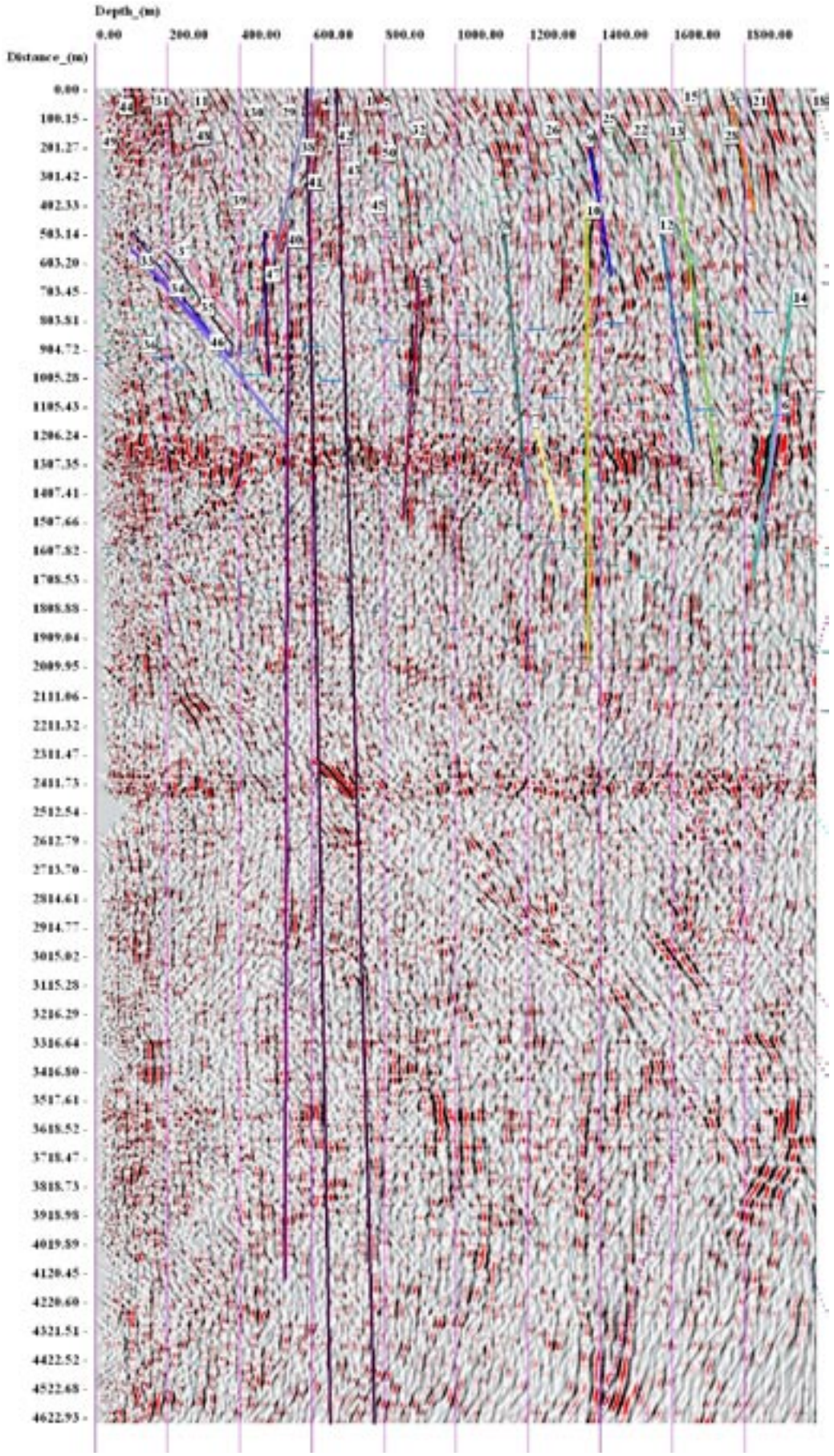

Figure 3-10. *2D depth migrated seismic profile along line 2, with interpreted reflector events.*

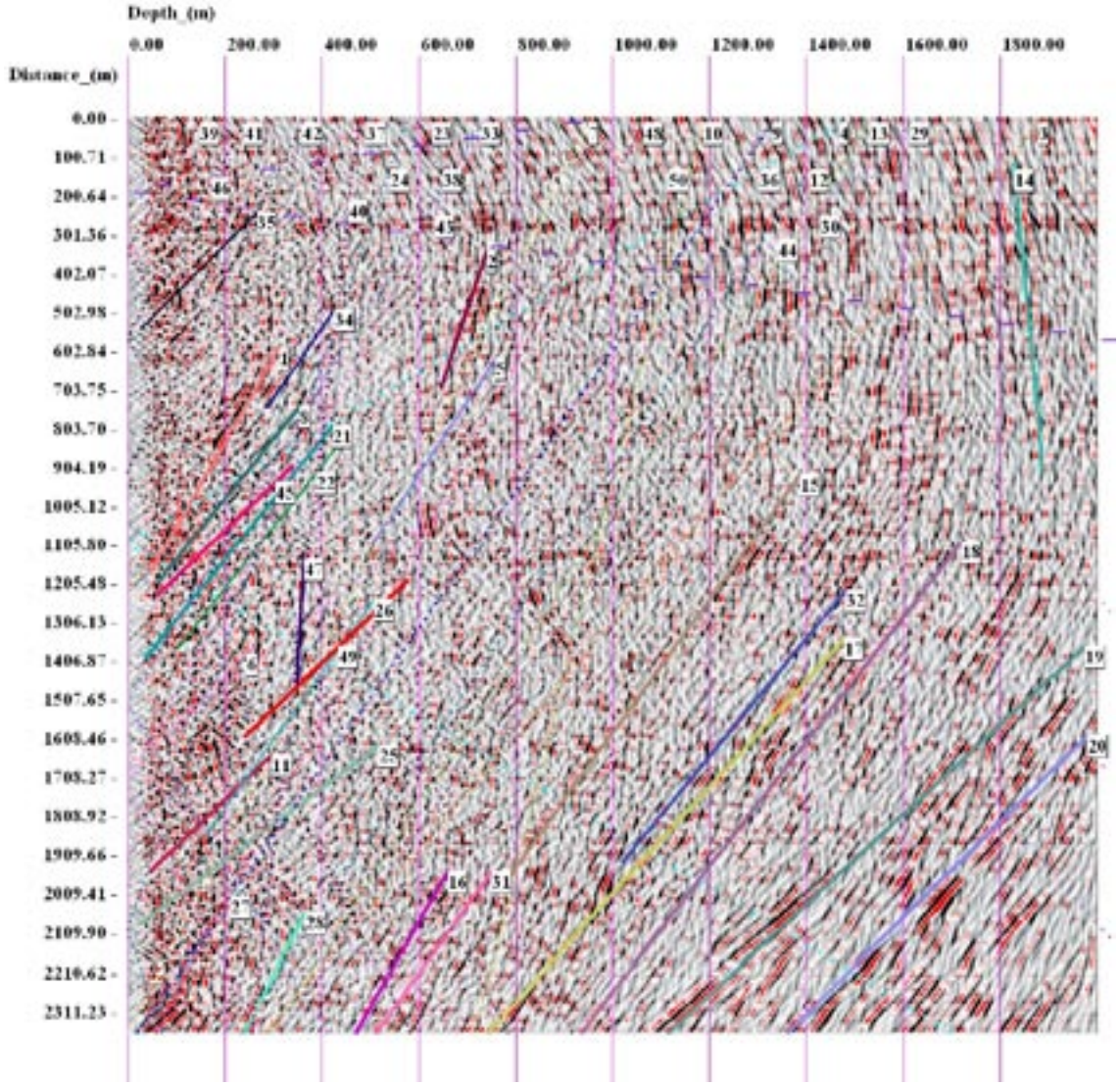

Figure 3-11. *2D depth migrated seismic profile along line 4, with interpreted reflector events.*

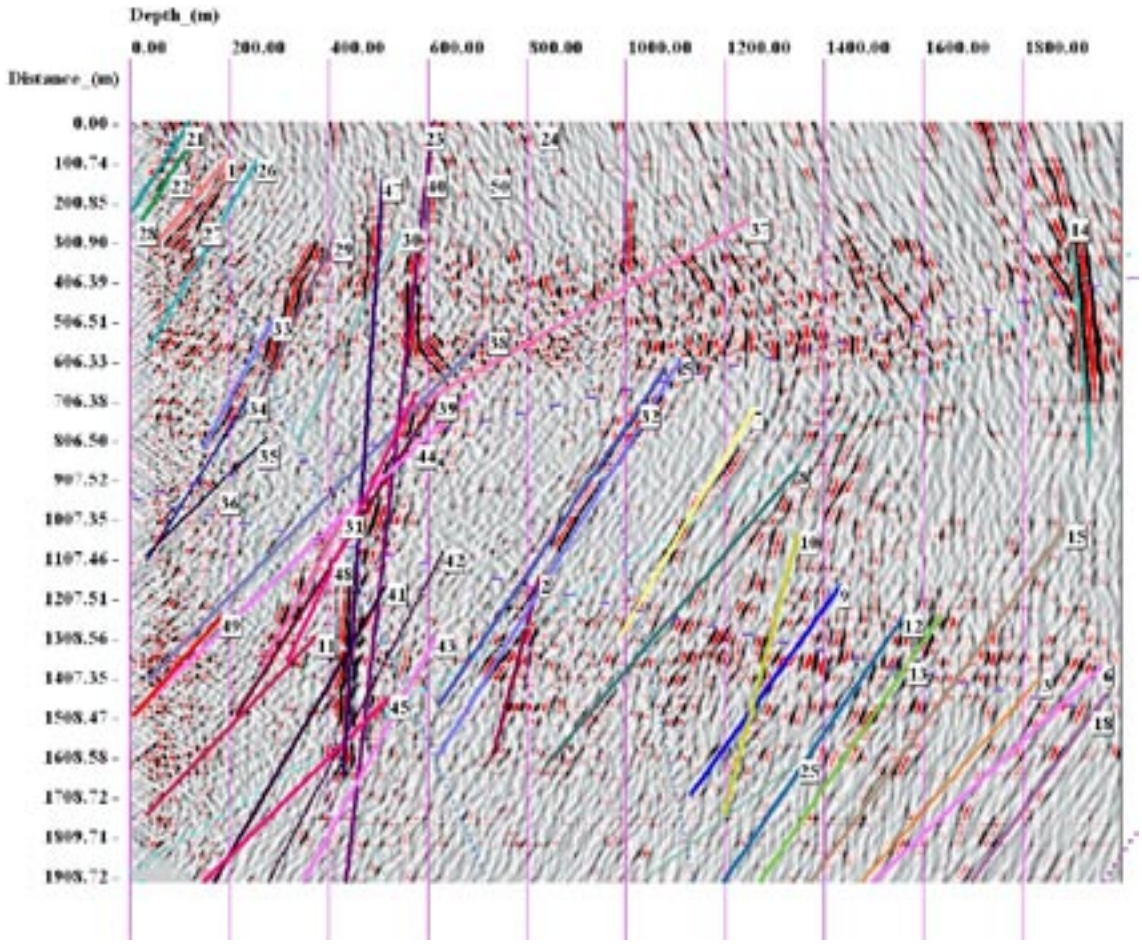

Figure 3-12. *2D depth migrated seismic profile along line 5, with interpreted reflector events.*

Table 3-1. Average parameters of the VSP reflectors interpreted from boreholes KFM01A and KFM02A. For the VSP profiles, *Depth (m)* is calculated from the top of the hole along an imaginary line along the hole. Similarly, for the 2D profiles, *Distance (m)* is calculated from the first receiver in the profile, along an imaginary line along the receiver line. The points at *Depth (Distance)* along these lines are the intersection points between the reflector (or its extension) and the line. The *Depth (Distance)* values are significant for reflectors physically intersecting the boreholes. The *Dip (°)* is calculated from horizontal. The *Azimuth (°)* is calculated from North. *Dip Direction (°)* is Azimuth +180° (modulo 360°). The coordinates of the Crux point are calculated with respect to a common origin (99000.0 33000.0 0.0). All coordinates are given in a reduced form. These translate to site coordinates by 6600000 on the Northing and 1600000 on the Easting. The *Profile* column specifies the 2D profile or borehole where the reflector parameters were estimated.

VSP reflector no.	Depth/ Distance (m)	Dip (°)	Dip Dir (°)	Azimuth (°)	Northing Crux (m)	Easting Crux (m)	Elev Crux (m)	Profile
1	1,150.0	40.0	213.0	33.0	98860.2	32909.2	198.7	P1_depth
1	1,282.9	40.0	213.0	33.0	98860.2	32909.2	198.7	P4_depth
1	385.0	35.5	171.6	351.6	98741.0	33038.5	367.6	P5_depth
2	16,443.2	15.0	121.0	301.0	99106.7	32822.4	–773.2	P2_depth
2	3,131.4	16.0	142.0	322.0	99192.1	32849.9	–850.3	P4_depth
2	5,152.8	14.0	124.0	304.0	99105.2	32844.0	–754.8	P5_depth
2	380.2	15.0	121.0	301.0	99106.7	32822.4	–773.2	KFM01A
2	850.0	18.0	125.0	305.0	99128.5	32816.4	–689.7	KFM02A

VSP reflector no.	Depth/ Distance (m)	Dip (°)	Dip Dir (°)	Azimuth (°)	Northing Crux (m)	Easting Crux (m)	Elev Crux (m)	Profile
3	–10,238.0	35.1	150.8	330.8	99806.6	32549.4	–1,312.8	P2_depth
3	4,042.7	35.1	150.8	330.8	99806.6	32549.4	–1,312.8	P5_depth
3	1,005.8	35.1	150.8	330.8	99806.6	32549.4	–1,312.8	KFM01A
3	2,100.0	35.1	150.8	330.8	99806.6	32549.4	–1,312.8	KFM02A
4	–122.2	54.0	170.0	350.0	99447.4	32921.1	–330.1	KFM01A
4	1,300.0	53.0	170.0	350.0	99457.8	32919.3	–350.3	KFM02A
5	6,145.6	27.5	166.5	346.5	99298.4	32928.4	–589.6	P1_depth
5	2,064.7	28.0	170.0	350.0	99357.6	32936.9	–682.9	P4_depth
5	2,881.7	27.0	172.0	352.0	99334.3	32953.0	–662.6	P5_depth
5	434.6	28.0	170.0	350.0	99357.6	32936.9	–682.9	KFM01A
5	1,025.0	29.0	170.0	350.0	99363.4	32935.9	–665.7	KFM02A
6	16,888.4	50.0	124.8	304.8	99715.3	31968.9	–1,053.0	P2_depth
6	3,691.1	50.2	124.5	304.5	99672.6	32021.7	–987.4	P5_depth
6	420.0	49.8	125.2	305.2	99679.3	32035.4	–998.3	KFM01A
6	2,496.4	49.8	125.2	305.2	99679.3	32035.4	–998.3	KFM02A
7	–33,172.7	25.0	160.0	340.0	99371.6	32864.8	–847.9	P1_depth
7	–5,240.6	25.0	160.0	340.0	99371.6	32864.8	–847.9	P2_depth
7	3,432.1	25.0	160.0	340.0	99371.6	32864.8	–847.9	P5_depth
7	524.0	25.0	160.0	340.0	99371.6	32864.8	–847.9	KFM01A
7	1,162.6	35.0	155.0	335.0	99414.9	32806.5	–653.9	KFM02A
8	1,318.4	36.0	140.0	320.0	99406.0	32659.4	–729.4	P1_depth
8	–17,180.4	36.0	140.0	320.0	99406.0	32659.4	–729.4	P2_depth
8	1,300.8	36.0	140.0	320.0	99406.0	32659.4	–729.4	P4_depth
8	2,867.5	36.0	140.0	320.0	99406.0	32659.4	–729.4	P5_depth
8	70.5	36.0	140.0	320.0	99406.0	32659.4	–729.4	KFM01A
8	1,290.0	36.0	140.0	320.0	99406.0	32659.4	–729.4	KFM02A
9	–9,484.1	30.0	150.0	330.0	99526.0	32696.3	–1,052.0	P2_depth
9	3,687.0	30.0	150.0	330.0	99526.0	32696.3	–1,052.0	P5_depth
9	636.0	30.0	150.0	330.0	99526.0	32696.3	–1,052.0	KFM01A
9	1,541.7	30.0	150.0	330.0	99526.0	32696.3	–1,052.0	KFM02A
10	–322,206.0	12.9	134.8	314.8	99200.6	32798.0	–1,240.0	P2_depth
10	7,427.0	12.9	134.8	314.8	99200.6	32798.0	–1,240.0	P5_depth
10	940.4	23.0	135.0	315.0	99413.5	32586.5	–1,377.6	KFM01A
10	1,366.6	23.0	134.8	314.8	99320.7	32677.2	–1,072.0	KFM02A
11	2,010.0	52.0	199.0	19.0	99359.3	33123.7	–296.9	P4_depth
11	1,800.0	53.0	198.0	18.0	99317.7	33103.2	–251.7	P5_depth
11	775.0	53.1	198.9	18.9	99355.7	33121.7	–281.8	KFM01A
11	1,060.0	54.0	198.0	18.0	99347.2	33112.8	–265.3	KFM02A
12	–12,755.6	28.8	147.9	327.9	99562.6	32646.4	–1,207.6	P2_depth
12	4,140.7	28.8	147.9	327.9	99562.6	32646.4	–1,207.6	P5_depth
12	808.0	28.8	147.9	327.9	99562.6	32646.4	–1,207.6	KFM01A
12	1,698.3	28.8	147.9	327.9	99562.6	32646.4	–1,207.6	KFM02A
13	–14,105.1	29.0	147.0	327.0	99586.4	32619.2	–1,261.4	P2_depth
13	4,267.8	29.0	147.0	327.0	99586.4	32619.2	–1,261.4	P5_depth
13	865.0	29.0	147.0	327.0	99586.4	32619.2	–1,261.4	KFM01A
13	1,771.0	29.0	147.0	327.0	99586.4	32619.2	–1,261.4	KFM02A
14	–22,300.0	6.0	28.0	208.0	98834.1	32911.8	–1,787.6	P1_depth

VSP reflector no.	Depth/ Distance (m)	Dip (°)	Dip Dir (°)	Azimuth (°)	Northing Crux (m)	Easting Crux (m)	Elev Crux (m)	Profile
14	18,847.9	6.3	30.1	210.1	98816.3	32893.7	–1,933.9	P2_depth
14	–24,340.9	6.3	30.1	210.1	98816.3	32893.7	–1,933.9	P4_depth
14	–28,500.0	6.3	30.1	210.1	98816.3	32893.7	–1,933.9	P5_depth
15	89,382.4	30.0	163.1	343.1	99758.9	32768.7	–1,374.2	P1_depth
15	–6,475.7	30.0	163.0	343.0	99740.6	32773.6	–1,341.4	P2_depth
15	3,330.0	30.0	163.0	343.0	99740.6	32773.6	–1,341.4	P4_depth
15	4,322.2	30.0	163.0	343.0	99740.6	32773.6	–1,341.4	P5_depth
15	1,161.9	30.0	163.0	343.0	99740.6	32773.6	–1,341.4	KFM01A
15	1,920.1	31.0	161.0	341.0	99745.1	32743.5	–1,311.4	KFM02A
16	–582.4	40.0	113.7	293.7	99519.2	31817.7	–1,537.4	P1_depth
16	3,389.5	40.0	113.7	293.7	99519.2	31817.7	–1,537.4	P4_depth
16	1,090.0	40.0	113.7	293.7	99519.2	31817.7	–1,537.4	KFM01A
16	2,659.5	40.0	113.7	293.7	99519.2	31817.7	–1,537.4	KFM02A
17	–2,686.3	42.1	134.3	314.3	100081.0	31892.1	–1,713.7	P1_depth
17	3,392.6	42.1	134.3	314.3	100081.0	31892.1	–1,713.7	P4_depth
17	1,551.0	42.1	134.3	314.3	100081.0	31892.1	–1,713.7	KFM01A
18	152,120.0	32.0	162.7	342.7	99980.5	32694.1	–1,643.8	P1_depth
18	3,881.9	31.8	162.7	342.7	99966.9	32698.4	–1,636.7	P4_depth
18	4,883.5	30.0	162.7	342.7	99872.9	32727.7	–1,583.8	P5_depth
18	1,518.9	31.0	162.7	342.7	99927.3	32710.7	–1,615.4	KFM01A
18	2,320.7	31.0	162.7	342.7	99927.3	32710.7	–1,615.4	KFM02A
19	110,795.0	40.8	162.9	342.9	100399.0	32570.2	–1,697.4	P1_depth
19	3,662.4	40.8	162.9	342.9	100399.0	32570.2	–1,697.4	P4_depth
19	1,940.4	40.8	162.9	342.9	100399.0	32570.2	–1,697.4	KFM01A
20	850,420.0	37.7	161.9	341.9	100368.0	32552.8	–1,860.2	P1_depth
20	4,049.7	39.0	161.9	341.9	100447.0	32526.9	–1,879.9	P4_depth
20	2,032.5	39.0	161.9	341.9	100403.0	32541.2	–1,823.1	KFM01A
21	1,285.4	63.0	216.3	36.3	98747.0	32814.3	159.9	P1_depth
21	1,458.7	66.0	217.0	37.0	98721.4	32790.1	155.3	P4_depth
21	233.5	64.2	216.3	36.3	98741.9	32810.5	155.1	P5_depth
21	265.5	64.2	216.3	36.3	98741.9	32810.5	155.1	KFM01A
21	–571.7	64.2	216.3	36.3	98741.9	32810.5	155.1	KFM02A
22	1,344.4	63.1	216.6	36.6	98771.8	32830.3	144.1	P1_depth
22	1,541.2	63.1	216.6	36.6	98771.8	32830.3	144.1	P4_depth
22	297.0	63.1	216.6	36.6	98771.8	32830.3	144.1	P5_depth
22	350.9	63.1	216.6	36.6	98771.8	32830.3	144.1	KFM01A
22	–472.3	63.1	216.6	36.6	98771.8	32830.3	144.1	KFM02A
23	675.6	70.0	233.8	53.8	98597.8	32450.9	247.1	KFM01A
24	2,809.5	82.2	237.7	57.7	98548.2	32285.6	116.1	KFM01A
24	–16,389.5	84.0	237.8	57.8	98532.9	32257.1	93.0	KFM02A
25	6,515.0	47.3	169.9	349.9	99903.3	32839.8	–845.8	P1_depth
25	–2,840.9	47.3	169.9	349.9	99903.3	32839.8	–845.8	P2_depth
25	2,113.0	47.3	169.9	349.9	99903.3	32839.8	–845.8	P4_depth
25	2,931.3	47.3	169.9	349.9	99903.3	32839.8	–845.8	P5_depth
25	882.5	47.3	169.9	349.9	99903.3	32839.8	–845.8	KFM01A
25	2,068.8	47.3	169.9	349.9	99903.3	32839.8	–845.8	KFM02A
26	1,713.7	65.0	220.0	40.0	98912.0	32926.1	53.6	P1_depth

VSP reflector no.	Depth/ Distance (m)	Dip (°)	Dip Dir (°)	Azimuth (°)	Northing Crux (m)	Easting Crux (m)	Elev Crux (m)	Profile
26	2,141.3	65.0	220.0	40.0	98912.0	32926.1	53.6	P4_depth
26	660.4	65.0	220.0	40.0	98912.0	32926.1	53.6	P5_depth
26	1,086.9	65.0	220.0	40.0	98912.0	32926.1	53.6	KFM01A
26	–73.0	65.0	220.0	40.0	98912.0	32926.1	53.6	KFM02A
27	3,037.3	78.3	226.2	46.2	98826.3	32818.9	52.1	KFM01A
27	–12,550.0	86.7	228.1	48.1	98779.6	32754.1	19.2	KFM02A
28	2,955.1	69.2	229.3	49.3	98891.7	32874.1	63.0	P4_depth
28	2,026.2	69.2	229.3	49.3	98891.7	32874.1	63.0	KFM01A
28	–404.2	69.2	229.3	49.3	98891.7	32874.1	63.0	KFM02A
29	2,163.2	56.0	223.0	43.0	99090.5	33084.4	–83.4	P1_depth
29	1,430.5	56.0	223.0	43.0	99102.9	33096.0	–94.9	P5_depth
29	1,520.0	58.9	221.7	41.7	99113.8	33101.3	–92.0	KFM01A
29	533.2	58.9	221.7	41.7	99113.8	33101.3	–92.0	KFM02A
30	2,305.3	63.0	223.3	43.3	99172.2	33162.4	–120.6	P1_depth
30	1,670.0	63.0	223.0	43.0	99176.0	33164.1	–122.6	P5_depth
30	1,961.0	61.3	223.3	43.3	99167.0	33157.5	–125.5	KFM01A
30	750.0	58.0	223.0	43.0	99186.3	33173.7	–159.1	KFM02A
31	2,400.0	62.0	220.0	40.0	99265.4	33222.7	–184.2	P1_depth
31	3,255.0	66.0	220.0	40.0	99300.9	33252.5	–174.9	P4_depth
31	1,985.0	62.0	220.0	40.0	99277.9	33233.2	–192.9	P5_depth
31	2,360.0	64.2	220.1	40.1	99289.7	33243.6	–183.3	KFM01A
31	1,251.6	63.0	220.1	40.1	99302.9	33254.8	–201.7	KFM02A
32	3,490.9	65.0	216.0	36.0	99559.7	33406.6	–322.6	P4_depth
32	2,640.0	66.0	216.0	36.0	99571.8	33415.4	–314.7	P5_depth
32	2,970.0	65.0	216.0	36.0	99559.7	33406.6	–322.6	KFM01A
32	2,169.2	66.0	216.0	36.0	99538.0	33390.9	–296.1	KFM02A
33	1,396.9	35.0	203.6	23.6	99018.3	33008.0	–28.5	P1_depth
33	376.3	35.0	203.6	23.6	99018.3	33008.0	–28.5	P2_depth
33	1,172.9	35.0	203.6	23.6	99018.3	33008.0	–28.5	P5_depth
33	151.9	35.0	203.6	23.6	99018.3	33008.0	–28.5	KFM01A
33	185.0	35.0	203.6	23.6	99018.3	33008.0	–28.5	KFM02A
34	327.1	35.5	197.8	17.8	99018.7	33006.0	–27.5	P2_depth
34	1,281.0	35.5	197.8	17.8	99018.7	33006.0	–27.5	P4_depth
34	1,186.6	35.5	197.8	17.8	99018.7	33006.0	–27.5	P5_depth
34	205.0	35.5	197.8	17.8	99018.7	33006.0	–27.5	KFM02A
35	210.0	42.5	180.0	0.0	98996.5	33000.0	3.9	P2_depth
35	582.7	40.0	178.0	358.0	98988.8	33000.4	13.3	P4_depth
35	1,142.4	42.5	178.0	358.0	98987.7	33000.4	13.5	P5_depth
35	245.0	42.5	178.0	358.0	98987.7	33000.4	13.5	KFM02A
36	1,184.7	66.0	108.9	288.9	98966.9	33096.7	45.5	P2_depth
36	1,182.9	66.0	108.9	288.9	98966.9	33096.7	45.5	P5_depth
36	275.9	66.0	108.9	288.9	98966.9	33096.7	45.5	KFM02A
37	137.6	57.0	170.0	350.0	98957.1	33007.6	28.3	P2_depth
37	1,127.3	57.0	170.0	350.0	98957.1	33007.6	28.3	P5_depth
37	370.4	57.0	170.0	350.0	98957.1	33007.6	28.3	KFM02A
38	3,338.6	48.5	120.0	300.0	99071.1	32876.9	–126.0	P2_depth
38	1,462.3	48.5	122.7	302.7	99037.7	32941.1	–62.0	P5_depth

VSP reflector no.	Depth/ Distance (m)	Dip (°)	Dip Dir (°)	Azimuth (°)	Northing Crux (m)	Easting Crux (m)	Elev Crux (m)	Profile
38	452.3	48.5	122.7	302.7	99037.7	32941.1	–62.0	KFM02A
39	1,932.9	28.0	140.5	320.5	99109.4	32909.8	–266.8	P5_depth
39	482.1	26.7	140.5	320.5	99099.9	32917.6	–258.0	KFM02A
40	220,236.0	5.8	132.3	312.3	99033.3	32963.4	–491.6	P2_depth
40	6,725.8	5.8	132.0	312.0	99033.0	32963.3	–490.1	P5_depth
40	369.1	6.2	132.3	312.3	99038.6	32957.6	–528.9	KFM01A
40	575.2	6.2	132.3	312.3	99038.6	32957.6	–528.9	KFM02A
41	–41,478.3	26.0	135.6	315.6	99130.1	32872.5	–373.5	P2_depth
41	2,293.5	26.9	135.6	315.6	99138.3	32864.5	–382.2	P5_depth
41	631.1	26.9	135.6	315.6	99138.3	32864.5	–382.2	KFM02A
42	–29,256.1	24.6	136.9	316.9	99155.6	32854.3	–466.4	P2_depth
42	2,586.2	24.6	136.9	316.9	99155.6	32854.3	–466.4	P5_depth
42	699.2	24.6	136.9	316.9	99155.6	32854.3	–466.4	KFM02A
43	118,385.0	23.3	161.9	341.9	99227.5	32925.7	–554.7	P1_depth
43	2,741.9	23.3	161.9	341.9	99227.5	32925.7	–554.7	P5_depth
43	220.8	23.3	161.9	341.9	99227.5	32925.7	–554.7	KFM01A
43	789.1	23.3	161.9	341.9	99227.5	32925.7	–554.7	KFM02A
44	1,627.8	61.6	200.2	20.2	99219.1	33080.5	–126.4	P1_depth
44	1,511.6	61.6	200.2	20.2	99219.1	33080.5	–126.4	P5_depth
44	624.8	61.6	200.2	20.2	99219.1	33080.5	–126.4	KFM01A
44	936.0	61.6	200.2	20.2	99219.1	33080.5	–126.4	KFM02A
45	1,312.7	40.0	170.2	350.2	99364.9	32936.8	–441.3	P4_depth
45	2,110.8	40.0	170.2	350.2	99364.9	32936.8	–441.3	P5_depth
45	981.9	40.0	170.2	350.2	99364.9	32936.8	–441.3	KFM02A
46	421.4	82.0	170.5	350.5	98780.6	33036.9	31.1	P2_depth
46	–4,089.6	81.8	170.0	350.0	98768.6	33040.8	34.1	KFM01A
46	463.4	82.0	170.5	350.5	98780.6	33036.9	31.1	KFM02A
47	–88,699.9	3.0	157.0	337.0	99021.8	32990.7	–452.0	P1_depth
47	–22,256.7	3.0	157.0	337.0	99021.8	32990.7	–452.0	P2_depth
47	8,782.9	2.8	157.0	337.0	99018.3	32992.2	–414.5	P4_depth
47	9,888.0	3.0	157.0	337.0	99021.8	32990.7	–452.0	P5_depth
47	399.6	3.0	157.0	337.0	99021.8	32990.7	–452.0	KFM01A
47	478.7	3.0	157.0	337.0	99021.8	32990.7	–452.0	KFM02A
48	2,472.0	31.7	204.7	24.7	99191.3	33088.0	–340.4	P1_depth
48	2,206.1	31.7	204.7	24.7	99191.3	33088.0	–340.4	P5_depth
48	586.8	31.7	204.7	24.7	99191.3	33088.0	–340.4	KFM01A
48	595.2	31.7	204.7	24.7	99191.3	33088.0	–340.4	KFM02A
49	1,896.3	59.0	205.0	25.0	99196.9	33091.8	–130.5	P4_depth
49	1,517.0	59.0	205.0	25.0	99196.9	33091.8	–130.5	P5_depth
49	797.4	59.0	205.0	25.0	99196.9	33091.8	–130.5	KFM01A
49	808.0	59.0	205.0	25.0	99196.9	33091.8	–130.5	KFM02A

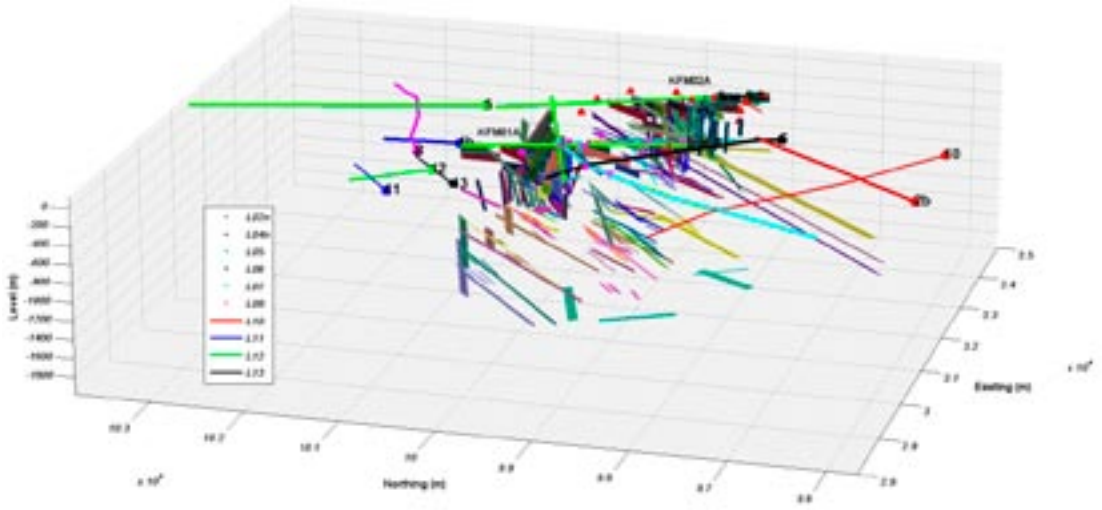

Figure 3-13. *Interpreted 3D reflector elements from the VSP (KFM01A and KFM02A) and surface reflection seismic data (lines 1, 2, 4 and 5). 3D perspective view from south-east.*

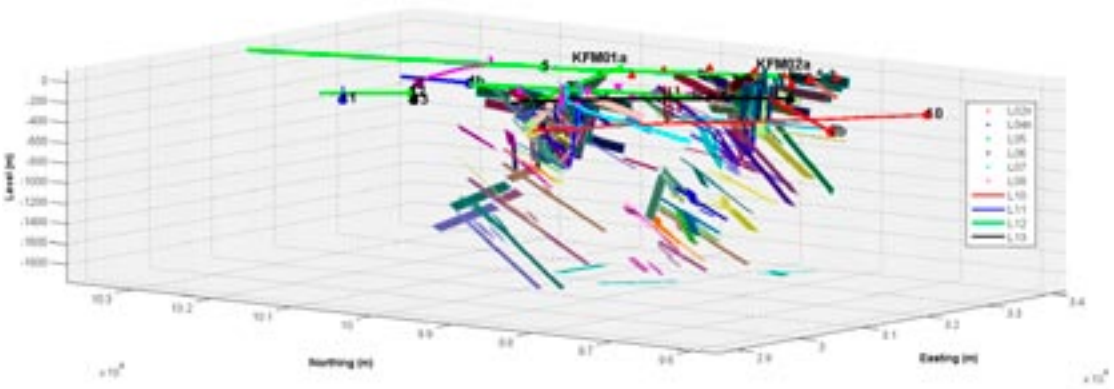

Figure 3-14. *Same as Figure 3-13. 3D orthographic projection, view from south-east.*

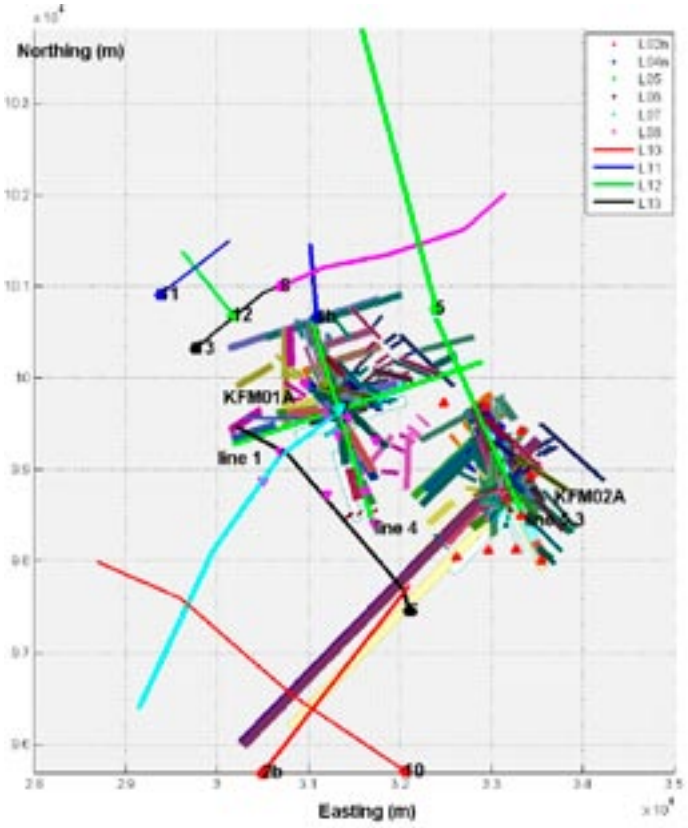

Figure 3-15. *Same as Figure 3-13. 2D view from top.*

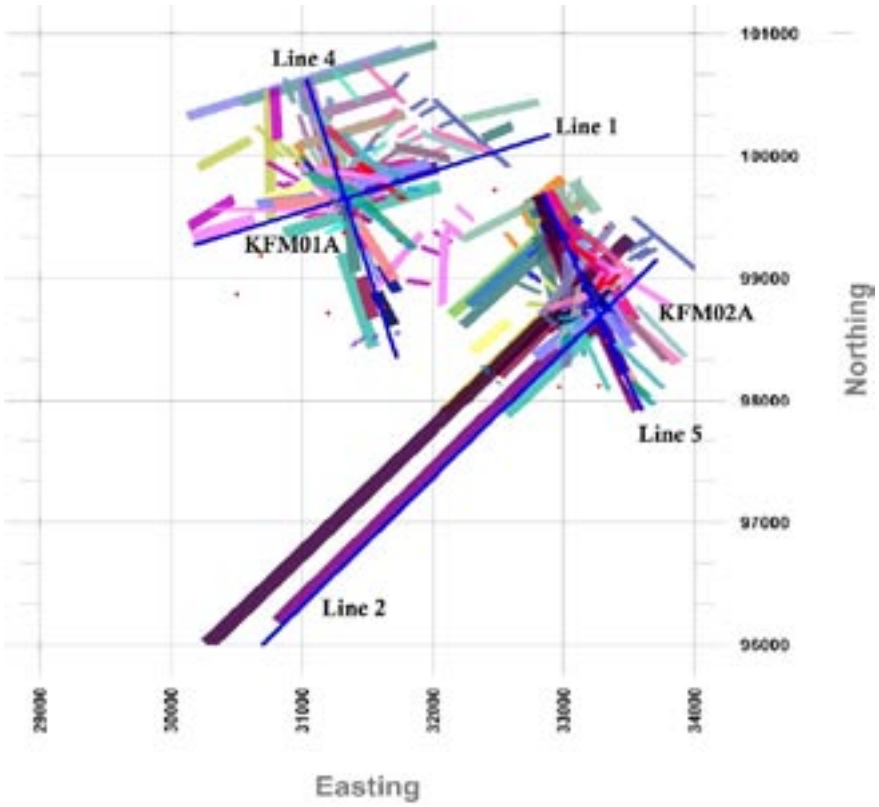

Figure 3-16. *Same as Figure 3-13. 2D more detailed view from top.*

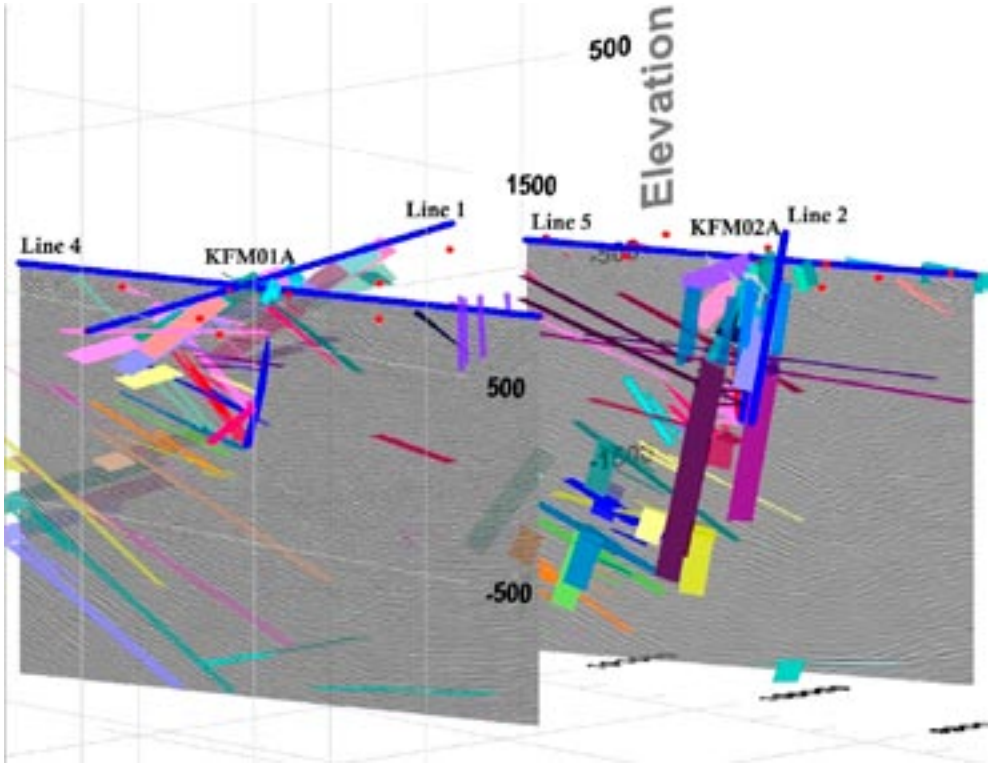

Figure 3-17. *Interpreted 3D reflector elements from the VSP (KFM01A and KFM02A) and surface reflection seismic data (lines 1, 2, 4 and 5), together with migrated profiles from lines 2 and 4. View from north-west.*

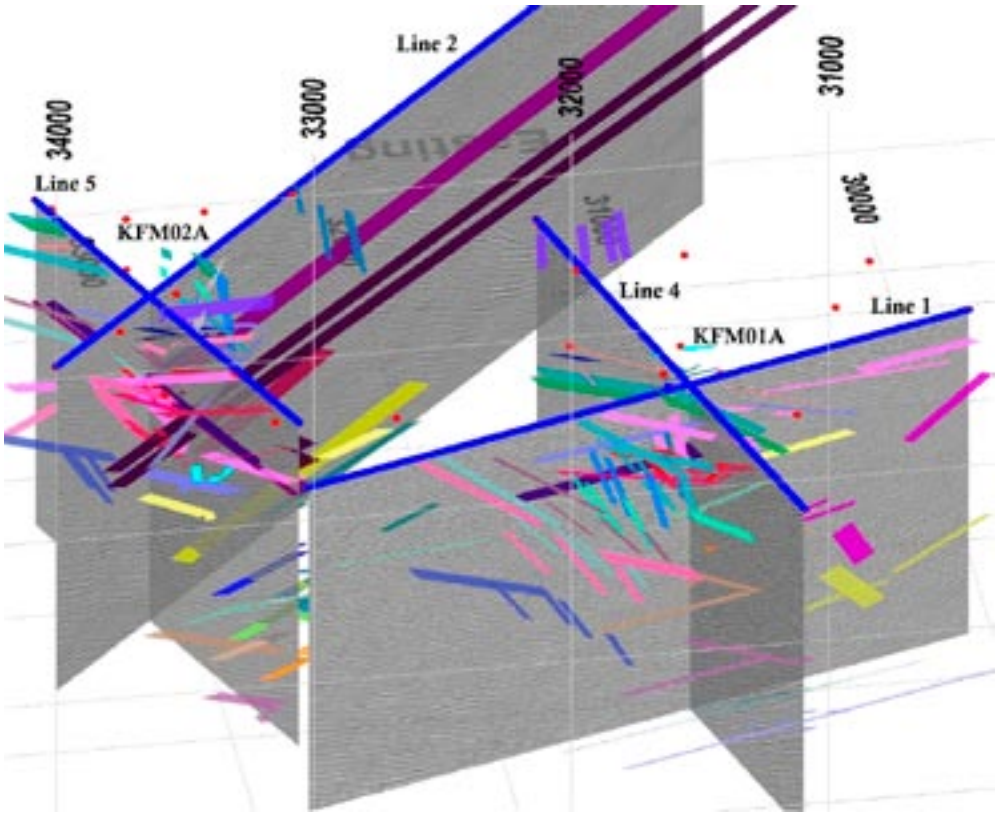

Figure 3-18. *Interpreted 3D reflector elements from the VSP (KFM01A and KFM02A) and surface reflection seismic data (lines 1, 2, 4 and 5), together with migrated profiles from all four lines. View from north-east.*

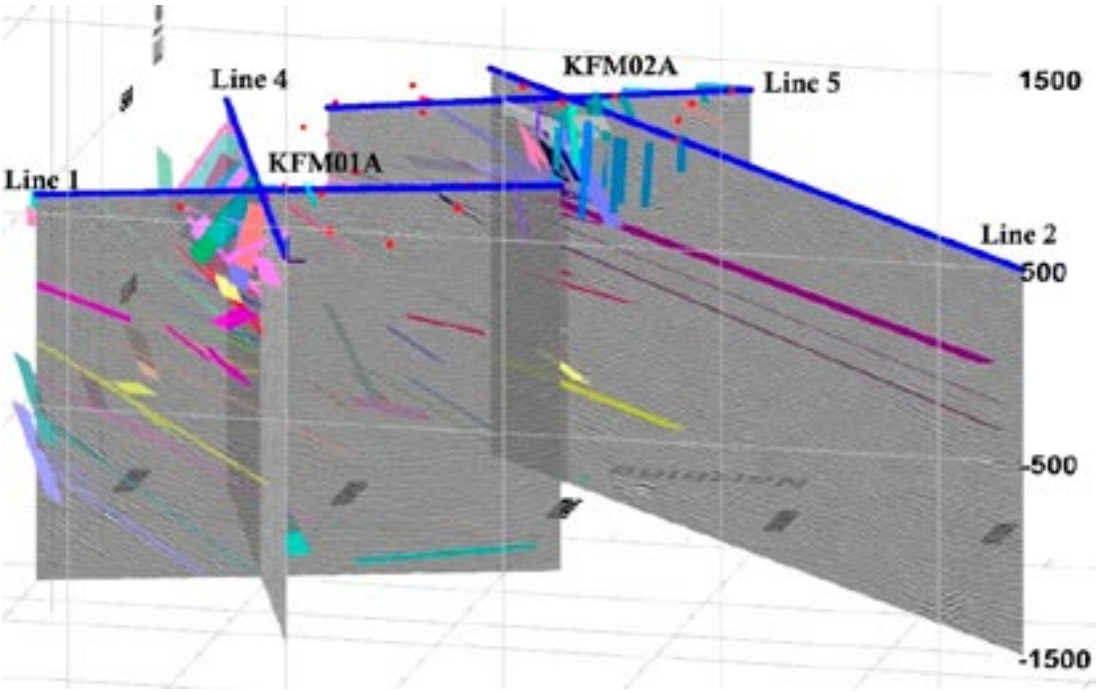

Figure 3-19. *Interpreted 3D reflector elements from the VSP (KFM01A and KFM02A) and surface reflection seismic data (lines 1, 2, 4 and 5), together with migrated profiles from all four lines. View from west.*

Reflector elements inferred to represent the same reflecting surface are grouped to form one reflector surface, which is defined by a fitted interpolation of all reflector elements in a group. Figure 3-20 illustrates this process for reflector elements labelled 1.

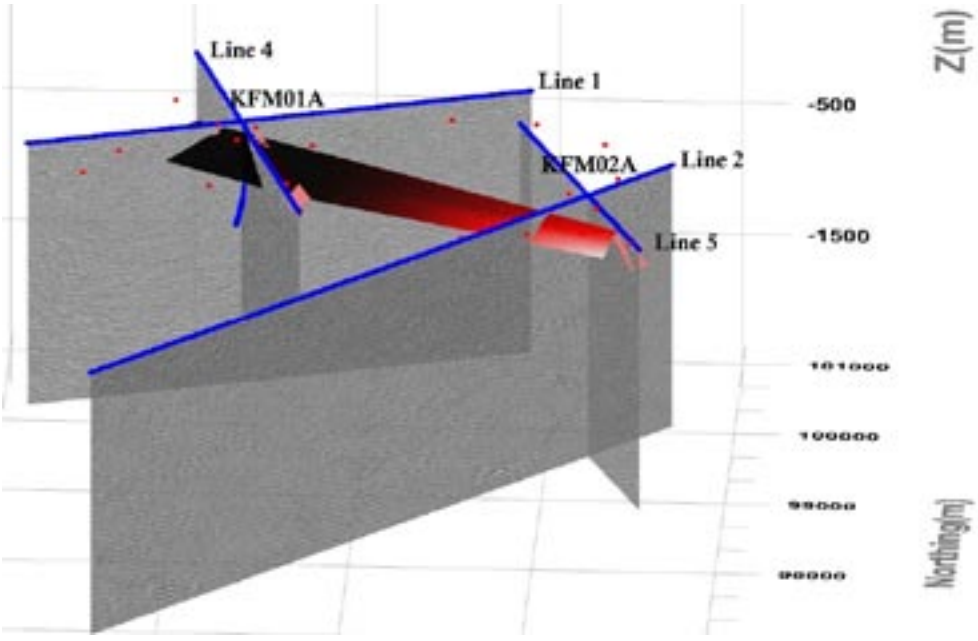

Figure 3-20. *Example of an interpolated reflector surface for the reflector 1. View from south.*

3.1 Borehole KFM01A, and 2D profiles 1 and 4

Reflector elements and inferred reflector surfaces computed from these elements are shown in Figures 3-21 to 3-24. The possible correlation between VSP reflectors interpreted from borehole KFM01A and the geological data in the borehole is presented in Table 3-2.

Table 3-2. VSP reflectors interpreted from borehole KFM01A, in relation to the single-hole interpretation of KFM01A /Carlsten et al. 2004a/.

Label	Depth (m)	Dip (°)	Dip Dir (°)	Azimuth (°)	Comment
46	–4,089.6	81.8	170.0	350.0	
4	–122.2	54.0	170.0	350.0	
8	70.5	36.0	140.0	320.0	RU1. Cannot observe DZ1 in the VSP data, since measurements were made from 100–774 m, DZ1 being too shallow.
33	151.9	35.0	203.6	23.6	RU1, amphibolite vein.
43	220.8	23.3	161.9	341.9	RU1, amphibolite vein.
21	265.5	64.2	216.3	36.3	RU1, amphibolite vein, alteration (oxidised) zone.
22	350.9	63.1	216.6	36.6	RU1, gabbro vein.
40	369.1	6.2	132.3	312.3	RU1
2	380.2	15.0	121.0	301.0	RU1
47	399.6	3.0	157.0	337.0	RU1, alteration (oxidised) zone.
6	420.0	49.8	125.2	305.2	RU1, sealed fractures. May correspond to DZ2.
5	434.6	28.0	170.0	350.0	RU1. May represent reflector B4 (see text below associated with Figure 3-35).
7	524.0	25.0	160.0	340.0	RU3, granite to grandiorite transition, fine- to medium-grained.
48	586.8	31.7	204.7	24.7	RU1, pegmatite.
44	624.8	61.6	200.2	20.2	RU1. May correspond to DZ3.
9	636.0	30.0	150.0	330.0	RU1, pegmatite.
23	675.6	70.0	233.8	53.8	RU1. May correspond to DZ3.
11	775.0	53.1	198.9	18.9	RU1, amphibolite / granite / pegmatite.
49	797.4	59.0	205.0	25.0	RU1
12	808.0	28.8	147.9	327.9	lower RU1 / upper RU2, Granite, granodiorite and tonalite, metamorphic, fine- to medium-grained.
13	865.0	29.0	147.0	327.0	lower RU2 / upper RU1.
25	882.5	47.3	169.9	349.9	RU1, pegmatite, steeply dipping, from NW.
10	940.4	23.0	135.0	315.0	RU1, Granite, granodiorite and tonalite, metamorphic, fine- to medium-grained.
3	1,005.8	35.1	150.8	330.8	RU1
26	1,086.9	65.0	220.0	40.0	
16	1,090.0	40.0	113.7	293.7	
15	1,161.9	30.0	163.0	343.0	
18	1,518.9	31.0	162.7	342.7	
29	1,520.0	58.9	221.7	41.7	
17	1,551.0	42.1	134.3	314.3	
19	1,940.4	40.8	162.9	342.9	May be related to reflector A1 (see Figure 3-33).
30	1,961.0	61.3	223.3	43.3	
28	2,026.2	69.2	229.3	49.3	
20	2,032.5	39.0	161.9	341.9	May represent reflector A1 (see Figure 3-33).
31	2,360.0	64.2	220.1	40.1	
24	2,809.5	82.2	237.7	57.7	May correspond to DZ2.
32	2,970.0	65.0	216.0	36.0	
27	3,037.3	78.3	226.2	46.2	

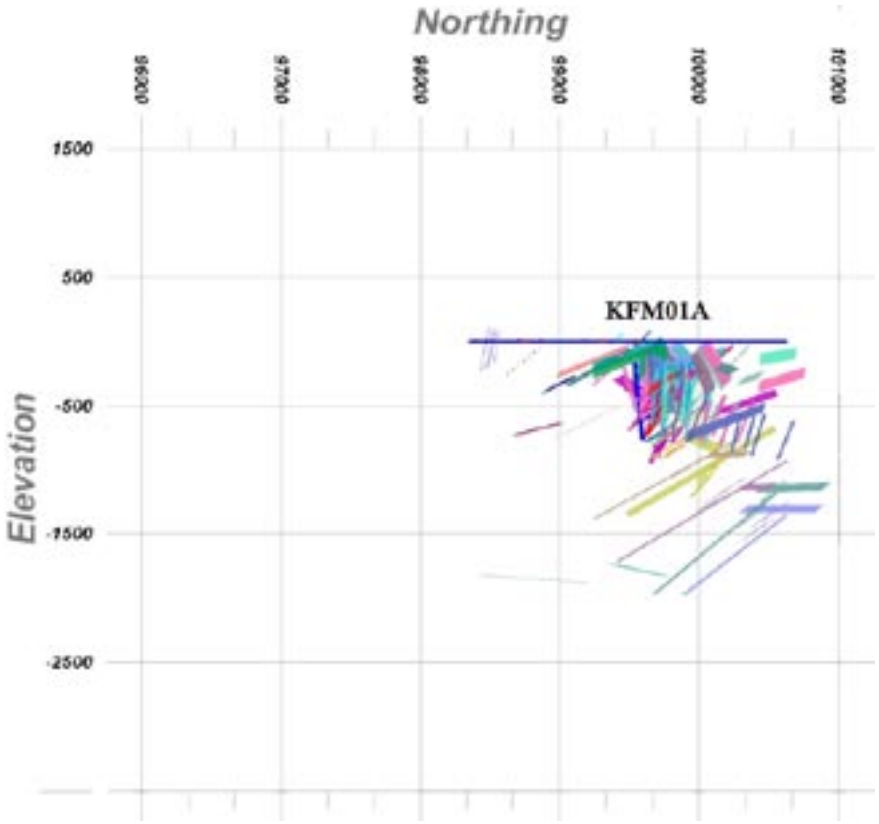

Figure 3-21. *Reflector elements interpreted from the VSP data acquired in borehole KFM01A and the 2D depth migrated profiles along lines 1 and 4. View from east.*

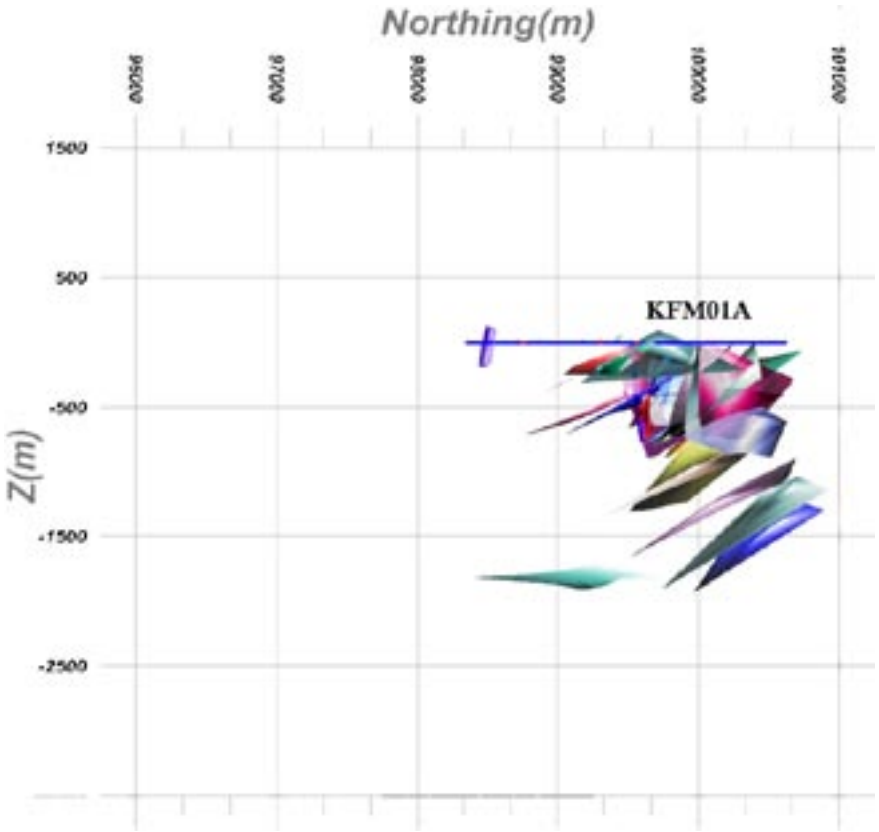

Figure 3-22. *Reflector surfaces computed from the reflector elements shown in Figure 3-21. View from east.*

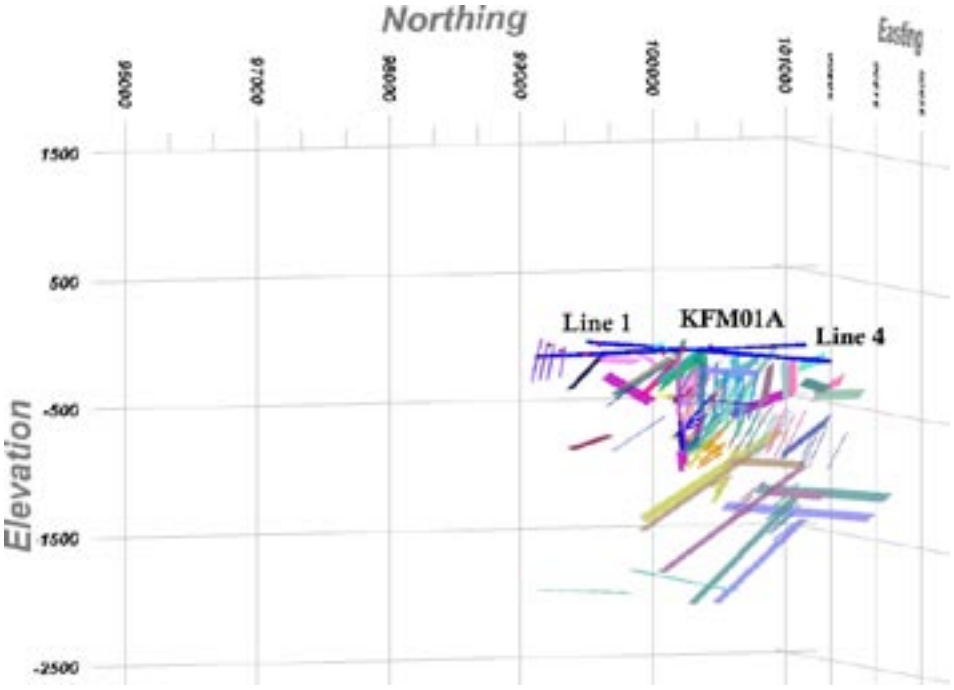

Figure 3-23. *Same as Figure 3-21. View from south-east.*

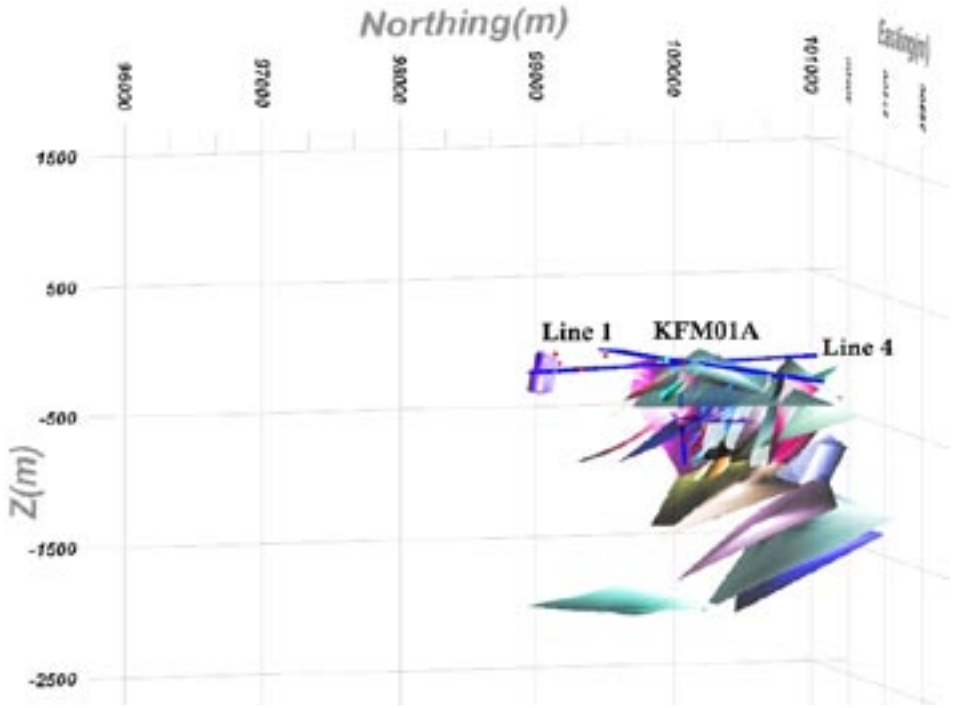

Figure 3-24. *Reflector surfaces computed from the reflector elements shown in Figure 3-21. View from south-east.*

3.2 Borehole KFM02A, and 2D profiles 2 and 5

Reflector elements and inferred reflector surfaces computed from these elements are shown in Figures 3-27 to 3-28. The possible correlation between VSP reflectors interpreted from borehole KFM02A and the geological data in the borehole is presented in Table 3-3.

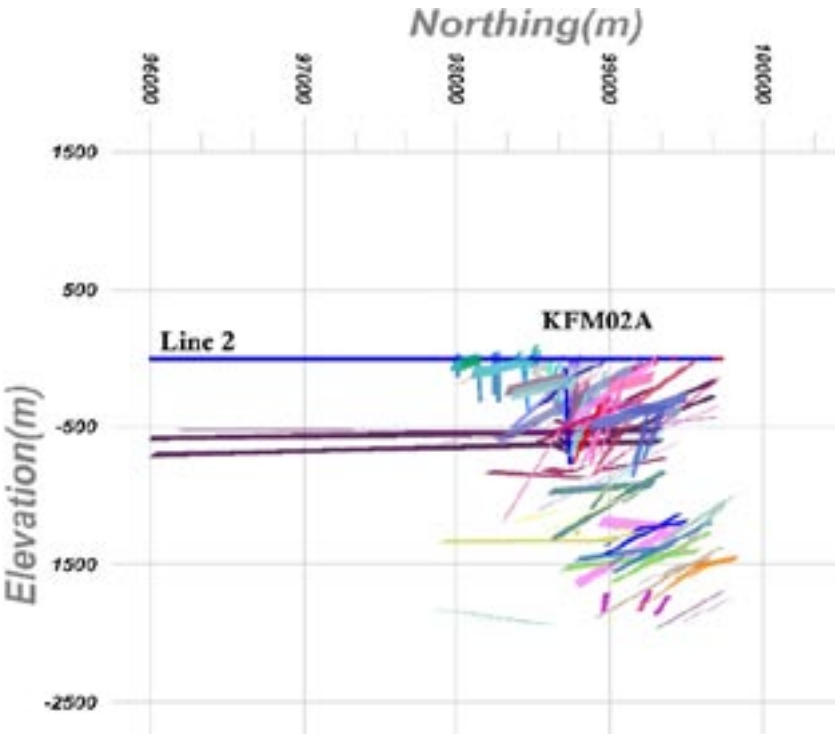

Figure 3-25. *Reflector elements interpreted from the VSP data acquired in borehole KFM02A and the 2D depth migrated profiles along lines 2 and 5. View from east.*

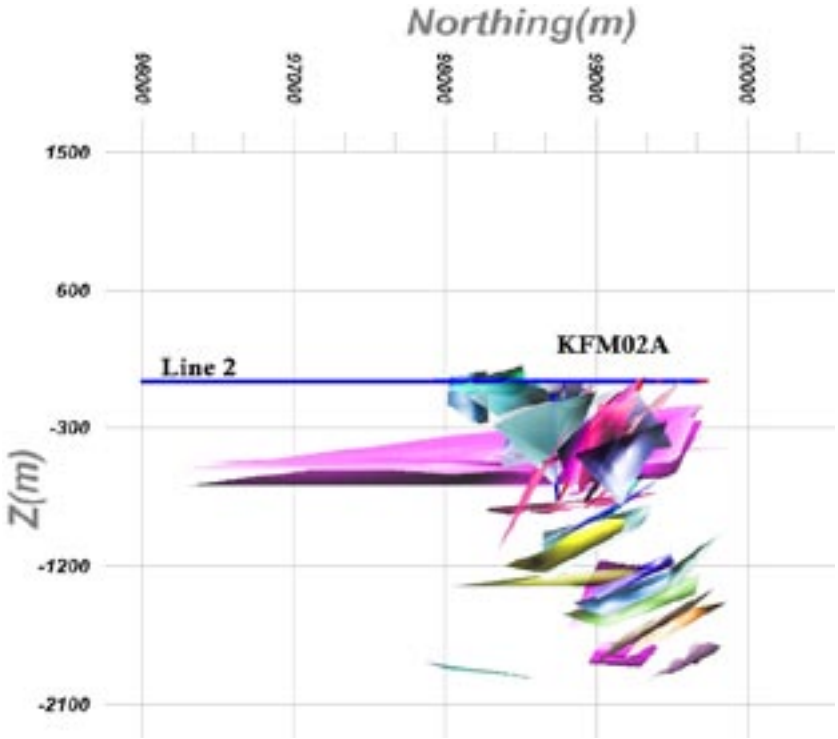

Figure 3-26. *Reflector surfaces computed from the reflector elements shown in Figure 3-25. View from east.*

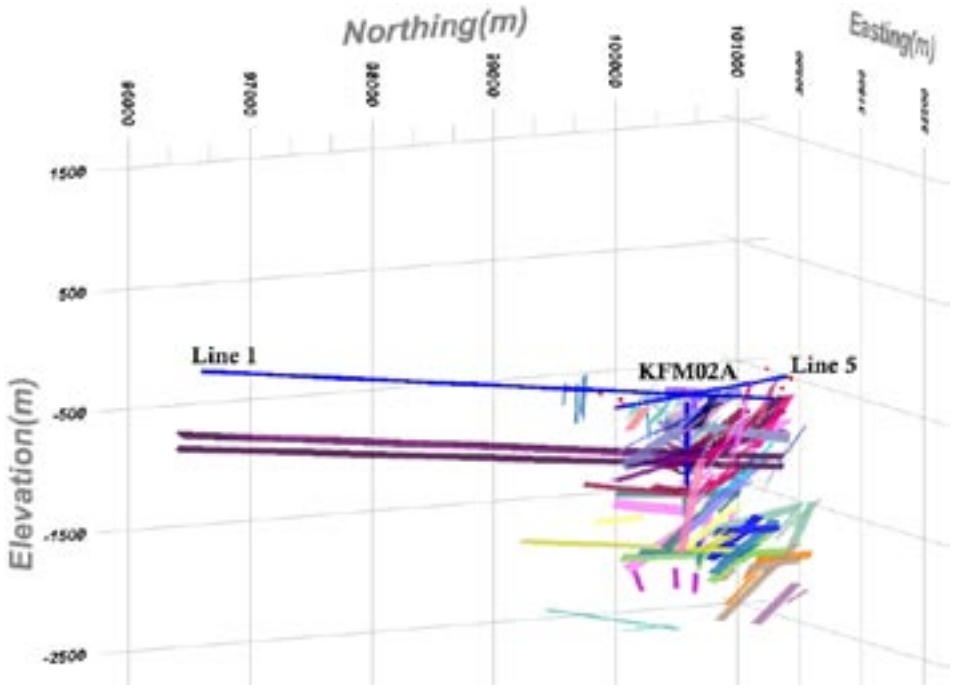

Figure 3-27. *Same as Figure 3-25. View from south-east.*

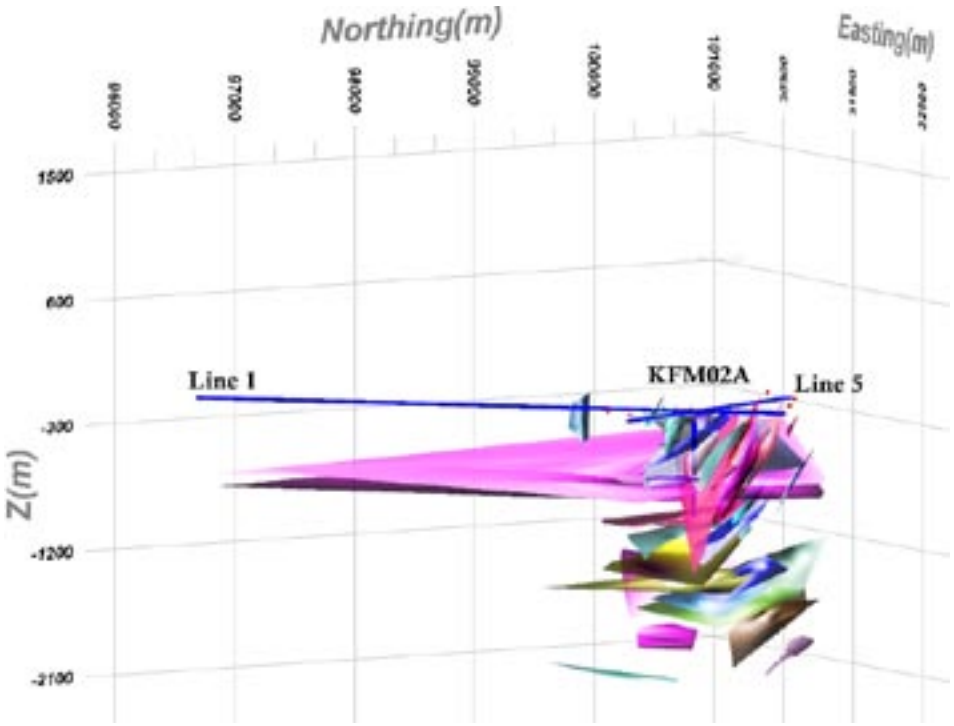

Figure 3-28. *Reflector surfaces computed from the reflector elements shown in Figure 3-25. View from south-east.*

Table 3-3. VSP reflectors interpreted from borehole KFM02A, in relation to the single-hole interpretation of KFM02A /Carlsten et al. 2004b/.

Label	Depth (m)	Dip (°)	Dip Dir (°)	Azimuth (°)	Comments
24	–16,389.5	84.0	237.8	57.8	
27	–12,550.0	86.7	228.1	48.1	
21	–571.7	64.2	216.3	36.3	
22	–472.3	63.1	216.6	36.6	
28	–404.2	69.2	229.3	49.3	
26	–73.0	65.0	220.0	40.0	RU1, Cannot observe DZ1 and DZ2 from the VSP data, because measurements were made from 100–774 m, these zones being too shallow.
33	185.0	35.0	203.6	23.6	RU3, amphibolite vein, DZ3 (lower boundary of the 170–185 m alteration zone).
34	205.0	35.5	197.8	17.8	RU3, amphibolite vein, DZ3 (lower boundary of DZ3 ?).
35	245.0	42.5	178.0	358.0	RU2, alteration (oxidised) zone, May correspond to the strongly altered vuggy metagranite.
36	275.9	66.0	108.9	288.9	RU2, alteration (albitisation) zone, DZ4 = crushed zone, May correspond to the strongly altered vuggy metagranite (see Figure 3-36).
37	370.4	57.0	170.0	350.0	RU1, granite to granodiorite transition, fine to medium grained, sealed fractures.
38	452.3	48.5	122.7	302.7	RU1, sealed fracture, may correspond to DZ6.
46	463.4	82.0	170.5	350.5	RU1, sealed fracture, may correspond to DZ6.
47	478.7	3.0	157.0	337.0	RU1, amphibolite vein.
39	482.1	26.7	140.5	320.5	RU1 / RU3 boundary, granite to granodiorite transition, fine- to medium-grained. May represent reflector A2 (see Figure 3-34).
29	533.2	58.9	221.7	41.7	RU3, alteration (oxidised) zone.
40	575.2	6.2	132.3	312.3	RU1, amphibolite (gabbro?) zone, 5 m thick.
48	595.2	31.7	204.7	24.7	RU1 / RU3 boundary, granite to granodiorite transition, fine- to medium-grained, Reflector B2.
41	631.1	26.9	135.6	315.6	RU3 / RU1 boundary, granite to granodiorite transition, fine- to medium-grained, alteration zone.
42	699.2	24.6	136.9	316.9	RU1, sealed fracture.
30	750.0	58.0	223.0	43.0	RU1, granite to granodiorite transition, fine- to medium-grained.
43	789.1	23.3	161.9	341.9	RU1, granite to granodiorite transition, fine- to medium-grained.
49	808.0	59.0	205.0	25.0	RU1, amphibolite vein.
2	850.0	18.0	125.0	305.0	RU3, granite to granodiorite transition, fine- to medium-grained; amphibolite vein.
44	936.0	61.6	200.2	20.2	RU4, granite to granodiorite transition, fine- to medium-grained; may correspond to DZ9.
45	981.9	40.0	170.2	350.2	RU1 sealed fractures, alteration zone; may correspond to DZ10.
5	1,025.0	29.0	170.0	350.0	May represent reflector B4 (see Figure 3-35).
11	1,060.0	54.0	198.0	18.0	
7	1,162.6	35.0	155.0	335.0	
31	1,251.6	63.0	220.1	40.1	
8	1,290.0	36.0	140.0	320.0	
4	1,300.0	53.0	170.0	350.0	
10	1,366.6	23.0	134.8	314.8	
9	1,541.7	30.0	150.0	330.0	
12	1,698.3	28.8	147.9	327.9	
13	1,771.0	29.0	147.0	327.0	
15	1,920.1	31.0	161.0	341.0	
25	2,068.8	47.3	169.9	349.9	

Label	Depth (m)	Dip (°)	Dip Dir (°)	Azimuth (°)	Comments
3	2,100.0	35.1	150.8	330.8	
32	2,169.2	66.0	216.0	36.0	
18	2,320.7	31.0	162.7	342.7	
6	2,496.4	49.8	125.2	305.2	
16	2,659.5	40.0	113.7	293.7	

3.3 Combined interpretation of reflectors from boreholes KFM01A and KFM02A together with 2D profiles 1, 2, 4 and 5, and some geological features presented in geological model, stage 2.1

The sub-set of gently dipping (dip < 37.5°) reflectors is presented in Figures 3-29 and 3-30. The sub-set of steeply dipping (dip > 60°) reflectors is presented in Figures 3-31 and 3-32. Figures 3-33 to 3-37 present some of the inferred reflectors from the surface seismic data and information in the geological model stage 2.1, in relation to reflectors interpreted from the VSP data from boreholes KFM1A and KFM02A. Reflectors A1, A2 and B4 are taken from /Juhlin et al. 2002/ and the porous granite (including zone ZFMNE1189) from the geological model stage 2.1 /SKB 2006/.

There is a confident correlation of reflectors A1 and A2 in the surface data with reflectors 19–20 and reflector 39, respectively, in the VSP data (Figures 3-33 and 3-34). If B4 is correlated with reflector 5 interpreted from the VSP data (Figure 3-35) and if the correlation of VSP reflector 5 between the boreholes KFM01A and KFM02A, as proposed here, is correct (see Table 3-1), it would mean that B4 will have to be reoriented from an intersect along KFM01A at c. 10 m, with an orientation 050/28 (strike/dip), to an intersect along KFM01A at c. 430–470m, with an orientation 080/28 (strike/dip). An alternative interpretation of reflector B4, in which there is no intersection in borehole KFM01A, was presented in /Juhlin and Bergman 2004/. Finally, zone ZFMNE1189 inside the porous granite interval in borehole KFM02A appears to correlate with VSP reflector 36 (Figures 3-36 and 3-37). A steep dip for this structure is inferred.

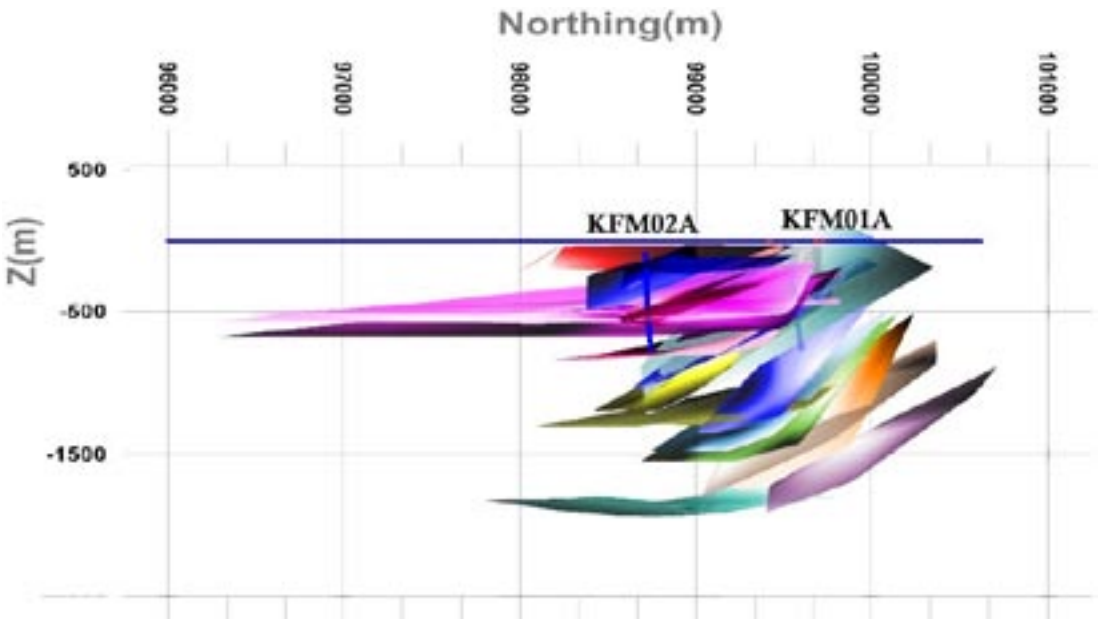

Figure 3-29. Gently dipping (dip < 37.5°) interpolated surfaces. View from east.

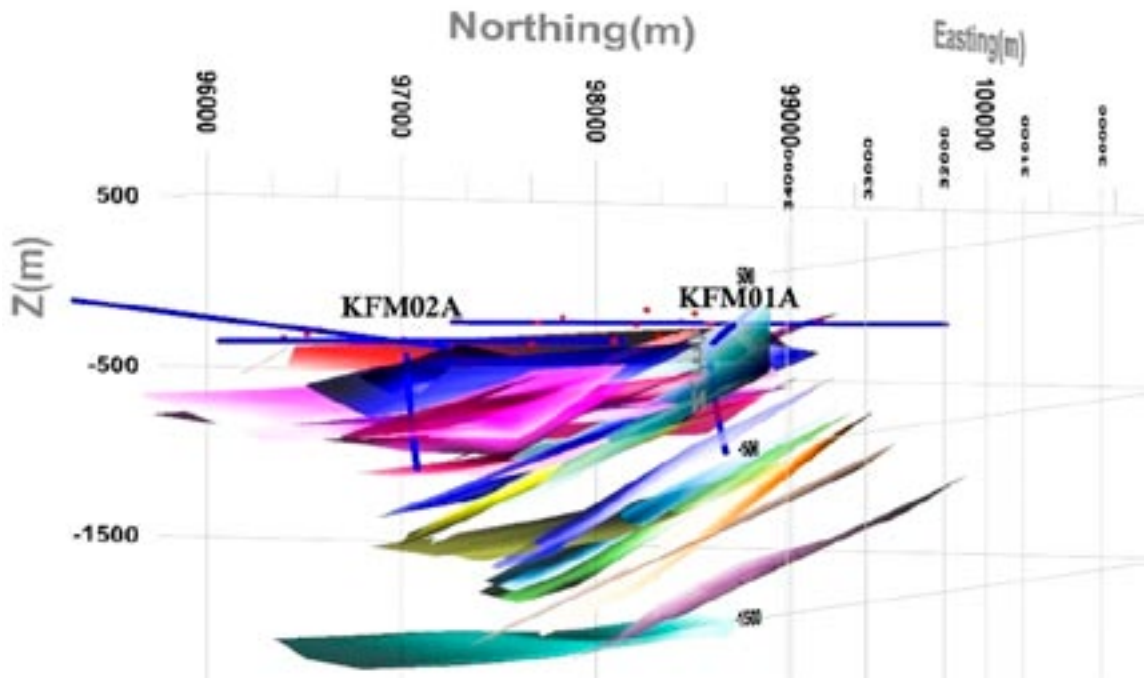

Figure 3-30. *Gently dipping (dip < 37.5°) interpolated surfaces. View from north-east.*

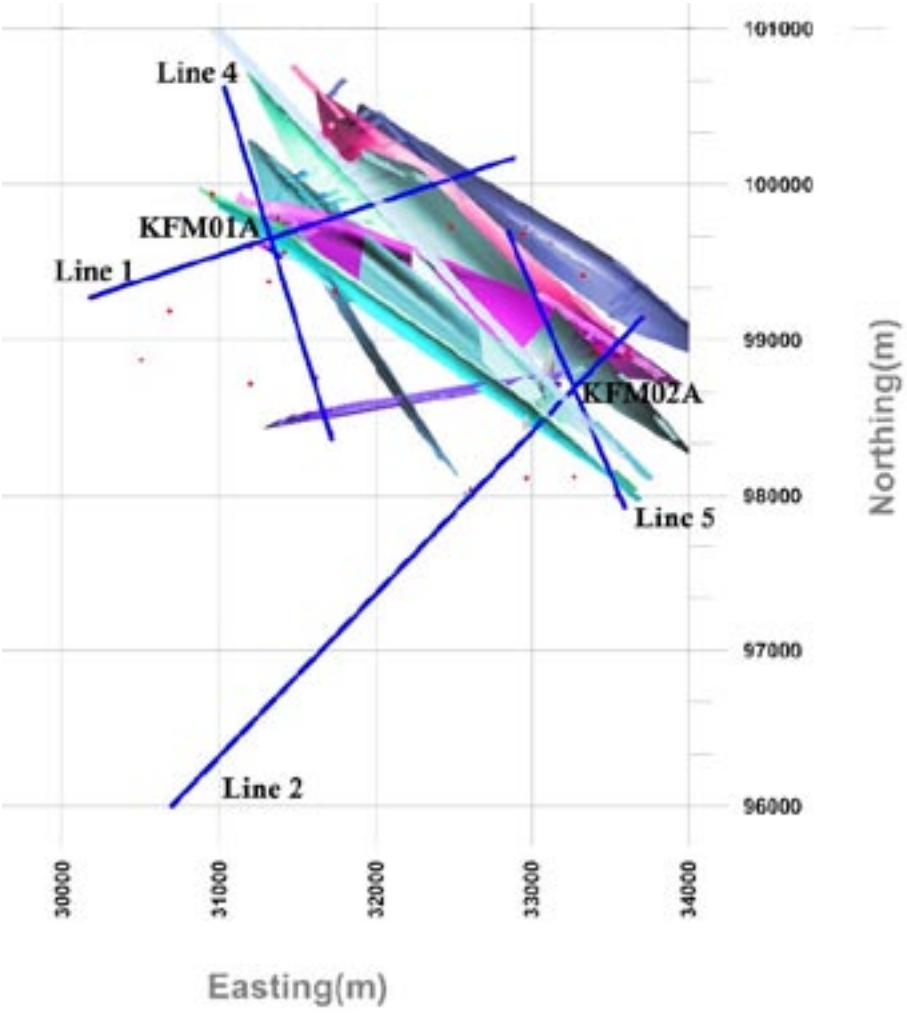

Figure 3-31. *Steeply dipping (dip > 60°) interpolated surfaces. View from top.*

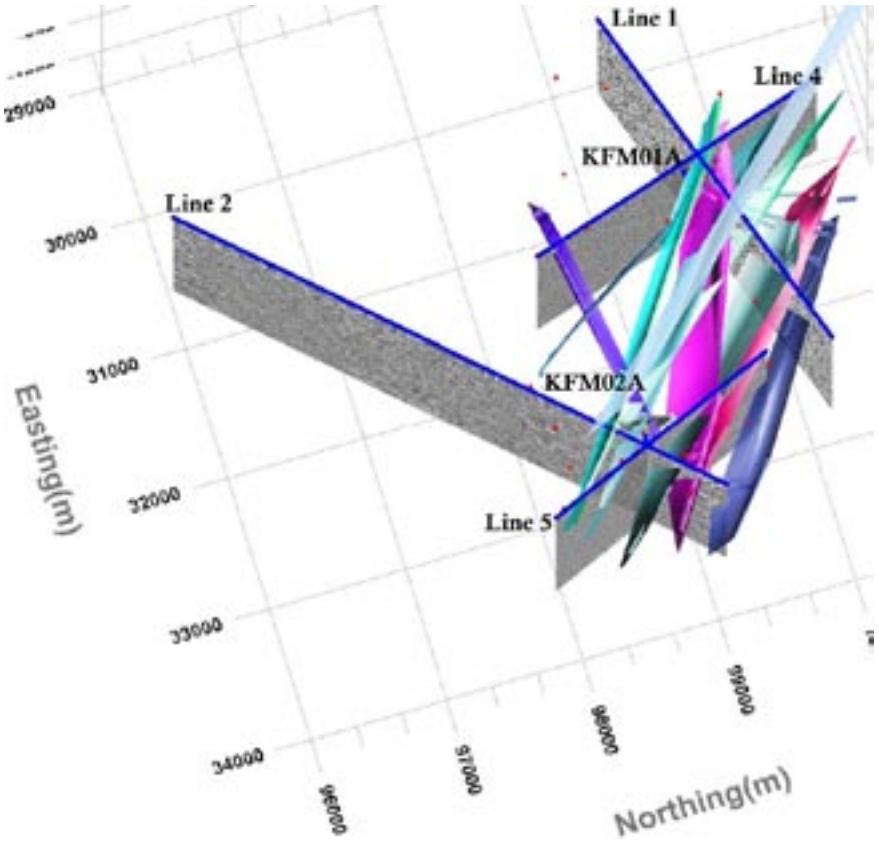

Figure 3-32. *Steeply dipping (dip > 60°) interpolated surfaces. 3D view from top.*

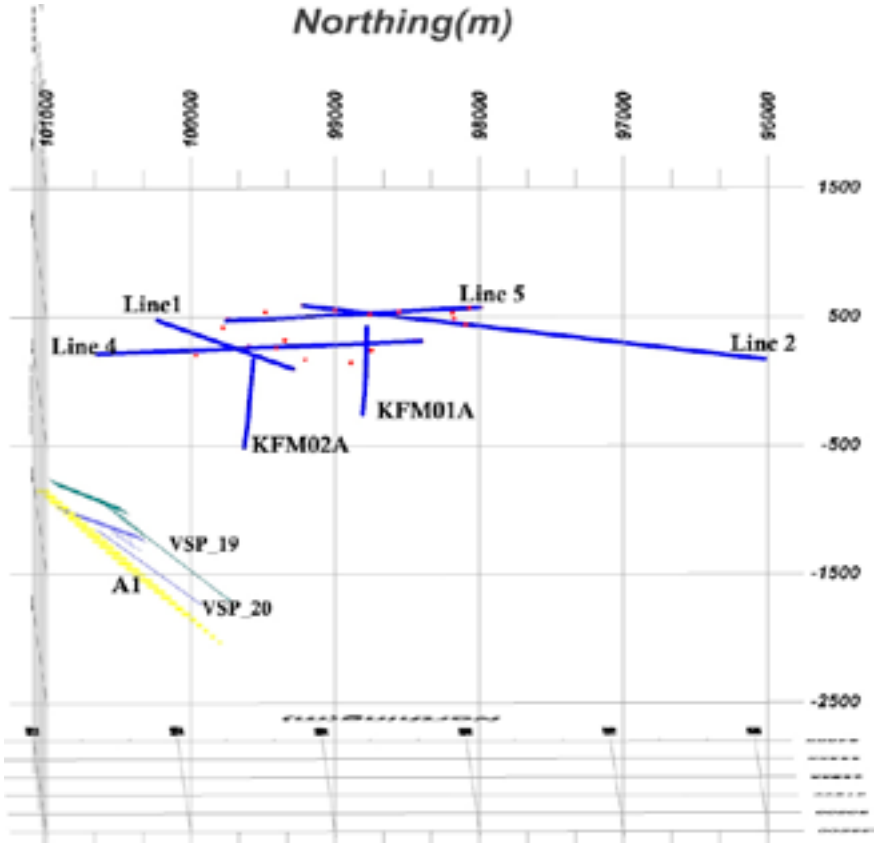

Figure 3-33. *Reflector A1 interpreted from the 2D seismic data and correlation with reflectors 19 and 20 interpreted from the VSP data.*

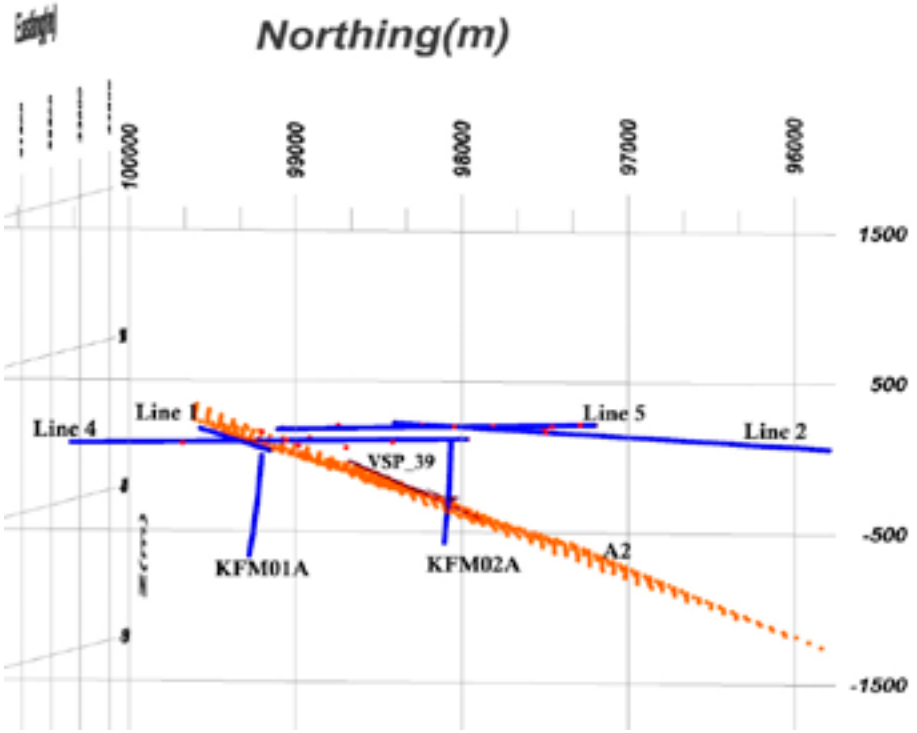

Figure 3-34. *Reflector A2 interpreted from the 2D seismic data and correlation with reflector 39 interpreted from the VSP data.*

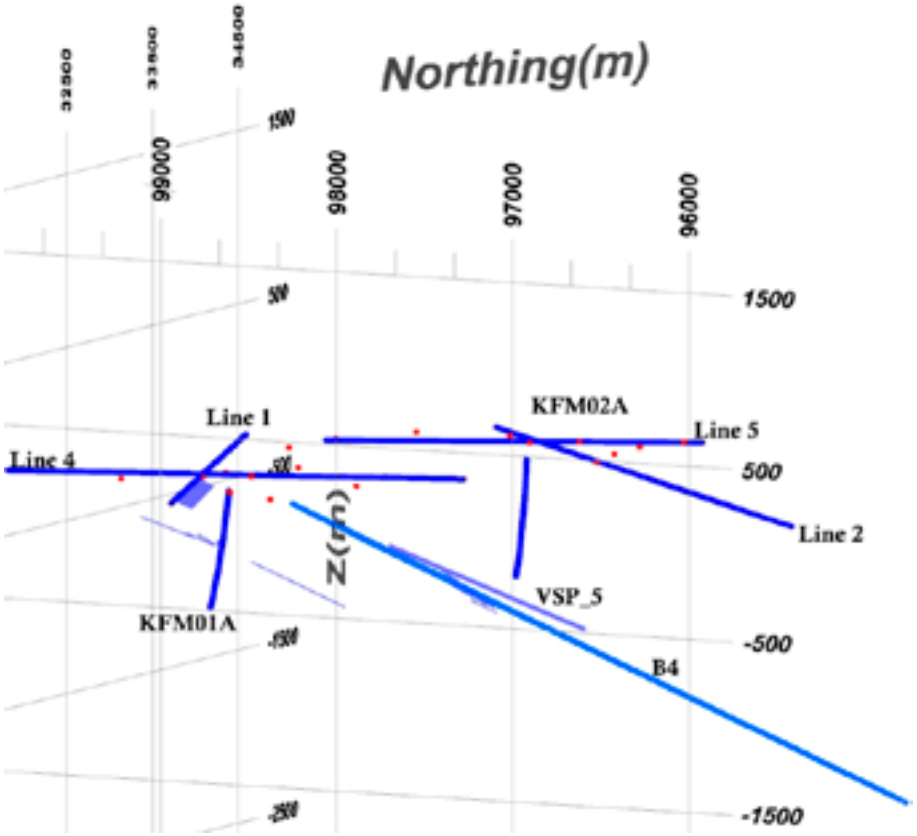

Figure 3-35. *Reflector B4 interpreted from the 2D seismic data and correlation with reflector 5 interpreted from the VSP data.*

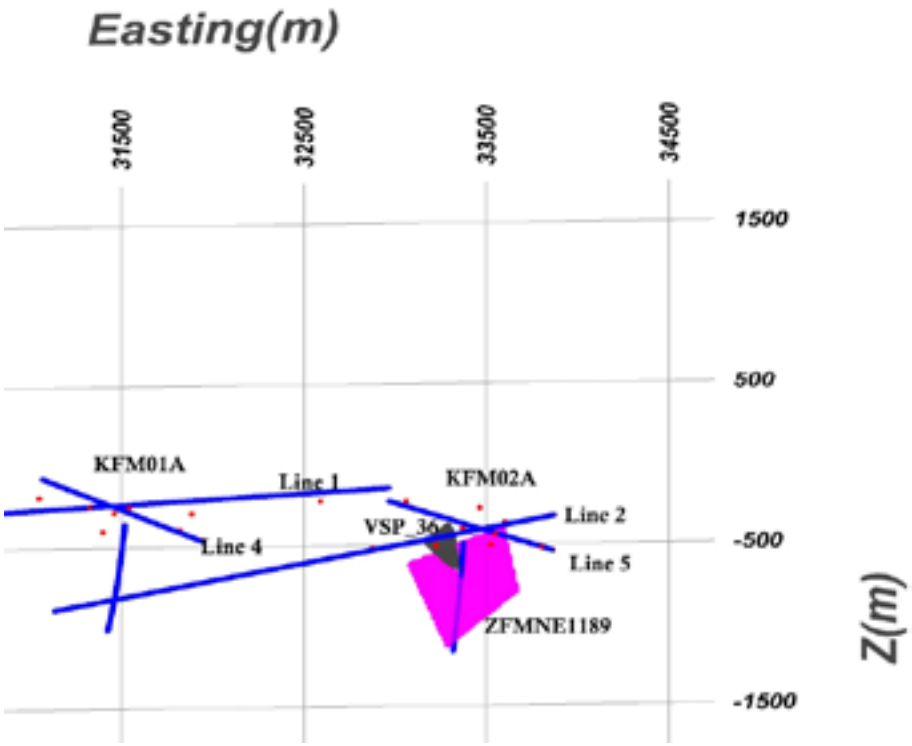

Figure 3-36. *Structure ZFMNE1189 (porous granite) and correlation with reflector 36 interpreted from the VSP data.*

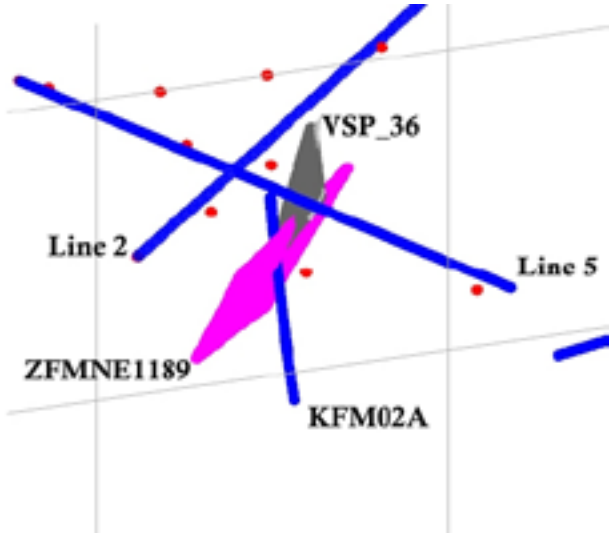

Figure 3-37. *Detailed view of Figure 3-36.*

4 References

Carlsten S, Petersson J, Stephens M, Mattsson H, Gustafsson J, 2004a. Geological single-hole interpretation of KFM01A, KFM01B and HFM01–03 (DS1). Forsmark site investigation. SKB P-04-116, Svensk Kärnbränslehantering AB.

Carlsten S, Petersson J, Stephens M, Mattsson H, Gustafsson J, 2004b. Geological single-hole interpretation of KFM02A and HFM04–05 (DS2). Forsmark site investigation. SKB P-04-117, Svensk Kärnbränslehantering AB.

Cosma C, Enescu N, Balu L, 2005. Vertical seismic profiling from the boreholes KFM01A and KFM02A. Forsmark site investigation. SKB P-05-168, Svensk Kärnbränslehantering AB.

Juhlin C, Bergman B, 2004. Reflection seismics in the Forsmark area. Updated interpretation of Stage 1 (previous report R-02-43). Updated estimate of bedrock topography (previous report P-04-99). SKB P-04-158, Svensk Kärnbränslehantering AB.

Juhlin C, Bergman B, Palm H, 2002. Reflection seismic studies in the Forsmark area Stage 1. SKB R-02-43, Svensk Kärnbränslehantering AB.

SKB 2006. Site descriptive modelling. Forsmark stage 2.1. Feedback for completion of the site investigation including input from safety assessment and repository engineering. SKB R-06-38, Svensk Kärnbränslehantering AB.

Stephens M B, Fox A, La Pointe P, Simeonov A, Isaksson H, Hermanson J, Öhman J, 2007. Geology. Forsmark modelling stage 2.2. SKB R-07-45, Svensk Kärnbränslehantering AB.

Appendix 1

Parameters of reflector elements interpreted from the VSP and 2D seismic data

No.	Depth	Dip (°)	Dip Dir (°)	Azimuth (°)	Visibility	Type	Northing Crux	Easting Crux	Elev Crux	Profile	1st receiver	last receiver
1	1,150.0	40.0	213.0	33.0	2	P-Reflection	98860.2	32909.2	198.7	P1_depth	135	215
1	1,282.9	40.0	213.0	33.0	2	P-Reflection	98860.2	32909.2	198.7	P4_depth	120	235
1	385.0	35.5	171.6	–8.4	2	P-Reflection	98741.0	33038.5	367.6	P5_depth	20	65
1		**38.5**	**199.2**	**19.2**			**98820.5**	**32952.3**	**255.0**			
2	16,443.2	15.0	121.0	301.0	2	P-Reflection	99106.7	32822.4	–773.2	P2_depth	130	300
2	3,131.4	16.0	142.0	322.0	2	P-Reflection	99192.1	32849.9	–850.3	P4_depth	70	140
2	5,152.8	14.0	124.0	304.0	2	P-Reflection	99105.2	32844.0	–754.8	P5_depth	230	320
2	380.2	15.0	121.0	301.0	2	P-Reflection	99106.7	32822.4	–773.2	KFM01A_01	1	49
2	380.2	15.0	121.0	301.0	1	P-Reflection	99106.7	32822.4	–773.2	KFM01A_02	1	57
2	380.2	15.0	121.0	301.0	1	P-Reflection	99106.7	32822.4	–773.2	KFM01A_03	1	57
2	380.2	15.0	120.0	300.0	1	P-Reflection	99103.8	32820.2	–774.7	KFM01A_05	1	57
2	850.0	18.0	125.0	305.0	2	P-Reflection	99128.5	32816.4	–689.7	KFM02A_01	1	136
2	850.0	18.0	125.0	305.0	1	P-Reflection	99128.5	32816.4	–689.7	KFM02A_07	1	136
2	850.0	20.0	120.0	300.0	1	P-Reflection	99121.9	32788.9	–669.6	KFM02A_08	1	136
2		**16.1**	**124.0**	**304.0**			**99120.7**	**32822.5**	**–752.2**			
3	–10,238.0	35.1	150.8	330.8	2	P-Reflection	99806.6	32549.4	–1,312.8	P2_depth	1	85
3	4,042.7	35.1	150.8	330.8	1	P-Reflection	99806.6	32549.4	–1,312.8	P5_depth	280	384
3	1,005.0	35.0	150.0	330.0	2	P-Reflection	99801.2	32537.4	–1,321.3	KFM01A_01	1	136
3	1,005.8	35.1	150.8	330.8	1	P-Reflection	99806.6	32549.4	–1,312.8	KFM01A_03	1	136
3	1,005.8	35.1	150.8	330.8	1	P-Reflection	99806.6	32549.4	–1,312.8	KFM01A_05	1	136
3	2,100.0	35.1	150.8	330.8	1	P-Reflection	99806.6	32549.4	–1,312.8	KFM02A_01	1	136
3	2,100.0	35.1	150.8	330.8	2	P-Reflection	99806.6	32549.4	–1,312.8	KFM02A_02	1	136
3	2,100.0	35.1	150.8	330.8	2	P-Reflection	99806.6	32549.4	–1,312.8	KFM02A_07	1	136
3	2,100.0	35.1	150.8	330.8	2	P-Reflection	99806.6	32549.4	–1,312.8	KFM02A_08	1	136

No.	Depth	Dip (°)	Dip Dir (°)	Azimuth (°)	Visibility	Type	Northing Crux	Easting Crux	Elev Crux	Profile	1st receiver	last receiver
3		**35.1**	**150.7**	**330.7**			**99806.0**	**32548.1**	**–1,313.8**			
4	–122.2	54.0	170.0	350.0	2	P-Reflection	99447.4	32921.1	–330.1	KFM01A_01	1	136
4	–122.2	54.0	170.0	350.0	2	P-Reflection	99447.4	32921.1	–330.1	KFM01A_02	1	136
4	–122.2	54.0	170.0	350.0	2	P-Reflection	99447.4	32921.1	–330.1	KFM01A_03	1	136
4	–122.2	54.0	170.0	350.0	2	P-Reflection	99447.4	32921.1	–330.1	KFM01A_05	1E+09	0
4	1,300.0	53.0	170.0	350.0	2	P-Reflection	99457.8	32919.3	–350.3	KFM02A_01	1	136
4	1,300.0	54.0	170.0	350.0	2	P-Reflection	99447.4	32921.1	–330.1	KFM02A_02	1	136
4	1,300.0	54.0	170.0	350.0	1	P-Reflection	99447.4	32921.1	–330.1	KFM02A_07	1	136
4	1,300.0	52.0	170.0	350.0	1	P-Reflection	99467.5	32917.6	–370.9	KFM02A_08	1	136
4		**53.6**	**170.0**	**350.0**			**99451.2**	**32920.4**	**–337.7**			
5	6,145.6	27.5	166.5	346.5	2	P-Reflection	99298.4	32928.4	–589.6	P1_depth	225	380
5	2,064.7	28.0	170.0	350.0	1	P-Reflection	99357.6	32936.9	–682.9	P4_depth	125	220
5	2,881.7	27.0	172.0	352.0	2	P-Reflection	99334.3	32953.0	–662.6	P5_depth	120	320
5	434.6	28.0	170.0	350.0	1	P-Reflection	99357.6	32936.9	–682.9	KFM01A_01	1	58
5	434.6	28.0	170.0	350.0	2	P-Reflection	99357.6	32936.9	–682.9	KFM01A_02	1	59
5	434.6	28.0	170.0	350.0	2	P-Reflection	99357.6	32936.9	–682.9	KFM01A_03	1	59
5	434.6	28.0	170.0	350.0	2	P-Reflection	99357.6	32936.9	–682.9	KFM01A_05	1	59
5	1,025.0	28.0	170.0	350.0	1	P-Reflection	99357.6	32936.9	–682.9	KFM02A_01	1	136
5	1,025.0	29.0	170.0	350.0	2	P-Reflection	99363.4	32935.9	–665.7	KFM02A_02	1	136
5	1,025.0	30.0	168.0	348.0	2	P-Reflection	99365.7	32922.3	–647.5	KFM02A_07	1	136
5	1,025.0	28.0	170.0	350.0	2	P-Reflection	99357.6	32936.9	–682.9	KFM02A_08	1	136
5		**28.1**	**169.7**	**349.7**			**99351.4**	**32936.2**	**–667.8**			
6	16,888.4	50.0	124.8	304.8	2	P-Reflection	99715.3	31968.9	–1,053.0	P2_depth	215	325
6	3,691.1	50.2	124.5	304.5	2	P-Reflection	99672.6	32021.7	–987.4	P5_depth	275	384
6	420.0	49.8	125.2	305.2	1	P-Reflection	99679.3	32035.4	–998.3	KFM01A_01	66	136
6	420.0	49.8	125.2	305.2	2	P-Reflection	99679.3	32035.4	–998.3	KFM01A_02	1	73
6	420.0	49.8	125.2	305.2	2	P-Reflection	99679.3	32035.4	–998.3	KFM01A_03	1	73
6	420.0	49.8	125.2	305.2	1	P-Reflection	99679.3	32035.4	–998.3	KFM01A_05	1	73

No.	Depth	Dip (°)	Dip Dir (°)	Azimuth (°)	Visibility	Type	Northing Crux	Easting Crux	Elev Crux	Profile	1st receiver	last receiver
6	2,496.4	49.8	125.2	305.2	1	P-Reflection	99679.3	32035.4	–998.3	KFM02A_01	1	136
6	2,496.4	49.8	125.2	305.2	1	P-Reflection	99679.3	32035.4	–998.3	KFM02A_02	1	136
6	2,496.4	49.8	125.2	305.2	1	P-Reflection	99679.3	32035.4	–998.3	KFM02A_08	1	136
6		**49.8**	**125.0**	**305.0**			**99682.6**	**32026.5**	**–1,003.2**			
7	–33,172.7	25.0	160.0	340.0	2	P-Reflection	99371.6	32864.8	–847.9	P1_depth	120	200
7	–5,240.6	25.0	160.0	340.0	2	P-Reflection	99371.6	32864.8	–847.9	P2_depth	225	300
7	3,432.1	25.0	160.0	340.0	2	P-Reflection	99371.6	32864.8	–847.9	P5_depth	145	260
7	524.0	25.0	160.0	340.0	1	P-Reflection	99371.6	32864.8	–847.9	KFM01A_02	1	85
7	524.0	25.0	160.0	340.0	1	P-Reflection	99371.6	32864.8	–847.9	KFM01A_03	1	85
7	524.0	25.0	160.0	340.0	2	P-Reflection	99371.6	32864.8	–847.9	KFM01A_05	1	85
7	1,162.6	30.0	155.0	335.0	1	P-Reflection	99394.5	32816.1	–753.9	KFM02A_01	1	136
7	1,162.6	25.0	155.0	335.0	1	P-Reflection	99358.6	32832.8	–848.5	KFM02A_02	1	136
7	1,162.6	35.0	155.0	335.0	2	P-Reflection	99414.9	32806.5	–653.9	KFM02A_07	1	136
7		**26.7**	**158.3**	**338.3**			**99377.5**	**32849.4**	**–816.0**			
8	1,318.4	36.0	140.0	320.0	2	P-Reflection	99406.0	32659.4	–729.4	P1_depth	470	520
8	–17,180.4	36.0	140.0	320.0	2	P-Reflection	99406.0	32659.4	–729.4	P2_depth	90	280
8	1,300.8	36.0	140.0	320.0	2	P-Reflection	99406.0	32659.4	–729.4	P4_depth	150	240
8	2,867.5	36.0	140.0	320.0	2	P-Reflection	99406.0	32659.4	–729.4	P5_depth	175	325
8	70.5	36.0	140.0	320.0	2	P-Reflection	99406.0	32659.4	–729.4	KFM01A_01	1	136
8	70.0	40.0	130.0	310.0	1	P-Reflection	99439.0	32476.8	–814.0	KFM01A_02	1	136
8	1,290.0	36.0	140.0	320.0	1	P-Reflection	99406.0	32659.4	–729.4	KFM02A_01	1	136
8	1,290.0	36.0	140.0	320.0	2	P-Reflection	99406.0	32659.4	–729.4	KFM02A_02	1	136
8	1,290.0	36.0	140.0	320.0	1	P-Reflection	99406.0	32659.4	–729.4	KFM02A_07	1	136
8	1,290.0	36.0	140.0	320.0	2	P-Reflection	99406.0	32659.4	–729.4	KFM02A_08	1	136
8		**36.4**	**139.0**	**319.0**			**99409.3**	**32641.1**	**–737.9**			
9	–9,484.1	30.0	150.0	330.0	2	P-Reflection	99526.0	32696.3	–1,052.0	P2_depth	30	130
9	3,687.0	30.0	150.0	330.0	2	P-Reflection	99526.0	32696.3	–1,052.0	P5_depth	235	340
9	636.0	30.0	150.0	330.0	1	P-Reflection	99526.0	32696.3	–1,052.0	KFM01A_01	1	114

No.	Depth	Dip (°)	Dip Dir (°)	Azimuth (°)	Visibility	Type	Northing Crux	Easting Crux	Elev Crux	Profile	1st receiver	last receiver
9	636.0	30.0	150.0	330.0	1	P-Reflection	99526.0	32696.3	–1,052.0	KFM01A_02	1	106
9	636.0	30.0	150.0	330.0	1	P-Reflection	99526.0	32696.3	–1,052.0	KFM01A_03	1	106
9	636.0	30.0	150.0	330.0	1	P-Reflection	99526.0	32696.3	–1,052.0	KFM01A_05	1	106
9	1,541.7	30.0	150.0	330.0	2	P-Reflection	99526.0	32696.3	–1,052.0	KFM02A_01	1	136
9	1,541.7	30.0	150.0	330.0	2	P-Reflection	99526.0	32696.3	–1,052.0	KFM02A_02	1	136
9	1,541.7	30.0	150.0	330.0	2	P-Reflection	99526.0	32696.3	–1,052.0	KFM02A_07	1	136
9	1,541.7	30.0	150.0	330.0	2	P-Reflection	99526.0	32696.3	–1,052.0	KFM02A_08	1	136
9		**30.0**	**150.0**	**330.0**			**99526.0**	**32696.3**	**–1,052.0**			
10	–322,206.0	12.9	134.8	314.8	2	P-Reflection	99200.6	32798.0	–1,240.0	P2_depth	80	400
10	7,427.0	12.9	134.8	314.8	2	P-Reflection	99200.6	32798.0	–1,240.0	P5_depth	208	350
10	940.4	23.0	135.0	315.0	2	P-Reflection	99413.5	32586.5	–1,377.6	KFM01A_01	1	131
10	940.4	12.9	134.8	314.8	2	P-Reflection	99200.6	32798.0	–1,240.0	KFM01A_02	1	131
10	940.4	23.0	135.0	315.0	1	P-Reflection	99413.5	32586.5	–1,377.6	KFM01A_03	1	131
10	940.4	23.0	135.0	315.0	2	P-Reflection	99413.5	32586.5	–1,377.6	KFM01A_05	1	131
10	1,366.6	23.0	135.0	315.0	1	P-Reflection	99321.7	32678.3	–1,071.9	KFM02A_02	1	136
10	1,366.6	23.0	134.8	314.8	2	P-Reflection	99320.7	32677.2	–1,072.0	KFM02A_07	1	136
10		**19.2**	**134.9**	**314.9**			**99310.6**	**32688.6**	**–1,249.6**			
11	2,010.0	52.0	199.0	19.0	2	P-Reflection	99359.3	33123.7	–296.9	P4_depth	330	390
11	1,800.0	53.0	198.0	18.0	2	P-Reflection	99317.7	33103.2	–251.7	P5_depth	260	350
11	775.0	53.1	198.9	18.9	2	P-Reflection	99355.7	33121.7	–281.8	KFM01A_01	1	136
11	775.0	53.1	198.9	18.9	1	P-Reflection	99355.7	33121.7	–281.8	KFM01A_02	1	135
11	775.0	53.1	198.9	18.9	1	P-Reflection	99355.7	33121.7	–281.8	KFM01A_03	1	135
11	775.0	53.1	198.9	18.9	2	P-Reflection	99355.7	33121.7	–281.8	KFM01A_05	1	135
11	1,060.0	54.0	198.0	18.0	1	P-Reflection	99347.2	33112.8	–265.3	KFM02A_01	1	136
11	1,063.4	54.0	198.9	18.9	2	P-Reflection	99348.6	33119.2	–267.6	KFM02A_02	1	136
11	1,063.4	53.1	198.9	18.9	2	P-Reflection	99355.7	33121.7	–281.8	KFM02A_07	1	136
11	1,060.0	54.0	198.0	18.0	2	P-Reflection	99347.2	33112.8	–265.3	KFM02A_08	1	136
11		**53.3**	**198.6**	**18.6**			**99349.9**	**33118.0**	**–275.6**			

No.	Depth	Dip (°)	Dip Dir (°)	Azimuth (°)	Visibility	Type	Northing Crux	Easting Crux	Elev Crux	Profile	1st receiver	last receiver
12	–12,755.6	28.8	147.9	327.9	2	P-Reflection	99562.6	32646.4	–1,207.6	P2_depth	90	250
12	4,140.7	28.8	147.9	327.9	2	P-Reflection	99562.6	32646.4	–1,207.6	P5_depth	250	384
12	808.0	28.8	147.9	327.9	2	P-Reflection	99562.6	32646.4	–1,207.6	KFM01A_01	1	136
12	808.0	28.8	147.9	327.9	2	P-Reflection	99562.6	32646.4	–1,207.6	KFM01A_02	1	136
12	808.0	28.8	147.9	327.9	2	P-Reflection	99562.6	32646.4	–1,207.6	KFM01A_03	1	136
12	808.0	28.8	147.9	327.9	2	P-Reflection	99562.6	32646.4	–1,207.6	KFM01A_05	1	136
12	1,698.3	28.8	147.9	327.9	2	P-Reflection	99562.6	32646.4	–1,207.6	KFM02A_01	1	136
12	1,698.3	28.8	147.9	327.9	2	P-Reflection	99562.6	32646.4	–1,207.6	KFM02A_02	1	136
12	1,698.3	28.8	147.9	327.9	2	P-Reflection	99562.6	32646.4	–1,207.6	KFM02A_07	1	136
12	1,698.3	28.8	147.9	327.9	1	P-Reflection	99562.6	32646.4	–1,207.6	KFM02A_08	1	136
12		**28.8**	**147.9**	**327.9**			**99562.6**	**32646.4**	**–1,207.6**			
13	–14,105.1	29.0	147.0	327.0	2	P-Reflection	99586.4	32619.2	–1,261.4	P2_depth	25	280
13	4,267.8	29.0	147.0	327.0	2	P-Reflection	99586.4	32619.2	–1,261.4	P5_depth	250	384
13	865.0	29.0	147.0	327.0	2	P-Reflection	99586.4	32619.2	–1,261.4	KFM01A_01	1	136
13	865.0	29.0	147.0	327.0	2	P-Reflection	99586.4	32619.2	–1,261.4	KFM01A_02	1	136
13	865.0	29.0	147.0	327.0	1	P-Reflection	99586.4	32619.2	–1,261.4	KFM01A_03	1	136
13	1,771.0	29.0	147.0	327.0	1	P-Reflection	99586.4	32619.2	–1,261.4	KFM02A_01	1	136
13	1,771.0	29.0	147.0	327.0	1	P-Reflection	99586.4	32619.2	–1,261.4	KFM02A_02	1	136
13	1,771.0	29.0	147.0	327.0	1	P-Reflection	99586.4	32619.2	–1,261.4	KFM02A_07	1	136
13	1,771.0	29.0	147.0	327.0	2	P-Reflection	99586.4	32619.2	–1,261.4	KFM02A_08	1	136
13		**29.0**	**147.0**	**327.0**			**99586.4**	**32619.2**	**–1,261.4**			
14	–22,300.0	6.0	28.0	208.0	2	P-Reflection	98834.1	32911.8	–1,787.6	P1_depth	135	385
14	18,847.9	6.3	30.1	210.1	2	P-Reflection	98816.3	32893.7	–1,933.9	P2_depth	140	340
14	–24,340.9	6.3	30.1	210.1	2	P-Reflection	98816.3	32893.7	–1,933.9	P4_depth	25	185
14	–28,500.0	6.3	30.1	210.1	2	P-Reflection	98816.3	32893.7	–1,933.9	P5_depth	50	170
14		**6.2**	**29.5**	**209.5**			**98820.8**	**32898.2**	**–1,897.3**			
15	89,382.4	30.0	163.1	343.1	2	P-Reflection	99758.9	32768.7	–1,374.2	P1_depth	200	370
15	–6,475.7	30.0	163.0	343.0	2	P-Reflection	99740.6	32773.6	–1,341.4	P2_depth	1	85

No.	Depth	Dip (°)	Dip Dir (°)	Azimuth (°)	Visibility	Type	Northing Crux	Easting Crux	Elev Crux	Profile	1st receiver	last receiver
15	3,330.0	30.0	163.0	343.0	2	P-Reflection	99740.6	32773.6	–1,341.4	P4_depth	185	400
15	4,322.2	30.0	163.0	343.0	2	P-Reflection	99740.6	32773.6	–1,341.4	P5_depth	205	384
15	1,161.9	30.0	163.0	343.0	1	P-Reflection	99740.6	32773.6	–1,341.4	KFM01A_05	1	136
15	1,920.1	30.0	161.0	341.0	1	P-Reflection	99732.7	32747.7	–1,342.2	KFM02A_01	1	136
15	1,920.1	30.0	163.0	343.0	2	P-Reflection	99740.6	32773.6	–1,341.4	KFM02A_02	1	136
15	1,920.1	31.0	161.0	341.0	1	P-Reflection	99745.1	32743.5	–1,311.4	KFM02A_07	1	136
15	1,920.1	32.0	160.0	340.0	1	P-Reflection	99752.0	32726.3	–1,280.7	KFM02A_08	1	136
15		**30.3**	**162.2**	**342.2**			**99743.5**	**32761.6**	**–1,335.1**			
16	–582.4	40.0	113.7	293.7	2	P-Reflection	99519.2	31817.7	–1,537.4	P1_depth	1	80
16	3,389.5	40.0	113.7	293.7	2	P-Reflection	99519.2	31817.7	–1,537.4	P4_depth	390	472
16	1,090.0	40.0	113.7	293.7	2	P-Reflection	99519.2	31817.7	–1,537.4	KFM01A_01	1	136
16	1,090.0	40.0	113.7	293.7	2	P-Reflection	99519.2	31817.7	–1,537.4	KFM01A_02	1	136
16	1,090.0	40.0	113.7	293.7	2	P-Reflection	99519.2	31817.7	–1,537.4	KFM01A_03	1	136
16	1,090.0	40.0	113.7	293.7	2	P-Reflection	99519.2	31817.7	–1,537.4	KFM01A_05	1	136
16	2,659.5	40.0	113.7	293.7	1	P-Reflection	99519.2	31817.7	–1,537.4	KFM02A_01	1	136
16	2,659.5	40.0	113.7	293.7	1	P-Reflection	99519.2	31817.7	–1,537.4	KFM02A_02	1	136
16	2,659.5	40.0	113.7	293.7	1	P-Reflection	99519.2	31817.7	–1,537.4	KFM02A_07	1	136
16		**40.0**	**113.7**	**293.7**			**99519.2**	**31817.7**	**–1,537.4**			
17	–2,686.3	42.1	134.3	314.3	2	P-Reflection	100081.0	31892.1	–1,713.7	P1_depth	45	135
17	3,392.6	42.1	134.3	314.3	2	P-Reflection	100081.0	31892.1	–1,713.7	P4_depth	270	472
17	1,551.0	42.1	134.3	314.3	2	P-Reflection	100081.0	31892.1	–1,713.7	KFM01A_01	1	136
17	1,551.0	42.1	134.3	314.3	2	P-Reflection	100081.0	31892.1	–1,713.7	KFM01A_02	1	136
17	1,551.0	42.1	134.3	314.3	2	P-Reflection	100081.0	31892.1	–1,713.7	KFM01A_03	1	136
17	1,551.0	42.1	134.3	314.3	2	P-Reflection	100081.0	31892.1	–1,713.7	KFM01A_05	1	136
17		**42.1**	**134.3**	**314.3**			**31892.1**	**–1713.7**				
18	152,120.0	32.0	162.7	342.7	2	P-Reflection	99980.5	32694.1	–1,643.8	P1_depth	235	370
18	3,881.9	31.8	162.7	342.7	2	P-Reflection	99966.9	32698.4	–1,636.7	P4_depth	220	472
18	4,883.5	30.0	162.7	342.7	2	P-Reflection	99872.9	32727.7	–1,583.8	P5_depth	290	384

No.	Depth	Dip (°)	Dip Dir (°)	Azimuth (°)	Visibility	Type	Northing Crux	Easting Crux	Elev Crux	Profile	1st receiver	last receiver
18	1,518.9	31.0	162.7	342.7	2	P-Reflection	99927.3	32710.7	–1,615.4	KFM01A_01	1	136
18	1,518.9	31.0	162.7	342.7	1	P-Reflection	99927.3	32710.7	–1,615.4	KFM01A_02	1	136
18	1,518.9	30.0	162.7	342.7	1	P-Reflection	99897.6	32720.0	–1,628.6	KFM01A_03	1	136
18	1,518.9	31.0	162.7	342.7	1	P-Reflection	99927.3	32710.7	–1,615.4	KFM01A_05	1	136
18	2,320.7	31.0	162.7	342.7	2	P-Reflection	99927.3	32710.7	–1,615.4	KFM02A_02	1	136
18	2,320.7	31.0	162.7	342.7	1	P-Reflection	99927.3	32710.7	–1,615.4	KFM02A_08	1	136
18		**31.0**	**162.7**	**342.7**			**99928.3**	**32710.4**	**–1,618.8**			
19	110,795.0	40.8	162.9	342.9	2	P-Reflection	100399.0	32570.2	–1,697.4	P1_depth	140	450
19	3,662.4	40.8	162.9	342.9	2	P-Reflection	100399.0	32570.2	–1,697.4	P4_depth	274	472
19	1,940.4	40.8	162.9	342.9	2	P-Reflection	100399.0	32570.2	–1,697.4	KFM01A_01	1	136
19	1,940.4	40.8	162.9	342.9	2	P-Reflection	100399.0	32570.2	–1,697.4	KFM01A_02	1	136
19	1,940.4	40.8	162.9	342.9	1	P-Reflection	100399.0	32570.2	–1,697.4	KFM01A_03	1	136
19	1,940.4	40.8	162.9	342.9	1	P-Reflection	100399.0	32570.2	–1,697.4	KFM01A_05	1	136
19		**40.8**	**162.9**	**342.9**			**100399.0**	**32570.2**	**–1,697.4**			
20	850,420.0	37.7	161.9	341.9	2	P-Reflection	100368.0	32552.8	–1,860.2	P1_depth	55	400
20	4,049.7	39.0	161.9	341.9	2	P-Reflection	100447.0	32526.9	–1,879.9	P4_depth	320	472
20	2,032.5	37.7	161.9	341.9	2	P-Reflection	100368.0	32552.8	–1,860.2	KFM01A_01	1	136
20	2,032.5	39.0	161.9	341.9	1	P-Reflection	100403.0	32541.2	–1,823.1	KFM01A_02	1	136
20	2,032.5	37.7	161.9	341.9	2	P-Reflection	100368.0	32552.8	–1,860.2	KFM01A_03	1	136
20	2,032.5	39.0	161.9	341.9	1	P-Reflection	100403.0	32541.2	–1,823.1	KFM01A_05	1	136
20		**38.4**	**161.9**	**341.9**			**100392.8**	**32544.6**	**–1,851.1**			
21	1,285.4	63.0	216.3	36.3	2	P-Reflection	98747.0	32814.3	159.9	P1_depth	200	250
21	1,458.7	66.0	217.0	37.0	2	P-Reflection	98721.4	32790.1	155.3	P4_depth	160	280
21	233.5	64.2	216.3	36.3	2	P-Reflection	98741.9	32810.5	155.1	P5_depth	1	45
21	265.5	64.2	216.3	36.3	1	P-Reflection	98741.9	32810.5	155.1	KFM01A_02	1	34
21	265.5	64.2	216.3	36.3	2	P-Reflection	98741.9	32810.5	155.1	KFM01A_03	1	34
21	–571.7	64.2	216.3	36.3	1	P-Reflection	98741.9	32810.5	155.1	KFM02A_01	1	136
21	–571.7	64.2	216.3	36.3	1	P-Reflection	98741.9	32810.5	155.1	KFM02A_02	1	136

No.	Depth	Dip (°)	Dip Dir (°)	Azimuth (°)	Visibility	Type	Northing Crux	Easting Crux	Elev Crux	Profile	1st receiver	last receiver
21	–571.7	64.2	216.3	36.3	1	P-Reflection	98741.9	32810.5	155.1	KFM02A_08	1	136
21		**64.2**	**216.4**	**36.4**			**98740.0**	**32808.4**	**155.7**			
22	1,344.4	63.1	216.6	36.6	1	P-Reflection	98771.8	32830.3	144.1	P1_depth	190	270
22	1,541.2	63.1	216.6	36.6	1	P-Reflection	98771.8	32830.3	144.1	P4_depth	160	275
22	297.0	63.1	216.6	36.6	2	P-Reflection	98771.8	32830.3	144.1	P5_depth	15	50
22	350.9	63.1	216.6	36.6	1	P-Reflection	98771.8	32830.3	144.1	KFM01A_02	1	51
22	350.9	63.1	216.6	36.6	1	P-Reflection	98771.8	32830.3	144.1	KFM01A_03	1	51
22	–472.3	63.1	216.6	36.6	2	P-Reflection	98771.8	32830.3	144.1	KFM02A_01	1	136
22		**63.1**	**216.6**	**36.6**			**32830.3**	**144.1**				
23	675.6	70.0	233.8	53.8	2	P-Reflection	98597.8	32450.9	247.1	KFM01A_01	1	116
23	675.6	70.0	233.8	53.8	2	P-Reflection	98597.8	32450.9	247.1	KFM01A_02	1	116
23	675.6	70.0	233.8	53.8	2	P-Reflection	98597.8	32450.9	247.1	KFM01A_03	1	116
23	675.6	70.0	233.8	53.8	1	P-S, S-P Conversion	98597.8	32450.9	247.1	KFM01A_05	1	108
23		**70.0**	**233.8**	**53.8**			**98597.8**	**32450.9**	**247.1**			
24	2,809.5	82.2	237.7	57.7	2	P-Reflection	98548.2	32285.6	116.1	KFM01A_01	1	136
24	2,809.5	82.2	237.7	57.7	2	P-Reflection	98548.2	32285.6	116.1	KFM01A_02	1	136
24	2,809.5	82.2	237.7	57.7	2	P-Reflection	98548.2	32285.6	116.1	KFM01A_03	1	136
24	–16,389.5	84.0	237.8	57.8	1	P-Reflection	98532.9	32257.1	93.0	KFM02A_01	1	136
24	–15,532.2	83.8	237.9	57.9	2	P-Reflection	98536.7	32262.2	94.6	KFM02A_02	1	136
24	–11,477.0	82.8	237.2	57.2	2	P-Reflection	98531.1	32273.5	109.9	KFM02A_07	1	136
24	–47,474.4	86.0	237.9	57.9	1	P-Reflection	98545.9	32275.5	59.7	KFM02A_08	1	136
24		**83.3**	**237.7**	**57.7**			**98541.6**	**32275.0**	**100.8**			
25	6,515.0	47.3	169.9	349.9	2	P-Reflection	99903.3	32839.8	–845.8	P1_depth	450	570
25	–2,840.9	47.3	169.9	349.9	2	P-Reflection	99903.3	32839.8	–845.8	P2_depth	15	180
25	2,113.0	47.3	169.9	349.9	2	P-Reflection	99903.3	32839.8	–845.8	P4_depth	325	417
25	2,931.3	47.3	169.9	349.9	1	P-Reflection	99903.3	32839.8	–845.8	P5_depth	323	384
25	882.5	47.3	169.9	349.9	2	P-Reflection	99903.3	32839.8	–845.8	KFM01A_01	1	136
25	882.5	47.3	169.9	349.9	2	P-Reflection	99903.3	32839.8	–845.8	KFM01A_02	1	136

No.	Depth	Dip (°)	Dip Dir (°)	Azimuth (°)	Visibility	Type	Northing Crux	Easting Crux	Elev Crux	Profile	1st receiver	last receiver
25	882.5	47.3	169.9	349.9	2	P-Reflection	99903.3	32839.8	–845.8	KFM01A_03	1	136
25	882.5	47.3	169.9	349.9	2	P-Reflection	99903.3	32839.8	–845.8	KFM01A_05	1	136
25	2,068.8	47.3	169.9	349.9	2	P-Reflection	99903.3	32839.8	–845.8	KFM02A_01	1	136
25	2,068.8	47.3	169.9	349.9	2	P-Reflection	99903.3	32839.8	–845.8	KFM02A_02	1	136
25	2,068.8	47.3	169.9	349.9	1	P-Reflection	99903.3	32839.8	–845.8	KFM02A_08	1	136
25		**47.3**	**169.9**	**349.9**			**99903.3**	**32839.8**	**–845.8**			
26	1,713.7	65.0	220.0	40.0	1	P-Reflection	98912.0	32926.1	53.6	P1_depth	275	337
26	2,141.3	65.0	220.0	40.0	1	P-Reflection	98912.0	32926.1	53.6	P4_depth	250	371
26	660.4	65.0	220.0	40.0	2	P-Reflection	98912.0	32926.1	53.6	P5_depth	20	115
26	1,086.9	65.0	220.0	40.0	2	P-Reflection	98912.0	32926.1	53.6	KFM01A_01	1	136
26	1,086.9	65.0	220.0	40.0	1	P-Reflection	98912.0	32926.1	53.6	KFM01A_02	1	136
26	1,086.9	65.0	220.0	40.0	1	P-Reflection	98912.0	32926.1	53.6	KFM01A_03	1	136
26	1,086.9	65.0	220.0	40.0	2	P-Reflection	98912.0	32926.1	53.6	KFM01A_05	1	136
26	–73.0	65.0	220.0	40.0	1	P-Reflection	98912.0	32926.1	53.6	KFM02A_02	1	136
26	–73.0	65.0	220.0	40.0	1	P-S, S-P Conversion	98912.0	32926.1	53.6	KFM02A_07	1	69
26		**65.0**	**220.0**	**40.0**			**98912.0**	**32926.1**	**53.6**			
27	3,037.3	78.3	226.2	46.2	2	P-Reflection	98826.3	32818.9	52.1	KFM01A_01	1	136
27	3,037.3	78.3	226.2	46.2	2	P-Reflection	98826.3	32818.9	52.1	KFM01A_02	1	136
27	3,037.3	78.3	226.2	46.2	2	P-Reflection	98826.3	32818.9	52.1	KFM01A_03	1	136
27	3,037.3	78.3	226.2	46.2	2	P-Reflection	98826.3	32818.9	52.1	KFM01A_05	1	136
27	–12,550.0	86.7	228.1	48.1	1	P-Reflection	98779.6	32754.1	19.2	KFM02A_01	1	136
27	11,152.3	89.4	228.4	48.4	1	P-Reflection	98769.9	32740.8	3.6	KFM02A_02	1	136
27	–12,550.0	86.7	228.1	48.1	1	P-S, S-P Conversion	98779.6	32754.1	19.2	KFM02A_07	1	136
27	4,935.1	89.1	49.1	229.1	1	P-Reflection	98793.6	32761.4	–5.1	KFM02A_08	1	136
27		**83.1**	**249.8**	**69.8**			**98803.5**	**32785.8**	**30.7**			
28	2,955.1	69.2	229.3	49.3	2	P-Reflection	98891.7	32874.1	63.0	P4_depth	411	472
28	2,026.2	69.2	229.3	49.3	2	P-Reflection	98891.7	32874.1	63.0	KFM01A_01	1	136
28	2,026.2	69.2	229.3	49.3	2	P-Reflection	98891.7	32874.1	63.0	KFM01A_02	1	136

No.	Depth	Dip (°)	Dip Dir (°)	Azimuth (°)	Visibility	Type	Northing Crux	Easting Crux	Elev Crux	Profile	1st receiver	last receiver
28	2,026.2	69.2	229.3	49.3	2	P-Reflection	98891.7	32874.1	63.0	KFM01A_03	1	136
28	2,026.2	69.2	229.3	49.3	2	P-Reflection	98891.7	32874.1	63.0	KFM01A_05	1	136
28	–404.2	69.2	229.3	49.3	1	P-Reflection	98891.7	32874.1	63.0	KFM02A_01	1	136
28	–404.2	69.2	229.3	49.3	1	P-Reflection	98891.7	32874.1	63.0	KFM02A_02	1	136
28	–404.2	69.2	229.3	49.3	2	P-Reflection	98891.7	32874.1	63.0	KFM02A_08	1	136
28		**69.2**	**229.3**	**49.3**			**98891.7**	**32874.1**	**63.0**			
29	2,163.2	56.0	223.0	43.0	2	P-Reflection	99090.5	33084.4	–83.4	P1_depth	340	414
29	1,430.5	56.0	223.0	43.0	2	P-Reflection	99102.9	33096.0	–94.9	P5_depth	60	150
29	1,520.0	58.9	221.7	41.7	2	P-Reflection	99113.8	33101.3	–92.0	KFM01A_01	1	136
29	1,520.0	58.9	221.7	41.7	2	P-Reflection	99113.8	33101.3	–92.0	KFM01A_02	1	136
29	1,520.0	58.9	221.7	41.7	2	P-Reflection	99113.8	33101.3	–92.0	KFM01A_05	1	136
29	533.2	58.9	221.7	41.7	2	P-S, S-P Conversion	99113.8	33101.3	–92.0	KFM02A_01	1	87
29	533.2	58.9	221.7	41.7	1	P-Reflection	99113.8	33101.3	–92.0	KFM02A_07	1	87
29	533.2	58.9	221.7	41.7	2	P-Reflection	99113.8	33101.3	–92.0	KFM02A_08	1	87
29		**58.1**	**222.0**	**42.0**			**99109.5**	**33098.5**	**–91.3**			
30	2,305.3	63.0	223.3	43.3	2	P-Reflection	99172.2	33162.4	–120.6	P1_depth	385	455
30	1,670.0	63.0	223.0	43.0	2	P-Reflection	99176.0	33164.1	–122.6	P5_depth	55	160
30	1,961.0	61.3	223.3	43.3	2	P-Reflection	99167.0	33157.5	–125.5	KFM01A_01	1	136
30	1,961.0	61.3	223.3	43.3	2	P-Reflection	99167.0	33157.5	–125.5	KFM01A_02	1	136
30	1,961.0	61.3	223.3	43.3	2	P-Reflection	99167.0	33157.5	–125.5	KFM01A_03	1	136
30	1,961.0	61.3	223.3	43.3	2	P-Reflection	99167.0	33157.5	–125.5	KFM01A_05	1	136
30	750.0	58.0	223.0	43.0	2	P-Reflection	99186.3	33173.7	–159.1	KFM02A_01	1	126
30	750.0	58.0	223.0	43.0	2	P-Reflection	99186.3	33173.7	–159.1	KFM02A_02	1	126
30	750.0	60.0	223.0	43.0	1	P-Reflection	99175.0	33163.2	–138.1	KFM02A_07	1	126
30	750.0	58.0	223.0	43.0	2	P-Reflection	99186.3	33173.7	–159.1	KFM02A_08	1	126
30		**60.5**	**223.2**	**43.2**			**99175.0**	**33164.1**	**–136.1**			
31	2,400.0	62.0	220.0	40.0	2	P-Reflection	99265.4	33222.7	–184.2	P1_depth	400	475
31	3,255.0	66.0	220.0	40.0	2	P-Reflection	99300.9	33252.5	–174.9	P4_depth	390	472

No.	Depth	Dip (°)	Dip Dir (°)	Azimuth (°)	Visibility	Type	Northing Crux	Easting Crux	Elev Crux	Profile	1st receiver	last receiver
31	1,985.0	62.0	220.0	40.0	2	P-Reflection	99277.9	33233.2	–192.9	P5_depth	200	275
31	2,360.0	64.2	220.1	40.1	2	P-Reflection	99289.7	33243.6	–183.3	KFM01A_01	1	136
31	2,360.0	64.2	220.1	40.1	2	P-Reflection	99289.7	33243.6	–183.3	KFM01A_02	1	136
31	2,360.0	65.5	220.1	40.1	2	P-Reflection	99254.0	33213.6	–151.2	KFM01A_03	1	136
31	2,360.0	64.2	220.1	40.1	2	P-Reflection	99289.7	33243.6	–183.3	KFM01A_05	1	136
31	1,251.6	63.0	220.1	40.1	2	P-Reflection	99302.9	33254.8	–201.7	KFM02A_01	1	136
31	1,251.6	63.0	220.1	40.1	2	P-Reflection	99302.9	33254.8	–201.7	KFM02A_02	1	136
31	1,251.6	64.2	220.1	40.1	1	P-Reflection	99289.7	33243.6	–183.3	KFM02A_07	1	136
31	1,251.6	64.2	220.1	40.1	1	P-Reflection	99289.7	33243.6	–183.3	KFM02A_08	1	136
31		**63.8**	**220.0**	**40.0**			**99286.6**	**33240.9**	**–183.9**			
32	3,490.9	65.0	216.0	36.0	2	P-Reflection	99559.7	33406.6	–322.6	P4_depth	245	385
32	2,640.0	66.0	216.0	36.0	2	P-Reflection	99571.8	33415.4	–314.7	P5_depth	125	295
32	2,970.0	63.0	214.0	34.0	2	P-Reflection	99685.4	33462.3	–421.3	KFM01A_01	1	136
32	2,970.0	65.0	216.0	36.0	1	P-Reflection	99559.7	33406.6	–322.6	KFM01A_02	1	136
32	2,970.0	65.5	216.0	36.0	1	P-Reflection	99543.4	33394.8	–306.1	KFM01A_03	1	136
32	2,970.0	65.0	216.0	36.0	2	P-Reflection	99559.7	33406.6	–322.6	KFM01A_05	1	136
32	2,169.2	66.0	216.0	36.0	2	P-Reflection	99538.0	33390.9	–296.1	KFM02A_01	1	136
32	2,169.2	64.5	216.0	36.0	2	P-Reflection	99570.2	33414.3	–336.2	KFM02A_02	1	136
32	2,169.2	66.0	216.0	36.0	2	P-Reflection	99538.0	33390.9	–296.1	KFM02A_07	1	136
32	2,169.2	66.0	216.0	36.0	2	P-Reflection	99538.0	33390.9	–296.1	KFM02A_08	1	136
32		**65.2**	**215.8**	**35.8**			**99566.4**	**33407.9**	**–323.4**			
33	1,396.9	35.0	203.6	23.6	2	P-Reflection	99018.3	33008.0	–28.5	P1_depth	110	200
33	376.3	35.0	203.6	23.6	2	P-Reflection	99018.3	33008.0	–28.5	P2_depth	115	240
33	1,172.9	35.0	203.6	23.6	2	P-Reflection	99018.3	33008.0	–28.5	P5_depth	100	165
33	151.9	35.0	203.6	23.6	1	P-Reflection	99018.3	33008.0	–28.5	KFM01A_03	1	11
33	185.0	35.0	203.6	23.6	1	P-Reflection	99018.3	33008.0	–28.5	KFM02A_01	1	18
33	185.0	35.0	203.6	23.6	2	P-Reflection	99018.3	33008.0	–28.5	KFM02A_07	1	18
33	185.0	35.0	203.6	23.6	1	P-Reflection	99018.3	33008.0	–28.5	KFM02A_08	1	18

No.	Depth	Dip (°)	Dip Dir (°)	Azimuth (°)	Visibility	Type	Northing Crux	Easting Crux	Elev Crux	Profile	1st receiver	last receiver
33		**35.0**	**203.6**	**23.6**			**99018.3**	**33008.0**	**–28.5**			
34	327.1	35.5	197.8	17.8	1	P-Reflection	99018.7	33006.0	–27.5	P2_depth	100	185
34	1,281.0	35.5	197.8	17.8	1	P-Reflection	99018.7	33006.0	–27.5	P4_depth	100	150
34	1,186.6	35.5	197.8	17.8	1	P-Reflection	99018.7	33006.0	–27.5	P5_depth	140	222
34	205.0	35.5	197.8	17.8	1	P-Reflection	99018.7	33006.0	–27.5	KFM02A_01	1	22
34	205.1	35.5	197.8	17.8	1	P-Reflection	99018.7	33006.0	–27.5	KFM02A_07	1	21
34	205.1	35.5	197.8	17.8	2	P-Reflection	99018.7	33006.0	–27.5	KFM02A_08	1	22
34		**35.5**	**197.8**	**17.8**			**99018.7**	**33006.0**	**–27.5**			
35	210.0	42.5	180.0	0.0	1	P-Reflection	98996.5	33000.0	3.9	P2_depth	115	180
35	582.7	40.0	178.0	358.0	1	P-Reflection	98988.8	33000.4	13.3	P4_depth	50	110
35	1,142.4	42.5	178.0	358.0	1	P-Reflection	98987.7	33000.4	13.5	P5_depth	160	220
35	245.0	42.5	178.0	358.0	1	P-Reflection	98987.7	33000.4	13.5	KFM02A_01	1	29
35	245.0	42.5	178.0	358.0	1	P-S, S-P Conversion	98987.7	33000.4	13.5	KFM02A_02	1	30
35	245.0	42.5	178.0	358.0	1	P-Reflection	98987.7	33000.4	13.5	KFM02A_07	1	29
35	245.0	42.5	178.0	358.0	1	P-Reflection	98987.7	33000.4	13.5	KFM02A_08	1	29
35		**42.1**	**126.9**	**306.9**			**98989.1**	**33000.3**	**12.1**			
36	1,184.7	66.0	108.9	288.9	2	P-Reflection	98966.9	33096.7	45.5	P2_depth	173	207
36	1,182.9	66.0	108.9	288.9	2	P-Reflection	98966.9	33096.7	45.5	P5_depth	180	225
36	275.9	66.0	108.9	288.9	2	P-Reflection	98966.9	33096.7	45.5	KFM02A_01	1	36
36	275.9	66.0	108.9	288.9	2	P-Reflection	98966.9	33096.7	45.5	KFM02A_02	1	36
36	275.9	66.0	108.9	288.9	2	P-S, S-P Conversion	98966.9	33096.7	45.5	KFM02A_07	1	36
36	275.9	66.0	108.9	288.9	2	P-S, S-P Conversion	98966.9	33096.7	45.5	KFM02A_08	1	36
36		**66.0**	**108.9**	**288.9**			**98966.9**	**33096.7**	**45.5**			
37	137.6	57.0	170.0	350.0	2	P-Reflection	98957.1	33007.6	28.3	P2_depth	108	171
37	1,127.3	57.0	170.0	350.0	2	P-Reflection	98957.1	33007.6	28.3	P5_depth	50	150
37	370.4	57.0	170.0	350.0	1	P-Reflection	98957.1	33007.6	28.3	KFM02A_01	1	49
37	370.4	57.0	170.0	350.0	2	P-S, S-P Conversion	98957.1	33007.6	28.3	KFM02A_02	1	49
37	370.4	57.0	170.0	350.0	2	P-Reflection	98957.1	33007.6	28.3	KFM02A_07	1	49

No.	Depth	Dip (°)	Dip Dir (°)	Azimuth (°)	Visibility	Type	Northing Crux	Easting Crux	Elev Crux	Profile	1st receiver	last receiver
37	370.4	57.0	170.0	350.0	2	P-Reflection	98957.1	33007.6	28.3	KFM02A_08	1	49
37		**57.0**	**170.0**	**350.0**			**98957.1**	**33007.6**	**28.3**			
38	3,338.6	48.5	120.0	300.0	2	P-Reflection	99071.1	32876.9	–126.0	P2_depth	1	185
38	1,462.3	48.5	122.7	302.7	2	P-Reflection	99037.7	32941.1	–62.0	P5_depth	107	282
38	452.3	48.5	122.7	302.7	2	P-Reflection	99037.7	32941.1	–62.0	KFM02A_01	1	77
38	452.3	48.5	122.7	302.7	1	P-Reflection	99037.7	32941.1	–62.0	KFM02A_02	1	71
38	452.3	48.5	122.7	302.7	1	P-Reflection	99037.7	32941.1	–62.0	KFM02A_07	1	71
38	452.3	48.5	122.7	302.7	2	P-Reflection	99037.7	32941.1	–62.0	KFM02A_08	1	71
38		**48.5**	**122.2**	**302.2**			**99043.3**	**32930.4**	**–72.6**			
39	1,932.9	28.0	140.5	320.5	2	P-Reflection	99109.4	32909.8	–266.8	P5_depth	140	300
39	482.1	26.7	140.5	320.5	2	P-Reflection	99099.9	32917.6	–258.0	KFM02A_01	1	86
39	482.1	26.7	140.5	320.5	2	P-Reflection	99099.9	32917.6	–258.0	KFM02A_02	1	86
39	482.1	26.7	140.5	320.5	1	P-Reflection	99099.9	32917.6	–258.0	KFM02A_07	1	86
39	482.1	26.7	140.5	320.5	1	P-Reflection	99099.9	32917.6	–258.0	KFM02A_08	1	86
39		**26.9**	**140.5**	**320.5**			**99101.8**	**32916.0**	**–259.7**			
40	220,236.0	5.8	132.3	312.3	2	P-Reflection	99033.3	32963.4	–491.6	P2_depth	100	825
40	6,725.8	5.8	132.0	312.0	2	P-Reflection	99033.0	32963.3	–490.1	P5_depth	1	384
40	369.1	6.2	132.3	312.3	1	P-Reflection	99038.6	32957.6	–528.9	KFM01A_01	1	54
40	369.1	6.2	132.3	312.3	1	P-Reflection	99038.6	32957.6	–528.9	KFM01A_03	1	54
40	369.1	6.2	132.3	312.3	1	P-Reflection	99038.6	32957.6	–528.9	KFM01A_05	1	52
40	575.2	6.2	132.3	312.3	1	P-Reflection	99038.6	32957.6	–528.9	KFM02A_01	1	96
40	575.2	6.2	132.3	312.3	1	P-Reflection	99038.6	32957.6	–528.9	KFM02A_02	1	96
40	575.2	6.2	132.3	312.3	2	P-Reflection	99038.6	32957.6	–528.9	KFM02A_07	1	96
40	575.2	6.2	132.3	312.3	2	P-Reflection	99038.6	32957.6	–528.9	KFM02A_08	1	96
40		**6.1**	**132.3**	**312.3**			**99037.4**	**32958.9**	**–520.4**			
41	–41,478.3	26.0	135.6	315.6	2	P-Reflection	99130.1	32872.5	–373.5	P2_depth	1	925
41	2,293.5	26.9	135.6	315.6	2	P-Reflection	99138.3	32864.5	–382.2	P5_depth	234	384
41	631.1	26.9	135.6	315.6	2	P-Reflection	99138.3	32864.5	–382.2	KFM02A_01	1	107

No.	Depth	Dip (°)	Dip Dir (°)	Azimuth (°)	Visibility	Type	Northing Crux	Easting Crux	Elev Crux	Profile	1st receiver	last receiver
41	631.1	26.9	135.6	315.6	2	P-Reflection	99138.3	32864.5	–382.2	KFM02A_02	1	107
41	631.1	26.9	135.6	315.6	2	P-Reflection	99138.3	32864.5	–382.2	KFM02A_07	1	107
41	631.1	26.9	135.6	315.6	2	P-Reflection	99138.3	32864.5	–382.2	KFM02A_08	1	107
41		**26.7**	**135.6**	**315.6**			**99136.9**	**32865.8**	**–380.7**			
42	–29,256.1	24.6	136.9	316.9	2	P-Reflection	99155.6	32854.3	–466.4	P2_depth	1	925
42	2,586.2	24.6	136.9	316.9	1	P-Reflection	99155.6	32854.3	–466.4	P5_depth	217	384
42	699.2	24.6	136.9	316.9	1	P-Reflection	99155.6	32854.3	–466.4	KFM02A_01	1	120
42	699.2	24.6	136.9	316.9	2	P-Reflection	99155.6	32854.3	–466.4	KFM02A_02	1	120
42	699.2	24.6	136.9	316.9	1	P-Reflection	99155.6	32854.3	–466.4	KFM02A_07	1	120
42	699.2	24.6	136.9	316.9	1	P-Reflection	99155.6	32854.3	–466.4	KFM02A_08	1	120
42		**24.6**	**136.9**	**316.9**			**99155.6**	**32854.3**	**–466.4**			
43	118,385.0	23.3	161.9	341.9	2	P-Reflection	99227.5	32925.7	–554.7	P1_depth	1	100
43	2,741.9	23.3	161.9	341.9	2	P-Reflection	99227.5	32925.7	–554.7	P5_depth	260	384
43	220.8	23.3	161.9	341.9	2	P-S, S-P Conversion	99227.5	32925.7	–554.7	KFM01A_01	1	24
43	220.8	23.3	161.9	341.9	2	P-Reflection	99227.5	32925.7	–554.7	KFM01A_02	1	136
43	220.8	23.3	161.9	341.9	1	P-Reflection	99227.5	32925.7	–554.7	KFM01A_03	1	136
43	220.8	23.3	161.9	341.9	1	P-Reflection	99227.5	32925.7	–554.7	KFM01A_05	1	80
43	789.1	23.3	161.9	341.9	2	P-Reflection	99227.5	32925.7	–554.7	KFM02A_01	1	136
43	789.1	23.3	161.9	341.9	2	P-Reflection	99227.5	32925.7	–554.7	KFM02A_02	1	136
43	789.1	23.3	161.9	341.9	2	P-Reflection	99227.5	32925.7	–554.7	KFM02A_07	1	136
43	789.1	23.3	161.9	341.9	1	P-Reflection	99227.5	32925.7	–554.7	KFM02A_08	1	136
43		**23.3**	**161.9**	**341.9**			**99227.5**	**32925.7**	**–554.7**			
44	1,627.8	61.6	200.2	20.2	2	P-Reflection	99219.1	33080.5	–126.4	P1_depth	214	316
44	1,511.6	61.6	200.2	20.2	2	P-Reflection	99219.1	33080.5	–126.4	P5_depth	137	295
44	624.8	61.6	200.2	20.2	2	P-Reflection	99219.1	33080.5	–126.4	KFM01A_01	1	105
44	624.8	61.6	200.2	20.2	1	P-Reflection	99219.1	33080.5	–126.4	KFM01A_02	1	105
44	624.8	61.6	200.2	20.2	2	P-Reflection	99219.1	33080.5	–126.4	KFM01A_03	1	100
44	624.8	61.6	200.2	20.2	1	P-Reflection	99219.1	33080.5	–126.4	KFM01A_05	1	100

No.	Depth	Dip (°)	Dip Dir (°)	Azimuth (°)	Visibility	Type	Northing Crux	Easting Crux	Elev Crux	Profile	1st receiver	last receiver
44	936.0	61.6	200.2	20.2	2	P-S, S-P Conversion	99219.1	33080.5	–126.4	KFM02A_01	1	136
44	936.0	61.6	200.2	20.2	2	P-Reflection	99219.1	33080.5	–126.4	KFM02A_02	1	136
44	936.0	61.6	200.2	20.2	2	P-Reflection	99219.1	33080.5	–126.4	KFM02A_07	1	136
44	936.0	61.6	200.2	20.2	2	P-S, S-P Conversion	99219.1	33080.5	–126.4	KFM02A_08	1	136
44		**61.6**	**200.2**	**20.2**			**99219.1**	**33080.5**	**–126.4**			
45	1,312.7	40.0	170.2	350.2	2	P-Reflection	99364.9	32936.8	–441.3	P4_depth	181	247
45	2,110.8	40.0	170.2	350.2	2	P-Reflection	99364.9	32936.8	–441.3	P5_depth	291	384
45	981.9	40.0	170.2	350.2	2	P-Reflection	99364.9	32936.8	–441.3	KFM02A_01	1	136
45	981.9	40.0	170.2	350.2	2	P-Reflection	99364.9	32936.8	–441.3	KFM02A_02	1	136
45	981.9	40.0	170.2	350.2	2	P-Reflection	99364.9	32936.8	–441.3	KFM02A_07	1	136
45	981.9	40.0	170.2	350.2	2	P-Reflection	99364.9	32936.8	–441.3	KFM02A_08	1	136
45		**40.0**	**170.2**	**350.2**			**99364.9**	**32936.8**	**–441.3**			
46	421.4	82.0	170.5	350.5	2	P-Reflection	98780.6	33036.9	31.1	P2_depth	112	186
46	–4,089.6	81.8	170.0	350.0	1	P-Reflection	98768.6	33040.8	34.1	KFM01A_01	1	136
46	–4,089.6	82.0	170.5	350.5	2	P-Reflection	98780.6	33036.9	31.1	KFM01A_02	1	136
46	–4,089.6	82.0	170.5	350.5	2	P-Reflection	98780.6	33036.9	31.1	KFM01A_03	1	136
46	–4,089.6	82.0	170.5	350.5	2	P-Reflection	98780.6	33036.9	31.1	KFM01A_05	1	136
46	463.4	82.0	170.5	350.5	2	P-Reflection	98780.6	33036.9	31.1	KFM02A_01	1	73
46	463.4	82.0	170.5	350.5	2	P-Reflection	98780.6	33036.9	31.1	KFM02A_07	1	73
46	463.4	82.0	170.5	350.5	2	P-Reflection	98780.6	33036.9	31.1	KFM02A_08	1	73
46		**82.0**	**170.4**	**350.4**			**98779.1**	**33037.4**	**31.5**			
47	–88,699.9	3.0	157.0	337.0	2	P-Reflection	99021.8	32990.7	–452.0	P1_depth	260	390
47	–22,256.7	3.0	157.0	337.0	2	P-Reflection	99021.8	32990.7	–452.0	P2_depth	100	200
47	8,782.9	2.8	157.0	337.0	2	P-Reflection	99018.3	32992.2	–414.5	P4_depth	229	294
47	9,888.0	3.0	157.0	337.0	2	P-Reflection	99021.8	32990.7	–452.0	P5_depth	30	330
47	399.6	3.0	157.0	337.0	1	P-Reflection	99021.8	32990.7	–452.0	KFM01A_01	1	57
47	399.6	3.0	157.0	337.0	1	P-Reflection	99021.8	32990.7	–452.0	KFM01A_02	1	57
47	399.6	3.0	157.0	337.0	1	P-Reflection	99021.8	32990.7	–452.0	KFM01A_03	1	57

No.	Depth	Dip (°)	Dip Dir (°)	Azimuth (°)	Visibility	Type	Northing Crux	Easting Crux	Elev Crux	Profile	1st receiver	last receiver
47	399.6	3.0	157.0	337.0	1	P-Reflection	99021.8	32990.7	–452.0	KFM01A_05	1	57
47	478.7	3.0	157.0	337.0	1	P-Reflection	99021.8	32990.7	–452.0	KFM02A_01	1	76
47	478.7	3.0	157.0	337.0	2	P-Reflection	99021.8	32990.7	–452.0	KFM02A_02	1	76
47	478.7	3.0	157.0	337.0	2	P-Reflection	99021.8	32990.7	–452.0	KFM02A_07	1	76
47	478.7	3.0	157.0	337.0	2	P-Reflection	99021.8	32990.7	–452.0	KFM02A_08	1	76
47		**3.0**	**157.0**	**337.0**			**99021.5**	**32990.8**	**–448.9**			
48	2,472.0	31.7	204.7	24.7	2	P-Reflection	99191.3	33088.0	–340.4	P1_depth	249	363
48	2,206.1	31.7	204.7	24.7	2	P-Reflection	99191.3	33088.0	–340.4	P5_depth	137	273
48	586.8	31.7	204.7	24.7	1	P-Reflection	99191.3	33088.0	–340.4	KFM01A_01	1	98
48	586.8	31.7	204.7	24.7	1	P-Reflection	99191.3	33088.0	–340.4	KFM01A_02	1	98
48	586.8	31.7	204.7	24.7	2	P-Reflection	99191.3	33088.0	–340.4	KFM01A_03	1	98
48	586.8	31.7	204.7	24.7	1	P-Reflection	99191.3	33088.0	–340.4	KFM01A_05	1	136
48	595.2	31.7	204.7	24.7	2	P-Reflection	99191.3	33088.0	–340.4	KFM02A_01	1	100
48	595.2	31.7	204.7	24.7	2	P-Reflection	99191.3	33088.0	–340.4	KFM02A_02	1	100
48	595.2	31.7	204.7	24.7	2	P-Reflection	99191.3	33088.0	–340.4	KFM02A_07	1	100
48	595.2	31.7	204.7	24.7	1	P-Reflection	99191.3	33088.0	–340.4	KFM02A_08	1	100
48		**31.7**	**204.7**	**24.7**			**99191.3**	**33088.0**	**–340.4**			
49	1,896.3	59.0	205.0	25.0	2	P-Reflection	99196.9	33091.8	–130.5	P4_depth	240	320
49	1,517.0	59.0	205.0	25.0	2	P-Reflection	99196.9	33091.8	–130.5	P5_depth	250	300
49	797.4	59.0	205.0	25.0	2	P-Reflection	99196.9	33091.8	–130.5	KFM01A_01	1	136
49	797.4	59.0	205.0	25.0	1	P-Reflection	99196.9	33091.8	–130.5	KFM01A_02	1	136
49	797.4	59.0	205.0	25.0	1	P-Reflection	99196.9	33091.8	–130.5	KFM01A_03	1	136
49	797.4	59.0	205.0	25.0	2	P-Reflection	99196.9	33091.8	–130.5	KFM01A_05	1	136
49	808.0	59.0	205.0	25.0	2	P-Reflection	99196.9	33091.8	–130.5	KFM02A_01	1	136
49	808.0	59.0	205.0	25.0	2	P-Reflection	99196.9	33091.8	–130.5	KFM02A_02	1	136
49	808.0	59.0	205.0	25.0	2	P-Reflection	99196.9	33091.8	–130.5	KFM02A_07	1	136
49	808.0	59.0	205.0	25.0	2	P-Reflection	99196.9	33091.8	–130.5	KFM02A_08	1	136
49		**59.0**	**205.0**	**25.0**			**99196.9**	**33091.8**	**–130.5**			

Refraction seismic data and bedrock velocity distribution at Forsmark

Johan Nissen, Malå Geoscience AB

Contents

1 Introduction

Refraction seismic profiling has been performed in the Forsmark investigation area during several campaigns (Table 1-1). In the present note, we discuss only data collected during the time period 2004–2006, in connection with the SKB site investigation work (Figure 1-1). These data are described in /Toresson 2005, 2006/. The data from the construction of the nuclear power plant and SFR (1970–1982) are presented in /Isaksson and Keisu 2005/ and the geological implications are discussed in /SKB 2005, p. 184–185/. The purpose of the present note is to discuss the bedrock velocity distribution based on the results of the refraction seismics.

The data from 2004–2006 are all collected with a digital seismograph (ABEM Terraloc Mk 6). The geophone separation was 5 metres except for some minor parts where the separation was 2–3 metres. Table 1-2 lists the 43 profiles. The values "Assumed Length" and "Actual Length" in this table differ slightly, due to the fact that the geophone cable is not completely straight between the geophone positions.

Table 1-1. Summary of refraction seismic campaigns at Forsmark.

Time period	Total length of profiles
1970–82	107.2 km
2004–06	30.3 km

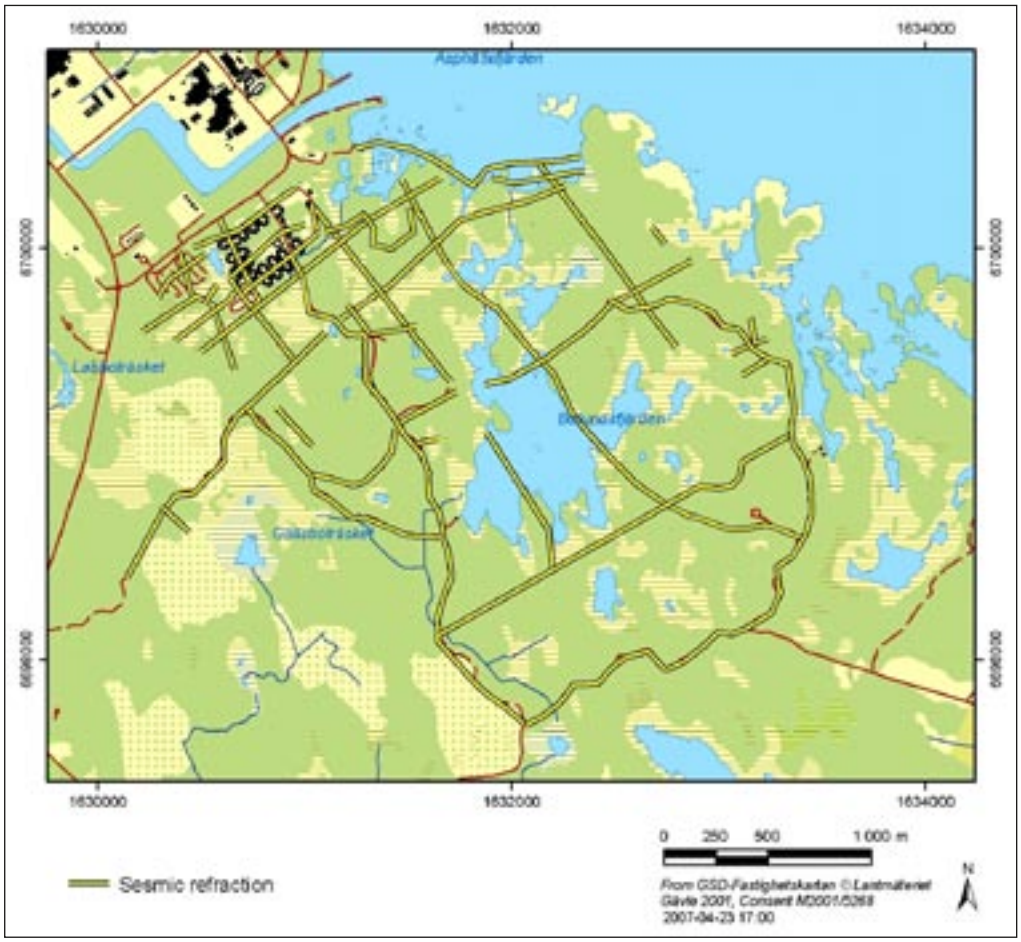

Figure 1-1. *Overview of the Forsmark investigation area, showing the location of the 43 refraction seismic profiles listed in Table 1-2. The campaign was focussed on the target area around Bolundsfjärden, in the north-western part of the candidate area.*

Table 1-2. 43 refraction seismic profiles completed during the 2004–2006 campaign. The column "Assumed length" is based upon the length of the geophone cable, and the column "Actual length" is based upon the coordinates of the geophone positions.

Idcode	Start Date	Assumed length (m)	Actual length (m)
LFM000825	2004-09-16 00:00	1,692.4	1,677.0
LFM000826	2004-09-24 00:00	175.1	174.8
LFM000827	2004-09-24 00:00	220.4	220.3
LFM000828	2004-09-16 00:00	316.4	316.1
LFM000829	2004-09-16 00:00	106.4	106.4
LFM000830	2004-09-19 00:00	1,208.0	1,206.8
LFM000831	2004-09-09 00:00	1,964.1	1,962.1
LFM000832	2004-09-15 00:00	126.0	126.0
LFM000833	2004-09-15 00:00	188.0	188.0
LFM000834	2004-09-15 00:00	162.0	161.9
LFM000835	2004-09-14 00:00	446.1	445.9
LFM000836	2004-09-23 00:00	730.9	728.6
LFM000889	2005-05-17 08:00	1,432.7	1,432.8
LFM000890	2005-05-15 08:00	452.3	452.2
LFM000891	2005-06-18 08:00	109.5	109.6
LFM000892	2005-06-18 08:00	310.5	310.4
LFM000893	2005-05-15 08:00	501.0	501.0
LFM000894	2005-05-12 08:00	115.0	115.0
LFM000895	2005-05-14 08:00	572.9	573.0
LFM000896	2005-05-14 08:00	324.0	324.0
LFM000897	2005-05-13 08:00	447.5	447.3
LFM000898	2005-05-13 08:00	110.0	110.0
LFM000899	2005-05-13 08:00	361.0	361.0
LFM000900	2005-05-16 08:00	672.5	672.4
LFM000901	2005-05-13 08:00	443.0	443.1
LFM000902	2005-09-30 08:00	583.0	582.9
LFM000903	2005-07-13 08:00	1,186.0	1,184.1
LFM000904	2005-10-07 08:00	1,804.5	1,797.3
LFM000905	2005-11-02 08:00	250.0	250.0
LFM000906	2005-11-24 08:00	100.0	100.0
LFM000907	2005-11-24 08:00	100.0	100.0
LFM000908	2005-11-01 08:00	178.0	178.0
LFM000915	2005-09-12 08:00	2,012.5	2,012.1
LFM000916	2006-03-15 08:00	1,185.0	1,184.6
LFM000917	2006-03-16 08:00	460.0	460.0
LFM000918	2005-09-28 08:00	755.0	755.0
LFM000919	2005-06-18 08:00	1,092.0	1,092.0
LFM001013	2005-07-05 08:00	1,293.0	1,293.0
LFM001014	2005-07-05 08:00	584.0	584.0
LFM001015	2005-10-30 08:00	1,007.5	1,007.0
LFM001016	2005-07-12 08:00	1,137.1	1,137.1
LFM001017	2005-06-21 17:00	2,332.5	2,327.0
LFM001018	2005-10-29 08:00	1,105.0	1,104.9
Total		30,352.7	30,314.3

2 Results

2.1 Bedrock velocity distribution

In order to study the distribution of the bedrock velocity, all velocity estimations from the campaigns 2004–2006 are compiled in the histogram in Figure 2-1. Table 2-1 presents a classification of velocity ranges observed in the present study and a comparison with the older data from 1970–1982 /Isaksson and Keisu 2005/. The most probable bedrock velocity in the area is 5,400 m/s (i.e. 5,350–5,450 m/s). Furthermore, along more than 88% of the total measured profile length, the bedrock velocity exceeds 5,000 m/s.

The old data from the Forsmark nuclear power plant and SFR show a similar velocity distribution. The most "typical" velocity is 5,500 m/s /Isaksson and Keisu 2005/, although the number of profiles with high velocity is lower than in the present data set.

Table 2-1. Classification of velocity ranges based upon the present data set (2004–2006) and from old data (1970–1982) taken from /Isaksson and Keisu 2005/.

	Velocity range	Amount of total profile length	
		1970–1982	2004–2006
High velocity	≥ 5,000 m/s	75%	88%
Medium velocity	4,000–5,000 m/s	23%	9.5%
Low velocity	≤ 4,000 m/s	2%	2.5%

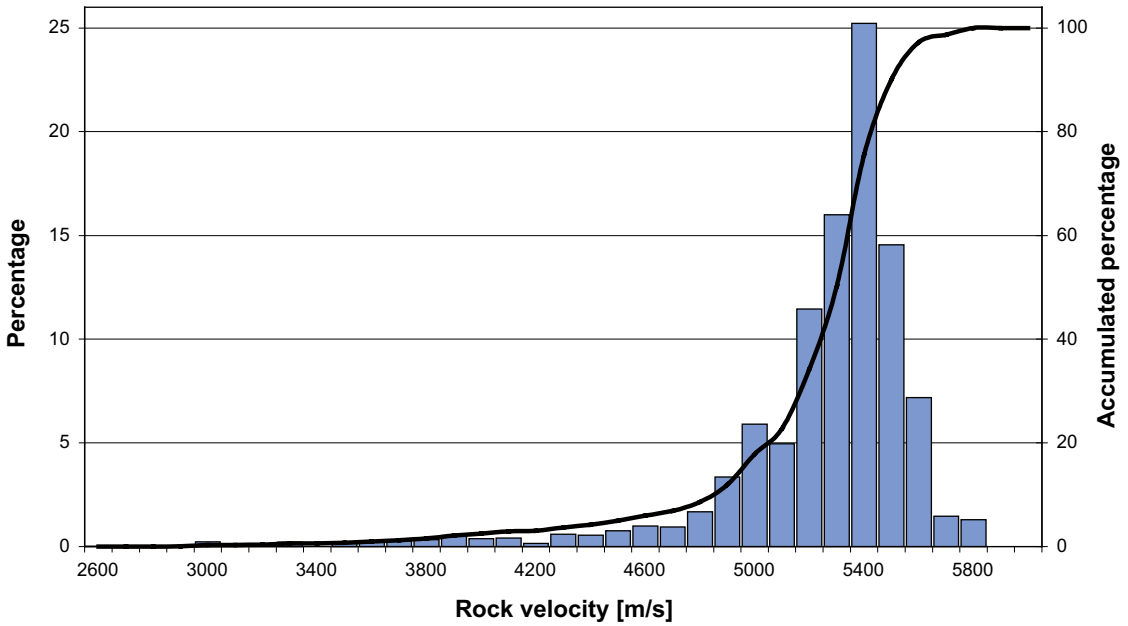

Figure 2-1. *The distribution of measured velocities, based upon the 30.3 km profile data from 2004–2006, together with the accumulated distribution (right scale). Each velocity bin covers a range of 100 m/s.*

3 References

Isaksson H, Keisu M, 2005. Interpretation of airborne geophysics and integration with topography Stage 2 (2002–2004). An integration of bathymetry. topography. refraction seismics and airborne geophysics. Forsmark site investigation. SKB P-04-282, Svensk Kärnbränslehantering AB.

SKB 2005. Preliminary site description. Forsmark area − version 1.2. SKB R-05-18, Svensk Kärnbränslehantering AB.

Toresson B, 2005. Seismic refraction survey 2004. Forsmark site investigation. SKB P-05-12, Svensk Kärnbränslehantering AB.

Toresson B, 2006. Seismic refraction survey 2005–2006. Forsmark site investigation. SKB P-06-138, Svensk Kärnbränslehantering AB.

Correlation between refraction seismic data, low magnetic lineaments and deformation zones (model stage 2.2)

Hans Isaksson, GeoVista AB

Contents

1 Introduction

This report addresses the correlation between refraction seismic data, low magnetic lineaments and deformation zones (model stage 2.2). The following data have been used in the study:

- Refraction seismic data and bedrock velocity from the construction of the nuclear power plant at Forsmark and SFR during 1970–1982 /Keisu and Isaksson 2004, Isaksson and Keisu 2005/ (Figure 1-1). These data are referred here to as old data.
- Refraction seismic data and bedrock velocity from the site investigations during 2004–2006 (Figure 1-1). Data from Sicada_06_148, 2006-06-30 have been used. These data are referred to here as new data.
- Large-scale airborne low magnetic lineaments that are present inside the regional model area and airborne low magnetic lineaments that intersect the local model area. These lineaments were established in connection with the modelling work stage 2.1 /SKB 2006/.
- Low magnetic lineaments from the detailed ground and marine magnetic survey 2006 /Isaksson et al. 2006/.
- An interim, stage 2.2 2D ground model for deformation zones, delivered by A. Simeonov and M. B. Stephens on 2007-04-18.
- A summary of the refraction seismic profiling completed in the Forsmark investigation area (see paper by Nissen on p. 107 in this report).

2 Methodology

Previous work has shown /e.g. Sjögren 1984/ that P-wave velocity correlates well to fracture intensity and hence can be used as an indicator of strong brittle deformation (Figure 2-1). Based on these considerations, a velocity magnitude of 4,000 m/s has been chosen as a threshold to identify low velocity anomalies in both the old and new data. For both sets of data, a buffer zone has been constructed that takes account of the uncertainty in the survey locations. The buffer zone is 5 and 10 m for the new and old data, respectively. Bearing in mind also the uncertainty in the position of the low magnetic lineaments (Figure 3-1) /Isaksson and Keisu 2005, Isaksson et al. 2006/, these structures have been treated in a similar manner. Lineaments identified from fixed-wing airborne survey data, helicopter survey data and detailed ground magnetic survey data have been given a buffer zone of 40, 20 and 10 m, respectively (Figure 3-2).

When low velocity and low magnetic lineament buffer zones intersect, this is considered as a match (Figure 3-2), and the lineament identity has been noted as a new attribute in the low velocity data set (Appendices 1 and 2 at the end of this report). The individual identity or the type of low magnetic lineament that matches has not been documented in this work.

A correlation between low velocity anomalies and deformation zones (site investigation model, stage 2.2) is registered when the low velocity anomaly occurs at or within the surface intersection of the inferred deformation zones (Figure 4-1). The width of the zone at the ground surface is accounted for in the analysis. This match is also noted in the low velocity data set as a new attribute (Appendices 1 and 2).

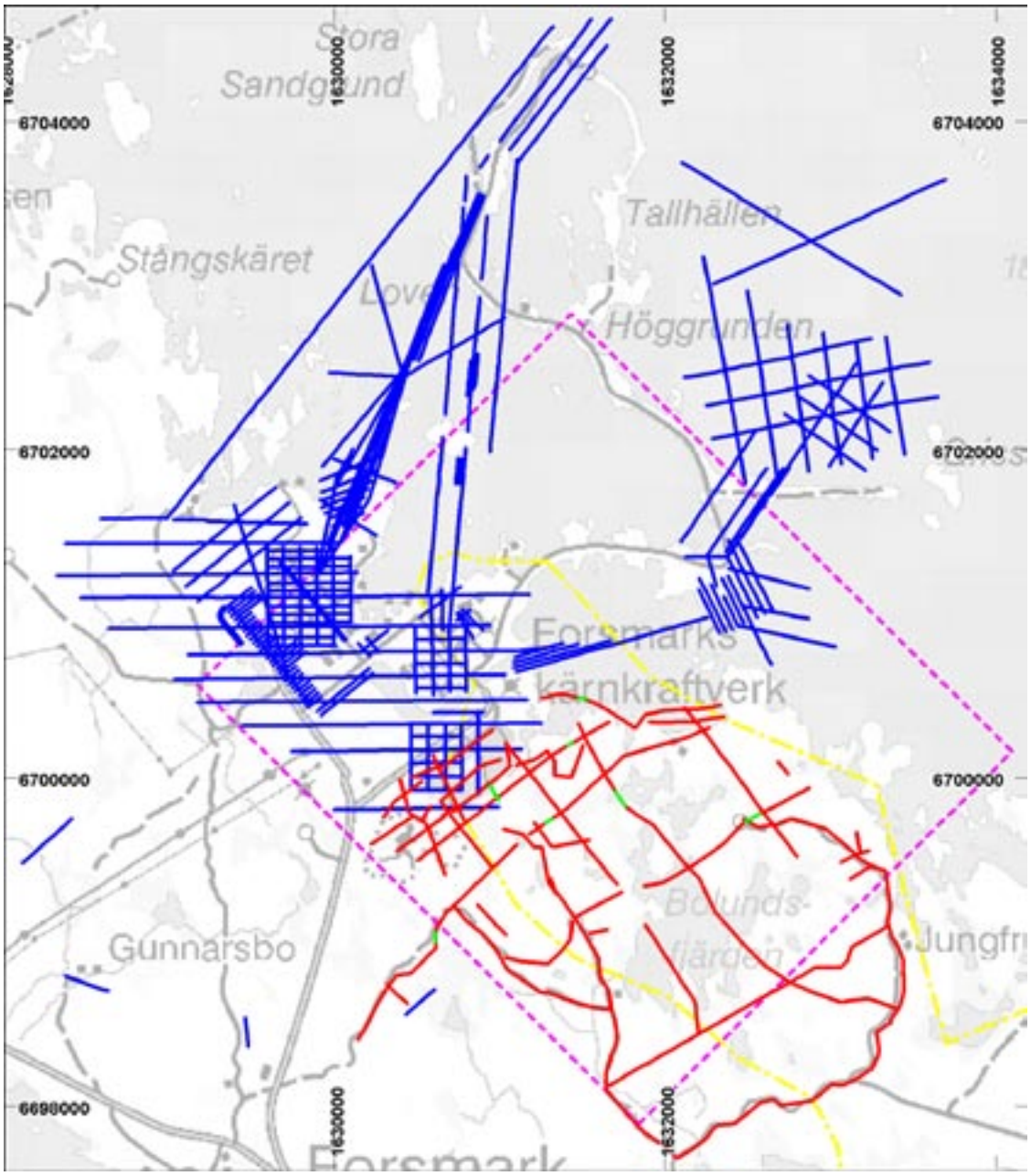

Figure 1-1. *Overview of refraction seismic profiles in the Forsmark area. Old surveys from 1970–1982 are shown with blue lines and the site investigation surveys from 2004–2006 in red. Green sections of the latter profiles show parts where no bedrock velocity data were determined. The local model area is shown with a dashed magenta line and the Forsmark candidate area with a yellow dot-dashed line. One short profile from the older surveys is located at Forsmarks bruk, immediately south of the viewed area.*

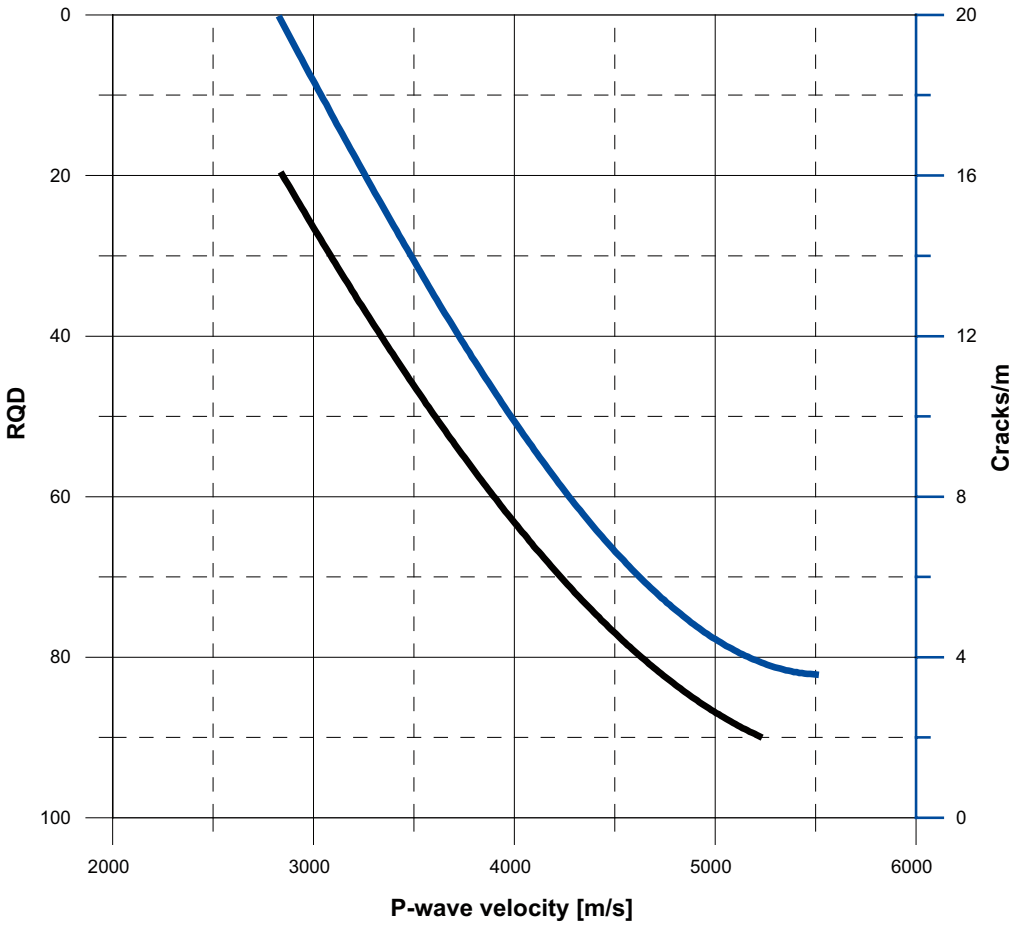

Figure 2-1. *P-wave velocity for bedrock in relation to cracks (fractures) per m (blue line) and RQD value (black line) according to /Sjögren 1984/.*

3 Correlation of low velocity anomalies and low magnetic lineaments

A comparison of the low velocity anomalies and the current interpretation of low magnetic lineaments (Figure 3-1) yields a total of 97 matches out of 266 possible low velocity sections, (Figure 3-2). Statistical data that address the correlation between low velocity anomalies and low magnetic lineaments indicate that the results are very similar for both the old and new data (Table 3-1). 36% of all low velocity anomalies (40% of the length) show a correlation with a low magnetic lineament, while 64% (60%) show no correlation. The number of correlations in the detailed, ground magnetic survey area is higher. This can be expected, bearing in mind the higher frequency of low magnetic lineaments. The low magnetic lineaments that correlate to low rock velocity anomalies are documented in Appendices 1 and 2 for the new and old data sets, respectively. Sections of low velocity within the detailed, magnetic ground survey area are marked with an asterisk in Appendices 1 and 2.

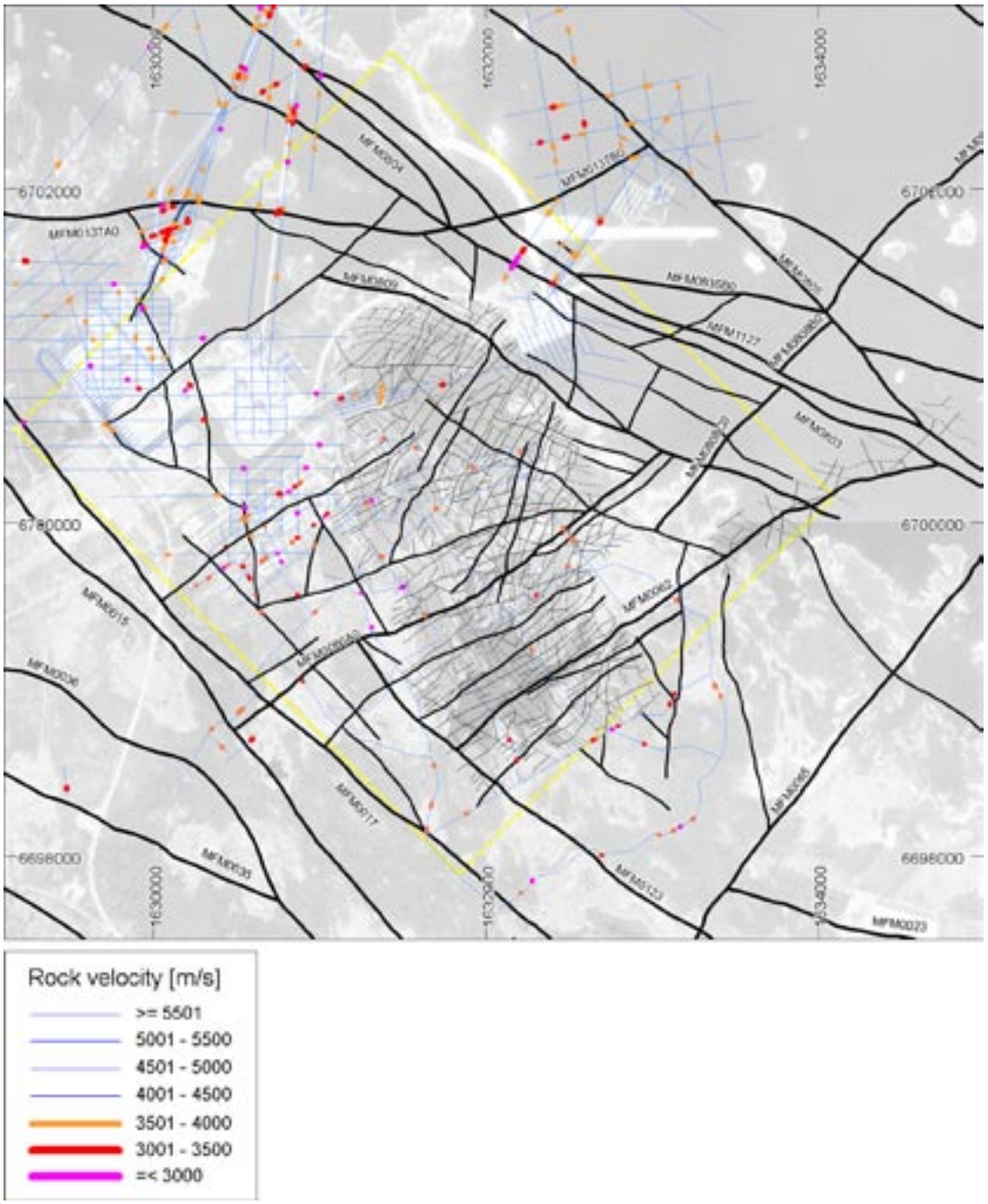

Figure 3-1. *Low velocity determinations in the bedrock (≤ 4,000 m/s) from both old and new data and their relationship to low magnetic lineaments according to /Isaksson et al. 2006/. Thick, medium and thin black solid lines represent discordant magnetic minima with a length of > 3 km, 1–3 km and < 1 km, respectively. Thin dashed lines show magnetic minima connections of concordant nature. The local model area is shown with a dashed yellow line. © Lantmäteriet, Gävle 2007, Consent 1 2007/1092.*

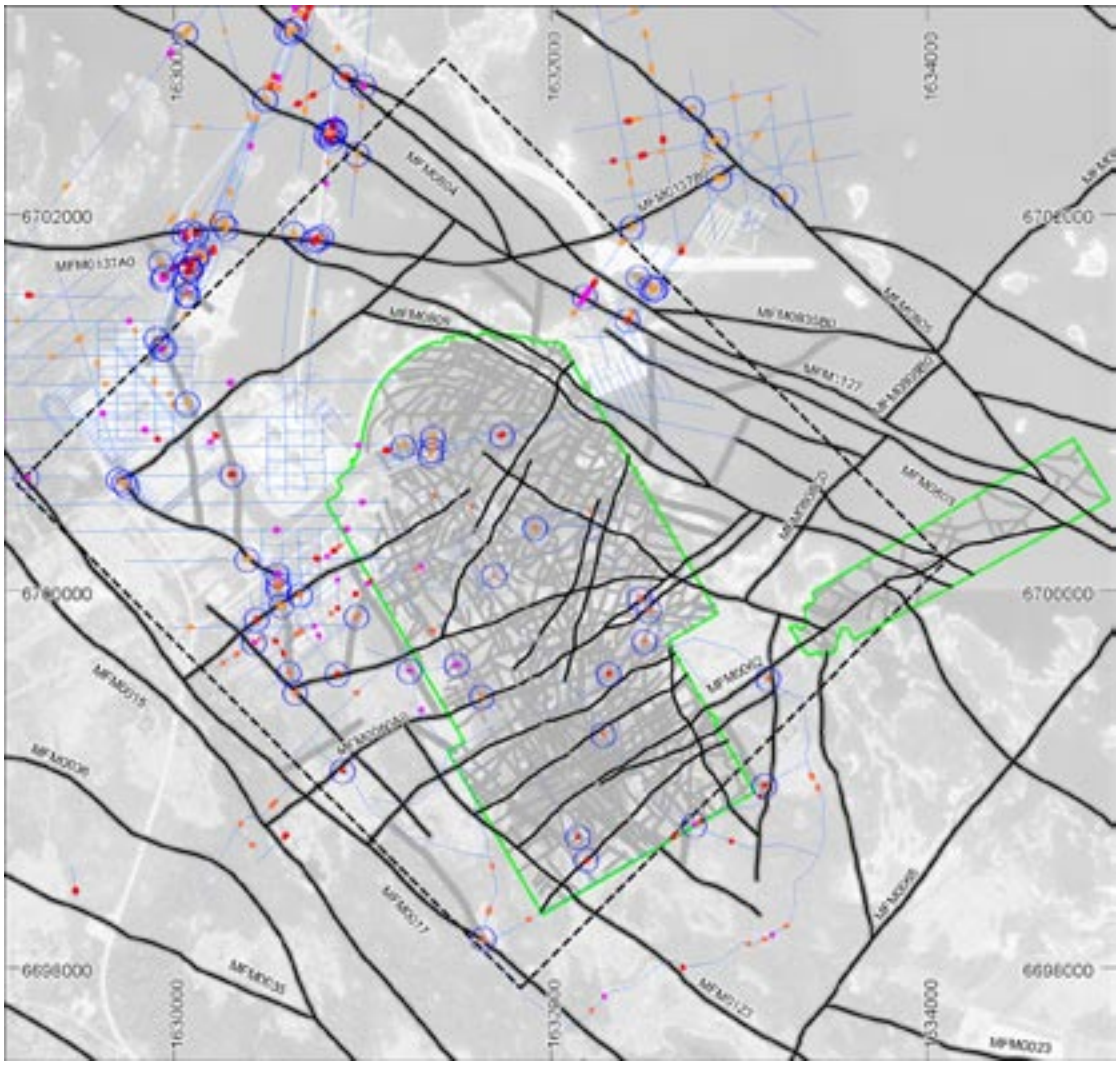

Figure 3-2. *Intersections between low velocity anomalies and low magnetic lineaments (blue circles). These intersections take into account the buffer zones that address the uncertainty in the location of the anomalies and the lineaments. The grey corridors indicate buffer zones around the lineaments and the corresponding low magnetic lineaments, > 1 km in length, are outlined with a black solid line. The local model area is shown with a dashed black line. The detailed ground magnetic survey area is shown with a green solid line. As in Figure 3-1, the parts of the refraction seismic profiles that indicate a rock velocity > 4,000 m/s are shown as blue solid lines. © Lantmäteriet, Gävle 2007, Consent 1 2007/1092.*

Table 3-1. Statistical summary of correlation between low velocity anomalies (LV) and low magnetic lineaments in and around the local model area (MFM), and within the detailed, ground magnetic survey area (DGM).

	Old data	New data	Total
Number of sections	1,322	494 *	1,816
Profile length (m)	108,485	29,656 *	138,141
Average velocity (m/s)	5,202	5,236	5,209
Mode velocity, ca (m/s)	5,400–5,500	5,400–5,500	5,400–5,500
LV, sections	195	71	266
(% of total number)	(15%)	(14%)	(15%)
LV, length (m)	3,189	746	3,935
(% of total length)	(2.9%)	(2.5%)	(2.8%)
LV, average velocity (m/s)	3,675	3,637	3,668
LV-MFM match, no. of sections	72	25	97
(% of LV, no. of sections)	(37%)	(35%)	(36%)
LV-MFM match, length (m)	1,287	294	1,581
(% of LV length)	(40%)	(39%)	(40%)
LV-MFM within DGM, match, no. of sections	5 of 9	12 of 22	17 of 31
(% of LV, no. of sections)	(56%)	(55%)	(55%)
LV-MFM within DGM, match length (m)	65 of 90	129 of 192	194 of 282
(% of LV length)	(72%)	(67%)	(69%)

* Sections with no rock velocity determined are omitted.

4 Correlation of low velocity anomalies and modelled deformation zones (stage 2.2)

A comparison of the low velocity anomalies and the current interpretation of deformation zones in model stage 2.2 (Figure 4-1) yields a total of 87 matches out of 266 possible low velocity sections, Statistical data that address the correlation between low velocity anomalies and deformation zones are presented in Table 4-1. As for low magnetic lineaments, the percentage of no correlation is higher and 2 out of 3 low velocity anomalies do not match deformation zones. The low rock velocity anomalies that correlate to deformation zones are documented in Appendices 1 and 2.

The number of deformation zones inside the detailed ground magnetic survey area is somewhat higher than outside. For this reason, it can be expected that there should be a higher matching frequency inside the ground magnetic survey area and this is indeed valid for the new data. However, the statistical basis is insufficient and the result is only indicative. Sections of low velocity within the detailed ground magnetic survey area are marked with an asterisk in Appendices 1 and 2.

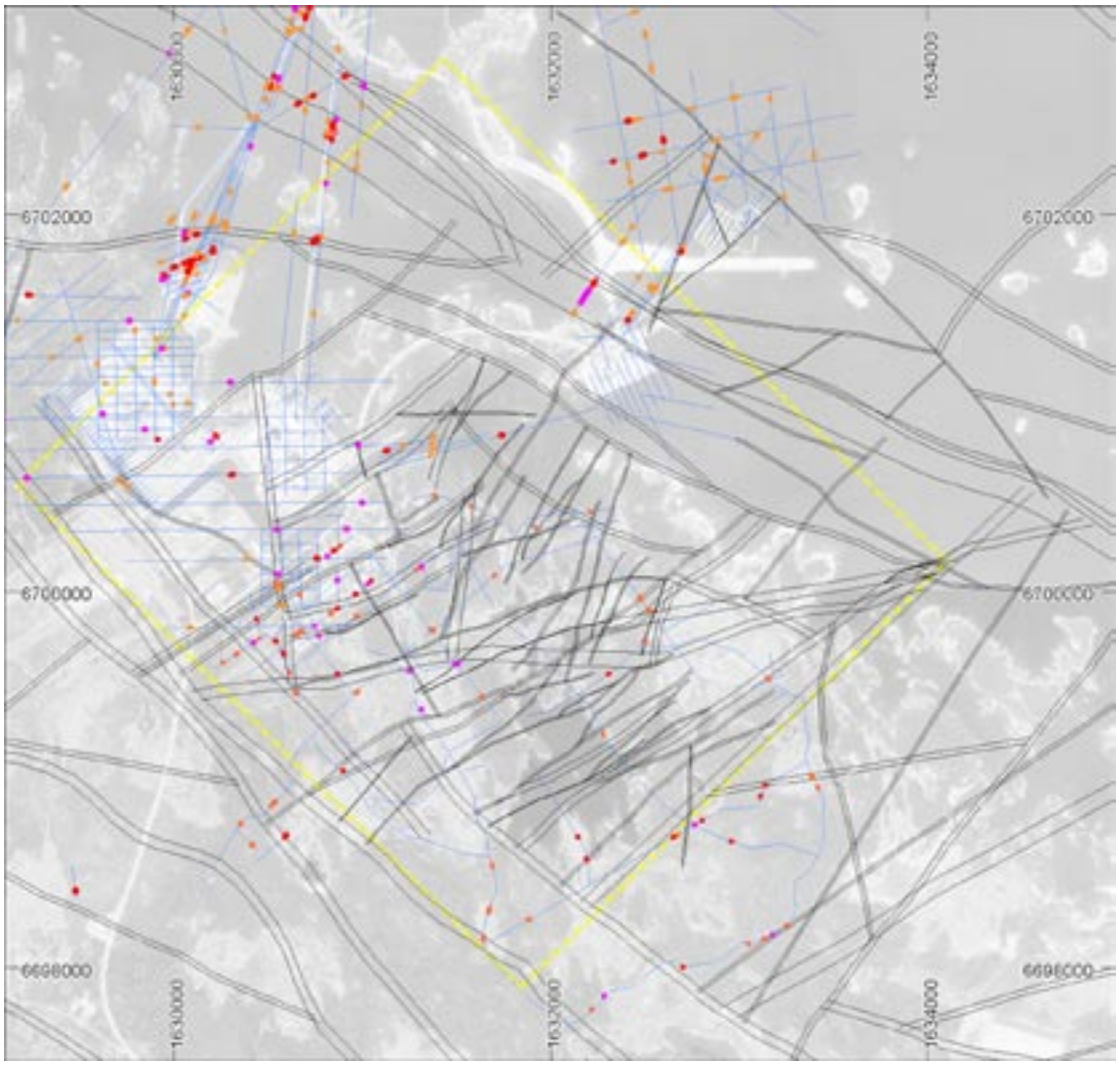

Figure 4-1. *Low velocity anomalies in the bedrock (≤ 4,000 m/s) from both old and new data and their relationship to the ground intersection of inferred deformation zones in the site investigation model, stage 2.2 (thin black lines). The width of the deformation zones at the surface is taken into account in the analysis work. The local model area is shown with a dashed yellow line. The rock velocity in refraction seismic profiles is illustrated in the same manner as in Figure 3-1. © Lantmäteriet, Gävle 2007, Consent 1 2007/1092.*

Table 4-1. Statistical summary of correlation between low velocity indications (LV) and deformation zones (DZ) in and around the local model area, and within the detailed ground magnetic survey area (DGM).

	Old data	New data	Total
LV-DZ match, no. of sections	62	25	87
(% of LVi, no. of sections)	(32%)	(35%)	(33%)
LVi-DZ match, length (m)	1,004	335	1,339
(% of LVi length)	(31%)	(45%)	(34%)
LV-DZ within DGM, match, no. of sections	0 of 9	9 of 22	9 of 31
(% of LVi, no. of sections)	(0%)	(41%)	(29%)
LV-DZ within DGM, match length (m)	0 of 90	112 of 192	112 of 282
(% of LVi of length)	(0%)	(58%)	(40%)

5 Discussion and conclusions

The analysis carried out here shows that there is moderate correlation between low velocity anomalies and low magnetic lineaments or modelled deformation zones. Typically, there are only one or a few low velocity anomalies along some of the intersecting profiles and several profiles lack anomalies. Both survey methodology and geological conditions need to be considered in the assessment of the relatively poor correlation. These two features are explored in more detail below.

A study of the refraction seismic data along the well-established Singö deformation zone (ZFMWNW0001) yields some interesting results. The c. 200 m wide surface extension of the Singö deformation zone is intersected by refraction seismics over a total length of c. 5,000 m (Figure 5-1). The zone can be considered as well-defined by three tunnels and by considerable drilling close to the seismic surveys. A comparison between the refraction seismic data and the intersection of the zone at the surface shows that only 11% of the total profile length within the zone has a velocity ≤ 4,000 m/s (Table 5-1). Another important difference to the surrounding data is that 46% of the total length is within the medium velocity interval compared to 17% overall.

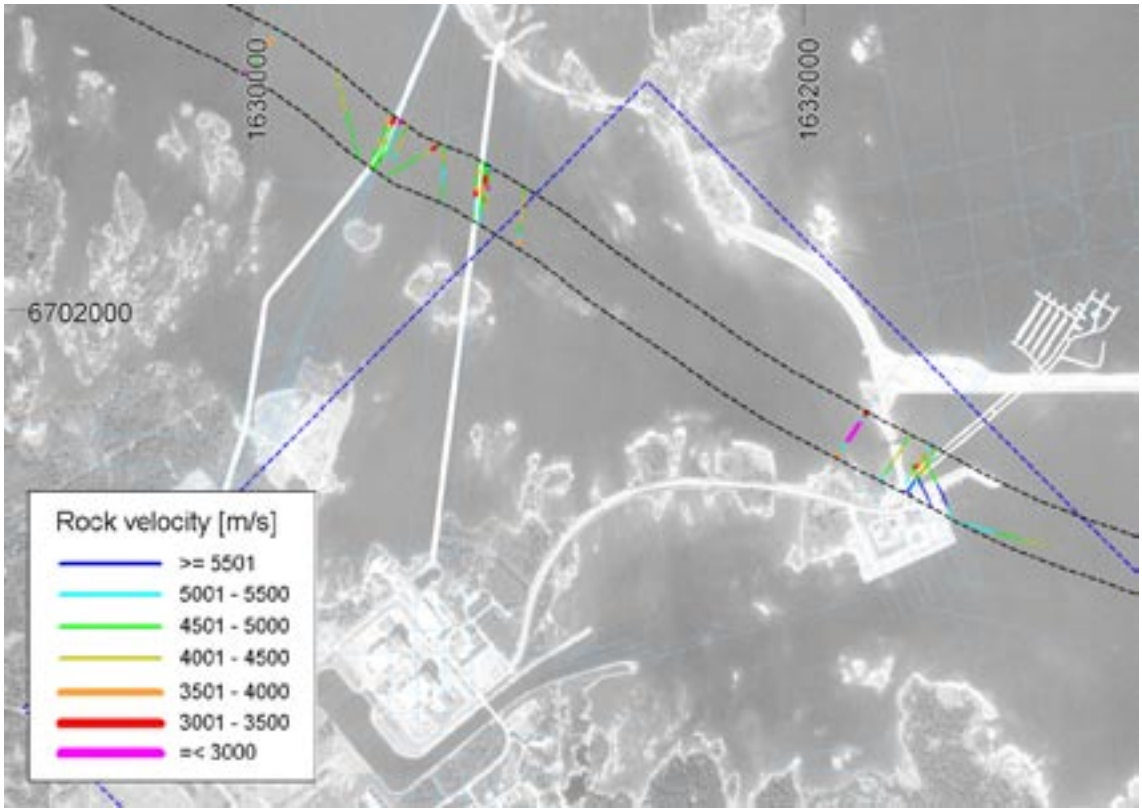

Figure 5-1. *Refraction seismic profiles and bedrock velocity magnitudes in the Singö deformation zone (ZFMWNW0001). Profiles outside the zone are shown as cyan lines. Blue dashed line shows the local model area. Background, GSD-ortofoto © Lantmäteriet, Gävle 2001, Permission M2001/5268.*

Table 5-1. Classification of velocity ranges based on Table 3 in paper by Nissen on p. 107 in this report. A column has been added for data intersecting ZFMWNW0001 (Singö deformation zone).

	Velocity range	Amount of total profile length			
		1970–1982	2004–2006	Total	ZFMWNW0001
High velocity	≥ 5,000 m/s	75%	88%	80%	43%
Medium velocity	4,000–5,000 m/s	23%	9.5%	17%	46%
Low velocity	≤ 4,000 m/s	2%	2.5%	2.8%	11%

The information along the Singö deformation zone indicates some difficulty to resolve individual narrow sections with low velocity in the refraction seismic data, since the given velocity is determined by an average velocity over longer sections composed of both normal and low velocity sections. Bearing in mind the high velocity for the intact bedrock in the Forsmark area, this also indicates that the average velocity for such a mixed section will show a bias towards a higher value. Interpretation templates for refraction seismic surveys, completed during the construction of the nuclear power plant and SFR /Isaksson and Keisu 2005, Figure 5-7/, show that velocities ≤ 4,000 m/s are characterized as crushed or fractured bedrock, while velocities ≥ 4,500 m/s indicate medium to good bedrock quality. Thus, the interval 4,000–4,500 m/s would possibly indicate poor to medium bedrock quality. /Fagerlund 1977/ also noted that sections within this velocity interval possibly can contain narrow fracture zones. It is concluded that the adoption of a single velocity threshold, such as ≤ 4,000 m/s, may lead to an underestimation of matches between low velocity anomalies and inferred deformation zones or low magnetic lineaments.

Together with the bedrock velocity contrasts, the geophone spacing has a strong influence on the spatial resolution of the velocity determinations. For most of the refraction seismic surveys in the Forsmark area, 5 m geophone station spacing has been used. In the sea area, 10 m geophone spacing is noted in a few cases from the old data and in the 2004–2006 survey, 2 m spacing was only used along a few lines. From all 1,816 velocity sections available (Table 3-1), only three sections (from the old survey) were determined as shorter than 5 m.

Figure 5-2 shows an example in which two close profiles (between 0 and 20 m apart) have been carried out with 5 m and 2 m geophone spacing, respectively. The profiles both traverse the inferred deformation zone ZFMENE0060A that corresponds to the low magnetic lineament MFM0060A0. The 5 m profile LFM000825 shows no indication of lower velocities, while the 2 m profile LFM000906 yields one 6 m wide section at 3,000 m/s and one 29 m section at 4,060 m/s intersecting the deformation zone. Along the adjacent 5 m profile LFM000919, a 10 m wide low velocity anomaly correlates well with the deformation zone. It is concluded that, with a geophone spacing of 5 m, there is a strong possibility that low velocity zones narrower than 5 m will not be detected.

Low velocity anomalies in the bedrock may represent brittle deformation zones that contain an anomalous concentration of open fractures or one or more open crush zones. However, there is an inherent heterogeneity along such zones, where it concerns the frequency of open fractures, and the methodology is considerably less efficient where it concerns the detection of brittle deformation zones with sealed fractures and sealed fracture networks. This type of steeply dipping deformation zone is common at Forsmark /SKB 2006/, not least inside the north-western part of the candidate volume where the new refraction seismic data have been acquired. Many of the low magnetic lineaments may be related to a bedrock alteration around sealed fractures or even other rock contrasts (e.g. Group D dykes, pegmatite and amphibolite) that do not result in a sufficiently decreased P-wave velocity. Thus, the geological character of the Forsmark area is a key factor that helps to explain the absence of a strong correlation between low velocity anomalies, deformation zones and low magnetic lineaments.

Figure 5-2. *Refraction seismic profiles LFM000825 (5 m geophone spacing) and LFM000906 (2 m geophone spacing) traversing the inferred deformation zone ZFMENE0060A (black dashed lines) and low magnetic lineament MFM0060A0 (black solid line) close to drill sites 1 and 5. Magnitude of bedrock velocity as in Figure 5-1. Roads and drill sites are shown with a red dashed line. The profile LFM000906 is 100 m long. Background, GSD-ortofoto © Lantmäteriet, Gävle 2001, Permission M2001/5268.*

Highly fractured bedrock close to the surface is one of the distinctive features of the Forsmark site. A continuously increasing velocity downwards, which is related to a decrease of fracturing in this direction, may obscure the occurrences of sub-vertical low velocity zones in the deeper parts of the bedrock. Furthermore, care needs to be taken in the interpretation work concerning the influence of older, well-packed boulder clay that shows a higher P-wave velocity relative to the normal Quaternary cover.

The low velocity anomalies that do not match low magnetic lineaments and/or deformation zones and that are as yet not explained may represent unidentified fracture zones. However, they may also be related to local narrow depressions in the bedrock surface that correlate with fractured near-surface bedrock or are simply filled with Quaternary cover material. Most of the low velocity anomalies that are so far not explained occur outside the Forsmark candidate area and in areas where the coverage of magnetic data is poor. Thus, mismatches may be explained by lack of magnetic data. The correlation rate between low velocity anomalies and low magnetic lineaments would probably increase significantly if detailed ground magnetic data was available over larger areas.

6 References

Fagerlund H, 1977. Rapport 58/21 över seismiska grundundersökningar för SFR, Forsmark. Statens Vattenfallsverk, arkivnummer: 764445/0917.

Keisu M, Isaksson H, 2004. Acquisition of geological information from Forsmarksverket. Information from the Vattenfall archive, Råcksta. SKB P-04-81, Svensk Kärnbränslehantering AB.

Isaksson H, Keisu M, 2005. Interpretation of airborne geophysics and integration with topography. Stage 2 (2002–2004). An integration of bathymetry, topography, refraction seismics and airborne geophysics. SKB P-04-282, Svensk Kärnbränslehantering AB.

Isaksson H, Thunehed H, Pitkänen T, Keisu M, 2006. Detailed ground and marine magnetic survey and lineament interpretation in the Forsmark area – 2006. SKB P-06-261, Svensk Kärnbränslehantering AB.

Sjögren B, 1984. Shallow refraction seismics. Chapman and Hall. ISBN 0 412 24210 9.

SKB, 2006. Site descriptive modelling Forsmark stage 2.1. Feedback for completion of the site investigation including input from safety assessment and repository engineering. SKB R-06-38, Svensk Kärnbränslehantering AB.

Appendix 1

Low rock velocity anomalies (LV), ≤ 4,000 m/s, from refraction seismics 2004–2006 and their relation to deformation zones and low magnetic lineaments.

Id code	Rock velocity [m/s]	Length [m]	DZ_Correlation	MFM_lineament correlation
LFM000825	3,000	10.00	NNW0404	MFM1196
LFM000827 *	3,000	15.00	ENE2254	MFM2233G, MFM2254G
LFM000830	3,200	5.00	none	MFM0060
LFM000831 *	3,800	10.00	NNE2008	MFM2008G
LFM000831	4,000	10.00	ENE0062A	MFM0126
LFM000831	3,700	17.50	ZFM866	None
LFM000831	3,700	10.00	none	None
LFM000836 *	3,000	7.50	ENE2320	None
LFM000889 *	3,800	10.00	ENE2320	None
LFM000889	3,950	15.00	none	MFM1197
LFM000890	3,000	5.00	none	None
LFM000892	3,600	5.00	none	None
LFM000892	3,000	5.00	none	MFM1200,(MFM0159)
LFM000892	3,850	15.00	none	None
LFM000892	3,600	5.00	none	None
LFM000893	3,300	5.00	ENE0061,ZFMA2	MFM0061
LFM000895	3,900	15.00	none	None
LFM000895	3,300	15.00	none	None
LFM000895	2,900	5.00	none	None
LFM000895	3,900	45.00	NNW0100,ENE1208A	MFM0100
LFM000897	3,300	5.00	none	None
LFM000897	2,600	5.00	none	None
LFM000897	3,300	10.00	none	None
LFM000897	3,500	5.00	ENE2320	None
LFM000897	3,800	10.00	none	None
LFM000898	3,800	40.00	ENE2325A	None
LFM000900	3,900	20.00	NW1200	MFM1200, MFM2254G, MFM0100
LFM000900	3,800	10.00	NNW0100	MFM0100
LFM000900	3,500	15.00	none	None
LFM000900	3,300	10.00	none	None
LFM000900	3,500	5.00	ENE0159A	MFM0159
LFM000901	3,000	5.00	ENE2325A	None
LFM000901	3,000	5.00	none	None
LFM000901	3,600	10.00	none	MFM0159
LFM000903 *	3,200	5.00	none	MFM2261G
LFM000904	4,000	10.00	ZFMA7	None
LFM000904	2,900	5.00	ZFMA7	None
LFM000904	3,700	10.00	ZFMA7	None
LFM000904	4,000	5.00	none	None
LFM000904	3,300	5.00	none	None
LFM000904	3,000	10.00	none	None
LFM000904	3,900	5.00	none	None
LFM000906 2	3,000	6.00	none	None
LFM000908 2	3,600	8.00	none	None

Id code	Rock velocity [m/s]	Length [m]	DZ_Correlation	MFM_lineament correlation
LFM000915	3,200	5.00	ZFM866	MFM0683
LFM000915	3,500	10.00	none	None
LFM000915 *	3,300	5.00	none	None
LFM000915 *	2,800	9.00	none	MFM2424G
LFM000915 *	4,000	5.00	none	None
LFM000915 *	3,500	5.00	none	None
LFM000915	3,600	10.00	none	None
LFM000916 *	3,700	5.00	none	None
LFM000916 *	4,000	10.00	ZFM1203	None
LFM000916 *	4,000	5.00	none	None
LFM000917 *	3,900	5.00	none	MFM0168
LFM000918 *	3,300	10.00	ENE2332	MFM2332G0
LFM000918 *	3,500	5.00	none	MFM2351G, MFM2354G
LFM000919 *	3,900	10.00	ENE0060A	MFM0060, MFM0060G0 and G1
LFM000919 *	4,000	5.00	none	None
LFM001013 *	4,000	10.00	none	MFM1198G
LFM001013 *	3,800	5.00	none	None
LFM001014	3,800	15.00	none	None
LFM001015	3,700	37.90	none	None
LFM001015	4,000	10.00	none	None
LFM001016 *	3,900	20.00	ENE0060B	MFM0060G1, (MFM2085G)
LFM001016 *	4,000	20.00	ENE0060A	MFM0060G0
LFM001017	3,100	5.00	none	None
LFM001017 *	4,000	10.00	none	MFM2445G, MFM2382G
LFM001018	3,600	20.00	NW0017	MFM0017
LFM001018	3,900	25.00	none	None
LFM001018	3,600	10.00	none	None

* Shows LV within the detailed, magnetic ground survey area. The digit 2 after the profile identity stands for 2 m geophone spacing.

Appendix 2

Low rock velocity anomalies (LV), ≤ 4,000 m/s, from refraction seismics 1970–1982 and their relation to deformation zones and low magnetic lineaments.

Id code	Rock velocity [m/s]	Length [m]	DZ_Correlation	MFM_lineament correlation
LFK000150	3,500	15.83	none	None
LFK000147	4,000	23.21	none	None
LFK000058	3,500	5.13	none	None
LFK000059	3,000	5.36	none	None
LFK000060	3,000	5.35	none	None
LFK000061	4,000	7.29	none	MFM1088
LFK000062	3,900	11.76	none	None
LFK000065	4,000	9.20	none	MFM1088
LFK000066	4,000	13.69	none	MFM1092, MFM1088
LFK000068	4,000	10.12	none	None
LFK000070	4,000	10.00	none	None
LFK000071	3,900	14.64	none	None
LFK000072	3,800	12.25	none	None
LFK000001	3,000	5.00	none	None
LFK000002	3,800	11.00	none	None
LFK000002	3,000	5.00	none	None
LFK000003	3,000	3.00	NNW1204	None
LFK000005	3,000	5.00	none	None
LFK000006	4,000	25.00	WNW1068	MFM1068
LFK000006	3,500	10.00	none	None
LFK000007	4,000	19.99	none	None
LFK000008	4,000	9.00	none	None
LFK000009	3,000	5.00	none	None
LFK000010	3,000	6.00	NW0017	MFM0017
LFK000010	3,500	11.00	none	MFM1072
LFK000011	3,000	5.00	NNW0100	None
LFK000011 *	3,000	5.01	none	None
LFK000021	3,000	5.01	WNW1068,NNW0100	MFM0100, MFM1068
LFK000022	3,600	18.00	NNW0100,ENE1208B	MFM0100
LFK000023	4,000	29.00	NNW0100,ENE0159A	MFM0100, MFM0159
LFK000030	4,000	14.00	none	None
LFK000030	4,000	10.00	none	MFM0137
LFK000030	3,000	5.01	none	None
LFK000030	4,000	6.00	none	None
LFK000030	3,600	30.00	WNW0001	MFM803
LFK000030	4,000	20.00	none	None
LFK000030	3,500	10.01	none	None
LFK000030	3,500	39.00	none	None
LFK000046	3,000	2.99	none	None
LFK000047	3,400	8.00	none	None
LFK000044	4,000	23.99	none	None
LFK000044	4,000	13.00	none	None
LFK000044	3,300	13.00	WNW0001	None
LFK000044	3,500	5.00	none	None
LFK000044	3,900	13.00	NW0002	MFM0804
LFK000044	3,800	7.00	none	None

Id code	Rock velocity [m/s]	Length [m]	DZ_Correlation	MFM_lineament correlation
LFK000045	3,700	10.00	none	None
LFK000045	4,000	19.00	none	None
LFK000045	3,000	16.00	WNW0001	None
LFK000045	3,900	18.00	WNW0001	MFM0803
LFK000045	4,000	30.01	WNW0001	None
LFK000045	3,500	9.99	NW0002	MFM0804
LFK000045	3,600	22.00	NW0002	None
LFK000045	3,700	11.00	none	None
LFK000045	3,850	10.00	none	None
LFK000039	3,000	5.01	none	None
LFK000039	3,700	5.00	none	None
LFK000039	3,000	5.00	none	None
LFK000039	4,000	20.00	NW0017	MFM0017
LFK000040	4,000	5.01	none	None
LFK000041	3,000	5.00	NW0017	MFM0017
LFK000041	3,000	5.01	none	None
LFK000043	3,000	5.01	none	MFM0015
LFK000031 *	3,500	10.00	none	None
LFK000031 *	4,000	15.00	none	MFM2126G
LFK000031 *	4,000	20.00	none	MFM2505G
LFK000032 *	4,000	10.00	none	None
LFK000033 *	4,000	15.00	none	MFM2165G
LFK000034 *	4,000	5.00	none	MFM2165G
LFK000034 *	3,500	10.00	none	MFM2310G
LFK000037	3,800	20.00	none	MFM0137
LFK000037	3,800	20.00	WNW0001	None
LFK000054	3,500	10.00	WNW0001	MFM803
LFK000054	3,800	15.00	WNW0001	MFM803
LFK000054	3,950	15.00	WNW0001	None
LFK000055	3,700	10.00	WNW0001	MFM803
LFK000055	3,000	6.00	WNW0001	MFM803
LFK000055	3,700	4.00	WNW0001	MFM803
LFK000055	3,000	5.00	WNW0001	None
LFK000056	3,500	15.00	EW0137	MFM0137
LFK000057	3,500	14.00	EW0137	MFM0137
LFK000081	3,700	15.00	none	None
LFK000082	4,000	22.00	none	None
LFK000082	4,000	8.00	none	None
LFK000083	3,500	12.00	WNW0001	None
LFK000083	3,600	15.00	none	None
LFK000083	3,200	12.00	none	None
LFK000083	3,400	15.01	NW0002,NW1127	MFM1127, MFM0804
LFK000076	3,000	7.00	none	MFM1093
LFK000077	3,500	5.99	none	None
LFK000077	3,900	29.99	none	MFM0137
LFK000078	3,900	35.01	WNW0001	None
LFK000078	3,600	10.01	NW0002	MFM0804
LFK000078	4,000	19.00	none	None
LFK000078	3,000	5.00	none	None
LFK000079	3,700	16.00	WNW0001	None

Id code	Rock velocity [m/s]	Length [m]	DZ_Correlation	MFM_lineament correlation
LFK000079	3,000	16.00	WNW0001	None
LFK000079	3,000	4.99	none	None
LFK000079	4,000	10.00	NW0002	MFM0804
LFK000079	3,900	15.00	none	None
LFK000080	3,600	17.00	WNW0001	None
LFK000080	3,600	5.00	none	None
LFK000080	3,300	19.00	none	None
LFK000080	3,400	10.00	none	None
LFK000103	3,800	8.00	WNW1068	MFM1068
LFK000104	3,800	5.00	WNW1068	MFM1068, MFM0810
LFK000105	4,000	10.00	WNW1068,ENE0810	MFM1068, MFM0810
LFK000142	3,500	13.00	none	MFM1093
LFR000013	3,300	10.00	NW0001	MFM0803
LFR000013	4,000	25.00	NW0001	None
LFK000130	4,000	25.00	none	MFM1093
LFK000132	4,000	15.01	none	None
LFK000133	3,000	12.00	none	MFM1093
LFK000133	3,800	65.00	none	MFM1092
LFK000134	3,500	16.01	none	None
LFK000134	3,200	40.01	none	MFM1092
LFK000134	3,200	30.00	none	MFM1092
LFK000134	3,500	10.00	none	None
LFK000135	4,000	18.00	none	MFM1093
LFK000136	3,500	10.00	none	None
LFK000136	3,300	10.01	EW0137	MFM0137
LFK000138	3,000	7.00	EW0137	MFM0137
LFK000138	3,800	35.00	none	None
LFK000125	3,700	14.99	none	None
LFK000137	3,900	25.00	none	MFM1092
LFK000137	3,700	70.01	none	MFM1092
LFK000137	4,000	20.01	none	MFM1092
LFK000137	3,700	48.01	none	None
LFK000126	3,500	55.00	none	MFM1092
LFK000139	4,000	16.00	EW0137	MFM0137
LFK000139	4,000	19.01	NW0001	None
LFK000139	4,000	17.01	NW0001	MFM0803
LFK000139	4,000	23.00	NW0001	None
LFK000141	3,000	5.00	none	MFM1088
LFK000141	4,000	10.00	none	None
LFK000141	4,000	27.01	EW0137	MFM0137
LFK000141	3,000	5.01	none	None
LFK000038	3,800	17.99	NW0001	None
LFK000038	4,000	11.99	NW0001	MFM0803
LFK000038	3,700	15.00	none	None
LFK000038	3,000	10.00	NW0002,NW1127	MFM1127, MFM0804
LFK000038	4,000	12.00	none	None
LFK000038	3,000	10.00	none	None
LFK000053	3,500	5.00	NW0001	MFM803
LFK000053	3,200	18.99	NW0001	None
LFK000151	4,000	35.00	none	None

Id code	Rock velocity [m/s]	Length [m]	DZ_Correlation	MFM_lineament correlation
LFR000013	3,800	15.00	none	MFM1035
LFR000014	3,800	15.00	none	MFM1035
LFR000014	3,500	10.01	NNE0869	None
LFR000015	3,700	10.00	none	MFM1035
LFK000152	3,500	17.00	none	None
LFK000152	3,500	18.00	none	None
LFK000153	3,500	10.00	none	None
LFK000153	3,500	13.00	none	None
LFK000154	3,500	10.01	none	None
LFK000155	3,200	14.99	NW0003	None
LFK000156	3,900	26.00	NW0004	MFM0014
LFK000156	3,500	10.00	NW0003	None
LFK000042	3,000	5.00	NW0017	MFM0017
LFK000042	3,000	5.00	none	None
LFK000042	3,500	10.99	none	MFM0015
LFR000018	3,800	16.61	none	None
LFR000018	3,800	26.27	none	None
LFR000019	4,000	21.52	none	None
LFR000019	3,700	22.79	none	None
LFR000019	3,500	14.26	none	None
LFR000024	4,000	34.51	none	None
LFR000021	3,700	13.62	none	MFM0805
LFR000021	3,600	12.96	none	None
LFR000022	4,000	27.75	none	None
LFR000020	3,300	15.65	none	None
LFR000020	4,000	31.05	none	None
LFR000020	4,000	15.78	none	MFM0805
LFR000020	4,000	32.86	none	None
LFR000025	4,000	18.18	NW0001	None
LFR000025	2,000	78.32	NW0001	MFM0803
LFR000025	3,200	24.63	NW0001	None
LFR000025	4,000	26.30	none	None
LFR000025	3,600	16.54	none	MFM0137B0
LFR000026	3,900	23.01	none	MFM1035
LFR000026	3,800	25.71	NNE0869	None
LFR000026	4,000	22.07	none	None
LFR000029	3,700	12.95	none	None
LFR000016	3,800	35.38	none	None
LFR000016	4,000	39.56	none	MFM0137B0
LFR000017	3,500	8.95	none	None
LFR000017	3,500	19.02	none	None
LFR000017	3,600	14.76	none	None
LFR000017	4,000	36.90	NW0805	MFM0805
LFR000031	3,700	18.49	none	None
LFR000031	3,950	48.10	none	None
LFR000031	3,700	17.83	none	None
LFR000032	3,800	22.03	none	None
LFR000032	3,900	41.52	none	None
LFR000032	3,400	23.55	none	None

* Shows LV within the detailed, magnetic ground survey area.

Interpretation of tomography inversion models for seismic refraction data along profile LFM001017 in Forsmark

Håkan Mattsson, GeoVista AB

Contents

1 Introduction

A test to use tomography inversion to model refraction seismic data along profile LFM001017 in Forsmark (Figure 1-1) was performed in order to evaluate the possibility of extracting more information from the raw data. LFM001017 was chosen since several magnetic lineaments cross-cut the profile, without any indications of decreased P-wave velocity along these sub-sections in the traditional velocity model /Toresson 2006/. Thus, the tomography inversion could possibly help explain uncertainties in the geological model for some deformation zones in the area.

Figure 1-1. *Location of the refraction seismic profile LFM001017. Labels denote section length coordinates in metres along the profile.*

2 Methodology and limitations − general considerations

The data processing was performed with the software Rayfract™, which uses inversion of first arrival travel time data to estimate a 2D velocity model based on Wavepath Eikonal Traveltime (WET) tomography. The Eikonal equations are obtained from the elastic wave equations and provide the travel time of the fastest arriving waves, which makes the Eikonal solvers especially suitable for refraction seismic data /Lecomte et al. 2000/. The technique assures valid travel time calculations, even in models with strong velocity contrasts, and the exact topography of the surface is also a part of the model.

Wave propagation is modelled in a physically meaningful way with ray paths. Rayfract™ handles several real life geological situations, such as sharp vertical or horizontal velocity gradients caused by e.g. brittle deformation zones. Quality control of velocity models is performed by direct graphical comparison of the measured travel-time data to those calculated from the model solution. Quantitative statistics (e.g. mean residual and maximum error) of the fit of the modelled travel times to the measured travel times is also presented. 2D plots of the ray coverage as a function of depth along the profile is displayed for all models, which provides information on areas with low data coverage.

As for traditional data processing, the tomography inversion of refraction seismic data will fail if it encounters site conditions that conflict with the underlying assumptions of the method. One example is laterally continuous constant velocity layers for which the method inserts a velocity gradient when none is present. This may occur if the rock underlying the soft soil is perfectly solid, fresh crystalline rock. Other possible pitfalls are artefacts caused by low data coverage in combination with low smoothing, or artefacts caused by low ray coverage.

To fully benefit from the possibilities of tomography inversion by Rayfract™, the data coverage should be high, preferably at least 7–8 shots/array of 24 geophones. Furthermore, the different geophone arrays should overlap with several geophone stations so as to avoid low data coverage at the boundaries. The data in this investigation were collected for traditional processing technique with 5–7 shots/array and only one or no overlapping geophones. The model resolution is therefore limited. Furthermore, the geophone distance is 5 m, which makes it very difficult to detect low velocity zones narrower than 5–10 m with any kind of processing technique, assuming that the velocity contrast is 2,000 m/s. Thus, all low velocity zones narrower than c. 10 m, and those located close to the array boundaries, should be handled with extreme care.

Some disadvantages with the WET-technique are the risk of velocity artefacts when using a low degree of smoothing in combination with low data coverage. This is the case especially if there are strong topography variations. The reason for using minimum smoothing in this test was to try to extract as much information as possible from the data. Another drawback is that the gradient approach used by the software may indicate increasing velocity with depth, even though the bedrock is almost homogenous rock with presumably more or less constant P-wave velocity.

Advantages with the WET-technique are that it is fast, automated and all arrival time data are used in the creation of the velocity model. The quality control is based on independent statistics such as uncertainty numbers, ray coverage plots and model fit parameters. In the traditional processing technique, the velocity model is the result of a combination of manual interpolation and personal judgements made by the interpreter. The interpreter may also have to decide if one shot is more “reliable” than another shot, even if the raw data quality is equally good for both shots. This makes the traditional velocity model less general compared with the tomography inversion model.

3 Data input

First arrival times, layout geometries and topography data were supplied by Björn Toresson at Impakt Geofysik.

4 Data processing

Data processing was performed by use of the software Rayfract™ version 2.64. Each geophone array was processed separately. However, the arrays 8–11 (section length 768.5–1,194.5 m) and 14–15 (section length 1,419.5–1,639.5 m) were also processed as continuous lines. Raw data were rearranged to fit the software specifications. A 2D velocity gradient model was constructed and a first smooth inversion was performed (10 iterations), which results in a "stable" low resolution model. Following this procedure, the data were re-processed starting with the 2D velocity gradient as starting model, with 40–100 iterations and minimal smoothing. Minimal smoothing gives high resolution but also increases the risk of artefacts in the resulting velocity model, especially in this test when the data coverage is close to the lower limits according to the software demands. The high and low smoothing models were subsequently interpreted with respect to velocity variations that indicate soil cover thickness, bedrock topography and areas or zones with decreased P-wave velocity possibly related to rock deformation.

Quality control of the resulting velocity models was performed by:

- Quantitative statistics of model fit to raw data (max error, mean error, relative misfit).
- Qualitative comparison between calculated and measured travel time curves.
- Inspection of ray coverage plots.

5 Results and interpretation

The velocity model for profile LFM001017 based on WET tomography inversion is presented in Figure 5-1 together with the model based on the traditional processing technique. In Figure 5-1 the intersection points between the seismic profile and discordant magnetic lineaments (possible deformation zones) from /Isaksson et al. 2006/ are shown by triangles. Lineaments longer and shorter than 1,000 m are shown by larger and smaller triangles, respectively. Two geophone arrays (117–232 m and 2,217.5–2,232.5 m) contain too few shots for a fully reliable model calculation. Notwithstanding this limitation, these sections have also been processed. Possible anomalies along these two sections should be viewed with considerable care.

Mean errors (mean residual between measured and modelled travel time) are generally below 0.3 ms, which indicates a good model fit to the measured data. Geophone arrays with anomalously high mean errors (error > 0.5 ms) and poor model fits occur at 430.5–530.5 m, 530.5–634.5 m, 883.5–998.5 m and 1,861.5–1,976.5 m. However, model fits to the data along these four sections are fair, and no mean errors exceed 0.8 ms. The combined inversion model for lines 8, 9,10 and 11 (768.5–1,194.5) shows a mean error of 0.7 ms (shot 1 of line 9 was disregarded). The combined inversion model for lines 14–15 (1,419.5–1,639.5 m) shows a mean error of 0.41 ms. In general, there is a good agreement between the tomography inversion models and the velocity model presented in /Toresson 2006/, but significant deviations between the two models do occur. The velocity intervals roughly correspond to the geological features indicated in the table below.

Velocity interval	Geological feature
0–1,500 m/s	soft soil or heavily crushed rock
1,500–3,000 m/s	moraine or fractured rock
3,000–4,000 m/s	fractured/weathered/altered rock (soil rock boundary at c. 3,000 m/s)
> 4,000 m/s	sound rock

The bedrock surface roughly corresponds to the magenta colour in the velocity model.

In the following text, comments to the velocity model for each line (geophone array) are presented. The term "soil" refers to the Quaternary cover.

Array 1 (0–115 m)

Major depression of the bedrock surface at 30–40 m, possibly in combination with a low velocity zone. Diffuse boundary between soil cover and bedrock surface at 0–30 m, possibly indicating weathering and/or increased fracturing in the uppermost part of the bedrock, or another type of moraine.

Array 2 (117–232 m) (few shots, extra care)

Thin soil cover, high P-wave velocities in the bedrock.

Array 3 (233–348 m)

Major depression of the bedrock surface at c. 250–285 m, which possibly indicates a low velocity zone. Diffuse boundary between soil cover and bedrock surface at 340–350 m, possibly indicating weathering and/or increased fracturing in the uppermost part of the bedrock or another type of moraine (also supported by the model for Array 4).

Array 4 (348–430 m)

Diffuse boundary between soil cover and bedrock surface at 380–400 m, possibly indicating weathering and/or increased fracturing in the uppermost part of the bedrock or another type of moraine.

Array 5 (430.5–530.5 m) (poor model fit)

Diffuse boundary between soil cover and bedrock surface at 420–450 m, possibly indicating weathering and/or increased fracturing in the uppermost part of the bedrock. Low velocity zone in the bedrock indicated at c. 488–494 m (high uncertainty).

Array 6 (530.5–634.5 m) (poor model fit)

Starting at 510 m (array 5) and ending at 540 m (array 6). Diffuse boundary between soil cover and bedrock surface, possibly indicating weathering and/or increased fracturing in the uppermost part of the bedrock or another type of moraine. High uncertainty due to poor model fit but bedrock surface shows good correlation with traditional model.

Array 7 (646.5–761.5 m)

Along the entire section the model indicates thin or "normal" soil cover with unusually high velocities. The reason could be fractured rock close to the ground surface or soil cover thickness of 1–2 m with anomalously high P-wave velocity (1,500–3,000 m/s), "solid moraine", or effects related to the fact that the profile cross-cuts a wetland or lake.

Array 8 (768.5–883.5 m)

Along the entire section, the model indicates thin or "normal" soil cover with unusually high velocities. The reason could be fractured rock close to the ground surface, a soil cover thickness of 1–2 m with anomalously high P-wave velocity (1,500–3,000 m/s), i.e. "solid moraine", or effects related to the fact that the profile cross-cuts a wetland or lake. Sharp bedrock depression in the bedrock indicated at c. 838–848 m (high uncertainty).

Array 9 (883.5–998.5 m) (poor model fit)

Area of indicated decreased P-velocity in the section c. 870–910 m may be related to increased soil cover thickness. Increased mean error of model fit lowers the certainty of the presented model.

Array 10 (998.5–1,113.5 m)

Increased soil cover thickness along major part of the section. Sharp bedrock depression indicated in the section c. 1,000–1,010 m.

Array 11 (1,113.5–1,194.5 m)

Bedrock depression in combination with either high soil or low rock velocities in the section 1,125–1,155 m. The depression is indicated along the section c. 1,060–1,155 m.

Arrays 8–11 combined processing (768.5–1,194.5 m)

The combined processing of these four arrays shows a similar result as the single-array processing apart from one major deviation. In the combined velocity model, a significant low velocity zone is indicated at c. 1,020–1,035 m. In the single-array model, there is no such anomaly in this part of the section, but there is a bedrock depression indicated at c. 1,000–1,010 m. Since no low velocity zone at c. 1,020–1,035 m is indicated in the model presented by /Toresson 2006/, the suggested low velocity zone is interpreted as an artefact caused by boundary condition problems in the combined model between the two geophone arrays at c. 1,000 m.

Array 12 (1,194.5–1,309 m)

The section 1,160–1,290 m is characterized by an inferred soil cover thickness of 0.5–2 m with partly anomalously high P-wave velocity (1,500–3,000 m/s). The reason could be fractured rock close to the ground surface, a soil cover thickness of 1–2 m with anomalously high P-wave velocity, i.e. "solid moraine", or effects related to the fact that the profile cross-cuts a wetland or lake. Bedrock depression and possible low velocity zone at c. 1,270–1,280 m.

Array 13 (1,309–1,424 m)

Topographic high that coincides with increased soil cover thickness of c. 2–4 m (normal soil P-wave velocities, c. 500–1,500 m/s). Indication of low velocity zone at 1,310 m. However, this anomaly is close to the array boundary, which makes it very uncertain (most likely artefact).

Array 14 (1,419.5–1,534.5 m)

Inferred soil cover thickness of 1–2 m and generally high P-wave velocities in the underlying bedrock. Low velocity zone indicated in the section c. 1,507–1,515 m. Decreased velocities in the bedrock along the interval c. 1,510–1,560 m.

Array 15 (1,534.5–1,639.5 m)

Inferred soil cover thickness of 1–2 m. Apart from the section c. 1,534–1,550 m, there are fairly high P-wave velocities in the underlying bedrock with a diffuse boundary between soil cover and bedrock surface. Possibly indicates weathering and/or increased fracturing in the uppermost part of the bedrock or another type of moraine.

Arrays 14–15 combined processing (1,419.5–1,639.5 m)

The combined velocity model fully supports the single-array models and their interpretations.

Array 16 (1,641.5–1,756.5 m)

Large variations in the bedrock surface topography. Decreased P-wave velocity present in the uppermost part of the bedrock along the entire profile, as well as a diffuse boundary between soil cover and bedrock surface. Possibly indicates weathering and/or increased fracturing in the uppermost part of the bedrock or another type of moraine.

Array 17 (1,861.5–1,976.5 m) (poor model fit)

The model indicates large variations in the bedrock topography along the major part of the profile. Possible low velocity zones in the bedrock are indicated in the sections c. 1,860–1,870 m and 1,942–1,953 m (high uncertainty). The model fit to the data is poor but the above result is also supported by a more low resolution model with maximum smoothing (100 iterations).

Array 18 (1,986.5–2,101.5 m)

Increased soil cover thickness (c. 3 m) along the entire profile. Fairly distinct depression of the bedrock surface in the section 2,058–2,073 m. Low velocity zone in the bedrock indicated at c. 2,093–2,100 m, which is at the boundary of the array. This renders the model interpretation as more uncertain.

Array 19 (2,101.5–2,216.5 m)

Increased soil cover thickness (c. 3–4 m) along the entire profile and large variations of the bedrock topography. Distinct depression of the bedrock surface in the section 2,145–2,161 m. This coincides with a near-surface high velocity anomaly that is most likely artificial. However, a similar depression is indicated in the high smoothing model (without any artefact) and also in the model by /Toresson 2006/. The depression coincides with indicated decrease in the P-wave velocity in the underlying bedrock.

Array 20 (2,217.5–2,332.5 m) (few shots, extra care)

Increased soil cover thickness (c. 2–4 m) along the entire profile and large variations of the bedrock topography. Distinct depression of the bedrock surface in the section 2,265–2,290 m. Diffuse boundary between soil cover and bedrock surface, possibly indicating weathering and/or increased fracturing in the uppermost part of the bedrock.

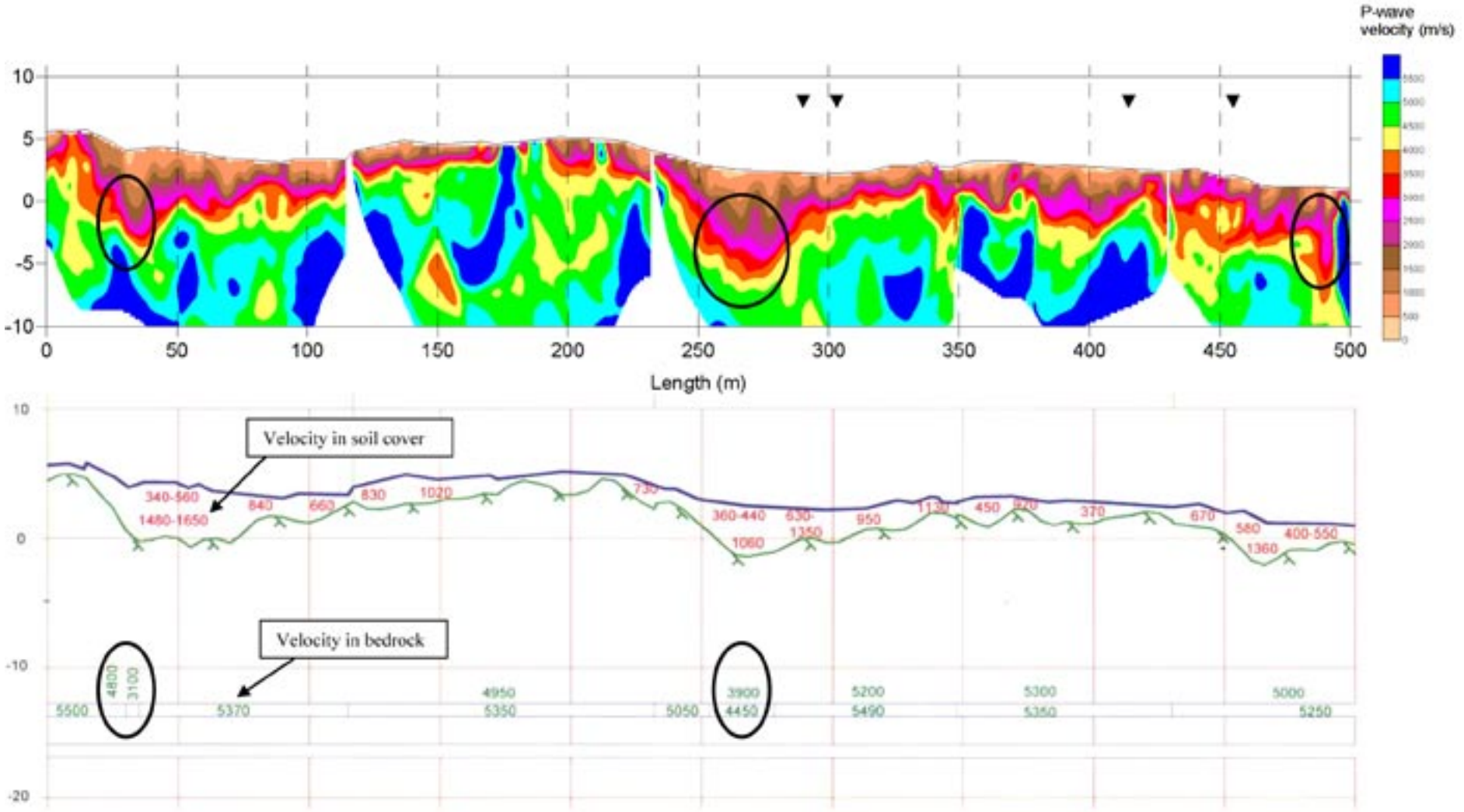
P-wave velocity (m/s)
10
5
0
-5
-10
0
50
100
150
200
250
300
350
400
450
500
Length (m)
Velocity in soil cover
340-560
1480-1650
840
660
830
1020
730
360-440
1060
630-1350
950
1130
450
320
370
670
580
1360
400-550
Velocity in bedrock
4800
3100
5500
5370
4950
5350
5050
3900
4450
5200
5490
5300
5350
5000
5250
-20

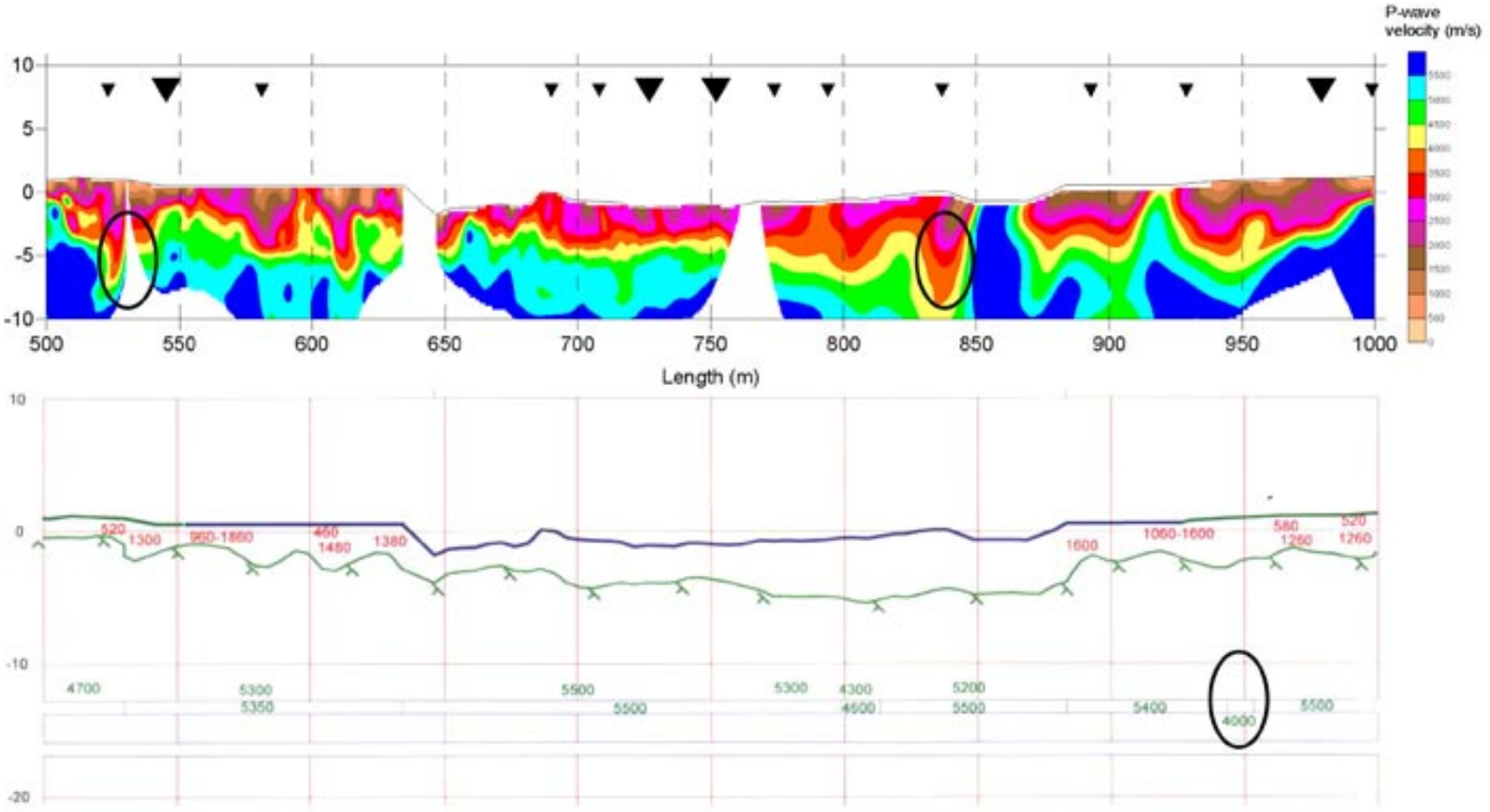
P-wave velocity (m/s)
10
5
0
-5
-10
500
550
600
650
700
750
800
850
900
950
1000
Length (m)
10
0
-10
-20
520
1300
950-1860
460
1480
1380
1600
1060-1600
580
1260
520
1260
4700
5300
5350
5500
5500
5300
4300
4600
5200
5500
5400
4000
5500

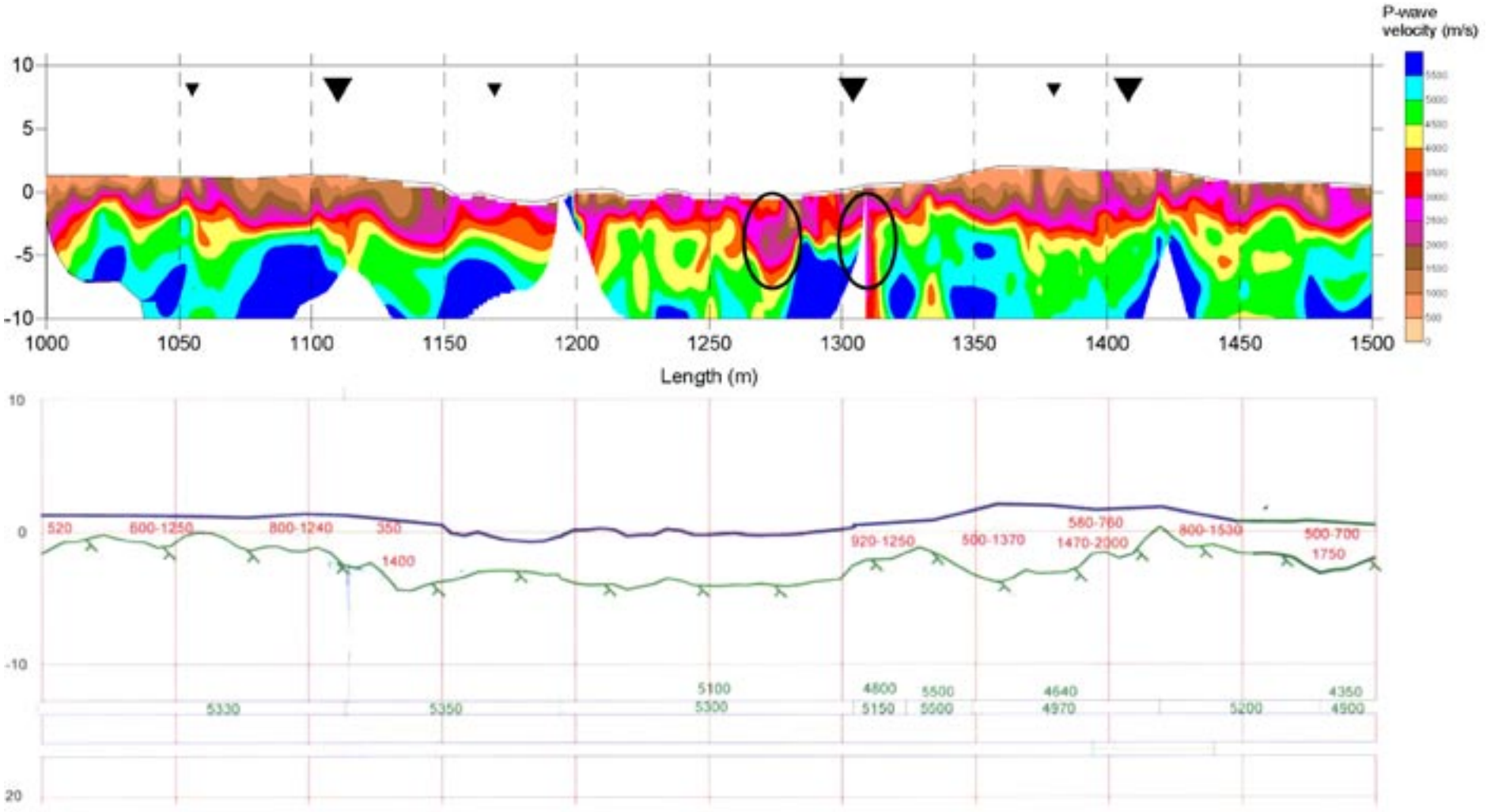
P-wave velocity (m/s)
10
5
0
-5
-10
1000
1050
1100
1150
1200
1250
1300
1350
1400
1450
1500
Length (m)
10
0
-10
20
520
600-1250
800-1240
350
1400
920-1250
500-1370
580-760
1470-2000
800-1530
500-700
1750
5330
5350
5100
5300
4800
5150
5500
5500
4640
4970
5200
4350
4900

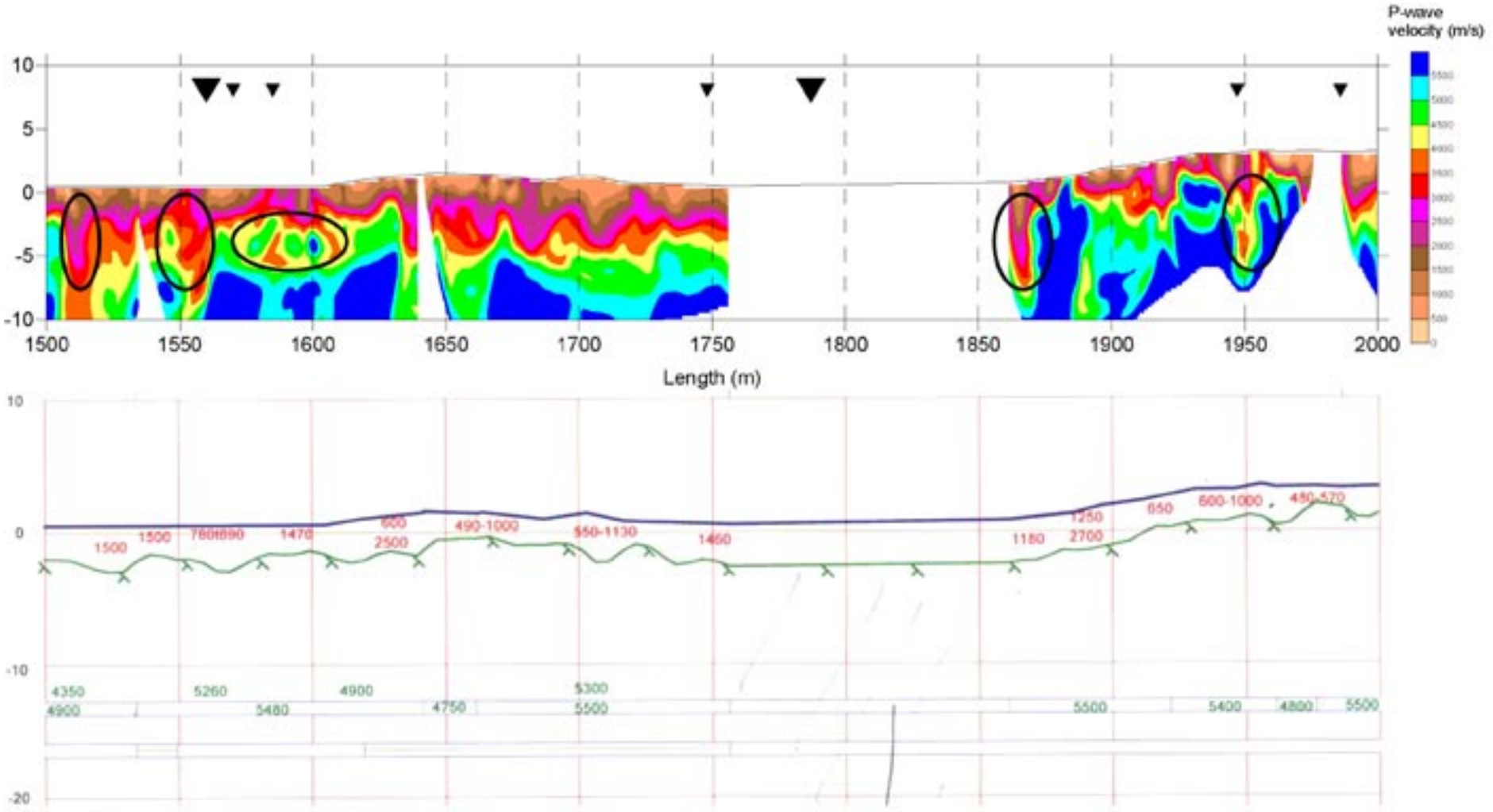
P-wave velocity (m/s)
10
5
0
-5
-10
1500
1550
1600
1650
1700
1750
1800
1850
1900
1950
2000
Length (m)
10
0
-10
-20
1500
1500
780/890
1470
600
2500
490-1000
550-1130
1460
1180
1250
2700
650
600-1000
450-570
4350
4900
5260
5480
4900
4750
5300
5500
5500
5400
4800
5500

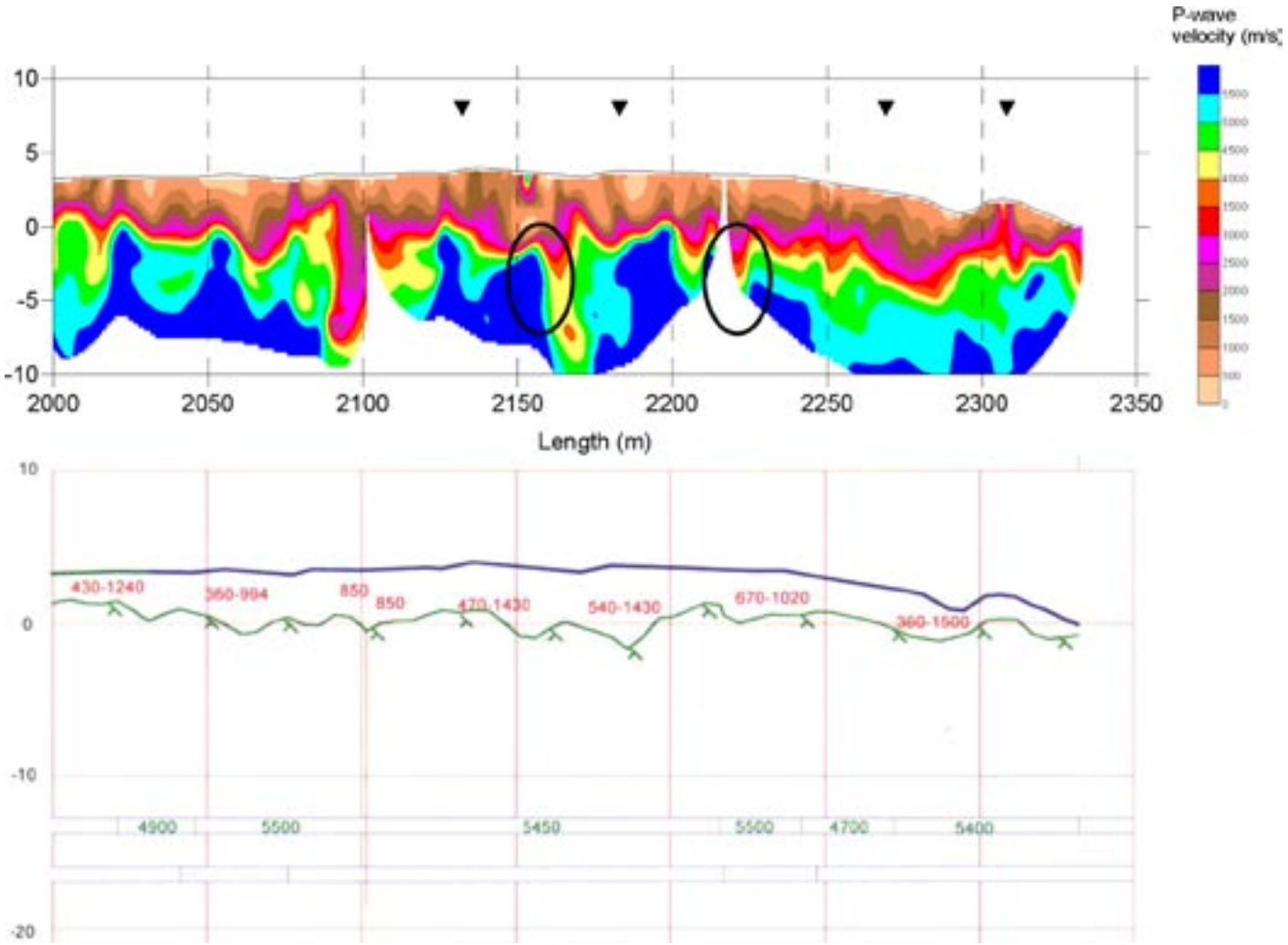

Figure 5-1. *Velocity model based on WET inversion tomography (top) and traditional processing (bottom) along the LFM001017 refraction seismic profile. Sections along each of the profiles with an inferred decreased P-wave velocity are indicated by the ellipses. The triangles indicate positions where discordant magnetic lineaments intersect the profile /Isaksson et al. 2006/. Lineaments longer than 1,000 m are shown by larger triangles. The section c. 0–270 m was not included in the interpretation of magnetic data.*

6 Discussion

The comparison between the traditional model and the WET-model shows a general agreement regarding major features such as long wave length variations in bedrock surface topography, the general velocity distribution and the fairly shallow soil cover thickness. In general, the traditional model is smoother compared to the WET-model. There are only two low velocity zones indicated in the traditional model along the entire 2,350 m long profile; these occur at c. 35–40 m and c. 945–955 m. The first is indicated also in the WET-model, but the second one is absent. However, this is one of the four lines that show a relatively poor WET-model fit, which may explain the deviating result between the two models.

There are more than 30 magnetic lineaments that cross-cut the profile (the triangles in Figure 5-1). A majority of these lineaments cannot be correlated to low velocity zones in any of the two seismic models. One reason could be that the 5 m geophone distance is too large to detect the narrow, highly fractured core part of the possible deformation zones. It is also possible that these lineaments represent sealed fracture zones or a lithological contrast (e.g. Group D granite dykes, pegmatite, amphibolite) that do not result in decreased P-wave velocity. These aspects are discussed in more detail in the paper by Isaksson on p. 113 in this report.

When looking at lineaments longer than 1,000 m (denoted by large triangles in Figure 5-1), the WET-model indicates low velocity zones in 3 of totally 8 possible cases. The traditional model does not indicate any. There are also several low velocity zones indicated in the WET-model that do not correspond to any lineaments. However, some of these anomalies may be related to artefacts caused by the low number of shot points and the absence of overlapping geophones, which is actually demanded by the WET software (see the paragraph Method above).

It is concluded that this test of using the tomography inversion model technique on refraction seismic data from the profile LFM001017 leads to ambiguous results, both regarding a comparison with the traditional interpretation techniques and also with reference to the magnetic lineament model. As stated earlier, the main reason for this is the lack of data, i.e. too few shot points, in combination with an insufficient number of overlapping geophones. However, it is also clear that the comparison between the traditional model and the magnetic lineament interpretation also leads to unsatisfactory results (see also paper by Isaksson on p. 113 in this report).

In this test of the profile LFM001017, the data collection technique in combination with the low amount of shots makes the benefit of the tomography inversion model limited compared to the traditional model. An independent investigation of Rayfract™ and two other inversion modelling-softwares, which is performed by use of synthetic data with several different geological anomaly situations, shows that the resulting velocity models generally fit well to the true velocity distribution /Sheehan et al. 2005/. In connection with the site investigation at Laxemar, a test that compared WET-models to the models achieved from the traditional processing technique showed very good results when the data coverage was sufficiently high /Mattsson et al. 2005/. With a sufficient number of shots in combination with overlapping geophone spreads, the inversion technique is most likely the future technique for the processing of refraction seismic data.

7 References

Isaksson H, Thunehed H, Pitkänen T, Keisu M, 2006. Detailed ground and marine magnetic survey and lineament interpretation in the Forsmark area – 2006. SKB P-06-261, Svensk Kärnbränslehantering AB.

Isaksson H, 2007. Correlation between refraction seismic data, low magnetic lineaments and deformation zones (model stage 2.2); in Geology − background complementary studies. Forsmark modelling stage 2.2. SKB R-07-56, Svensk Kärnbränslehantering AB.

Lecomte I, Gjøstdal H, Dahle A, Pedersen O C, 2000. Improving modelling and inversion in refraction seismics with first-order Eikonal solver. Geophysical Prospecting, v 48, pp 437–454.

Mattsson H, Triumf C-A, Lindqvist G, 2005. Re-interpretation of the refraction seismic profiles 277, 280 and 506 by use of Wavepath Ekonal Traveltime Tomography – a comparison with the traditional interpretation technique. SKB P-05-179, Svensk Kärnbränslehantering AB.

Sheehan J R, Doll W E, Mandell W A, 2005. An evaluation of methods and available software for Seismic Refraction Tomography Analysis. JEEG, v 10, pp 21–34.

Toresson B, 2006. Seismic refraction survey 2005–2006. SKB P-06-138, Svensk Kärnbränslehantering AB.

Correlation of oriented radar reflectors with geological features in boreholes at Forsmark

Seje Carlsten, GeoSigma AB

Contents

1 Aim of study

This report aims to correlate oriented borehole radar reflectors with geological features from geological Boremap-mapping in the Forsmark investigation area. Only radar reflectors located within possible deformation zones from the single-hole interpretation work and their extension according to model stage 2.1 have been assessed in the correlation process. The correlation aims to address the key question − what is the geological significance of the oriented radar reflectors inside the zones?

A separate study was made on the correlation of borehole radar reflectors with vuggy rock sections. This study aims to establish whether these rocks correlate with radar reflectors and whether the reflectors provide any information on the orientation of the vuggy rock sections.

2 Description of borehole radar

The description of the borehole radar system in this chapter is mainly from the radar reports /Aaltonen and Gustafsson 2004, Gustafsson and Gustafsson 2004a–f, 2005a–f, 2006a–e/.

2.1 Radar measurements with RAMAC

The RAMAC GPR system, which is owned by SKB, is a fully digital GPR system, where emphasis has been laid on rapid survey execution and easy field operation. The system operates dipole and directional antennae (see Figure 2-1).

The directional antenna

Figure 2-1. *Example of a borehole radar antenna.*

The borehole radar system consists of a transmitter and a receiver antenna. During operation, an electromagnetic pulse, within the frequency range of 20 MHz up to 250 MHz, is generated inside the bedrock. Once a feature, e.g. a water-filled fracture or a lithological contact, with sufficiently different electrical properties is encountered, the pulse is reflected back to the receiver and recorded.

2.2 Radar interpretation

The results from radar measurements are presented in the form of a radargram, where the position of the probe in the borehole is shown along one axis (denoted Distance (metre) in Figure 2-2) and the radar wave propagation and reflection is shown along the other axis (denoted Depth (metre) in Figure 2-2). An example of a radargram from a borehole in Forsmark is shown in Figure 2-2. The amplitude of the received signal is visualized in the radargram using a grey scale where black colour corresponds to large positive signals and white colour to large negative signals. Grey colour corresponds to no reflected signals. Reflectors from the surrounding rock constitute lines in the radargram. The data are adjusted for the measurement point of the antennae. The measurement point is defined to be the central point between the transmitter and the receiver antenna.

The two basic patterns to interpret in borehole measurements are point and planar reflectors. In the reflection mode, borehole radar essentially gives a high-resolution image of the rock mass. It shows the geometry of planes or structures, which may or may not intersect the borehole (contact between layers, thin marker beds, fractures), or the presence of local features around the borehole (cavities, lenses etc).

The distance to a reflecting feature or plane is determined by measuring the difference in arrival time between the direct and the reflected pulse. The basic assumption is that the speed of propagation is the same everywhere.

Only the larger, clearly visible structures are interpreted in RadinterSKB. A number of minor structures also exist but are not interpreted. Commonly, several structures can be identified, but they are most probably situated so close to each other that it is impossible to distinguish one from the other. If present, larger structures parallel to the borehole are also documented. It should also be pointed out that interpreted reflections include an intersection point with the borehole, even if they are located far away from the borehole. In some cases, they may not intersect the borehole.

The resolution and penetration of radar waves depend on the antenna frequency used. Low antenna frequency (20 MHz) yields lower resolution but higher penetration depth compared to a higher frequency. If structures can be identified with all three antenna frequencies, it is probable that the structure is a significant geological feature.

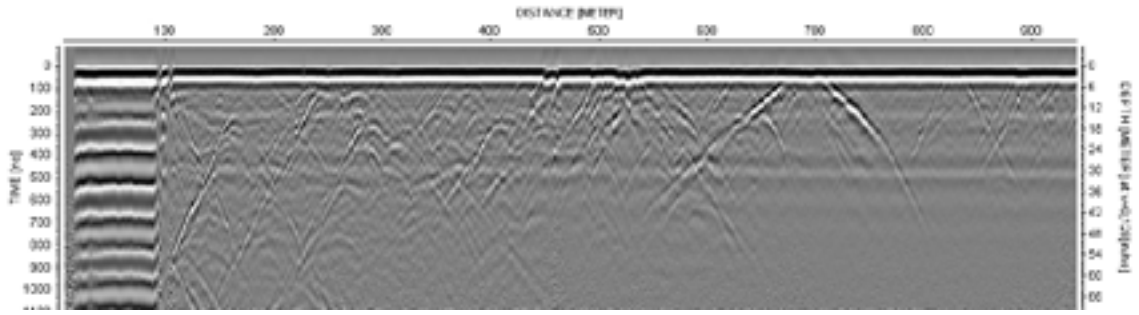

Figure 2-2. *Radargram showing an overview (20 MHz data) of the borehole radar measurements in KFM08C.*

The orientation of the feature (reflector) can also be provided. The data from directional antenna consists of several radargrams displayed individually in RadinterSKB. There is one radargram for each 3 degrees step around the borehole. The interpretor changes the radargrams during the interpretation process, in order to find the correct direction to the feature. The interpretation for some radar reflectors is uncertain. In these cases, the direction from the probe to the feature (reflector) can be ±180 degrees, for example the direction to an feature can be either 70° or 250°. The direction to the feature is defined in Figure 2-3. As the borehole inclination is less than 85°, the direction to the feature is calculated using gravity roll. The direction to the feature and the intersection angle (alpha) are recalculated to strike and dip. The strike of a plane is the angle between the line of the plane's cross-section with the surface and the magnetic north direction. It is counted clockwise and can be between 0 and 359°. A strike of 0° implies a dip to the east while a strike of 180° implies a dip to the west. The plane dip is the angle between the plane and the surface. It can vary between 0 and 90°, where 0° is horizontal and 90° is vertical.

It should be noted that the interpretation of orientation from the directional radar antenna is based on the internal deviation measurements in the directional antenna. For this reason, the radar interpretations are unaffected by any revisions in borehole deviations. It should also be noted that a structure may have several different angles, if the structure (reflector) is undulating in the radargram. These different intersection depths are given for some structures (reflectors). Normally, the part that is interpreted closest to the borehole is the one that can be connected to a mapped geological structure in the borehole.

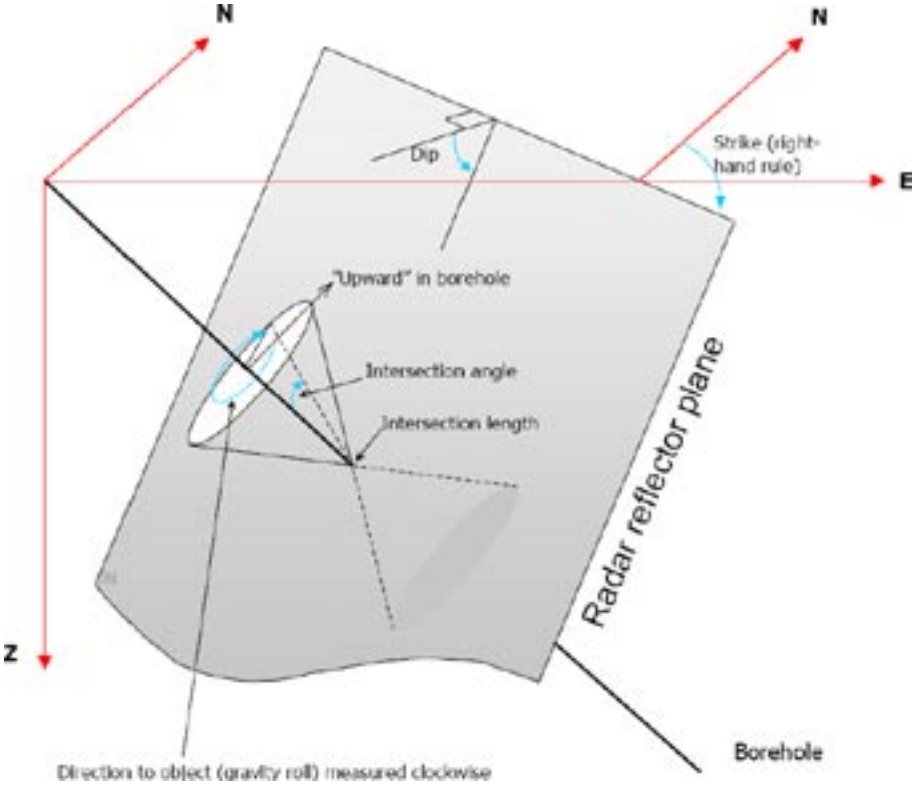

Figure 2-3. *Definition of intersection angle, direction to feature using gravity roll, and inferred strike and dip using the right-hand-rule method.*

3 Data used for the radar correlation

The following data and interpretations have been used for the radar correlation of the boreholes:

- Possible deformation zones from the single-hole interpretation work and their extensions as defined in model stage 2.1 /SKB 2006/.
- Revised Boremap data from Sicada (including BIPS and geological mapping data) for these zones that takes account of the orientation corrections completed during early 2007. In Table 3-1 the date for extraction and delivery of data is presented. Data were extracted from Sicada by Allan Stråhle.
- Radar data and their interpretation, with tables and radargrams /Aaltonen and Gustafsson 2004, Gustafsson and Gustafsson 2004a–f, 2005a–f, 2006a–e/. Accuracy for interpreted radar data is presented in Table 3-2. If the reflector is not planar, the accuracy of intersection decreases. Furthermore, the angle close to the borehole may differ from the angle further away from the borehole.

Table 3-1. Date for extraction of Boremap data from Sicada.

Borehole	Date for extraction and delivery of Boremap data in Sicada
KFM01A	2007-03-09
KFM01B	2007-03-05
KFM01D	2007-03-05
KFM02A	2007-03-05
KFM03A	2007-05-23
KFM03B	2007-03-05
KFM04A	2007-03-05
KFM05A	2007-03-05
KFM06A	2007-03-05
KFM06B	2007-03-05
KFM06C	2007-03-05
KFM07A	2007-03-05
KFM07B	2007-03-05
KFM07C	2007-03-08
KFM08A	2007-03-05
KFM08B	2007-03-05
KFM08C	2007-03-08
KFM09A	2007-03-05
KFM09B	2007-03-05
KFM10A	2007-03-05

Table 3-2. Accuracy of intersection length, angle to borehole axis and direction (azimuth) for a reflector. From SKB MD 252.020 vers. 3.0.

Antenna type (MHz)	Angle to borehole axis (interval) 0–29°	30–59°	60–90°	Parameter
20	> ± 5 m	± 4–5 m	< ± 5 m	Intersection length
100	> ± 3 m	± 2–3 m	< ± 2 m	Intersection length
250	> ± 2 m	± 1–2 m	< ± 1 m	Intersection length
100	± 2°	± 5°	± 10°	Angle to borehole axis
250	± 2°	± 5°	± 10°	Angle to borehole axis
60 (Directional)	± 2°	± 5°	± 5°	Direction (azimuth)

4 Execution of the radar correlation

4.1 General

20 boreholes were included in the radar correlation study (Table 4-1 and Appendix 1). 78 possible deformation zones from the single-hole interpretation work and their extensions, as defined in model stage 2.1 /SKB 2006/, were used. A total number of 271 oriented radar reflectors were defined within the possible deformation zones and their extended parts. Some possible deformation zones were excluded due to the absence of oriented radar reflectors within the zones. A few oriented radar reflectors were excluded due to the absence of BIPS-images.

A separate study was made on the correlation between vuggy rock sections in the boreholes and radar reflectors (Table 4-2 and Appendix 2). In this study, both oriented radar reflectors and non-oriented radar reflectors were included. All the occurrences of vuggy rock in 9 boreholes were studied. Most occurrences contain more than one borehole interval that are separated by one or several, short intervals of fresh, unaltered rock (Table 4-2).

The general working procedure relies on a careful visual inspection. It is summarized in Figure 4-1 and in the text below.

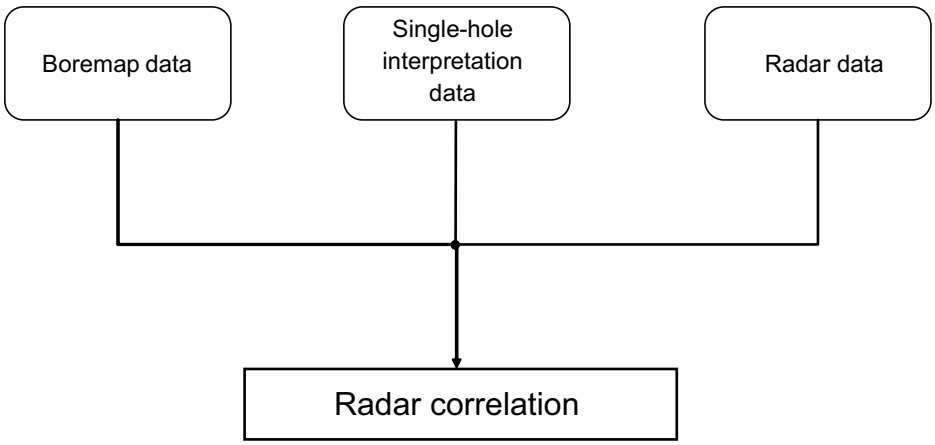

Figure 4-1. *Schematic chart that shows the procedure for the development of the radar correlation.*

Table 4-1. Boreholes, possible deformation zones, oriented radar reflectors and confidence of correlation included in the correlation study.

Borehole	Number of possible deformation zones	Number of radar reflectors	Number of confidence levels between radar reflector and geological feature			
			None	Low	Medium	High
KFM01A	2	6	1	3	1	1
KFM01B	3	7	3	–	2	2
KFM01D	5	7	–	–	3	4
KFM02A	4	24	2	9	6	7
KFM03A	5	13	–	1	7	5
KFM03B	2	4	–	–	1	3
KFM04A	5	19	2	4	7	6
KFM05A	5	38	2	20	7	9
KFM06A	10	27	1	3	9	14
KFM06B	1	4	–	–	3	1
KFM06C	5	32	1	–	10	21
KFM07A	4	11	–	2	3	6
KFM07B	3	5	–	–	1	4
KFM07C	2	4	–	1	2	1
KFM08A	5	23	–	5	12	6
KFM08B	0	0	–	–	–	–
KFM08C	4	13	2	4	4	3
KFM09A	5	10	–	3	3	4
KFM09B	5	17	–	1	5	11
KFM10A	3	7	–	4	2	1

Table 4-2. Occurrence of altered vuggy rock in the boreholes /Olofsson et al. 2007/.

Occurrence	Borehole	Adjusted SECUP (m)	Adjusted SECLOW (m)	Intensity
1	KFM02A	171.4017	172.0464	Medium
1	KFM02A	174.3257	174.6049	Medium
1	KFM02A	174.6069	175.1762	Weak
1	KFM02A	175.1792	175.2756	Medium
1	KFM02A	176.9033	177.0077	Faint
1	KFM02A	179.4226	180.0532	Medium
2	KFM02A	247.8602	248.2394	Faint
2	KFM02A	248.8501	264.6114	Weak
2	KFM02A	264.6143	266.0617	Medium
2	KFM02A	266.0638	272.9400	Weak
2	KFM02A	272.9420	274.9207	Medium
2	KFM02A	274.9238	276.6634	Strong
2	KFM02A	276.6664	279.6094	Medium
2	KFM02A	279.6124	283.1108	Strong
2	KFM02A	283.1138	283.4965	Medium
2	KFM02A	283.4985	284.3242	Strong
2	KFM02A	284.3262	284.8857	Weak
2	KFM02A	284.8867	296.5319	Strong
2	KFM02A	298.8883	299.0470	Strong

Occurrence	Borehole	Adjusted SECUP (m)	Adjusted SECLOW (m)	Intensity
2	KFM02A	299.2398	299.5151	Strong
2	KFM02A	301.6063	301.7067	Weak
3	KFM06A	332.4962	332.7465	Medium
4	KFM06A	610.6420	611.0861	Weak
5	KFM06A	770.8406	770.8858	Weak
6	KFM06B	66.5638	66.9108	Weak
6	KFM06B	68.6588	69.0540	Medium
6	KFM06B	69.0570	70.1661	Weak
7	KFM06C	451.4576	452.2256	Strong
8	KFM08A	409.8545	412.0399	Strong
9	KFM08C	454.9640	458.2870	Medium
9	KFM08C	462.0960	462.2760	Faint
9	KFM08C	462.2790	462.4950	Medium
10	KFM08C	497.8410	497.9030	Weak
10	KFM08C	497.9040	498.9950	Strong
11	KFM08C	511.6210	511.6410	Faint
11	KFM08C	512.8850	512.9310	Faint
11	KFM08C	517.2170	517.2880	Faint
11	KFM08C	519.1460	519.9780	Medium
11	KFM08C	520.4340	520.7890	Weak
11	KFM08C	523.1160	523.4460	Weak
11	KFM08C	523.4510	525.7750	Medium
11	KFM08C	526.2380	526.4410	Weak
11	KFM08C	531.5300	531.7940	Medium
12	KFM09A	511.7505	513.9343	Faint
12	KFM09A	513.9343	515.4333	Weak
12	KFM09A	515.4344	515.7068	Medium
12	KFM09A	515.7068	520.0322	Weak
13	KFM09B	382.3123	382.3254	Weak
14	KFM09B	568.9249	569.3978	Weak
14	KFM09B	569.3998	572.6340	Medium
14	KFM09B	572.6360	573.4531	Weak
15	KFM10A	86.9287	88.7894	Weak
15	KFM10A	89.3205	89.9060	Weak
15	KFM10A	92.6009	93.0834	Faint
15	KFM10A	93.0864	94.2436	Weak
15	KFM10A	96.6878	97.4517	Weak
15	KFM10A	98.7714	98.9686	Faint
15	KFM10A	98.9706	99.8841	Weak
15	KFM10A	99.8851	100.3489	Medium
15	KFM10A	100.3509	101.0936	Weak
15	KFM10A	104.0204	104.7111	Faint
15	KFM10A	104.9550	105.4848	Faint
15	KFM10A	111.4764	111.5854	Faint
15	KFM10A	111.5874	114.6291	Weak
15	KFM10A	114.6341	118.5576	Faint
16	KFM10A	483.5521	487.7752	Faint

4.2 Correlation procedure

The first step in the working procedure is to define the oriented radar reflectors occurring within the possible deformation zones from the single-hole interpretation work and their extension. The ID of the oriented radar reflector, the borehole length, the alpha angle, the orientation and the radargrams are collected from the radar P-reports.

The second step is to interpret the radius and the strength of the radar reflectors (Figure 4-2) and the presence of low radar amplitude. The strength is a subjective judgement of a combination of the intensity and the extension of a radar structure in the radargram. The strength is judged on the following basis: 3 = strong, 2 = medium and 1 = weak. The strength and the radius have been judged in one or several of the different radargrams with different frequency. The frequency radargram, where the reflector is most distinct, is used for judgement of radius and strength. However, the orientation of the reflector is always taken from the 60 MHz directional radargram.

The radar amplitude is the first arrival of the radar wave travelling along the borehole wall. The amplitude variation indicates changes of the electrical conductivity in the borehole wall and the closest surroundings. Low radar amplitude may indicate the presence of a fracture zone, clay, a different lithology or a higher porosity of the rock. This step is made on the basis of the radargrams in the radar P-reports.

The third step is to correlate the oriented radar reflector with a geological feature from Boremap. This is made on the basis of BIPS-images and the Boremap mapping. The first criterion for the correlation is the borehole length of the radar reflector. The borehole length ± 2–3 m is searched for suitable geological features with a similar alpha angle as the oriented radar reflector. If more than one candidate is present, the orientation of the geological feature is compared with the orientation of the radar reflector and the one with best agreement is selected. In some cases, when the alpha angle is small, an interval up to ± 3–5 m in the borehole is searched for suitable geological features. This is based on the fact that the interpreted intersection of radar reflectors

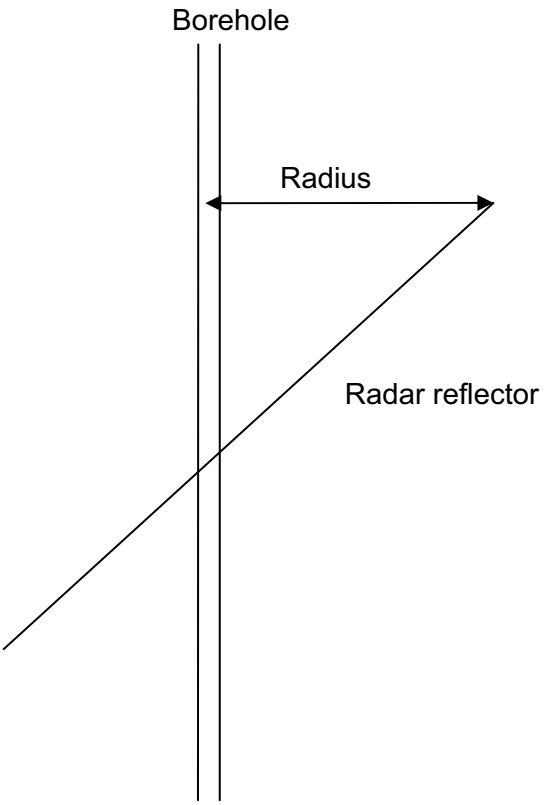

Figure 4-2. *Principle for calculation of the radius of a radar reflector outside a borehole.*

with borehole length is more uncertain for radar reflectors with small alpha angle compared to those with large alpha angle. In many cases, a single fracture can be correlated with the radar reflector. The single fracture may be one of several parallel single fractures occurring close to each other.

The fourth step is to place a confidence level on each correlation between oriented radar reflector and geological feature. The confidence level is a subjective judgement of the agreement between the oriented radar reflector and the geological feature, based on a combination of the borehole length, the alpha angle and the orientation of the radar reflector and the geological feature. The confidence level is made on the following basis: 3 = high, 2 = medium, 1 = low and 0 = none. In some cases, there are no Boremap data available and the confidence level is set to N/A, and is not included in the statistics.

The fifth step is a statistical analysis of the correlated data. The results of this analysis are presented in Tables 5-1 to 5-4. The correlation between radar reflectors and vuggy rock is presented in Table 5-5. An explanation of the columns in the correlation tables in Appendices 1 and 2 are provided below.

Borehole radar

DZ	Possible deformation zone from the single-hole interpretation work and their extension (indicated by Ext in the table) as defined in model stage 2.1 /SKB 2006/.
ID	Identification number of oriented radar reflector from the radar interpretation report.
Borehole length	Adjusted length of the oriented radar reflector from the radar interpretation report.
Alpha	The angle between a plane and the borehole axis. If the alpha angle is 0°, the plane is parallel to the borehole axis. If the alpha angle is 90°, the plane is perpendicular to the borehole axis.
Ori1	The orientation of the radar reflector from the radar interpretation report. The strike and dip of the oriented radar reflectors make use of the right-hand-rule method, e.g. 040°/80° corresponds to a strike of N40°E and a dip of 80° to the SE.
Ori2	An alternative orientation of the radar reflector from the radar interpretation report. This alternative is presented only in the cases where the interpretation of the direction to the feature (reflector) is uncertain. Selected alternative for the correlation is indicated by extra bold type.
Radius	The distance between the borehole and the point furthest away from the borehole where the reflector can still be observed. The radius is always perpendicular to the borehole axis (Figure 4-2). The radius is interpreted from the radargram in the radar interpretation report.
Strength	A subjective judgement of a combination of the intensity and the extension of a radar structure in the radargram. The strength is interpreted from the radargram in the radar interpretation report. The strength is assessed on the following basis: 3 = strong, 2 = medium and 1 = weak.
Low radar amplitude	The amplitude of the first arrival of the radar wave travelling along the borehole wall. The amplitude variation indicates changes of the electrical conductivity in the borehole wall and the closest surroundings. Low radar amplitude might indicate the presence of a fracture zone, clay, a different lithology or a higher porosity in the rock. The amplitude is from the radargram in the radar report.

Inferred geological feature from Boremap

Borehole length	Adjusted length of the geological feature from the Boremap data in Sicada.
Alpha	The angle between the geological feature (plane) and the borehole axis. If the alpha angle is 0° the plane is parallel to borehole axis. If the alpha angle is 90° the plane is perpendicular to the borehole axis.
Ori	The orientation of the geological feature from Boremap data. The strike and dip of the orientation of geological structures make use of the right-hand-rule method, e.g. 040°/80° corresponds to a strike of N40°E and a dip of 80° to the SE.
Feature	Description of the geological feature from Boremap data.
Comment	Description of the geological feature.
Confidence level	Subjective judgement of the agreement between the oriented radar reflector and the geological feature, based on a combination of the borehole length, the alpha angle and the orientation. The confidence is made on the following basis: 3 = high, 2 = medium, 1 = low and 0 = none. N/A indicates intersection above or below available Boremap data.

5 Results

5.1 Correlation of oriented radar reflectors with geological features in possible deformation zones

The results of the correlation of oriented radar reflectors with geological features in possible deformation zones are presented in Appendix 1. The correlation of oriented radar reflectors shows that 45% of all oriented radar reflectors can be correlated with contacts between different rock types (Table 5-1). 37% of the oriented radar reflectors can be correlated with broken fractures, crush zones or breccias, and only 10% can be correlated with unbroken fractures or sealed networks. Alteration is shown by 1% and foliation by 2% of the oriented radar reflectors. Finally, 5% of the oriented radar reflectors within possible deformation zones show no correlation with geological features. Since the correlation is made with reflectors that are observed some distance (up to at least 3–4 m) from the borehole, it is probable that the radar reflectors that fail to correlate with a geological feature simply do not intersect the borehole along the possible deformation zone.

The confidence level is high for 41% of the correlations between oriented radar reflectors and geological features, medium for 32% and low for 22%. For 5% of the oriented radar reflectors no correlation could be carried out (Table 5-2).

Oriented radar reflectors that have been correlated with contact between rock types show a high confidence level for 50%, medium confidence level for 30% and low confidence level for 20% (Table 5-3).

The corresponding confidence level for oriented radar reflectors that have been correlated with a broken fracture, a crush zone or a breccia is high for 36%, medium for 40% and low for 24% (Table 5-4).

It is apparent that the directional antenna detects rock contacts to a higher degree than broken fractures, crush zones or breccias. The correlation with unbroken fractures, sealed networks, alteration and foliation is very limited.

Table 5-1. Oriented radar reflectors and correlation with geological features from Boremap.

Oriented radar reflectors in DZ	Contact between rock types	Broken fracture, crush zone or breccia	Unbroken fracture or sealed fracture network	Alteration	Foliation	No correlation
271	121	101	28	3	5	13
	45%	37%	10%	1%	2%	5%

Table 5-2. Oriented radar reflectors and confidence of correlation with geological features from Boremap.

Oriented radar reflectors in DZ	Confidence 3 = high	Confidence 2 = medium	Confidence 1 = low	Confidence 0 = none
271	110	88	60	13
	41%	32%	22%	5%

Table 5-3. Oriented radar reflectors and confidence of correlation with contact between rock types.

Oriented radar reflectors in DZ	Confidence 3 = high	Confidence 2 = medium	Confidence 1 = low
121	60	36	25
	50%	30%	20%

Table 5-4. Oriented radar reflectors and confidence of correlation with a broken fracture, crush zone or a breccia.

Oriented radar reflectors in DZ	Confidence 3 = high	Confidence 2 = medium	Confidence 1 = low
101	36	41	24
	36%	40%	24%

5.2 Correlation between radar reflectors and vuggy rock

The results of the correlation between radar reflectors and vuggy rock are presented in Appendix 2. For 57% of the vuggy rock occurrences, there is no correlation with the radar data (Table 5-5). It is suggested that either there is no radar reflector at the location or there is a very poor agreement between the orientation of the radar reflector and the orientation of the vuggy rock. Low confidence is shown by 26% of the occurrences, 8.5% show medium confidence and only 8.5% show a high confidence of correlation between radar reflector and vuggy rock.

Table 5-5. Sections with vuggy rock and confidence of correlation with with radar reflectors.

Sections with vuggy rock	Confidence 3 = high	Confidence 2 = medium	Confidence 1 = low	Confidence 0 = none
47	4	4	12	27
	8.5%	8.5%	26%	57%

One explanation for the results presented above can be that the contrast in electrical properties between vuggy rock and its surroundings is not distinct enough to favour detection by borehole radar. The radar waves need a rather sharp electrical contrast to be reflected i.e. a distinct rock contact or a fracture zone. A second explanation can be that the boundary between the vuggy rock and its surroundings is not a planar structure, cf. a fracture zone or a rock contact. For this reason, it is not detected by borehole radar. Thirdly, the vuggy rock may form diffuse, scattered areas in the rock mass and the data from Boremap may simply not be representative of the orientation of the vuggy rock anomaly. In this case, vuggy rock is represented in the borehole radar and the orientation of the reflector may provide a better interpretation of the orientation of this rock.

In summary, this study shows that there is no simple correlation between borehole radar and the occurrences of vuggy rock. For this reason, it can be concluded that borehole radar is not an efficient method to detect or evaluate the orientation of vuggy rock in boreholes. However, the second statement is only valid if it is assumed that the vuggy rock sections are planar structures in the rock mass and if the Boremap data represent the orientation of these structures.

6 Summary and conclusions

- The attempt to correlate oriented radar reflectors with geological features along possible deformation zones in boreholes shows that 45% of all oriented radar reflectors can be correlated with contacts between different rock types, 37% can be correlated with a broken fracture, a crush zone or a breccia and only 10% can be correlated with an unbroken fracture or a sealed network. Alteration is shown by 1% and foliation by 2% of the correlated oriented radar reflectors. Finally, 5% of the correlated oriented radar reflectors within possible deformation zones show no correlation with geological features.
- The confidence level is high for 41% of oriented radar reflectors that have been correlated with geological features, a medium confidence level exists for 32%, a low confidence level for 22% and 5% lack a correlation.
- The confidence level for the correlation of oriented radar reflectors with the contact between rock types is high for 50% of the reflectors, medium for 30% and low for 20%. The corresponding confidence level for oriented radar reflectors, which have been correlated with a broken fracture, a crush zone or a breccia, is high for 36%, medium for 40% and low for 24%.
- It is concluded that the directional antenna is able to detect rock contacts more efficiently than broken fractures, crush zones or breccias. The method is not effective for the detection of unbroken fractures, sealed networks, alteration and foliation.
- The separate study of vuggy rock shows that if the vuggy rock sections are planar structures in the rock mass and if the Boremap data is representative of the orientation of these structures, then the borehole radar is not an effective method to detect this type of geological feature. For 57% of the vuggy rock occurrences, there is no correlation at all between these occurrences and radar data, 26% show a low confidence, 8.5% show a medium confidence and only 8.5% show a high confidence of correlation between radar reflector and vuggy rock.
- One explanation for the poor correlation between borehole radar and vuggy rock may be that the electrical properties between vuggy rock and its surrounding are not distinct enough to favour detection by borehole radar. The radar waves need a rather sharp electrical contrast to be reflected, i.e. a rock contact or a fracture zone. A second explanation can be that the boundary between the vuggy rock and its surroundings is not a planar structure, cf. a fracture zone or a rock contact. For this reason, it is not detected by borehole radar. Thirdly, the vuggy rock may form diffuse, scattered areas in the rock mass and the data from Boremap may simply not be representative of the orientation of the vuggy rock anomaly. In this case, vuggy rock

is represented in the borehole radar and the orientation of the reflector may provide a better interpretation of the orientation of this rock.

7 References

Aaltonen J, Gustafsson C, 2004. Forsmark site investigation. RAMAC and BIPS logging in borehole KFM01A. SKB P-03-45, Svensk Kärnbränslehantering AB.

Gustafsson J, Gustafsson C, 2004a. Forsmark site investigation. RAMAC and BIPS logging in borehole KFM01B and RAMAC directional re-logging in borehole KFM01A. SKB P-04-79, Svensk Kärnbränslehantering AB.

Gustafsson J, Gustafsson C, 2004b. Forsmark site investigation. RAMAC and BIPS logging in borehole KFM02A. SKB P-04-40, Svensk Kärnbränslehantering AB.

Gustafsson J, Gustafsson C, 2004c. Forsmark site investigation. RAMAC and BIPS logging in borehole KFM03A and KFM03B. SKB P-04-41, Svensk Kärnbränslehantering AB.

Gustafsson J, Gustafsson C, 2004d. Forsmark site investigation. RAMAC and BIPS logging in boreholes KFM04A, KFM04B, HFM09 and HFM10. SKB P-04-67, Svensk Kärnbränslehantering AB.

Gustafsson J, Gustafsson C, 2004e. Forsmark site investigation. RAMAC and BIPS logging in boreholes KFM05A. SKB P-04-152, Svensk Kärnbränslehantering AB.

Gustafsson J, Gustafsson C, 2004f. Forsmark site investigation. RAMAC and BIPS logging in boreholes KFM06A, HFM16, HFM17, HFM18 and HFM19. SKB P-04-69, Svensk Kärnbränslehantering AB.

Gustafsson J, Gustafsson C, 2005a. Forsmark site investigation. RAMAC and BIPS logging in borehole KFM06B. SKB P-05-53, Svensk Kärnbränslehantering AB.

Gustafsson J, Gustafsson C, 2005b. Forsmark site investigation. RAMAC and BIPS logging in borehole KFM06C. SKB P-05-242, Svensk Kärnbränslehantering AB.

Gustafsson J, Gustafsson C, 2005c. Forsmark site investigation. RAMAC and BIPS logging in borehole KFM07A (0–100 m), HFM20 and HFM21. SKB P-05-64, Svensk Kärnbränslehantering AB.

Gustafsson J, Gustafsson C, 2005d. Forsmark site investigation. RAMAC and BIPS logging in borehole KFM07A. SKB P-report P-05-52, Svensk Kärnbränslehantering AB.

Gustafsson J, Gustafsson C, 2005e. Forsmark site investigation. RAMAC and BIPS logging in borehole KFM08A. Revised April 2006. SKB P-05-158, Svensk Kärnbränslehantering AB.

Gustafsson J, Gustafsson C, 2005f. Forsmark site investigation. RAMAC and BIPS logging in borehole KFM08B. Revised April 2006.SKB P-05-58, Svensk Kärnbränslehantering AB.

Gustafsson J, Gustafsson C, 2006a. Forsmark site investigation. RAMAC and BIPS logging in boreholes KFM07B, KFM09A, HFM25 and HFM28. SKB P-06-44, Svensk Kärnbränslehantering AB.

Gustafsson J, Gustafsson C, 2006b. Forsmark site investigation. RAMAC and BIPS logging in boreholes KFM07C, HFM36, HFM37 and BIPS re-logging in HFM26. SKB P-06-120, Svensk Kärnbränslehantering AB.

Gustafsson J, Gustafsson C, 2006c. Forsmark site investigation. RAMAC and BIPS logging in boreholes KFM08C, HFM30, HFM31, HFM33 and HFM34. SKB P-06-178, Svensk Kärnbränslehantering AB.

Gustafsson J, Gustafsson C, 2006d. Forsmark site investigation. RAMAC and BIPS logging in boreholes KFM09B, HFM24, HFM26, HFM27, HFM29 and HFM32. SKB P-06-64, Svensk Kärnbränslehantering AB.

Gustafsson J, Gustafsson C, 2006e. Forsmark site investigation. RAMAC and BIPS logging in boreholes KFM10A, HFM35 and HFM38. SKB P-06-177, Svensk Kärnbränslehantering AB.

Olofsson O, Simeonov A, Stephens M B, Follin S, Nilsson A-C, Röshoff K, Lindberg U, Lanaro F, Frederiksson A, Persson L, 2007. Site descriptive modelling, Forsmark stage 2.2. Presentation of a fracture domain concept as a basis for the statistical modeling of fractures and minor deformation zones, and interdisciplinary coordination. SKB R-07-15, Svensk Kärnbränslehantering AB.

SKB, 2006. Site descriptive modelling, Forsmark stage 2.1. Feedback for completion of the site investigation including input from safety assessment and repository engineering. SKB R-06-38, Svensk Kärnbränslehantering AB.

Appendix 1

Correlation between oriented radar reflectors and geological features in possible deformation zones

KFM01A

DZ	Borehole radar								Inferred geological feature from boremap					Confidence level
	In data					Interpretation			Correlation					
	Id	Borehole length (m)	Alpha	Ori1	Ori2	Radius (m)	Strength	Low radar amplitude (m)	Borehole length (m)	Alpha	Ori	Feature	Comment	
2	Mxx	387.0	53	044/45	232/25	5–10	2	390–400	–	–	–	None	Reflector outside borehole	0
2	Mx	398.6	16	236/66	**054/82**	5	1	390–400	398.6	9	061/89	Unbroken fractures	4 parallel to Ori2	3
3	Vxx	641.3	47	191/32	–	5	1	650–653	640.8	53	339/41	Rock occurrence	101057/101061	1
3	X	651.9	50	055/55	248/29	4	1	650–653	651.7	51	359/49	Rock occurrence	101057/111058	2
3	QQ	659.3	8	223/86	–	18–24	3	650–653	659.0	23	259/58	Rock occurrence	101057/111058 Reflector outside borehole	1
3	1	663.5	45	348/53	–	4–6	1	650–653	663.6	33	270/50	Broken fracture	Quartz, 16 mm Reflector outside borehole	1

KFM01B

DZ	Borehole radar								Inferred geological feature from boremap					Confidence level
	In data					Interpretation			Correlation					
	ID	Borehole length (m)	Alpha	Ori1	Ori2	Radius (m)	Strength	Low radar amplitude (m)	Borehole length (m)	Alpha	Ori	Feature	Comment	
1	E	40.8	85	033/09	341/15	2	1	20–25 27–31 38–42 45–50	40.8	82	086/13	Crush zone		3
1	F	49.2	69	025/33	240/15	5	1	20–25 27–31 38–42 45–50	49.7	69	132/11	Crush zone		2
2	1	111.1	8	153/71	–	7	3	129–132	112.2	7	156/85	Unbroken fracture	Epidote 2 mm	3
2	Q	122.4	70	339/33	–	3	1	129–132	123.7	71	150/07	Broken fracture	Clay 6 mm	2
2	R	131.4	59	018/43	216/22	2	1	129–132	–	–	–			0
3	30	417.5	42	018/66	205/33	6	2	416–420	417.7	43	354/65	Rock type	101057/101057	3
3	35	445.7	55	028/49	238/19	3	1	416–420	–	–	–			0

KFM01D

DZ	Borehole radar								Inferred geological feature from boremap					Confidence level
	In data					Interpretation			Correlation					
	Id	Borehole length (m)	Alpha	Ori1	Ori2	Radius (m)	Strength	Low radar amplitude (m)	Borehole length (m)	Alpha	Ori	Feature	Comment	
1	22	182.3	56	137/71	–	10	1	179–184	182.4	48	161/68	Broken fracture		2
2	72	414.4	21	351/89	**–**	12	2	–	414.7	17	347/77	Broken fracture		3
3	169	488.4	45	144/80	032/27	18	2	488–491	488.3	39	149/88	Rock occurrence	101058/101057	3
3	87	489.8	59	067/13	–	60	3	488–491	490.2	43	013/13	Rock occurrence	101057/102017	2
4	131	676.8	58	162/40	–	15	2	688–697	676.8	50	160/69	Albitization	Alteration	2
4	130	692.2	60	076/52	**158/52**	17	2	688–697	692.2	52	158/67	Rock type	101057/102017, Ori2	3
5	141	772.0	19	219/51	**247/82**	21	3	–	772.0	19	250/81	Rock occurrence	101057/8022, Ori2	3

KFM02A

DZ	Borehole radar								Inferred geological feature from boremap					Confidence level
	In data					Interpretation			Correlation					
	Id	Borehole length (m)	Alpha	Ori1	Ori2	Radius (m)	Strength	Low radar amplitude (m)	Borehole length (m)	Alpha	Ori	Feature	Comment	
2	2	112.5	49	090/41	–	10	2	109–112 116–121	112.4	44	350/50	Rock occurrence	101057/102017	1
2	4	113.7	85	090/05	–	10	2	109–112 116–121	–	–				0
2	3	121.6	38	090/52	090/46	10	2	109–112 116–121	121.7	35	026/59	Unbroken fracture		1
3	8b	164.4	72	105/17	314/20	4	1	160–184	164.4	75	144/12	Broken fracture		3
3	10a	173.9	76	043/18	251/11	4	1	160–184	173.9	71	337/21	Broken fracture	Hematite	2
3	10b	176.3	51	038/44	–	4	1	160–184	176.4	63	004/32	Rock occurrence	101057/101061	3
6	24	419.6	75	275/12	061/17	18–30	2	514–518	419.9	78	248/07	Rock occurrence	101057/111058	3
6	23	419.9	18	099/73	**283/71**	20	3	514–518	420.5	20	282/69	Rock occurrence	101057/101061 Ori2	3
6	25	425.9	16	232/71	–	11	2	514–518	423.9	19	302/72	Broken fracture		2
6	25a	426.7	63	217/22	–	11	2	514–518	426.8	68	360/27	Broken fracture		1
6	26	437.2	90	021/05	–	12	2	514–518	437.6	79	041/15	Broken fracture		2
6	25b	443.9	77	013/18	–	8	2	514–518	444.2	74	042/21	Broken fracture		3
6	26a	456.0	49	033/46	–	7	2	514–518	456.4	68	054/27	Broken fracture		2
6	28	474.9	53	261/34	–	7	2	514–518	474.3	63	257/23	Rock occurrence	101057/101061	2
6	29	484.6	90	028/05	005/04	4	1	514–518	484.6	76	136/13	Broken fracture		3
6	30	492.0	90	337/06	–	10	2	514–518	492.4	64	042/32	Broken fracture		1
6	31	512.1	90	044/32	–	60	3	514–518	512.5	75	335/17	Broken fracture		1
7	32	532.9	57	075/36	–	6	1	564 565–567 574 576–577	533.4	45	011/51	Rock occurrence	101057/102017	2

KFM02A

DZ	Borehole radar								Inferred geological feature from boremap					Confidence level
	In data					Interpretation			Correlation					
	Id	Borehole length (m)	Alpha	Ori1	Ori2	Radius (m)	Strength	Low radar amplitude (m)	Borehole length (m)	Alpha	Ori	Feature	Comment	
7	33	549.8	63	193/22	–	20	2	564 565–567 574 576–577	549.4	41	105/51	Rock occurrence	101051/101061	1
7	34a	560.8	66	355/29	158/20	4	1	564 565–567 574 576–577	–	–				0
7	BB	566.2	28	013/68	**191/56**	20–30	3	564 565–567 574 576–577	566.2	24	220/60	Rock occurrence	101061/102017 Ori2	3
7	36a	596.9	36	045/60	**228/48**	3	1	564 565–567 574 576–577	570.6	27	182/57	Broken fracture	Ori2	1
Ext	Q	914.7	57	309/33	**–**	12	2	912–920	914.7	53	097/41	Unbroken fracture	Prehnite	1
Ext	QQQ	917.3	73	098/19	**–**	10	2	912–920	917.5	52	048/46	Rock occurrence	108019/101051	1

KFM03A

DZ	Borehole radar								Inferred geological feature from boremap					Confidence level
	In data					Interpretation			Correlation					
	ID	Borehole length (m)	Alpha	Ori1	Ori2	Radius (m)	Strength	Low radar amplitude (m)	Borehole length (m)	Alpha	Ori	Feature	Comment	
1	Y	359	61	353/36	**171/26**	3	1	364–366 369–374 386–390	359.1	56	180/29	Broken fracture	Ori2	3
1	X	365	73	116/14	321/21	6	1	364–366 369–374 386–390	364.5	70	302/22	Broken fracture	Or2	3
1	U	367	16	040/78	222/70	10	1	364–366 369–374 386–390	369.1	15	015/79	Unbroken fracture	Pyrite	3
1	Zx	375	62	194/23	010/33	10	2	364–366 369–374 386–390	375.1	45	156/41	Broken fracture		2
1	2	389	71	277/22	**073/23**	18	3	364–366 369–374 386–390	388.6	71	095/19	Crush	Ori2	3
1	3	399	66	082/24	–	12	3	364–366 369–374 386–390	399.3	74	044/20	Rock occurrence	101057/102017	2
2	10	452	58	043/36	235/27	6	2	450–455	452.6	61	070/31	Rock type	101057/102017	2
3	32	640	63	183/20	**008/34**	12	3	645–650	640.8	61	126/27	Rock occurrence	101061/102017	2
3	33	644	69	045/30	–	15	3	645–650	644.4	62	084/30	Rock occurrence	101057/102017	2
4	47	804	58	268/27	–	16	3	803–805 813–817	803.8	51	110/39	Rock occurrence	101057/101061	1
4	47x	811	68	092/23	–	4	1	803–805 813–817	811.0	64	130/24	Rock occurrence	101061/101051	2
4	48	815	81	328/21	109/17	6	2	803–805 813–817	815.4	71	351/24	Broken fracture		3
5	56	944	76	031/26	223/10	6	2	942–946	944.6	71	025/50	Broken fracture	Muscovite, clay	2

KFM03B

DZ	Borehole radar								Inferred geological feature from boremap					Confidence level
	In data					Interpretation			Correlation					
	Id	Borehole length (m)	Alpha	Ori1	Ori2	Radius (m)	Strength	Low radar amplitude (m)	Borehole length (m)	Alpha	Ori	Feature	Comment	
1	C	27	62	276/25	**096/25**	3	1	26–28	27.2	58	054/35	Rock type	101061/102017 Ori2	2
1	Cx	29	46	096/44	–	10	1	26–28	28.6	55	105/33	Broken fracture		3
1	D	37	59	180/33	**000/33**	8	2	26–28	36.5	61	009/34	Rock occurrence Vein	101057/101061 Ori2	3
2	H	66	59	359/36	–	12	2	64–67	65.1	61	025/34	Crush		3

KFM04A

DZ	Borehole radar								Inferred geological feature from boremap					Confidence level
	In data					Interpretation			Correlation					
	Id	Borehole length (m)	Alpha	Ori1	Ori2	Radius (m)	Strength	Low radar amplitude (m)	Borehole length (m)	Alpha	Ori	Feature	Comment	
Ext	D	132.4	46	320/19	**129/71**	12	3	–	132.0	36	137/82	Rock occurrence	102017/101056 Ori2	3
Ext	I	153.8	46	343/17	–	18	2	–	153.6	59	215/10	Broken fracture		1
Ext	J	156.3	38	129/80	313/24	5	1	–	156.0	41	134/77	Broken fracture	Ap = 3	3
1	L	170.9	31	326/32	–	9	2	170–176	170.9	29	326/90	Rock occurrence	101056/102017	1
2	T	205.9	46	128/73	–	12	2	202–206 206–214	205.5	42	148/76	Rock occurrence	Dyke 101057/101058	3
2	V	210.9	49	316/11	–	5	1	202–206 206–214	–					0
3	Y	234.7	61	136/57	**044/09**	15	2	232–242	235.5	52	022/17	Broken fracture	Ap = 10 mm Ori2	3
Ext	9	321.6	52	346/12	–	6	2	317–324	321.8	57	043/14	Broken fracture		2
Ext	12	353.9	54	134/76	016/09	5	1	–	353.5	44	122/78	Broken fracture		3
Ext	13	361.7	62	131/57	–	13	2	358–362	361.9	61	109/58	Rock occurrence	101051/101057	3
Ext	14	370.3	53	121/03	**063/42**	6	1	–	370.2	54	125/69	Broken fracture	Hematite Ori2	2

KFM04A

DZ	Borehole radar								Inferred geological feature from boremap					Confidence level
	In data					Interpretation			Correlation					
	Id	Borehole length (m)	Alpha	Ori1	Ori2	Radius (m)	Strength	Low radar amplitude (m)	Borehole length (m)	Alpha	Ori	Feature	Comment	
Ext	16	392.4	50	146/76	–	7	1	–	392.3	46	078/60	Rock occurrence	101061/101051	1
Ext	17	406.6	43	165/63	043/41	8	2	–	406.5	56	129/70	Rock occurrence	Shear zone	2
4	24	425.0	9	243/61	–	25	3	414–426 445–450 458–461	412.7	9	234/69	Breccia Rock occurrence	Brecciated 101051/6015	2
4	19	434.5	54	338/07	–	8	1	414–426 445–450 458–461	–					0
4	20	447.6	55	253/06	**120/70**	5	1	414–426 445–450 458–461	447.6	35	114/88	Rock occurrence	101061/102017 Ori2	2
4	21	455.2	51	350/08	–	10	2	414–426 445–450 458–461	455.4	43	137/82	Rock occurrence	Vein 101057/101061	1
4	30	459.3	7	206/87	–	–	1	414–426 445–450 458–461	458.0	9	259/75	Broken fracture		2
5	45	658.0	48	143/78	–	16	3	656–661	657.9	49	136/80	Structure	Foliation strong	2
Ext	79	986.2	54	141/81	–	3	1	984–988					No boremap data	N/A

KFM05A

DZ	Borehole radar								Inferred geological feature from boremap					Confidence level
	In data					Interpretation			Correlation					
	Id	Borehole length (m)	Alpha	Ori1	Ori2	Radius (m)	Strength	Low radar amplitude (m)	Borehole length (m)	Alpha	Ori	Feature	Comment	
1	A	111.3	62	192/53	100/20	19	3	–	111.5	51	322/11	Broken fracture	Clay, Aperture = 3	1
Ext	28	402.4	41	164/81	–	15	2	404–409	402.5	42	149/77	Rock occurrence	101061/101057	3
Ext	29	405.6	41	224/76	–	27	3	404–409	405.7	39	220/81	Breccia	6005/101057	3
2	31a	417.3	22	011/80	–	4	1	426–433	417.5	22	347/79	Rock occurrence	101057/102017	3
2	32	424.2	34	151/88	–	18	2	426–433	423.5	33	164/90	Rock occurrence	101061/102017	3
2	33	424.7	50	166/72	299/02	4	1	426–433	424.4	60	176/64	Alteration		1
2	34	427.6	53	092/24	**200/65**	8	2	426–433	427.8	58	140/55	Rock occurrence	101057/101061 Ori2	1
3	66	604.5	52	260/27	–	6	1	590–600 613–617 629–631 704–708 714–723 752–753	–					0
3	65	604.6	36	308/31	–	11	2	590–600 613–617 629–631 704–708 714–723 752–753	–					0
3	62	605.5	62	154/64	249/23	8	1	590–600 613–617 629–631 704–708 714–723 752–753	605.2	55	114/17	Rock occurrence	101057/101051	1
3	64a	606.2	19	305/47	–	12	1	590–600 613–617 629–631 704–708 714–723 752–753	605.4	13	055/80	Broken fracture		1

KFM05A

DZ	Borehole radar								Inferred geological feature from boremap					Confidence level
	In data					Interpretation			Correlation					
	Id	Borehole length (m)	Alpha	Ori1	Ori2	Radius (m)	Strength	Low radar amplitude (m)	Borehole length (m)	Alpha	Ori	Feature	Comment	
3	69a	610.2	56	167/74	284/14	10	3	590–600 613–617 629–631 704–708 714–723 752–753	610.6	39	186/86	Broken fracture		2
3	68	610.9	61	232/25	–	12	2	590–600 613–617 629–631 704–708 714–723 752–753	611.0	73	191/52	Broken fracture		1
3	71	613.9	46	258/36	141/67	12	2	590–600 613–617 629–631 704–708 714–723 752–753	613.5	31	027/89	Breccia Rock occurrence	101057/6005 Breccia	1
3	72	628.2	37	158/86	–	10	2	590–600 613–617 629–631 704–708 714–723 752–753	628.0	33	007/88	Broken fracture		2
3	73a	641.1	42	301/20	–	4	1	590–600 613–617 629–631 704–708 714–723 752–753	640.7	34	107/55	Rock occurrence	101057/101061	1

KFM05A

DZ	Borehole radar								Inferred geological feature from boremap					Confidence level
	In data					Interpretation			Correlation					
	Id	Borehole length (m)	Alpha	Ori1	Ori2	Radius (m)	Strength	Low radar amplitude (m)	Borehole length (m)	Alpha	Ori	Feature	Comment	
3	76	657.4	41	311/20	–	20	2	590–600 613–617 629–631 704–708 714–723 752–753	656.9	41	031/14	Unbroken		1
3	78	671.7	56	258/22	–	7	2	590–600 613–617 629–631 704–708 714–723 752–753	671.9	31	160/89	Broken fracture		1
3	79	678.8	63	159/55	–	5	1	590–600 613–617 629–631 704–708 714–723 752–753	679.6	34	115/58	Structural feature	Foliated	1
3	82	694.8	45	259/38	142/68	6	1	590–600 613–617 629–631 704–708 714–723 752–753	694.5	37	212/84	Sealed network		1
3	85a	700.0	15	285/62	–	9	3	590–600 613–617 629–631 704–708 714–723 752–753	701.1	21	284/59	Broken fracture	Pyrite	3

KFM05A

DZ	Borehole radar								Inferred geological feature from boremap					Confidence level
	In data					Interpretation			Correlation					
	Id	Borehole length (m)	Alpha	Ori1	Ori2	Radius (m)	Strength	Low radar amplitude (m)	Borehole length (m)	Alpha	Ori	Feature	Comment	
3	85	712.8	32	123/71	–	3	1	590–600 613–617 629–631 704–708 714–723 752–753	712.4	21	121/81	Rock occurrence	101061/102017	3
3	138	717.1	8	063/80	–	18	2	590–600 613–617 629–631 704–708 714–723 752–753	717.2	25	030/82	Broken fracture		3
3	86	718.1	19	338/37	–	4	1	590–600 613–617 629–631 704–708 714–723 752–753	718.8	24	044/85	Rock occurrence	Vein 101051/101061	1
3	89	734.9	38	288/30	**155/79**	6	2	590–600 613–617 629–631 704–708 714–723 752–753	735.2	39	152/82	Rock occurrence	101057/101061 Ori2	3
3	90	741.4	38	271/32	–	8	2	590–600 613–617 629–631 704–708 714–723 752–753	741.7	38	325/20	Broken fracture		2

KFM05A

DZ	Borehole radar								Inferred geological feature from boremap					Confidence level
	In data					Interpretation			Correlation					
	Id	Borehole length (m)	Alpha	Ori1	Ori2	Radius (m)	Strength	Low radar amplitude (m)	Borehole length (m)	Alpha	Ori	Feature	Comment	
3	91	749.2	29	276/51	–	5	2	590–600 613–617 629–631 704–708 714–723 752–753	748.0	28	012/82	Rock occurrence	101057/111058	1
3	92	750.2	39	248/62	–	4	1	590–600 613–617 629–631 704–708 714–723 752–753	751.3	27	035/84	Rock type	101057/102017	1
3	94	757.8	36	268/55	–	3	1	590–600 613–617 629–631 704–708 714–723 752–753	757.8	31	011/85	Broken fracture		1
3	97	779.2	24	032/82	–	8	1	590–600 613–617 629–631 704–708 714–723 752–753	778.9	38	120/64	Rock occurrence	Dyke 101057/101061	1
4	110	903.2	28	086/48	–	10	3	905–912	903.5	46	230/70	Broken fracture		1
4	111	909.3	34	041/26	–	6	2	905–912	909.3	28	233/89	Unbroken fract.		1
5	115	932.9	22	001/33	005/75	7	2	936–950	931.5	16	051/43	Rock occurrence	101057/101061	2
5	117	946.1	30	258/65	–	12	2	936–950	946.1	32	230/87	Unbroken fract.	Laumontite	2
Ext	118	950.9	30	241/81	–	8	2	–	952.1	38	217/85	Sealed network	Calcite, laumontite	2
Ext	120	960.8	47	071/15	–	10	2	–	961.9	36	041/20	Unbroken fract	Prehnite	2
Ext	127	977.8	26	220/79	–	2	7	978–979	978.1	40	214/83	Broken fracture		3
Ext	122a	980.2	34	331/28	–	2	4	981–982	980.9	23	077/45	Broken fracture		1

KFM06A

DZ	Borehole radar								Inferred geological feature from boremap					Confidence level
	In data					Interpretation			Correlation					
	Id	Borehole length (m)	Alpha	Ori1	Ori2	Radius (m)	Strength	Low radar amplitude (m)	Borehole length (m)	Alpha	Ori	Feature	Comment	
Ext	Dx	112.2	48	030/76	–	2	1	–	112.5	42	038/78	Rock type	102017/101057	3
1	J	133.6	63	340/16	158/53	6	1	128–131 134–136 140–146	–					0
1	Lx	142.6	42	050/75	–	16	3	128–131 134–136 140–146	142.9	46	024/73	Broken fracture	Asphalt 4 mm	3
1	K	145.6	30	014/84	–	11	2	128–131 134–136 140–146	145.5	40	024/80	Rock occurrence	101057/101061	2
1	L	145.9	46	043/72	–	50	3	128–131 134–136 140–146	145.7	41	024/80	Rock occurrence	101057/101061	3
2	X	206.0	78	033/15	–	24	2	217–221 236–240 241–244	206.2	61	105/10	Broken fracture	2.5 mm	2
2	2	218.8	73	045/16	032/45	18	2	217–221 236–240 241–244	218.1	70	050/11	Broken fracture	Clay 5 mm	3
2	Z	225.9	21	207/38	**211/81**	14	2	217–221 236–240 241–244	224.5	13	241/76	Broken fracture	Clay Ori2	2
2	14	226.0	25	228/85	056/66	21	2	217–221 236–240 241–244	226.1	19	187/82	Broken fracture		2
2	5	238.8	63	041/51	018/10	23	2	217–221 236–240 241–244	237.9	58	134/05	Broken fracture	Pyrite	1

KFM06A

DZ	Borehole radar								Inferred geological feature from boremap					Confidence level
	In data					Interpretation			Correlation					
	Id	Borehole length (m)	Alpha	Ori1	Ori2	Radius (m)	Strength	Low radar amplitude (m)	Borehole length (m)	Alpha	Ori	Feature	Comment	
2	6	243.7	55	027/65	–	10	2	217–221 236–240 241–244	244.1	65	020/54	Rock occurrence	101057/101061	3
3	11	269.3	46	217/09	–	18	2		268.7	51	289/17	Crush		2
3	11x	269.4	75	043/47	–	16	2	267–270	269.2	62	005/62	Rock type	101057/111058	2
4	27	335.6	33	209/26	**034/89**	12	2	330–338 347–359	334.2	49	040/73	Unbroken fract.	Pyrite Ori2	3
4	28xx	354.0	20	209/79	202/38	6	1	330–338 347–359	353.6	27	210/86	Unbroken fract.	Oxidized walls	3
5	85x	622.6	38	209/81	–	18	2	620–625	622.5	32	207/90	Sealed network	Quartz	3
5	85	624.0	37	117/42	–	6	2	620–625	624.6	52	100/49	Rock occurrence	101051/101061	3
6	88x	656.2	38	047/88	–	5	1	651–658	656.3	44	053/80	Rock occurrence	111058/101061	3
7	105	743.4	40	168/25	–	18	3	743–746 768–773	744.3	53	107/45	Rock type	101061/102017	1
7	105xx	756.7	25	249/80	–	14–18	2	743–746 768–773	756.6	31	210/89	Broken fracture	Laumontite	2
7	164	771.2	37	236/17	057/89	9	1	743–746 768–773	770.8	30	099/42	Crush		1
7	111x	772.3	70	027/35	**080/44**	14	2	743–746 768–773	772.7	69	086/39	Broken fracture	Ori2	2
7	111	772.4	57	011/39	–	18	3	743–746 768–773	772.0	63	012/43	Rock occurrence	101058/101061	3
9	137	886.1	16	276/76	294/45	12	2	884–890	885.3	20	331/68	Rock occurrence	101058/101061	2
9	133	887.2	29	241/23	**241/81**	3	1	884–890	887.1	24	241/76	Sealed network	Laumontite Hematite Ori2	3
10	136	925.7	23	239/76	–	17	2	926–931	925.4	23	215/78	Unbroken fract.	Chlorite Laumontite	3
11	144	962.5	68	062/10	**062/66**	4	1	964–969	962.6	77	068/50	Rock occurrence	101058/101061 Ori2	3

KFM06B

DZ	Borehole radar								Inferred geological feature from boremap					Confidence level
	In data					Interpretation			Correlation					
	ID	Borehole length (m)	Alpha	Ori1	Ori2	Radius (m)	Strength	Low radar amplitude (m)	Borehole length (m)	Alpha	Ori	Feature	Comment	
1	13	55.6	80	084/09	–	10	2	20–27 48–52 65–70	55.2	88	019/08	Crush		3
1	25	68.5	63	235/33	–	13–28	2	20–27 48–52 65–70	68.5	65	092/27	Broken fracture	Clay, reflector outside borehole	2
1	18	86.1	51	029/49	–	3	1	20–27 48–52 65–70	86.3	66	060/30	Broken fracture		2
Ext	16	94.8	12	234/72	–	4	1	88–94	94.2	23	037/74	Broken fracture		2

KFM06C														
DZ	Borehole radar								Inferred geological feature from boremap					Confidence level
	In data					Interpretation			Correlation					
	Id	Borehole length (m)	Alpha	Ori1	Ori2	Radius (m)	Strength	Low radar amplitude (m)	Borehole length (m)	Alpha	Ori	Feature	Comment	
1	21x	138.5	11	180/89	–	6–8	2	106–110 114–121 126–131 154–156	138.9	16	180/88	Sealed network	Reflector outside the borehole	3
1	8	139.8	52	209/17	090/68	12	2	106–110 114–121 126–131 154–156	139.4	51	017/17	Broken fracture		2
1	11	145.9	55	104/67	–	30	2	106–110 114–121 126–131 154–156	145.5	54	132/68	Rock occurrence	101057/101061	3
1	14	151.9	57	112/64	**020/03**	7	1	106–110 114–121 126–131 154–156	152.2	59	045/12	Broken fracture	Ori2	2
1	21	152.6	15	183/82	–	6	2	106–110 114–121 126–131 154–156	154.7	16	184/88	Broken fracture	Aperture = 13 mm, Ca, Qz, Zeol, Py	3
2	92	361.7	57	190/09	102/67	10	2	–	361.1	53	219/09	Crush		3
2	93	376.6	46	135/79	002/19	6	2	–	375.5	43	135/85	Rock occurrence	101057/101061	3
2	96	380.9	32	140/90	–	9	1	–	380.5	50	114/74	Rock occurrence	101057/101061	2
2	100	388.4	60	116/66	161/05	15	1	–	387.7	57	103/63	Rock occurrence	101057/101061	3
2	99x	392.9	46	262/11	111/79	40	3	–	394.4	27	293/27	Crush		2
3	109	425.9	69	091/46	161/38	12	2	451–459 466–471	426.0	61	106/54	Rock occurrence	101058/102017	3
3	111	430.0	65	160/39	**090/45**	8	2	451–459 466–471	430.0	69	105/43	Rock occurrence	101058/102017, Ori2	3
3	327	444.9	55	084/57	–	21	3	451–459 466–471	444.9	50	095/63	Rock occurrence	101058/108019	3

KFM06C

DZ	Borehole radar								Inferred geological feature from boremap					Confidence level
	In data					Interpretation			Correlation					
	Id	Borehole length (m)	Alpha	Ori1	Ori2	Radius (m)	Strength	Low radar amplitude (m)	Borehole length (m)	Alpha	Ori	Feature	Comment	
3	317x	449.0	13	048/89	313/75	25	3	451–459 466–471					Reflector outside the borehole	–
3	117	449.4	66	084/45	163/43	16	2	451–459 466–471	448.9	61	092/41	Rock occurrence	101058/102017	3
3	118	453.8	65	089/48	167/41	10	2	451–459 466–471	453.8	68	105/43	Rock occurrence	101058/102017	3
3	122	460.8	70	094/32	–	24	2	451–459 466–471	460.7	69	106/42	Rock occurrence	101058/102017	3
3	128	480.1	59	144/64	077/20	3	1	451–459 466–471	478.8	67	109/48	Rock occurrence	101058/101061	2
4	141	507.4	26	340/89	014/37	6	1	533–540	507.6	24	003/85	Broken fracture	Clay	3
4	140	509.8	64	150/56	**085/29**	18	2	533–540	509.7	54	080/34	Rock occurrence	101058/101061, Ori2	3
4	148	533.8	66	171/38	**097/51**	10	2	533–540	534.0	57	099/50	Rock occurrence	101058/102017, Ori2	3
4	317	537.3	9	223/88	–	30–36	3	533–540					Reflector outside the borehole, part of 317x	–
4	152	540.2	55	090/62	–	25	2	533–540	540.6	52	078/31	Rock occurrence	101051/101061	2
5	176	630.2	51	106/74	211/27	5	1	–	630.1	48	118/73	Rock occurrence	101058/101061	3
5	177	633.9	56	200/13	**119/74**	15	2	–	634.2	43	106/71	Rock occurrence	101058/101061, Ori2	3
5	333	640.1	10	354/65	–	6	1	–	638.5	8	292/65	Sealed network		2
5	205x	653.6	17	217/79	–	24–40	3	–	651.7	23	023/89	Broken fracture	Reflector outside the borehole, part of 205	2
5	330	655.6	46	230/06	**130/80**	9	1	–	655.1	45	137/85	Rock occurrence	101058/101061, Ori2	3
5	205	659.3	19	210/81	–	24	3	–	659.9	18	224/81	Sealed network		3
5	183	662.6	14	059/84	–	13	2	–						0
5	185x	662.6	25	208/67	066/71	6	1	–	662.8	19	290/78	Rock occurrence	101058/101061	2
5	184	663.6	18	203/81	048/70	12	2	–	663.7	15	224/86	Broken fracture		3
5	185	666.3	22	052/69	–	20	2	–	666.1	37	033/89	Sealed network		2
5	185xxxx	675.8	19	222/68	066/83	18–30	3	–	675.5	26	220/75	Sealed network	Reflector outside the borehole	3

KFM07A

DZ	Borehole radar								Inferred geological feature from boremap					Confidence level
	In data					Interpretation			Correlation					
	Id	Borehole length (m)	Alpha	Ori1	Ori2	Radius (m)	Strength	Low radar amplitude (m)	Borehole length (m)	Alpha	Ori	Feature	Comment	
1	5	108.0	15	133/82	–	9	2	111–113 118–121 150–170	108.1	7	253/78	Broken fracture		2
1	2	111.6	71	326/18	**001/45**	3	1	111–113 118–121 150–170	111.5	76	017/33	Broken fracture	1.5 mm Ori2	3
1	3x	120.9	65	343/55	–	3	1	111–113 118–121 150–170	120.7	52	127/11	Broken fracture	1.5 mm	2
1	4	133.4	55	250/10	002/63	18	3	111–113 118–121 150–170	133.7	52	097/18	Crush		2
1	8	134.2	14	161/73	–	12	3	111–113 118–121 150–170	136.7	7	127/75	Rock occurrence	101057/102017	3
1	8x	159.3	37	342/82	–	6	1	111–113 118–121 150–170	159.7	37	200/24	Broken fracture		1
1	18	169.6	18	148/80	–	13	2	111–113 118–121 150–170	168.7	23	170/82	Broken fracture		3
1	10	178.4	68	303/15	–	21	3	111–113 118–121 150–170	178.4	54	256/17	Crush		3
2	15	203.0	30	343/87	–	5	1	195–205	203.8	44	230/21	Unbroken fract		1
3	53	419.9	30	175/89	–	3	1	418–422	420.6	27	190/84	Rock occurrence	101057/101061	3
4	157	827.1	29	208/85	–	9	1	823–827 835–840 854–861 874–879 880–886 896–899 921–924 933–937 960–972	827.2	31	175/86	Broken fracture		3

KFM07B

DZ	Borehole radar								Inferred geological feature from boremap					Confidence level
	In data					Interpretation			Correlation					
	Id	Borehole length (m)	Alpha	Ori1	Ori2	Radius (m)	Strength	Low radar amplitude (m)	Borehole length (m)	Alpha	Ori	Feature	Comment	
1	1	52.9	31	295/61	**153/71**	70	3	N/A	50.7	40	167/63	Rock occurrence	101057/102017, Ori2	3
2	10	96.1	74	221/54	**209/19**	20	3	95–102	96.0	76	225/24	Rock occurrence	101057/102017, Ori2	3
3	14	120.1	33	195/90	–	20	2	118–123 132–136	122.2	27	170/81	Rock occurrence	101057/102058	2
3	22	127.1	30	145/64	–	6	1	118–123 132–136	127.4	28	150/64	Rock occurrence	101057/102017	3
4	42	231.7	24	153/79	–	48	3	232–240	232.3	15	147/80	Rock occurrence	101057/101061	3

KFM07C

DZ	Borehole radar								Inferred geological feature from boremap					Confidence level
	In data					Interpretation			Correlation					
	Id	Borehole length (m)	Alpha	Ori1	Ori2	Radius (m)	Strength	Low radar amplitude (m)	Borehole length (m)	Alpha	Ori	Feature	Comment	
1	2x	94.0	22	160/68	–	36	3	–	–				No boremap data	N/A
1	10	98.0	38	151/49	320/50	25	3	–	–				No boremap data	N/A
1	4	102.6	22	151/68	–	5	2	–	102.6	23	140/65	Rock occurrence	102017/101061	3
2	48	332.4	21	**264/73**	086/62	3	1	365–372	333.2	12	214/83	Unbroken	Hematite, oxidized walls	1
2	61	340.6	13	130/76	–	16	2	365–372	343.2	12	157/78	Rock occurrence	101061/101057	2
2	66	388.5	27	**276/70**	102/58	12	1	365–372	388.7	15	240/81	Broken fracture	–	2

KFM08A

DZ	Borehole radar								Inferred geological feature from boremap					Confidence level
	In data					Interpretation			Correlation					
	Id	Borehole length (m)	Alpha	Ori1	Ori2	Radius (m)	Strength	Low radar amplitude (m)	Borehole length (m)	Alpha	Ori	Feature	Comment	
1	25	190.1	58	076/62	–	14	2	256–260 272–276 308–311 339–344	189.9	57	086/55	Rock occurrence	101057/101061	3
1	30	198.3	58	319/05	–	25	2	256–260 272–276 308–311 339–344	197.8	44	204/14	Broken fracture		2
1	31	202.3	60	050/67	–	20	2	256–260 272–276 308–311 339–344	203.4	60	089/50	Rock occurrence	101058/101061	2
1	235	217.9	12	332/76	–	8–14	3	256–260 272–276 308–311 339–344	216.8	15	323/73	Structural feat.	Foliation, radar reflector outside the borehole, do not reach borehole in radargram	3
1	37	224.4	45	055/77	225/10	6	1	256–260 272–276 308–311 339–344	224.6	57	079/59	Rock occurrence	101057/101061	2
1	38	229.6	34	014/78	–	30	3	256–260 272–276 308–311 339–344	229.8	44	070/78	Broken fracture		1
1	234	243.2	42	064/81	–	15	1	256–260 272–276 308–311 339–344	242.5	44	032/79	Broken fracture		2

KFM08A

DZ	Borehole radar								Inferred geological feature from boremap					Confidence level
	In data					Interpretation			Correlation					
	Id	Borehole length (m)	Alpha	Ori1	Ori2	Radius (m)	Strength	Low radar amplitude (m)	Borehole length (m)	Alpha	Ori	Feature	Comment	
1	43	247.7	33	172/36	–	10	2	256–260 272–276 308–311 339–344	248.4	29	340/68	Rock type	101057/101061	1
1	53	307.0	56	122/43	–	12	2	256–260 272–276 308–311 339–344	307.5	43	142/34	Broken fracture	Oxidized	2
1	55	312.5	31	008/80	–	3	1	256–260 272–276 308–311 339–344	311.8	35	355/70	Rock type	101057/101061	3
1	57x	318.6	51	002/51	–	4	1	256–260 272–276 308–311 339–344	318.4	40	009/74	Rock occurrence	101057/101061	2
1	236	321.7	51	124/42	015/59	6	1	256–260 272–276 308–311 339–344	321.2	74	073/45	Rock occurrence	101057/101061	1
1	60x	332.9	47	341/39	–	15–20	3	256–260 272–276 308–311 339–344	332.9	40	003/69	Rock occurrence	101057/101061	2
1	60	341.6	33	354/68	–	15	3	256–260 272–276 308–311 339–344	342.0	28	004/85	Broken fracture		3

KFM08A

DZ	Borehole radar								Inferred geological feature from boremap					Confidence level
	In data					Interpretation			Correlation					
	Id	Borehole length (m)	Alpha	Ori1	Ori2	Radius (m)	Strength	Low radar amplitude (m)	Borehole length (m)	Alpha	Ori	Feature	Comment	
2	96	495.6	64	107/39	032/52	30	3	476–483 490–497	496.2	78	070/48	Rock occurrence	101057/101061 Ori2	2
3	104	530.2	58	111/50	–	14	2	542–545 552–557	530.0	63	051/67	Rock occurrence	101057/101061, probably a point reflector	1
3	240	535.1	51	102/65	–	16–24	2	542–545 552–557	535.6	47	078/80	Rock occurrence	101057/101061	1
3	107	544.1	69	098/42	–	7	1	542–545 552–557	544.4	73	034/44	Rock occurrence	101057/101061	2
4	140	675.4	69	072/20	–	12	2	686–690	673.3	63	095/21	Sealed network	Adularia	2
4	143	686.1	47	001/30	–	8	2	686–690	686.8	49	354/08	Rock occurrence	101057/8021 Quartz	3
5	243	807.3	15	149/84	–	9	1	800–803 820–823	807.0	13	184/85	Unbroken fract.		2
5	244	810.4	51	127/50	–	9	1	800–803 820–823	810.5	55	103/69	Rock type	101058/102017	2
5	169	812.5	69	059/29	086/67	10	2	800–803 820–823	812.5	79	070/57	Rock occurrence	101058/101061 Ori2	3

KFM08B

DZ	Borehole radar								Inferred geological feature from boremap					Confidence level
	In data					Interpretation			Correlation					
	Id	Borehole length (m)	Alpha	Ori1	Ori2	Radius (m)	Strength	Low radar amplitude (m)	Borehole length (m)	Alpha	Ori	Feature	Comment	
NO DIRECTIONAL RADAR REFLECTORS														

KFM08C

DZ	Borehole radar								Inferred geological feature from boremap					Confidence level
	In data					Interpretation			Correlation					
	Id	Borehole length (m)	Alpha	Ori1	Ori2	Radius (m)	Strength	Low radar amplitude (m)	Borehole length (m)	Alpha	Ori	Feature	Comment	
1	38	173.9	50	279/08	–	3	1	185–188	174.2	53	111/67	Rock occurrence	101058/101057	1
1	237	174.3	23	178/86	–	20	2	185–188	174.4	10	248/85	Broken fracture		1
1	33	178.4	9	027/73	–	9	2	185–188	178.5	13	297/72	Broken fracture		1
2	93	439.9	31	212/55	**072/71**	10	2	453–465 496–500 518–535	440.3	37	060/53	Rock occurrence	101061/101057, Ori2	2
2	97	456.6	36	074/69	–	12	2	453–465 496–500 518–535	–	–	–			0
2	100	457.6	50	211/22	107/66	9	2	453–465 496–500 518–535	–	–	–			0
2	101	468.1	33	084/77	–	30	3	453–465 496–500 518–535	468.4	47	080/55	Rock occurrence	8021/101057	2
2	109	509.0	37	042/44	–	24	2	453–465 496–500 518–535	509.1	28	052/60	Rock occurrence	101061/101057	3
2	223	520.5	42	213/45	–	6	1	453–465 496–500 518–535	521.0	45	215/39	Broken fracture		3
3	138	683.2	30	196/71	–	12	2	692–696	683.6	29	046/54	Rock occurrence	102017/101057	1
3	143	698.0	16	320/71	–	20	3	692–696	698.3	17	300/71	Unbroken fracture		3
3	145	701.5	36	025/34	164/82	14	2	692–696	701.1	40	061/50	Rock occurrence	101061/101057	2
4	177	829.7	46	179/61	–	12	2	827–832	829.7	32	195/72	Unbroken fracture		2

KFM09A

DZ	Borehole radar								Inferred geological feature from boremap					Confidence level
	In data					Interpretation			Correlation					
	Id	Borehole length (m)	Alpha	Ori1	Ori2	Radius (m)	Strength	Low radar amplitude (m)	Borehole length (m)	Alpha	Ori	Feature	Comment	
1	2	18.8	55	192/11	–	20	2	16–21 30–32	19.4	51	149/09	Broken fracture		2
2	39	83.0	26	180/44	**336/89**	20	2	92–106	82.7	23	340/88	Rock type	101058/8021, Ori2	3
2	22	97.5	48	318/70	–	20	2	92–106	97.4	35	341/75	Rock occurrence	101057/101061	3
2	24	110.7	17	206/67	–	20	3	92–106	110.8	19	154/85	Rock occurrence	101057/101061	2
3	70	246.8	8	154/71	–	6	2	226–237	247.5	11	163/76	Structural feature	Brittle ductile shear z.	3
3	90	265.8	40	139/16	–	15	2	226–237	264.8	35	075/25	Rock occurrence	101057/101061	2
3	91	273.9	30	219/57	–	30	3	226–237	273.9	29	109/85	Rock type	101057/101061	1
3	84	277.8	32	195/44	–	24	2	226–237	277.8	36	345/77	Broken fracture		1
4	246x	730.0	51	360/07	–	20	3	731–754	731.1	45	146/88	Rock occurrence	101057/102017	1
5	253	783.9	48	313/84	044/14	6	1	782–785	783.8	50	330/89	Broken fracture		3

KFM09B

DZ	Borehole radar								Inferred geological feature from boremap					Confidence level
	In data					Interpretation			Correlation					
	Id	Borehole length (m)	Alpha	Ori1	Ori2	Radius (m)	Strength	Low radar amplitude (m)	Borehole length (m)	Alpha	Ori	Feature	Comment	
1	3	28.2	56	235/70	–	4	1	13–21 26–50 106–110 119–122	28.8	58	233/67	Rock occurrence	101057/101061	3
1	5	40.4	40	230/86	–	4	1	13–21 26–50 106–110 119–122	40.5	43	256/77	Sealed network		3
1	9	49.6	46	095/11	234/79	14	2	13–21 26–50 106–110 119–122	49.9	41	085/16	Broken fracture	Aperture = 5 mm, clay, asphalt	3
1	11	76.5	17	139/71	299/82	10	2	13–21 26–50 106–110 119–122	76.4	14	129/65	Rock type	101061/101061 foliated	3
1	20	81.6	25	009/88	–	12	2	13–21 26–50 106–110 119–122	80.7	26	046/81	Broken fracture		2
1	17	101.7	52	124/08	**233/74**	15	2	13–21 26–50 106–110 119–122	101.7	42	212/81	Broken fracture	Ori2	2
1	16	105.5	20	131/62	–	24	3	13–21 26–50 106–110 119–122	105.8	18	167/87	Rock occurrence	101057/101061	2

KFM09B

DZ	Borehole radar								Inferred geological feature from boremap					Confidence level
	In data					Interpretation			Correlation					
	Id	Borehole length (m)	Alpha	Ori1	Ori2	Radius (m)	Strength	Low radar amplitude (m)	Borehole length (m)	Alpha	Ori	Feature	Comment	
1	18	123.7	24	148/69	–	10	2	13–21 26–50 106–110 119–122	123.4	22	168/83	Alteration		2
2	61	311.7	38	094/16	–	30	3	–	311.4	39	094/17	Broken fracture	Laum, hematite	3
2	63x	327.9	29	029/23	**046/81**	25	3	–	327.6	32	059/84	Broken fracture	Ori2	3
2	64	335.0	30	074/85	–	15	1	–	335.0	37	250/89	Broken fracture		3
2	57x	336.4	9	130/77	299/89	9–13	2	–	336.5	8	147/85	Rock occurrence	101057/101061, outside borehole	3
3	82	407.8	27	154/65	–	7	1	–	407.7	22	359/88	Structural feature		1
3	122	411.8	41	276/73	155/46	6	1	–	412.2	37	278/78	Alteration	Albitization	3
4	102	522.7	26	145/61	–	18	3	522–529	522.4	31	177/76	Rock occurrence	101057/1056	2
4	139	538.3	11	122/58	–	10–14	2	522–529	537.3	7	096/61	Rock type	101057/101061 Outside borehole	3
5	109	569.2	63	196/60	**262/37**	4	1	566–573	570.5	64	231/20	Rock type	101057/101061, Ori2	3

KFM10A

DZ	Borehole radar								Inferred geological feature from boremap					Confidence level
	In data					Interpretation			Correlation					
	Id	Borehole length (m)	Alpha	Ori1	Ori2	Radius (m)	Strength	Low radar amplitude (m)	Borehole length (m)	Alpha	Ori	Feature	Comment	
1	1	78.3	46	030/48	**133/63**	9	2	84–125 131–136	78.4	40	142/77	Rock occurrence	102017/101057, Ori2	3
1	6	86.8	52	034/50	–	12	2	84–125 131–136	86.6	43	064/79	Broken fracture		2
1	9	106.1	85	085/41	**092/44**	3	1	84–125 131–136	106.0	67	096/64	Broken fracture	Asphalt, Ori2	2
1	16	133.3	49	033/51	–	12	2	84–125 131–136	133.0	32	142/89	Rock occurrence	102017/101057	1
1	19	143.9	45	028/51	–	15	2	84–125 131–136	144.2	69	092/63	Crush		1
2	96	435.4	35	**337/09**	287/74	40	3	428–433	431.8	42	048/13	Broken fracture	Aperture = 5 mm	1
3	101	480.7	35	**345/11**	290/74	15	2	483–488	480.6	52	099/17	Broken fracture		1

Appendix 2

Correlation between radar reflectors and occurrences of vuggy rock

Vuggy rock Boremap Vuggy rock section					Borehole radar In data						Interpretation			
Borehole	From	To	Alpha	Ori	Low radar amplitude	Reflector ID	Borehole length	Alpha	Ori1	Ori2	Strength	Radius (m)	Comment	Confi-dence
KFM02A	171.40		62	102/28	165–185	–								0
		172.04	42	102/28	165–185	–								0
KFM02A	174.3		34	306/23	165–185	10a	173.9	76	043/18	251/11	2	15	Straight reflector, probably indicates a natural fracture with hematite at 173.8 m with alpha 72 and orientation 012/23	0
		175.27	65	306/23	165–185	–								0
KFM02A	176.90		63	325/30	165–185	10b	176.3	51	038/44	–	2	20	Straight reflector. Probably indicates rock occurrence (pegmatite) at 176.1 m with alpha 64 and orientation 038/30 or rock occurrence (fine-grained granite) at 176.5 m with alpha 64 and the orientation 028/31	1
		177.00	58	325/30	165–185	–								0
KFM02A	179.42		26	032/69	165–185	–								0
		180.05	75	032/69	165–185	–								0
KFM02A	247.86		48	074/46	240–320	17a	240.3	50	036/45	–	3	24	Straight reflector which bends close to the borehole and probably intersects deeper	2
		296.53	21	137/67	240–320	16	280.2	16	090/74	**118/73**	2	20	Reflector parallel to borehole along 180–240 m borehole length	2
KFM02A	298.89		67	066/27	240–320	–								0
		299.05			240–320	–								0
KFM02A	299.24	299.51	49	079/44	240–320	–								0
KFM02A	301.60	301.71	66	042/28	240–320	19	300.9	70	–		1	6		1

Vuggy rock														
Boremap					Borehole radar									
Vuggy rock section					In data						Interpretation			
Borehole	From	To	Alpha	Ori	Low radar amplitude	Reflector ID	Borehole length	Alpha	Ori1	Ori2	Strength	Radius (m)	Comment	Confi-dence
KFM06A	332.49		63	037/59	330–340	25	332.8	56	–	–	1	3		2
		332.75	64	092/22	330–340	–								0
KFM06B	66.56		27	019/69	65–72	–								0
		70.16	62	199/22	65–72	25	68.5	63	235/33	–	3	30	Curved reflector	2
KFM06C	451.46		50	171/70	450–460	117	449.4	66	084/45	163/43	3	20	Straight reflector, probably indicates amphibolite at 448.9 m with alpha 60 and orientation 097/48	0
		452.23	28	351/86	450–460	118	453.8	65	089/48	167/41	3	12	Straight reflector, probably indicates amphibolite at 453.8 m with alpha 68 and orientation 105/43	0
KFM08A	409.85		54	095/59	409–414	74	410.1	43	123/58	358/58	3	12	Reflectors 74x and 74xx probably part of 74, they are observed outside the borehole	3
						74x	(415.8)							
						74xx	(432.8)							
		412.04	39	013/77	409–414	75	413.2	48	–	–	2	6	Reflector probably indicates a broken fracture with clay at 413.0 m, 49 degr.	0
KFM08C	454.96	458.29	35	041/43	453–466	97	456.6	36	074/69	–	2	10		1
						100	457.6	50	211/22	107/66	1	9		0
KFM08C	462.09	462.50	50	029/15	453–466	–								0
KFM08C	497.84	499.0	41	195/61	495–501	108	497.9	61	–		1	3		0
						107	499.2	41	–		1	10		1
KFM08C	511.62	511.64	33	211/60	495–501	111	511.7	49	–		1	3		1
KFM08C	512.89	512.93	28	166/83	495–501	–								0
KFM08C	519.15	519.98	40	075/56	516–535	112	520.4	44	–		1	2		1
KFM08C	520.43	520.79	20	044/65	516–535	223	520.5	42	213/45		1	4		0

Vuggy rock														
Boremap					Borehole radar									
Vuggy rock section					In data						Interpretation			
Borehole	From	To	Alpha	Ori	Low radar amplitude	Reflector ID	Borehole length	Alpha	Ori1	Ori2	Strength	Radius (m)	Comment	Confi-dence
KFM08C	523.12	525.77	39	246/28	516–535	–								0
KFM08C	526.24	526.44	26	031/48	516–535	–								0
KFM08C	531.5	531.8	58	176/53	516–535	–								0
KFM09A	511.75		31.8	306/82	510–520	259	511.0	36	–	–	3	12		3
		520.03	37.6	135/88	510–520	194	518.8	40	–	–	2	12	Reflector dislocated at 12 m	3
					510–520	192	517.0	38	–	–	3	60	Strong and persistent reflector	3
KFM09B	382.31		41	224/89	–	77	383.8	38	–	–	2	6	Reflector might as well indicate broken fracture with hematite at 383.9 m with alpha 35 and orientation 191/86	1
		382.32	41	222/90	–									
KFM09B	568.92		38	280/84	566–573	109	569.2	63	196/60	262/37	1	3	Reflector might indicate rock type (pegmatite) at 570.49 m with alpha 64 and orientation 231/21	0
		573.45	47	210/82	566–573	110	572.1	72	–	–	1	3	Reflector might indicate rock occurrence (pegmatite) at 573.0 m with alpha 70 and orientation 258/31	0
KFM10A	86.93	88.79	48	135/72	82–124	6	86.8	52	034/50		2	10		1
KFM10A	89.32	89.91	47	030/38	82–124	–								0
KFM10A	92.60	94.25	39	137/82	82–124	7	92.4	78	–		1	3		0
KFM10A	96.69	97.45	63	122/63	82–124	8	98.1	46	–		1	2		1
KFM10A	98.77	101.09	62	122/64	82–124	–								0
KFM10A	104.02	104.71	57	127/67	82–124	–								0
KFM10A	104.96	105.48	62	121/64	82–124	10	105.0	54			1	2		1
KFM10A	111.48	118.56	61	126/63	82–124	12	113.3	66	–		1	2		1
						13	116.6	62	–		1	2		1
KFM10A	483.55	487.78	79	117/66	483–488	112	485.5	61	–		1	6		1